UNSATURATED ZONE STUDIES AT THE PROPOSED LOW-LEVEL RADIOACTIVE WASTE DISPOSAL FACILITY, EAGLE FLAT BASIN, TEXAS

by

Bridget R. Scanlon, Jiannan Xiang, and Richard S. Goldsmith

assisted by Jun Liao, Sreevathsa Ramachandra, and Liang Chen

Final Report

Prepared for

Texas Low-Level Radioactive Waste Disposal Authority
under Interagency Contract Number IAC(92-93)-0910

Bureau of Economic Geology
W. L. Fisher, Director
The University of Texas at Austin
Austin, Texas 78713-7508

December 1993

CONTENTS

Figures

Tables

EXECUTIVE SUMMARY

Hydrologic studies were conducted to characterize unsaturated zone processes at the proposed low-level radioactive waste disposal site and surrounding area in southern Hudspeth County, Texas. The study area is in northwest Eagle Flat basin, which is within the Basin and Range Physiographic Province. Fractured Cretaceous bedrock crops out to the southeast of the site. The thickness of the basin-fill sediments at the proposed site ranges from 164 ft (50 m) to ≥ 656 ft (200 m). Northwest Eagle Flat basin is an internally drained basin that drains through the ephemeral Blanca Draw into Grayton Lake playa. The climate in the study area is subtropical arid and the long-term average annual rainfall is 12.6 in (320 mm). Unsaturated zone studies were conducted in ephemeral stream and interstream geomorphic settings. In addition to studies of areas typical of these settings, the impact of pseudofissures, an earth fissure, and borrow pits on shallow zone unsaturated processes was also investigated.

To evaluate unsaturated zone processes, 57 boreholes were drilled in the various geomorphic settings for collection of soil samples and installation of monitoring equipement. Soil samples were analyzed in the laboratory for particle size, water content, water potential, and chloride concentration. Water potential data are used to evaluate the direction of the driving force for water movement. Chloride concentration data provide information on water fluxes because chloride concentrations are inversely proportional to water flux; low chloride concentrations indicate high water fluxes because chloride is flushed through the soil, whereas high chloride concentrations indicate low water fluxes because chloride is concentrated by evapotranspiration. In addition to laboratory analyses, a monitoring program was initiated by installing neutron probe access tubes in the different geomorphic settings to monitor water content. Field psychrometers were installed to a depth of 60.7 ft (18.5 m) in the interstream setting to monitor water potential and temperature.

Hydraulic conductivity was also measured in the field using permeameter tests, constant-head borehole infiltration tests, and multistep constant-head borehole infiltration tests.

Sediments beneath Blanca Draw were fine grained and ranged from clay to clay loam. In the interstream setting, some profiles were predominantly clay whereas others were primarily clay loam and sandy loam. Sediments beneath the borrow pit and adjacent profile were coarse grained and ranged from clay to muddy gravel. The fissured sediments were primarily loam whereas those adjacent to the fissure were predominantly clay.

Spatial variability in water content is controlled primarily by variations in sediment grain size. Discontinuities in water content across different soil types indicate that water-content variations with depth cannot be used to determine the direction of water movement. Temporal variations in water content were restricted to the fissured sediments and some areas in Blanca Draw. The maximum depth of water penetration in these areas was 5 ft (1.5 m). The absence of temporal variations in water content monitored in the remainder of the neutron probe access tubes indicates that water pulses did not move through these areas. Because a constant flux could result in temporally invariant water content, the absence of such variations does not preclude downward water movement.

Typical water potential profiles at the site, which is located in an interstream setting, were low in the upper 7 ft (2 m) (~-12 to -2 MPa) except after rainfall and increase with depth below the minimum to maximum values of -6 to -0.4 MPa in different profiles. The monitoring record for the in situ psychrometers was insufficient to evaluate long-term fluctuations in water potential. A vertical profile based on data collected on August 13, 1993, showed low water potentials at 1 ft (0.3 m) depth (-6 MPa) that increased to a maximum value of -2 MPa at 60.7 ft (18.5 m) depth. The low water potentials indicate that the sediments are dry, and the upward water potential gradients indicate an upward driving force for liquid flow. Boreholes drilled after rainfall had high water potentials in the surficial sediments that decreased sharply at the base of the wetting front. Exceptions to this typical profile were found in the profile in the fissured sediments and beneath the borrow pit. The fissured sediments had much higher water potentials in the upper 43 ft (13 m) than

the sediments 33 ft (10 m) distant from the fissure. Water potentials in soil samples from the borrow pit were much higher than those in soil samples from the profile 33 ft (10 m) distant from the borrow pit.

In addition to water potential data, information on hydraulic conductivity is also required to calculate water fluxes. New solutions were developed to analyze the field-saturated flow component of the hydraulic conductivity using permeameter data, constant-head borehole data, and multistep constant-head borehole data. These new solutions provide a more accurate distribution of pressure along the test hole or boreholes and thus result in more accurate estimates of hydraulic conductivity. A total of 26 permeameter tests were conducted in different soil textures to evaluate spatial variability in hydraulic conductivity of sediments in the upper 1.6 ft (0.5 m). K_{fs} based on the Guelph permeameter data ranged from $\leq 10^{-7}$ to 10^{-4} m s^{-1}. Hydraulic conductivities were highest in the coarse-grained sediments beneath the borrow pit and were lowest in fine-grained sediments in Blanca Draw. A total of 11 constant-head borehole infiltration tests were conducted in the study area. Results based on Xiang's (1994a) newly developed solution for the constant-head borehole test were similar to those of Reynolds and others and were up to 60% higher than those based on Glover's (1953) solution. The range in K_{fs} values for the constant-head borehole tests was 10^{-8} to 10^{-6} m s^{-1}. Hydraulic conductivities estimated from the constant-head borehole tests did not vary systematically with geomorphic setting, and the lowest and highest hydraulic conductivities were measured in the interstream setting. Multistep constant-head borehole tests were conducted in 7 of the 11 boreholes used for the constant-head borehole test to evaluate the effect of soil heterogeneity. There were no existing solutions for the multistep constant-head borehole tests. Results indicated that the hydraulic conductivity of individual layers within a borehole varied up to three orders of magnitude. Geometric average conductivities based on the multistep constant-head borehole tests differed from conductivities based on the regular constant-head tests by up to two orders of magnitude. Hydraulic conductivities based on the regular constant-head borehole tests depend on the location of the high-conductivity zone. When the high-conductivity zone is located in the upper portion of the borehole, the calculated hydraulic

conductivity based on the constant-head borehole test is lower than the average hydraulic conductivity, whereas when the high-conductivity zone is located in the lower portion of the borehole, the calculated hydraulic conductivity based on the constant-head borehole test is higher than the average hydraulic conductivity.

Typical chloride profiles in the study area are bulge shaped and have low chloride concentrations near the surface, generally less than 100 g m^{-3}, which increase to maximum concentrations of 3,000 to 18,000 g m^{-3} at depths of generally between 1.6 and 16 ft (0.5 and 5 m) and gradually decrease with depth below the peak to concentrations of 1,000 to 6,000 g m^{-3}. Water fluxes estimated from the chloride data were highest at the surface and decreased to less than .04 in (1 mm) yr^{-1} within the top meter. Flux estimates for profiles in the ephemeral stream were a minimum because chloride in runon and runoff was neglected. Deviations from the typical profiles were found in parts of Blanca Draw where maximum chloride concentrations in some profiles were less than 400 to 900 g m^{-3}, whereas chloride in other profiles in Blanca Draw reached maximum concentrations of 17,821 g m^{-3}. Chloride was leached in the upper 20 to 30 ft (6 to 9 m) depth in the fissure, whereas chloride concentrations in profiles 33 ft (10 m) distant from the fissure were much higher in this zone. Below 20 to 30 ft (6 to 9 m), chloride concentrations in the fissure increased to concentrations similar to those found in samples at the same depth in the profiles 33 ft (10 m) from the fissure. Chloride concentrations in the profile in the borrow pit were less than 50 g m^{-3} to a depth of 60.04 ft (18.3 m), whereas the profile 33 ft (10 m) distant from the borrow pit had maximum chloride concentrations of 2,622 g m^{-3}.

Because of the limited monitoring data at the Eagle Flat site, numerical simulations of unsaturated flow were based on long-term monitoring data at the Hueco Bolson site. These simulations were conducted to evaluate unsaturated zone processes. The results from these simulations are considered applicable to the Eagle Flat study area because the range in water potentials is similar at both sites. The sediments in the upper 5 ft (1.5 m) of the model domain (silty clay to clay) are finer grained than sediments found in this depth interval in the area of the proposed Eagle Flat repository (sandy loam). The gravel lens at depths of 5 to 23 ft (1.5 to 7 m) is

similar to that found in some of the profiles at the Eagle Flat site. Precipitation for the one year simulated (October 1, 1989, to September 30, 1990; 8 in [207 mm]) is lower than the long-term average annual precipitation at Eagle Flat (13 in [320 mm]) but is within the range of variability of annual precipitation at Eagle Flat. Results of the simulations showed that seasonal water potential variations below the subsurface active zone (1.6 ft [0.5 m]) are controlled by seasonal temperature fluctuations and do not reflect water movement. Analysis of water fluxes in the upper 0.98 ft (0.3 m) revealed that the dominant process for downward water movement was liquid flow. Below 0.98 ft (0.3 m) depth, water fluxes varied relatively little. The dominant term was thermal vapor flux.

The hydrologic data were integrated to develop a conceptual flow model of the vadose zone of the Eagle Flat study area. Profiles in the ephemeral stream setting are characterized by variable water content, low water potentials, upward water potential gradients below the shallow subsurface after rainfall, and variable chloride profiles. The generally low water potentials and upward water potential gradients suggest dry soils and an upward driving force for water movement under present conditions. The low chloride concentrations in some of the profiles in Blanca Draw indicate that at some time in the past the chloride was leached, probably when these sites were ponded. The typical profiles in the interstream setting have variable water contents, low water potentials, upward water potential gradients, and high maximum chloride concentrations. In this setting the water potential data indicate upward driving forces for liquid flow, and the chloride data indicate very low fluxes for thousands of years. In the borrow pit, the sediments are disturbed and ponded water occurs for long periods, which results in downward water movement as indicated by high water potentials and low chloride concentrations. The fissured sediments also have ponded water after rainfall. High water potentials and low chloride concentrations in the upper 20 to 30 ft (6 to 9 m) of the fissured sediments indicate downward fluxes to this depth. Water content monitoring data showed downward movement of water to 5 ft (1.5 m) depth after rainfall. The sharp decrease in water potentials and increase in chloride at 20 to 30 ft (6 to 9 m)

may occur because the fissure has not been present long enough for water to move deeper or may mark the location of a clay zone.

Long-term water potential monitoring data from the Hueco Bolson provide valuable information on unsaturated zone processes in response to climatic variations. These data indicate that the penetration depth of the wetting front after rainfall is greater in coarse textured soils (2.6 ft [0.8 m] in sand) than in fine-textured soils (1 ft [0.3 m] in clay loam). The progressive increase in water potentials with depth during infiltration and redistribution suggests piston flow.

The soil physics and chemical data for the area of the proposed Eagle Flat repository are consistent and suggest negligible fluxes. Long-term net water fluxes estimated from the soil water chloride concentrations were less than 1 mm yr^{-1} below the top meter of soil. The upward decrease in water potentials indicates an upward driving force for water movement.

INTRODUCTION

Purpose of Study

The objective of this study was to characterize the unsaturated zone in northwest Eagle Flat basin for low-level radioactive waste disposal. Hydraulic and chemical approaches were used to evaluate subsurface water movement at the site. Hydraulic approaches included laboratory measurement of water content and water potential of soil samples collected from 33 boreholes (table 1). These data provide information on spatial variability in water content and water potential throughout the study area. Profiles of water potential can be used to determine the direction of the driving force for water flow. In addition to laboratory data, neutron probe access tubes were installed in the field to monitor water content, and thermocouple psychrometers were installed to monitor water potential and temperature. Field-saturated hydraulic conductivity was also measured in situ. The hydraulic data provide information on water movement at the time of sampling or for the duration of the monitoring period. In contrast, chemical data such as the chloride concentrations in soil water provide information on water movement for up to several thousands of years in the

Table 1. Summary of boreholes drilled, samples collected, monitoring equipment, and tests conducted. Wc = water content, wp = water potential, Cl = chloride, BI = regular constant-head borehole infiltration test, BI* = regular and multistep constant-head borehole infiltration test, np = neutron probe, and p = thermocouple psychrometer.

Borehole no.	Location	Total depth (m)	Type of analysis	Monitoring equipment
YM9	ephemeral stream (slope)	14.63	wc, wp, Cl	
YM10	ephemeral stream (slope)	10.33	wc, wp, Cl	
YM11	ephemeral stream (floor)	9.30	wc, wp, Cl	
YM12	ephemeral stream (floor)	5.64	wc, wp, Cl	
YM13	interstream	11.34	wc, wp, Cl	
YM14	interstream	9.57	wc, wp, Cl	
YM15	borrow pit	16.55	wc, wp, Cl	
YM16	adjacent to borrow pit	14.51	wc, wp, Cl	
YM21	interstream	8.69		BI*
YM24NP	interstream	4.97		NP
YM25NP	interstream	5.18		NP
YM26NP	in borrow pit	7.92		NP
YM28	interstream	27.43	wc, wp, Cl	
YM30NP	adjacent to borrow pit	12.50		NP
YM32	interstream	2.62	wc, wp, Cl	
YM34	interstream	2.71	wc, wp, Cl	BI
YM35	in Hoover fissure	21.18	wc, wp, Cl	
YM36	adjacent to Hoover fissure	30.63	wc, wp, Cl	
YM41	ephemeral stream	24.02	wc, wp, Cl	
YM43	ephemeral stream	24.69	wc, wp, Cl	
YM45	interstream	11.95		BI*
YM46	interstream	9.47		BI*
YM47	interstream	7.32		BI
YM48	interstream	4.15		BI
YM49	interstream	15.24		P
YM50	interstream	14.33		P
YM51	interstream	10.39		BI*
YM54	interstream	23.65	wc, wp, Cl	
YM55NP	in earth fissure	8.58		NP
YM56NP	adjacent to earth fissure	8.46		NP
YM57NP	ephemeral stream	5.12		NP
YM58NP	ephemeral stream	5.09		NP
YM59	interstream	27.49	wc, wp, Cl	
YM60	interstream	17.59	wc, wp, Cl	
YM61	interstream	21.28	wc, wp, Cl	
YM64	interstream	14.69	wc, wp, Cl	
YM66	interstream	13.41	wc, wp, Cl	
YM67	interstream	18.50		P
YM68NP	in pseudo-fissure	8.66		NP
YM69NP	adjacent to pseudo-fissure	8.60		NP
YM70	interstream	10.39	wc, wp, Cl	

Table 1. cont.

Borehole no.	Location	Total depth (m)	Type of analysis	Monitoring equipment
YM71	interstream	10.39	wc, wp, Cl	
YM72	interstream	10.42	wc, wp, Cl	
YM73	interstream	10.45	wc, wp, Cl	
YM74	interstream	10.45	wc, wp, Cl	
YM75	interstream	10.36	wc, wp, Cl	
YM76	interstream	10.42	wc, wp, Cl	
YM77	interstream	10.42	wc, wp, Cl	
YM78	interstream	10.42	wc, wp, Cl	BI*
YM79	interstream	18.17	wc, wp, Cl	
YM80	interstream	10.39	wc, wp, Cl	BI*
YM81	interstream	10.42	wc, wp, Cl	
YM82NP	ephemeral stream (floor)	8.49		NP
YM83NP	ephemeral stream (floor)	8.55		NP
YM84	ephemeral stream (floor)	13.53	wc, wp, Cl	BI*
YM85	ephemeral stream (floor)	17.86	wc, wp, Cl	
YM86	in pseudo-fissure	20.63	wc, wp, Cl	
YM87	adjacent to pseudo-fissure	21.95	wc, wp, Cl	
YM88	in earth fissure	13.32	wc, wp, Cl	
YM89	adjacent to earth fissure	12.01	wc, wp, Cl	

past. Chloride concentrations were measured in soil water collected from 36 boreholes. The hydraulic and chemical approaches were integrated in this study to evaluate present-day and long-term water fluxes in different geomorphic settings.

Site Description

The study area (~ 60 km^2 in area; 31°7'N, 105°16'W), ~75 mi (120 km) southeast of El Paso, lies within the Chihuahuan Desert of Texas (fig. 1) in the northwest Eagle Flat basin. Northwest Eagle Flat basin is a sediment-filled basin within the Basin and Range Physiographic Province (Gile and others, 1981). The sediment fill lies on fractured Cretaceous bedrock that is exposed on Faskin Ranch southeast of the proposed site. On Faskin Ranch, the thickness of the sedimentary fill increases to 715 ft (218 m) in the northwest (Jackson and others, 1993). The sediment fill was laid down by alluvial fan, fluvial, and eolian processes (Jackson and others, 1993). Three calcic soil horizons are found at depths of 0 to 3 ft (0 to 1 m), 10 ft (3 m), and 20 ft (6 m) (Jackson and others, 1993). The upper two calcic soil horizons are better developed than the horizon at 20-ft (6-m) depth (Langford, 1993). Ground water flows to the south–southeast toward the Rio Grande (Darling and Hibbs, 1993). The unsaturated zone ranges from 673 to 754 ft (205 to 230 m) thick at the proposed site.

The topography of most of northern Faskin Ranch is relatively flat—slopes are less than 1 percent—and the elevation is approximately 4,364 ft (1,330 m) (fig. 1). Northwest Eagle Flat basin drains internally through the ephemeral Blanca Draw into Grayton Lake. The topographic relief in Blanca Draw is approximately 7 to 10 ft (2 to 3 m). Blanca Draw is generally dry except after high rainfall. The surface geomorphology of the area can be subdivided into ephemeral stream (Blanca Draw) and interstream settings. The ephemeral stream setting has no active channel with mobile sediment and is vegetated with tobosa grass (*Hilaria mutica*) and mesquite (*Prosopis glandulosa*). Pseudo-fissures are also restricted to the ephemeral stream setting and consist of an alignment of shallow holes, pipes, and depressions. A detailed description of these features can be

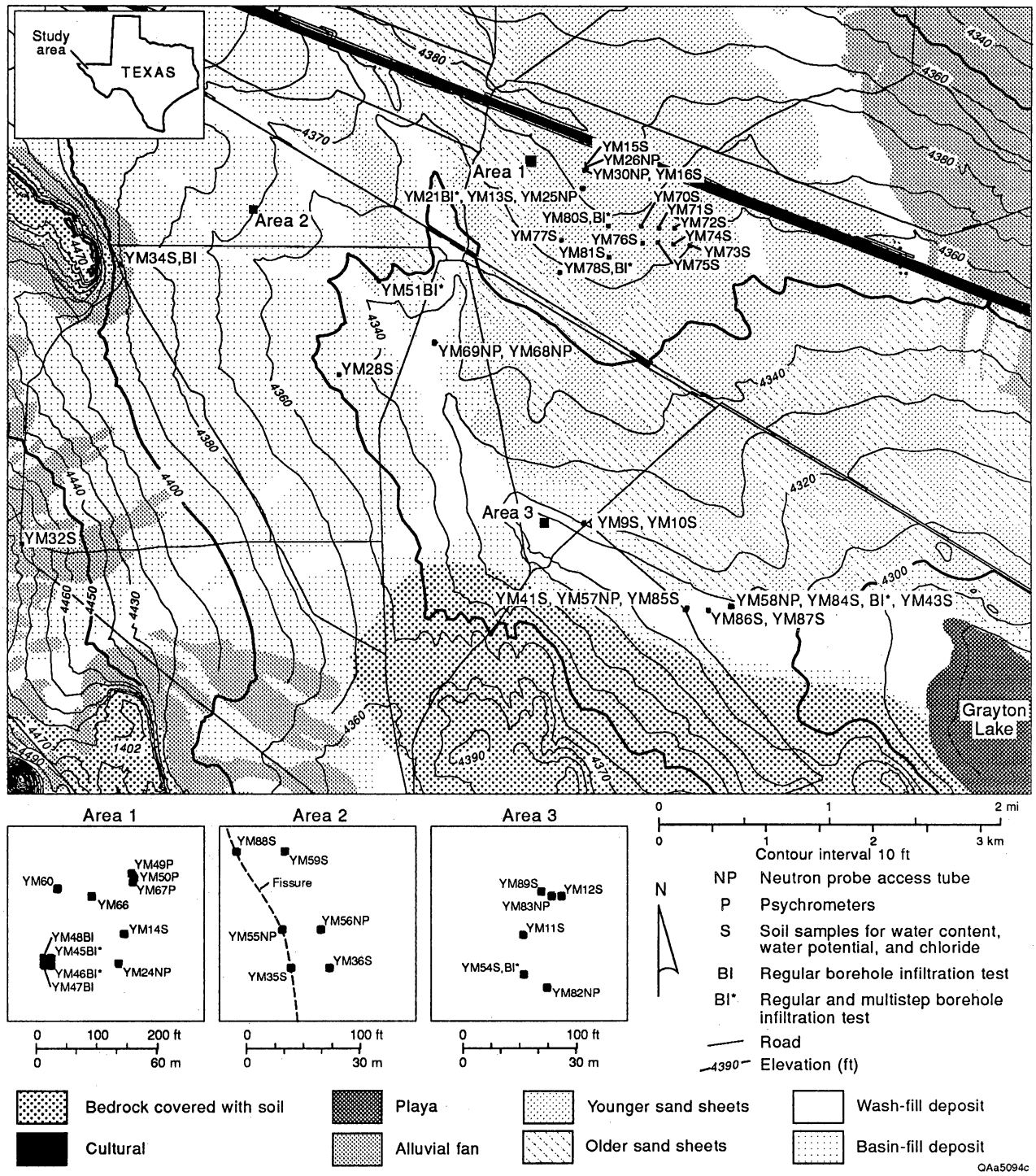

Figure 1. Location of sampled boreholes, unsaturated zone monitoring equipment, and borehole infiltration tests.

found in Jackson and others (1993). The term pseudo-fissure is used because these features are similar in scale and probable origin to pseudo-fissures described in California by Schlemon and La Chapelle (1992). The average size of individual depressions is 2 ft (0.6 m) long by 1 ft (0.3 m) deep by 1.3 ft (0.4 m) wide. Trenches dug at right angles to these fissures showed that these surface depressions are not underlain by open or filled cracks. Possible origins of these features include desiccation or sediment compaction. The interstream setting has areas characterized by sandy and silty surficial sediments. Vegetation in the interstream setting consists of black grama grass (*Bouteloua eriopoda*) and widely scattered mesquite and soaptree yucca (*Yucca elata*). An earth fissure called Hoover fissure because it is located mostly on the adjacent Hoover property was found in the northwest part of the study area and is described in Jackson and others (1993). Hoover fissure is much longer (4,000 ft [1.2 km]) and wider (7 ft [2 m]) than the pseudo-fissures but is similar in depth. It is approximately 1,000 ft (0.3 km) west of Blanca Draw in an interstream setting. It can be distinguished by a vegetation linear on aerial photos as far back as 1957. Depressions along Hoover fissure have average dimensions of 67 ft (20 m) long, 7 ft (2 m) wide, and 1 ft (0.3 m) deep. Trenches showed funnel-shaped areas of sand 0.3 ft (0.1 m) wide by several meters long that were offset from the surface depressions. Two continuous calcic soil horizons were disrupted beneath the fissure. The uppermost calcic soil horizon appears to be dissolved and reprecipitated at greater depth. No large continuous open or filled cracks were found beneath the fissure. A possible reason for the lack of subsurface cracks may be because the fissure is old and such cracks may be masked by soil processes. Possible origins of the fissure include differential subsidence related to a bedrock high or natural groundwater withdrawal related to a lowering of base level associated with incision of the Rio Grande (Gile and others, 1981). Other features in the interstream setting that affect the subsurface hydrology include borrow pits. These are anthropogenic in origin and the excavated material was used in road construction. The borrow pits have been open since at least 1964 and pond frequently after rainfall.

The regional climate is subtropical arid (Larkin and Bomar, 1983). Long-term meteorologic data were obtained at Sierra Blanca (1964–1992), situated on the western edge of the study area.

Mean annual precipitation is 12.6 in (320 mm). Precipitation in the region is characterized by large interannual variations (5.2 in [133 mm] in 1964 to 20.3 in [516 mm] in 1974). Most of the precipitation falls as local, intense, short-duration convective storms during the summer, when temperature and potential evaporation are highest. Minor winter frontal storms are of longer duration.

Previous Work

Site characterization studies for low-level radioactive waste disposal were previously conducted in the Hueco Bolson, which is northwest of the Eagle Flat basin. Studies were conducted at this site from 1988 to 1990, and long-term monitoring of certain hydraulic parameters has continued to the present. Work at the Hueco Bolson site was discontinued in 1990 except for long-term monitoring of some hydraulic parameters and characterization of the Eagle Flat study area begun in 1991. The work conducted in the Hueco Bolson has been described in papers (Scanlon, 1992a, 1992b, Appendices A and B).

Hydrodynamic Approach

Although much of the previous work on unsaturated flow in arid regions has concentrated on flow in the shallow zone in response to agricultural irrigation (Gaudet and others, 1977; van de Pol and others, 1977), recent interest in unsaturated systems of arid regions has developed because of their potential suitability as repositories of radioactive materials. The suitability of arid regions for waste disposal is related to high evapotranspiration rates relative to precipitation, which results in low net downward fluxes. In addition, thick unsaturated zones provide a natural barrier to radionuclide transport to ground water (Winograd, 1981). Studies of unsaturated flow related to radioactive-waste disposal are being conducted at Hanford, Washington; Beatty and Yucca Mountain, Nevada; and Las Cruces, New Mexico (Enfield, 1973; Gee, 1985; Montazer and

Wilson, 1985; Nichols, 1987). This study is part of a program to characterize a site in the Chihuahuan Desert of Texas for low-level radioactive waste disposal.

Various methods have been used to evaluate the direction and rate of water movement in the unsaturated zone, which is critical in predicting contaminant migration. The water balance approach estimates the downward rate of water percolation or recharge (Ababou and others, 1987) according to the following equation:

$$I = P - ET \pm R_s + \Delta S \tag{1}$$

where I is net infiltration, P is the precipitation, ET is the actual evapotranspiration, R_S is the surface runoff, and ΔS is the change in storage. Although the water balance approach may be suitable in irrigated agricultural regions, it is generally unsuitable in natural arid regions because precipitation and evapotranspiration measurements are not precise enough to allow confidence in the differencing of two numbers of nearly equal value (Gee and Hillel, 1988). Micrometeorological techniques for estimating actual evapotranspiration in partially vegetated desert regions are highly inaccurate. Weighing lysimeters were used at the Hanford site (Gee and Heller, 1985) to measure directly evapotranspiration and drainage. The disadvantages of lysimeters are that the natural soil structure is disturbed, and boundary conditions may affect flow.

Temporal variations in water content monitored with a neutron probe are often used to evaluate the movement of water pulses through the unsaturated zone. Comparison of water profiles monitored with time at the Beatty site showed deep percolation and redistribution of water down to a depth of 7 ft (2 m) after an intense rainfall event (Nichols, 1987). In general, however, monitoring water content may not be sufficiently accurate to detect the small fluxes that move through the unsaturated zone of arid regions. In addition, even under equilibrium conditions with no flow, water content is discontinuous across different lithologies, and variations in water content with depth do not indicate the direction of water movement.

In contrast to water content data, energy potential is continuous across different materials and is typically used to infer flow direction. In the unsaturated zone, many potential gradients may be important, as indicated by the generalized flow law (modified from de Marsily [1986]):

$$q = -L_1 \nabla \Phi - L_2 \nabla T - L_3 \nabla C \quad (2)$$

where q is flux, L_1, L_2, and L_3 are proportionality constants, L_1 is hydraulic conductivity, ∇ is gradient operator, Φ is hydraulic head, T is the temperature, and C is the chemical concentration. The hydraulic head is the sum of matric (ψ_m) and gravitational (ψ_g) potentials. Matric potential results from capillary and adsorptive forces. Gravitational potential is the elevation above the water table, which is used as a reference datum. Water flow in response to temperature gradients occurs primarily in the vapor phase at low water contents. Chemical-concentration gradients are equivalent to osmotic-potential (ψ_π) gradients, which are calculated from chloride concentrations of the soil water according to the Vant Hoff equation (Campbell, 1985):

$$\Psi_\pi = -(\nu C \chi R T) / 1000 \quad (3)$$

where ν is number of osmotically active particles (2 for NaCl), C is chemical concentration (moles/kg), χ is the osmotic coefficient (Robinson and Stokes, 1959), R is the gas constant (8.3142 J mole^{-1} °K^{-1}), and T is the temperature (°K). In some flow systems, temperature and osmotic potential gradients are negligible and the flow law can be simplified to the Buckingham-Darcy Law (the first term on the right of the equals sign in equation 2).

Various methods are used to measure the potential gradients in the generalized flow equation. Tensiometer measurements are restricted to matric potentials between 0 and –0.08 mega pascals (MPa; 1 MPa is equivalent to 10 bars or 102 m). In areas of shallow water tables (≤ 26 ft [≤ 8 m]), such as near Socorro, New Mexico, matric potentials were high (≥–0.08 MPa) and calculated Darcy fluxes ranged from 8 to 37 mm yr^{-1} (Stephens and Knowlton, 1986). To measure lower water potentials recorded in most other arid regions, which reflect, in part, deeper (>328 ft [≥100 m]) water tables, thermocouple psychrometers are generally required. Thermocouple psychrometers measure water (matric and osmotic) potentials of less than –0.1 MPa. Because thermocouple psychrometry forms an integral part of soil-physics monitoring in arid systems, principles of operation and potential sources of errors of psychrometers are described in Rawlins and Campbell (1986). Psychrometers have been employed at very few sites because these

instruments are difficult to calibrate and install and their life span is generally fairly short. Much of the psychrometric data in the literature is questionable because of poor installation procedures and lack of sophisticated data loggers for recording water potentials accurately.

Water potential data can be used to assess the direction of water movement; however, information on the relationship between water potential and water content and between hydraulic conductivity and water content is required for quantifying water flux and for numerical modeling. These relationships vary according to soil type and are highly nonlinear in arid systems. Water retention data measured in the field according to the instantaneous profile technique are only applicable in moist systems (Rose and others, 1965; Stephens and Knowlton, 1986) and are generally unsuitable in most arid regions. Water retention data for arid systems are generally measured in the laboratory. Although saturated hydraulic conductivity can be readily measured in the field or in the laboratory, unsaturated hydraulic conductivity measurements are extremely difficult and time consuming. Estimates of unsaturated hydraulic conductivity are generally obtained from measurements of water retention and saturated hydraulic conductivity according to Van Genuchten (1980). Because most studies do not measure data for water retention curves (Tyler and others, 1986; Montazer and Wilson, 1985; Isaacson and others, 1974), soil water fluxes cannot be quantified for these sites.

Chemical Approach

Meteoric Chloride

Chloride concentrations in soil water have been used to evaluate water fluxes in semi-arid systems (Bresler, 1973; Johnston, 1987; Peck and others, 1981; Sharma and Hughes, 1985). Chloride is an ideal tracer because it is chemically conservative. The source of soil water chloride is in precipitation and dry fallout. Because chloride is nonvolatile, its concentration increases in the root zone as a result of evapotranspiration. If the hydrodynamic dispersion coefficient is assumed

to be negligible (Allison and others, 1985), the soil water flux (q_w) can be approximated by:

$$q_w = D_{Cl} / C_{Cl} \tag{4}$$

where D_{Cl} is the chloride deposition rate (g m^{-2} yr^{-1}) and C_{Cl} is the measured soil-water chloride concentration (g m^{-3}). In the ephemeral streams, fissures, and borrow pits examined in the present study, sources of chloride other than precipitation exist such as runon. Because runon, runoff, and the chloride concentrations in these waters were not quantified, chloride profiles in these settings were only used qualitatively to evaluate the amount of downward water movement relative to other geomorphic settings. The chloride deposition rate (0.076 g m^{-2} yr^{-1}) for the study area was estimated from the prebomb $^{36}Cl/Cl$ ratio in soil water samples from below a depth of 5 ft (1.5 m) in borehole YM66 (4.9×10^{-13}) as discussed later and the natural ^{36}Cl fallout at the site estimated as 20 atoms ^{36}Cl m^{-2} s^{-1} (Bentley and others, 1986). This corresponds to a chloride concentration in precipitation and dry fallout of 0.24 g m^{-3} based on a long-term mean annual precipitation of 12.60 in (320 mm). The residence time (t) represented by chloride at depth z can be evaluated by dividing the cumulative total mass of chloride from the surface to that depth by the annual chloride deposition

$$t = \frac{\int_0^z \theta C_{cl} dz}{D_{Cl}} \tag{5}$$

where θ is the volumetric water content. Chloride profiles provide a qualitative estimate of water flux because there are many assumptions associated with the chloride mass balance approach. These assumptions are: (1) one-dimensional, vertical, downward, piston-type flow; (2) precipitation as the only source of chloride; (3) annual chloride deposition constant with time; and (4) steady-state chloride flux equal to the chloride deposition rate. The accuracy of the flux estimates from chloride data depends on the reliability of the physical flow model used to interpret the data. Although this model of chloride movement predicts that chloride concentrations should increase through the root zone and remain constant below the root zone, many previously published chloride profiles show that chloride concentration decreases below the peak; therefore, some of the assumptions associated with the model may not be valid for different systems. The

reduction in chloride concentration below the peak has been attributed to ground-water dilution (Phillips and others, 1988), nonpiston-type flow (Sharma and Hughes, 1985), or failure of the steady-state flow assumption as a result of paleoclimatic variations (Allison and others, 1985; Phillips and Stone, 1985; Scanlon, 1991).

Cosmogenic Chlorine-36

Variations in the geomagnetic field intensity during the past 50 kyr may have caused variations in the rate of production of cosmogenic radionuclides such as ^{14}C (Mazaud and others, 1991) and ^{36}Cl (Zreda and others, 1991). Variations in geomagnetic dipole intensity have been used to construct variations of cosmogenic ^{14}C production. High ^{14}C production between 18 and 45 kyr is attributed to a period of weaker geomagnetic dipole field intensity at that time (Mazaud and others, 1991). Good agreement was found between constructed ^{14}C production and calibration ^{14}C ages of corals by U-Th dating. A similar curve of variations in cosmogenic production of ^{36}Cl based on variations in geomagnetic dipole field intensity was constructed (Phillips, pers. comm., 1993). To test the hypothesis that cosmogenic production of ^{36}Cl varied with time, $^{36}Cl/Cl$ ratios of fossil packrat urine were measured (Phillips and others, 1988). The $^{36}Cl/Cl$ ratio of the urine preserves a record of meteoric ^{36}Cl fallout variations. Results suggest that $^{36}Cl/Cl$ ratios in urine radiocarbon dated at 12 kyr and 21 kyr B.P. are 28% and 41% higher than in urine dated 3 kyr, which is consistent with the reconstruction of cosmogenic production of ^{36}Cl based on paleomagnetic field intensity. This secular variation in ^{36}Cl production should provide a signal of transport times back to 50 kyr. Radioactive decay of ^{36}Cl should have a negligible effect because the residence time of soil water considered here is small relative to the half life of ^{36}Cl (301 kyr). Comparison of $^{36}Cl/Cl$ ratios in soil water with the reconstructed ^{36}Cl production should allow dating of soil water to 50 kyr.

METHODS

Field Methods

Water Content

Soil samples were collected from 36 boreholes for laboratory determination of gravimetric water content (fig. 1). Undisturbed samples were collected for dry bulk density analysis. Soil samples for bulk density analysis were collected in the upper 0.4 ft (0.12 m) adjacent to boreholes and down to 7 ft (2 m) in pits that were dug for psychrometer installation. Samples were also collected from 10 boreholes at depths ≥ 7 ft (2 m) where the sediment was sufficiently cohesive. Most of the boreholes sampled for bulk density are in the area of the proposed repository.

Water content was monitored by means of a Campbell Pacific Nuclear neutron moisture probe (Model 503 DR; CPN Corporation, Martinez, CA) in 12 neutron probe access tubes (fig. 1). The shallowest depth monitored was 1 ft (0.3 m). The maximum depth monitored ranged from 7.3 ft (2.2 m) in YM24NP and YM25NP to about 25 to 28 ft (7.5 to 8.5 m) in the remainder of the access tubes. The depth interval ranged from 0.33 ft (0.1 m) near the surface to 1.33 ft (0.4 m) at depth. The monitoring period ranged from June to October 1993. The access tubes were installed in boreholes drilled with a solid stem auger (76 mm diameter). This method of access tube installation minimized disturbance of the surrounding material. Because of drilling difficulties, steel drill pipe (70-mm O.D., 60-mm I.D.) was used instead of conventional aluminum access tubes. Steel is also preferred because it is much more resistant to corrosion than aluminum.

The neutron probe was calibrated in the laboratory within both aluminum and steel access tubing by the manufacturer. These data show that approximately 50 percent more fast neutrons are attenuated through the steel than through the aluminum. The calibration of the neutron probe in the Hueco Bolson site is described in Scanlon and others (1991). Because neutron-count ratios (neutron counts/standard counts) may introduce more uncertainty into water-content measurements than the natural drift of the count rate (Hudson and Wierenga, 1988), neutron counts were used in

the calibration equation. The calibration curve was calculated by least-squares linear regression of the volumetric water content and neutron counts:

$$\theta = (-6.4674 + 0.003921\ Cn)/100 \quad (6)$$

where θ is the volumetric water content and Cn is the neutron count/min. The calibration equation had a coefficient of determination (r^2) of 0.98 and a standard error of estimate of 0.01 $m^3\ m^{-3}$. Electronic problems with the neutron probe resulted in loss of data for many access tubes for June and July 1993.

Water Potential

Soil samples were collected from 33 boreholes down to 98 ft (30 m) depth for water-potential (sum of matric and osmotic potential) measurements in the laboratory (fig. 1). Many of the samples were collected from the same boreholes as those sampled for water content. The boreholes were drilled using a hollow-stem auger, and samples were collected in split tube core barrels (5 ft [1.5 m] long). The samples were transferred in the field to mason jars and their lids sealed with paraffin to minimize water loss.

Field psychrometers consisted of screen-caged, thermocouple psychrometers (Model 74, PST 66; J.R.D. Merrill Specialty Equip., Logan, UT). To install psychrometers at shallow depths, a pit was dug to 7 ft (2 m) and psychrometers were placed into pilot holes (13-mm diameter, 0.5-m length) drilled horizontally into the pit wall with a Bosch rotary hammer drill (Model 11209) that uses a solid stem auger. The psychrometers were staggered with depth over a horizontal distance of 8 ft (2.4 m). This installation procedure ensured that the material overlying the psychrometers was undisturbed and that a good contact existed between the psychrometers and the surrounding sediments. Because the psychrometers were not retrievable, they were installed in duplicate for data verification. Psychrometers were installed at a depth of 1 ft (0.3 m) and at 1-ft (0.3-m) intervals between depths of 1.7 ft (0.5 m) and 7 ft (2 m). The psychrometers were placed so that their symmetry axis was perpendicular to temperature gradients to minimize the effect of such

gradients on psychrometer output (Rawlins and Campbell, 1986). After these holes were sealed with sediment from the pit, the pit was backfilled with the original sediments.

At depths greater than 7 ft (2 m), duplicate psychrometers were installed in three adjacent boreholes (YM49, 50 ft [15.24 m], YM50, 47 ft [14.33 m], and YM67, 60.7 ft [18.50 m]) that were drilled using a solid-stem auger (76.2-mm diameter) (fig. 1). Wetting or drying of native material was expected to be minimal because no drilling fluid was used. For protection during installation, the psychrometers were emplaced in a PVC screen (25.4 mm diameter, 0.010 slot size, 152 mm long) that was filled with commercial (Ottawa) sand (0.1- to 0.4-mm grain size) to prevent bridging during backfilling. Commercial Ottawa sand was used to backfill each of the boreholes. Epoxy (DER324/DEH24, Dow Chemical Company) was used to prevent preferential water or air flow between psychrometer stations within the borehole and to form a seal at the surface that would preclude surface drainage into the borehole. Epoxy also was chosen because it does not introduce water into the system. Epoxy properties (curing time, viscosity, and exothermic curing temperature) were tested in the laboratory before field use to ensure that the epoxy would neither become viscous while being poured down the tremie pipe nor emit too much heat to the surroundings. Sand was poured down a separate tremie pipe immediately after the epoxy to form a sand/epoxy column that reduced the reaction temperature to 80°C. The small diameter of the borehole and use of natural materials as a backfill were designed to minimize psychrometer equilibration time. The psychrometers were connected to a data logger (Model CR7; Campbell Scientific, Incorporated, Logan, UT) that was powered by a solar panel and a rechargeable internal battery, backed up by an external (7 V) marine-type battery. Water potentials and temperatures were logged daily at 0900 hr local time.

Hydraulic Conductivity

Field-saturated hydraulic conductivity (K_{fs}) in the surficial sediments (0.17 to 1 ft [0.05 to 0.3 m] deep) was measured with a Guelph permeameter (fig. 2) (Reynolds and Elrick, 1985, 1986). The permeameter test operates in the range of H/a from 1 to 10, where H is the water height

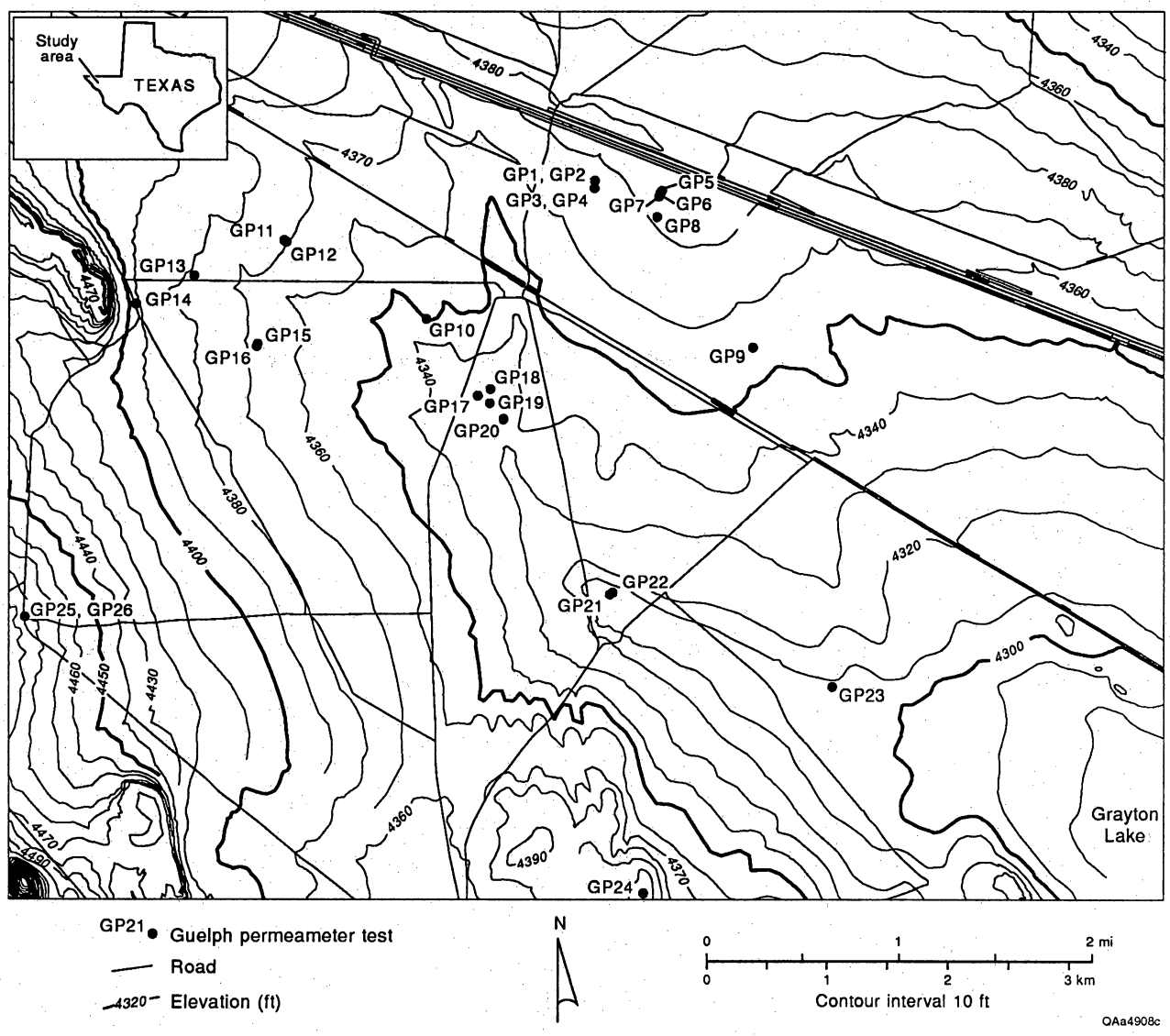

Figure 2. Location of Guelph permeameter tests.

in the test hole and a is the test hole radius. To evaluate hydraulic conductivity in the deeper unsaturated zone, constant-head borehole infiltration tests were conducted in 11 boreholes (8.8 to 77.8 ft [2.7 to 23.7 m] deep; fig. 1). The constant-head borehole test assumes that the soil is homogeneous; however, the soil is generally heterogeneous. Multistep constant-head borehole infiltration tests were conducted in 7 of the 11 borehole tests to evaluate soil heterogeneity (Xiang, 1994b) (fig. 1).

Permeameter Tests

A total of 26 permeameter tests were conducted in different soil textures to evaluate spatial variability in hydraulic conductivity of sediments in the upper 1.7 ft (0.5 m). Field-saturated hydraulic conductivity (K_{fs}) is calculated from the Guelph permeameter data by using an equation for steady-state flow from a cylindrical test hole:

$$2\pi H^2 K_{fs} + C\pi a^2 K_{fs} + 2\pi H \phi_m = CQ \tag{7}$$

where H *(m)* is the steady-state depth of water in the test hole, C is a dimensionless proportionality constant primarily dependent on H, and a *(m)* (the radius of the test hole), ϕ_m (m s^{-1}) is the matric flux potential, and Q (m^3 s^{-1}) is the steady-state flow rate out of the test hole (Reynolds and Elrick, 1985). The matric flux potential, ϕ_m, is

$$\phi_m = \int_{\psi_i}^{0} K(\psi) d\psi \tag{8}$$

where ψ_i is the initial matric potential in the soil and $K(\psi)$ is the hydraulic conductivity/matric potential relationship for infiltration (Reynolds and Elrick, 1985). The matric flux potential represents the matric effects of the unsaturated envelope and can be used to calculate the unsaturated hydraulic conductivity. The three terms on the left-hand side of equation 7 represent water flow resulting from pressure potential, gravitational potential, and matric potential, respectively. The first two terms combined yield the field-saturated flow component, and the third term represents the unsaturated-flow component. The field-saturated and unsaturated-flow

components are considered separable. Early work on analysis of the permeameter data was restricted to evaluation of the field saturated flow component (Glover, 1953)

$$K_{fs}=\frac{CQ}{2\pi H^2} \tag{9}$$

Because the ratio H/a generally ranges from 1 to 10 in the permeameter tests, flow through the bottom of the borehole may be important; therefore, Reynolds and others (1983) suggested the following equation, which includes bottom flow:

$$K_{fs}=\frac{CQ}{2\pi H^2[1+C(a/H)^2/2]} \tag{10}$$

Equations 9 and 10 neglect the effects of unsaturated flow. As shown in equations 9 and 10, only one measurement of both Q and H is necessary to evaluate the field-saturated flow component of hydraulic conductivity.

The C coefficient can be obtained using different methods. Glover (1953) developed the following equation to evaluate the C coefficient:

$$C=\sinh^{-1}\frac{H}{a}-\sqrt{\left(\frac{a}{H}\right)^2+1}+\frac{a}{H} \tag{11}$$

Because the pressure solution in Glover's development is too large, the coefficient C and K_{fs} are underestimated. Reynolds and others (1983) developed another equation to improve the evaluation of the C coefficient:

$$C=4\left[\frac{1}{2}\sinh^{-1}\frac{H}{2a}-\sqrt{\left(\frac{a}{H}\right)^2+\frac{1}{4}}+\frac{a}{H}\right] \tag{12}$$

Because existing solutions (Glover, 1953; Reynolds and others, 1983) do not accurately evaluate water pressure or hydraulic conductivity in the test hole (they overestimate pressure and underestimate hydraulic conductivity), Xiang (1994a) developed a new solution to evaluate the saturated flow component of the field-saturated hydraulic conductivity. According to this new solution, the following boundary conditions are considered:

$$\psi_p=0 \qquad at \quad r=a, \quad z=H \tag{13}$$

$$\psi_p = H \qquad at \quad r=a, \quad z=0 \tag{14}$$

where ψ_p is the pressure head in the test hole. Another necessary condition is the flow rate out of the borehole:

$$Q = \int_0^H dq \tag{15}$$

Using equations 13, 14, and 15, the coefficient C can be expressed as:

$$C = \sinh^{-1}\frac{H}{a} \tag{16}$$

In dry soils, the unsaturated effect should be considered in the evaluation of the hydraulic conductivity. Reynolds and Elrick (1985) were the first to consider the unsaturated effect as represented by equation 7. In order to determine the parameters K_{fs} and ϕ_m, permeameter tests should be conducted at two different ponded depths H_1 and H_2. The simultaneous equations approach can be used to solve for K_{fs}:

$$\begin{aligned} 2\pi H_1^2 K_{fs} + C_1 \pi a^2 K_{fs} + 2\pi H_1 \phi_m &= C_1 Q_{t1} \\ 2\pi H_2^2 K_{fs} + C_2 \pi a^2 K_{fs} + 2\pi H_2 \phi_m &= C_2 Q_{t2} \end{aligned} \tag{17}$$

where Q_{t1} and Q_{t2} are the total flow rates from the test hole with ponded depths H_1 and H_2 respectively, C_1 and C_2 can be obtained from H_1/a and H_2/a respectively based on equation 11, 12, or 16. In equation 17, we assume that the soil at both depths (H_1 and H_2) is homogeneous. We can solve equation 17 for the hydraulic conductivity and the matric flux potential as follows (Xiang, 1994b):

$$\begin{aligned} K_{fs} &= \frac{1}{\pi}\frac{C_1 H_2 Q_{t1} - C_2 H_1 Q_{t2}}{[2H_1 H_2 (H_1 - H_2) + a^2 (C_1 H_2 - C_2 H_1)]} \\ \phi_m &= \frac{1}{2\pi}\frac{2[C_2 H_1^2 Q_{t2} - C_1 H_2^2 Q_{t1}] + a^2 C_1 C_2 (Q_2 - Q_1)}{[2H_1 H_2 (H_1 - H_2) + a^2 (C_1 H_2 - C_2 H_1)]} \end{aligned} \tag{18}$$

When coefficients C_1 and C_2 are evaluated by equations 11, 12, or 16, the calculated hydraulic conductivities and matric flux potentials differ, as shown in equation 18. If the soil in the test hole is heterogeneous, equation 18 should not be used.

Permeameter data were analyzed to evaluate the field-saturated flow component of the hydraulic conductivity according to equation 10. Three different equations (11, 12, and 16) were used to evaluate the C coefficient in equation 10, which resulted in three estimates of hydraulic conductivity for each test hole. Estimates of the field-saturated flow component of hydraulic conductivity ignore the unsaturated effect and require only one head measurement; therefore, the two ponded depths for each test hole resulted in two estimates of hydraulic conductivity for each method (equations 11, 12, and 16) and a total of six estimates for each test hole. For each method of estimating the C coefficient, K_{fs} estimates based on the two head measurements (equation 10) in each test hole should be similar if the soil in the test hole is homogeneous. The unsaturated effect was also considered in the permeameter data analysis using equation 18 to estimate the hydraulic conductivity and the matric flux potentials. The three methods for evaluating the C coefficient discussed above were also used in this analysis. When the unsaturated effect is considered, two head measurements are required; therefore, this analysis resulted in three K_{fs} estimates for each test hole (table 2).

Constant-Head Borehole Infiltration Test

The constant-head borehole test is a single borehole test technique, designed to measure the field-saturated hydraulic conductivity of deep soil. The unsaturated effect is generally not considered in the constant-head borehole test because only one ponded depth is used. Traditionally equation 11 (Glover, 1953) has been used to analyze the data; however, equations 12 (Reynolds and others, 1983) and 16 (Xiang, 1994a, b) can also be used. Assuming steady-state flow, the measured constant flow rate and the water level in the borehole are used to determine the hydraulic conductivity.

Table 2. Grain size, and gravimetric water content of soil samples.

Borehole number	Depth (m)	Gravel (%)	Sand (%)	Silt (%)	Clay (%)	Soil Texture	Water content (g/g)
	0.08	0	47.77	24.26	27.98	SANDY CLAY LOAM	0.09
	0.39	0	40.03	24.14	35.83	CLAY LOAM	0.11
	1.10	0	34.52	24.44	41.03	CLAY	0.09
	1.71	0	35.12	26.16	38.72	CLAY LOAM	0.09
	1.76	0	34.23	25.32	40.45	CLAY	0.09
	2.07	0	40.98	25.77	33.25	CLAY LOAM	0.09
	2.31	0	68.24	18.49	13.28	SANDY LOAM	0.05
	2.37	0	55.72	26.00	18.28	SANDY LOAM	0.05
	2.67	0	30.25	24.95	44.80	CLAY	0.10
	3.26	0	18.22	26.13	55.65	CLAY	0.12
	3.62	0	34.51	20.74	44.75	CLAY	0.09
	4.11	0	23.38	18.57	57.87	CLAY	0.07
	4.24	0	21.44	21.89	56.66	CLAY	0.10
	4.75	0	19.64	25.06	55.29	CLAY	0.12
	4.99	1	19.09	21.66	58.08	CLAY	0.14
YM9	5.37	0	16.46	25.65	57.65	CLAY	0.14
	5.74	0	29.94	25.25	44.81	CLAY	0.11
	5.95	0	36.72	20.80	42.17	CLAY	0.11
	6.20	0	35.85	23.92	39.86	CLAY LOAM	0.09
	6.62	0	45.23	21.06	33.56	SANDY CLAY LOAM	0.09
	6.65	0	38.80	25.52	35.68	CLAY LOAM	0.09
	6.99	0	38.79	22.75	38.36	CLAY LOAM	0.09
	7.32	0	37.02	25.10	37.85	CLAY LOAM	0.08
	7.93	0	27.87	25.74	46.34	CLAY	0.12
	8.54	0	21.79	24.06	54.09	CLAY	0.13
	8.83	0	29.81	29.34	40.81	CLAY	0.13
	9.17	0	33.99	32.14	33.64	CLAY LOAM	0.11
	9.70	0	27.97	33.70	38.08	CLAY LOAM	0.11
	10.05	0	26.94	37.70	35.14	CLAY LOAM	0.09
	10.69	1	39.53	26.98	32.23	CLAY LOAM	0.10
	11.25	1	29.44	31.50	38.08	CLAY LOAM	0.10
	12.64	6	50.91	24.53	19.02	GMS	0.06
	13.17	1	71.45	14.27	12.99	SANDY LOAM	0.05
	13.82	0	49.20	30.28	20.52	LOAM	0.07
	1.81	0	22.38	29.02	48.55	CLAY	0.10
	2.11	0	40.45	22.34	36.88	CLAY LOAM	0.09
	2.39	0	35.62	23.09	41.25	CLAY	0.08
	2.78	0	35.55	25.08	39.37	CLAY LOAM	0.09
	3.09	0	43.55	26.38	30.01	CLAY LOAM	0.12
	3.42	0	17.18	79.92	2.90	SILT LOAM	0.11
	3.73	0	39.55	21.14	39.19	CLAY LOAM	0.11
YM11	4.00	2	36.23	26.92	35.27	CLAY LOAM	0.09
	4.34	1	36.55	20.40	41.57	CLAY	0.09
	4.67	0	27.84	27.27	44.51	CLAY	0.10
	5.40	10	20.43	31.72	38.01	GMS	0.13
	5.71	0	28.19	23.42	48.31	CLAY	0.14
	6.41	0	25.72	30.94	43.29	CLAY	0.15

Table 2. cont.

Borehole number	Depth (m)	Gravel (%)	Sand (%)	Silt (%)	Clay (%)	Soil Texture	Water content (g/g)
	7.26	0	27.53	31.34	41.07	CLAY	0.15
	8.21	0	38.84	29.89	30.93	CLAY LOAM	0.11
	0.22	0	17.89	31.71	50.40	CLAY	0.13
	0.46	0	18.75	32.34	48.92	CLAY	0.11
	0.83	0	25.01	31.08	43.92	CLAY	0.09
	1.15	0	20.60	29.20	50.20	CLAY	0.10
	1.42	0	9.63	38.95	51.42	CLAY	0.12
	1.81	0	11.83	35.54	52.58	CLAY	0.11
	2.10	0	40.74	23.06	36.20	CLAY LOAM	0.09
YM12	2.40	0	38.79	23.72	37.49	CLAY LOAM	0.08
	2.69	0	39.55	26.32	34.12	CLAY LOAM	0.09
	2.99	0	19.66	28.68	51.66	CLAY	0.12
	3.30	0	43.29	20.38	36.33	CLAY LOAM	0.09
	3.91	0	37.13	21.47	41.40	CLAY	0.13
	4.40	0	44.26	18.88	36.85	CLAY LOAM	0.12
	0.08	0	76.83	11.39	11.58	SANDY LOAM	0.11
	0.27	0	79.19	9.30	11.51	SANDY LOAM	0.10
	0.51	1	53.31	16.77	29.27	SANDY CLAY LOAM	0.08
	1.00	0	44.45	27.70	27.74	CLAY LOAM	0.10
	1.14	0	57.33	17.36	25.20	SANDY CLAY LOAM	0.07
	1.53	0	84.20	6.81	8.99	LOAMY SAND	0.03
	2.08	5	81.78	5.31	8.26	GMS	0.02
	2.51	20	74.64	1.19	3.80	GMS	0.02
	2.75	7	89.16	0.43	2.97	GMS	0.01
YM13	3.09	17	77.02	1.06	4.84	GMS	0.02
	3.39	23	72.18	1.46	3.67	GMS	0.03
	3.79	16	79.68	0.83	3.93	GMS	0.01
	4.09	0	81.46	6.54	12.00	SANDY LOAM	0.04
	4.40	0	80.01	7.61	12.38	SANDY LOAM	0.04
	4.84	0	56.93	14.48	28.59	SANDY CLAY LOAM	0.09
	5.28	0	51.94	17.53	30.29	SANDY CLAY LOAM	0.07
	5.86	0	66.48	9.08	24.22	SANDY CLAY LOAM	0.07
	6.35	3	65.19	14.34	17.66	GMS	0.07
	7.23	0	27.56	31.52	40.91	CLAY	0.13
	7.72	0	27.42	41.22	31.34	CLAY LOAM	0.09
	8.39	0	38.56	36.03	25.39	LOAM	0.08
	9.40	8	45.45	18.14	28.88	GMS	0.08
	10.71	2	66.67	11.70	19.63	SANDY LOAM	0.06
	11.29	5	71.06	10.65	13.64	GMS	0.05
	0.01	0	72.22	15.23	12.52	SANDY LOAM	0.07
	0.10	1	60.19	19.87	19.35	SANDY LOAM	0.14
	0.19	1	53.29	21.64	24.30	SANDY CLAY LOAM	0.13
	0.37	0	34.17	21.78	43.79	CLAY	0.11
	0.86	0	28.78	27.88	43.34	CLAY	0.10
	1.17	0	43.44	19.30	37.05	CLAY LOAM	0.08
	1.47	0	13.04	35.49	51.47	CLAY	0.13
	1.99	0	55.50	19.30	25.12	SANDY CLAY LOAM	0.07

Table 2. cont.

Borehole number	Depth (m)	Gravel (%)	Sand (%)	Silt (%)	Clay (%)	Soil Texture	Water content (g/g)
YM14	2.45	0	70.94	10.03	18.74	SANDY LOAM	0.06
	2.81	0	21.73	30.93	47.34	CLAY	0.08
	3.15	0	18.85	26.79	54.32	CLAY	0.12
	3.42	0	21.69	27.46	50.85	CLAY	0.14
	3.76	0	14.55	32.40	52.91	CLAY	0.14
	4.15	0	27.73	22.76	49.46	CLAY	0.13
	4.61	0	32.18	20.48	47.34	CLAY	0.09
	5.31	1	42.24	22.67	34.48	CLAY LOAM	0.09
	5.80	0	18.67	45.34	35.99	SILTY CLAY LOAM	0.10
	6.44	2	41.79	30.99	24.92	LOAM	0.07
	7.23	0	2.98	49.79	47.22	SILTY CLAY	0.13
	7.75	0	22.54	42.75	34.71	CLAY LOAM	0.10
	8.51	0	34.49	25.31	40.21	CLAY	0.11
	9.52	0	63.42	13.86	22.60	SANDY CLAY LOAM	0.07
	2.52	11	82.10	1.56	5.08	GMS	0.03
	2.61	11	84.69	0.37	3.46	GMS	0.02
	2.71	33	55.39	4.28	7.48	GMS	0.04
	2.80	1	91.78	1.79	5.54	SAND	0.10
	2.89	10	85.54	0.13	4.34	GMS	0.03
	3.04	22	72.97	0.98	4.06	GMS	0.03
	3.47	1	96.15	0.51	2.78	SAND	0.06
	3.65	64	22.21	6.39	7.80	GMS	0.05
	4.20	0	72.43	12.42	15.06	SANDY LOAM	0.09
	4.29	0	28.34	42.03	29.22	CLAY LOAM	0.24
	4.47	0	14.50	56.34	29.17	SILTY CLAY LOAM	0.29
YM15	4.79	0	9.55	50.72	39.73	SILTY CLAY LOAM	
	5.43	0	16.10	39.14	44.74	CLAY	
	5.39	0	64.73	11.79	23.00	SANDY CLAY LOAM	0.11
	5.55	0	65.66	12.52	21.45	SANDY CLAY LOAM	0.11
	5.74	0	64.11	15.68	20.21	SANDY CLAY LOAM	0.12
	6.07	0	22.78	43.63	33.59	CLAY LOAM	0.21
	6.29	0	40.15	17.82	42.00	CLAY	0.16
	6.62	0	37.59	17.45	44.67	CLAY	0.16
	6.96	0	40.02	17.41	42.26	CLAY	0.13
	7.48	0	22.54	24.62	52.79	CLAY	0.16
	8.34	0	46.12	21.64	32.17	SANDY CLAY LOAM	0.15
	9.24	11	84.56	1.35	3.43	GMS	0.02
	9.76	0	44.48	32.83	22.69	LOAM	0.15
	10.25	2	59.41	13.57	24.90	SANDY CLAY LOAM	0.14
	11.24	2	65.58	12.03	19.99	SANDY LOAM	0.11
	11.53	0	86.25	6.17	7.58	LOAMY SAND	0.05
	12.82	0	26.57	39.13	34.30	CLAY LOAM	0.17
	13.62	0	33.90	21.23	44.87	CLAY	0.17
	14.65	0	17.87	23.35	58.77	CLAY	0.22
	15.52	0	14.95	37.55	47.50	CLAY	0.20
	17.26	0	20.57	40.68	38.75	CLAY LOAM	0.18
	18.33	2	92.46	1.78	3.54	SAND	0.13

Table 2. cont.

Borehole number	Depth (m)	Gravel (%)	Sand (%)	Silt (%)	Clay (%)	Soil Texture	Water content (g/g)
	0.01	1	79.82	9.84	9.37	LOAMY SAND	0.03
	0.10	0	75.06	11.09	13.56	SANDY LOAM	0.06
	0.19	0	78.23	9.74	11.89	SANDY LOAM	0.05
	0.28	0	75.66	10.46	13.82	SANDY LOAM	0.07
	0.37	1	72.71	11.37	15.13	SANDY LOAM	0.08
	0.86	1	59.87	13.22	26.21	SANDY CLAY LOAM	0.09
	1.14	1	54.90	18.62	25.68	SANDY CLAY LOAM	0.09
	1.38	2	60.11	18.12	20.27	SANDY CLAY LOAM	0.07
	1.71	8	77.83	5.35	8.91	GMS	0.03
	2.02	4	82.76	4.45	8.40	GMS	0.03
YM16	2.35	16	80.98	0.74	2.49	GMS	0.01
	2.66	47	43.77	3.08	6.18	GMS	0.03
	2.99	1	94.07	0.82	4.28	SAND	0.02
	3.88	22	73.21	1.23	4.04	GMS	0.02
	4.18	19	77.01	0.48	3.73	GMS	0.03
	4.52	19	76.36	1.21	3.80	GMS	0.02
	5.04	1	76.42	9.92	12.22	SANDY LOAM	0.04
	5.88	4	88.51	1.29	6.06	GMS	0.02
	6.13	0	16.25	32.26	51.39	CLAY	0.14
	6.74	1	53.86	12.44	32.62	SANDY CLAY LOAM	0.07
	7.96	1	51.47	18.45	29.50	SANDY CLAY LOAM	0.07
	8.66	1	52.19	18.26	29.04	SANDY CLAY LOAM	0.06
	10.01	0	67.95	10.66	20.95	SANDY CLAY LOAM	0.05
	11.50	3	84.26	4.93	8.24	GMS	0.01
	12.47	0	25.67	45.98	28.35	CLAY LOAM	0.07
	13.39	0	41.61	14.26	44.14	CLAY	0.10
	14.42	0	53.00	12.08	34.67	SANDY CLAY LOAM	0.11
	0.29	2	40.75	30.33	27.23	CLAY LOAM	0.10
	0.59	0	39.55	35.70	24.43	LOAM	0.11
	0.90	0	48.54	29.70	21.75	LOAM	0.11
	1.26	1	54.73	25.15	19.03	SANDY LOAM	0.12
	1.57	1	43.52	30.81	24.43	LOAM	0.15
	1.87	0	30.62	45.69	23.63	LOAM	0.19
	2.18	0	22.05	52.89	25.06	SILT LOAM	0.16
	2.58	1	30.31	44.78	24.31	LOAM	0.17
	2.82	0	35.90	41.91	22.11	LOAM	0.16
	3.12	1	48.29	32.83	18.27	LOAM	0.15
	3.43	0	30.80	47.35	21.63	LOAM	0.20
	3.73	1	36.74	37.15	24.78	LOAM	0.15
YM35	4.10	2	43.24	33.66	21.48	LOAM	0.14
	4.37	4	45.54	28.65	22.14	GMS	0.13
	4.68	2	50.10	26.12	21.31	SANDY CLAY LOAM	0.13
	4.95	33	49.09	10.85	6.85	GMS	0.07
	5.41	0	89.97	5.98	4.05	SAND	0.04
	5.93	4	50.56	24.95	20.25	GMS	0.11
	6.23	0	52.66	17.65	29.69	SANDY CLAY LOAM	0.12
	6.54	0	20.91	45.21	33.88	CLAY LOAM	0.19

Table 2. cont.

Borehole number	Depth (m)	Gravel (%)	Sand (%)	Silt (%)	Clay (%)	Soil Texture	Water content (g/g)
	7.09	0	28.27	46.81	24.82	LOAM	0.16
	7.76	0	29.46	40.19	30.35	CLAY LOAM	0.15
	8.21	0	13.61	42.40	43.99	SILTY CLAY	0.16
	8.73	0	42.46	35.87	21.58	LOAM	0.13
	9.16	0	42.28	31.38	26.34	LOAM	0.13
	9.68	0	13.16	52.40	34.44	SILTY CLAY LOAM	0.19
	10.32	0	65.44	17.97	16.59	SANDY LOAM	0.08
	10.71	0	3.28	66.24	30.37	SILTY CLAY LOAM	0.21
	11.32	0	31.31	48.70	19.96	LOAM	0.15
	11.84	0	23.74	57.46	18.56	SILT LOAM	0.16
	12.88	0	50.04	31.65	17.87	LOAM	0.08
	13.40	2	26.02	38.33	33.31	CLAY LOAM	0.09
	14.31	0	14.71	57.95	27.32	SILTY CLAY LOAM	0.15
	14.95	0	18.19	60.28	21.46	SILT LOAM	0.15
	15.86	1	17.55	60.04	21.83	SILT LOAM	0.17
	16.54	3	19.07	55.59	22.68	GMS	0.14
	17.42	0	32.21	47.71	20.07	LOAM	0.13
	18.09	8	15.62	47.50	28.90	GMS	0.13
	18.91	0	15.18	56.30	28.51	SILTY CLAY LOAM	0.17
	19.46	0	12.60	60.08	27.20	SILTY CLAY LOAM	0.17
	20.47	0	18.97	57.92	23.09	SILT LOAM	0.16
	0.29	0	35.43	24.77	39.73	CLAY LOAM	
	0.59	0	35.50	19.47	44.92	CLAY	0.05
	1.05	0	54.18	22.70	23.11	SANDY CLAY LOAM	0.06
	1.36	0	32.36	23.83	43.59	CLAY	0.10
	1.97	0	30.25	21.19	48.44	CLAY	0.12
	2.27	0	26.15	23.44	50.34	CLAY	0.10
	2.58	0	28.38	21.29	50.23	CLAY	0.08
	2.91	0	34.87	23.78	41.06	CLAY	0.09
	3.22	0	50.43	19.79	29.63	SANDY CLAY LOAM	0.09
	3.52	0	27.22	20.31	52.42	CLAY	0.11
	3.83	1	38.75	23.90	36.74	CLAY LOAM	0.09
	4.13	1	46.65	19.91	32.87	SANDY CLAY LOAM	0.09
	4.47	2	45.14	20.46	32.48	SANDY CLAY LOAM	0.09
	4.77	1	66.05	12.45	20.50	SANDY CLAY LOAM	0.05
	5.07	1	61.76	19.81	17.41	SANDY LOAM	0.05
	5.47	0	71.77	14.31	13.89	SANDY LOAM	0.04
	6.02	0	53.53	24.51	21.96	SANDY CLAY LOAM	0.07
	6.32	0	62.82	18.96	18.23	SANDY LOAM	0.06
	6.63	0	26.27	28.37	45.36	CLAY	0.11
	7.30	0	23.38	24.35	52.08	CLAY	0.11
	7.70	0	26.10	26.81	47.08	CLAY	0.12
	8.21	0	41.10	23.33	35.57	CLAY LOAM	0.09
	8.67	0	4.80	38.65	56.54	CLAY	0.14
	9.25	0	31.25	43.74	25.01	LOAM	0.06
	9.86	0	16.26	39.24	44.51	CLAY	0.11
	10.35	0	23.76	33.60	42.56	CLAY	0.11

Table 2. cont.

Borehole number	Depth (m)	Gravel (%)	Sand (%)	Silt (%)	Clay (%)	Soil Texture	Water content (g/g)
	10.81	0	3.72	27.37	68.91	CLAY	0.17
YM36	11.29	0	34.32	16.49	49.17	CLAY	0.19
	11.96	0	23.42	16.65	59.92	CLAY	0.14
	12.36	0	25.84	18.90	55.10	CLAY	0.14
	12.85	0	44.91	24.40	30.46	CLAY LOAM	0.07
	13.27	1	33.75	26.67	38.80	CLAY LOAM	0.10
	14.10	0	24.43	27.01	48.44	CLAY	0.12
	14.52	0	17.36	29.08	53.57	CLAY	0.13
	15.47	0	18.69	23.67	57.51	CLAY	0.15
	16.08	0	17.81	24.22	57.90	CLAY	0.16
	17.02	0	16.57	23.85	59.57	CLAY	0.16
	17.63	0	26.58	23.42	49.99	CLAY	0.14
	18.58	1	18.72	25.40	55.10	CLAY	0.15
	19.19	0	29.05	24.75	46.20	CLAY	0.12
	19.95	0	19.78	22.77	57.27	CLAY	0.16
	20.86	0	13.45	26.17	60.34	CLAY	0.16
	22.17	1	11.49	20.32	67.58	CLAY	0.18
	23.76	0	13.20	28.94	57.71	CLAY	0.17
	25.31	0	13.44	31.29	55.26	CLAY	0.16
	26.87	0	9.80	31.81	58.32	CLAY	0.15
	28.42	0	9.69	36.25	54.06	CLAY	0.17
	29.98	0	13.25	31.67	55.08	CLAY	0.17
	0.22	0	32.29	25.74	41.93	CLAY	0.11
	0.53	0	41.09	19.88	39.00	CLAY LOAM	0.09
	0.92	0	45.00	21.34	33.58	CLAY LOAM	0.07
	1.29	0	44.91	22.32	32.67	CLAY LOAM	0.07
	1.56	10	60.94	10.85	17.80	GMS	0.04
	1.90	0	27.37	25.77	46.39	CLAY	0.10
	2.20	0	24.48	26.24	49.10	CLAY	0.09
	2.60	0	26.79	24.06	48.80	CLAY	0.09
	2.84	1	31.12	24.12	44.18	CLAY	0.09
	3.15	0	36.48	25.39	38.10	CLAY LOAM	0.09
	3.45	1	35.93	26.91	36.39	CLAY LOAM	0.09
	3.76	0	28.59	35.22	35.81	CLAY LOAM	0.09
	4.06	2	45.20	21.53	31.36	GMS	0.08
	4.58	0	24.14	33.01	42.85	CLAY	0.08
	4.88	1	53.32	22.37	23.61	SANDY CLAY LOAM	0.06
	5.19	5	72.62	9.20	13.61	GMS	0.04
	5.95	63	22.36	5.83	8.40	LOAMY SAND	0.03
	6.26	0	6.40	37.82	55.78	CLAY	0.14
	6.56	1	28.41	29.45	41.43	CLAY	0.11
YM59	6.87	0	19.14	26.26	54.58	CLAY	0.13
	6.96	0	32.38	23.09	44.47	CLAY	0.10
	7.51	1	19.83	37.13	42.37	CLAY	0.10
	7.90	0	34.81	26.98	38.14	CLAY LOAM	0.09
	8.21	0	48.65	22.57	28.76	SANDY CLAY LOAM	0.07
	9.76	0	17.05	31.83	51.12	CLAY	0.12

Table 2. cont.

Borehole number	Depth (m)	Gravel (%)	Sand (%)	Silt (%)	Clay (%)	Soil Texture	Water content (g/g)
	11.13	0	7.28	29.22	63.49	CLAY	0.16
	11.83	0	13.04	20.63	66.15	CLAY	0.12
	12.69	2	30.06	23.70	44.60	CLAY	0.12
	14.24	0	16.79	28.43	54.71	CLAY	0.14
	15.80	0	16.15	26.20	57.65	CLAY	0.15
	17.35	0	23.66	42.16	34.17	CLAY LOAM	0.09
	18.91	0	11.92	32.00	56.08	CLAY	0.15
	20.46	0	16.08	26.10	57.76	CLAY	0.17
	22.01	0	12.26	28.05	59.69	CLAY	0.17
	25.21	0	18.56	34.34	47.01	CLAY	0.13
	26.68	0	18.92	36.59	44.23	CLAY	0.13

In principle, the theory of conductivity measurements for the constant-head borehole test is the same as that for the permeameter test. The only difference is that the ratio H/a for the constant-head borehole test is much larger (20 to 400) than that for the permeameter test. Existing solutions (Glover, 1953; Reynolds and others, 1983) cannot provide accurate results. Xiang's solution for permeameter tests (equation 16) only performs well for ratios $H/a \leq 10$. To improve the existing solution for the case with a ratio of $H/a \geq 10$, on the basis of Glover's (1953) solution, we use the following boundary condition:

$$\psi_p = \beta H \text{ at } z^* = z_o{}^*, \text{ and } r^* = a^* \tag{19}$$

where z_o is the coordinate of maximum pressure from Glover's pressure solution, the * denotes dimensionless parameters (divided by H), and β is a weighting factor to reduce the water pressure on the basis of Glover's (1953) solution. Using the boundary condition described in equation 19 results in the following expression for hydraulic conductivity (Xiang and Chen, 1994):

$$K_{fs} = \frac{Q}{2\pi H^2 \beta}[(1-z_o^*)(\sinh^{-1}\frac{1-z_o^*}{a^*}+\sinh^{-1}\frac{z_o^*}{a^*})-\sqrt{a^{*2}+(1-z_o^*)^2}+\sqrt{a^{*2}+z_o^{*2}}] \tag{20}$$

For the borehole test, the ratio a/H is very small; therefore, equation 20 reduces to equation 9. Comparing equation 9 and equation 20 results in the following:

$$C = \frac{1}{\beta}[(1-z_o^*)(\sinh^{-1}\frac{1-z_o^*}{a^*}+\sinh^{-1}\frac{z_o^*}{a^*})-\sqrt{a^{*2}+(1-z_o^*)^2}+\sqrt{a^{*2}+z_o^{*2}}] \tag{21}$$

The solution for pressure potential is:

$$\psi_p^* = \beta\frac{(1-z^*)(\sinh^{-1}\frac{1-z^*}{r^*}+\sinh^{-1}\frac{z^*}{r^*})-\sqrt{r^{*2}+(1-z^*)^2}+\sqrt{r^{*2}+z^{*2}}}{(1-z_o^*)(\sinh^{-1}\frac{1-z_o^*}{a^*}+\sinh^{-1}\frac{z_o^*}{a^*})-\sqrt{a^{*2}+(1-z_o^*)^2}+\sqrt{a^{*2}+z_o^{*2}}} \tag{22}$$

After the maximum point $z_o{}^*$ is found, equation 22 can be used to evaluate the pressure distribution. Xiang and Chen (1994) have shown that the pressure calculated by equation 22 is closer to the actual pressure than the pressure calculated by the other solutions and have shown that

equations 12 and 21 provide a better match of the C coefficient with those obtained from numerical simulations. The roots z_o and the C coefficients for different ratios of H/a are available from Tables 1 and 2 in Appendix A of Xiang and Chen (1994). Once the C coefficient is calculated, the conductivity can be calculated according to equation 9.

Multistep Constant-Head Borehole Infiltration Test

In the previous analysis of the constant-head borehole test, the soil is assumed to be homogeneous; however, most subsurface soils consist of different layers, particularly on the scale of the borehole. (Xiang, 1994b) proposed a technique, the multistep constant-head borehole infiltration test, to estimate the field-saturated hydraulic conductivity of layered soils. In this technique, the constant-head borehole tests are repeated at different depths depending on the location of the layers. Considering n tests at n different depths results in the following n equations:

$$\begin{aligned} &2\pi K_{fs1} D_{11} = Q_{t1} \\ &2\pi K_{fs1} D_{21} + 2\pi K_{fs2} D_{22} = Q_{t2} \\ &\cdots \qquad\qquad \cdots \qquad\quad \cdots \\ &2\pi K_{fs1} D_{n1} + 2\pi K_{fs2} D_{n2} + \ldots + 2\pi K_{fsn} D_{nn} = Q_{tn} \end{aligned} \tag{23}$$

where D_{ij} is the coefficients for the j th test and the i th layer. It is equal to the flow rate from layer i of the borehole at the test j for $K_{fSi} = 1$. It can be expressed as

$$D_{ij} = -a^* H^2 \int_{h^*_{ij-1}}^{h^*_{ij}} \frac{\partial \psi^*_p}{\partial r^*} \Big|_{r^*=a^*} dz \quad \mathrm{j} \neq 1 \tag{24}$$

Assuming that the soil below the borehole is the same as the layer one (j = 1) results in:

$$D_{i1} = H^2 \left[-a^* \int_{h^*_{io}}^{h^*_{i1}} \frac{\partial \psi^*_p}{\partial r^*} \Big|_{r^*=a^*} dz + \frac{1}{\pi} \int_o^{a^*} \frac{\partial \psi^*_p}{\partial z^*} \Big|_{z^*=o} dz^* + \frac{a^{*2}}{2\pi} \right] \tag{25}$$

$$\text{where } h^*_{ij} = h_i / H_j \tag{26}$$

and H_j is the water column height in the borehole for the j th test, and h_i is defined as the distance from the bottom of the borehole to the top of the layer i. The integration in equations 24 and 25 can be obtained from Xiang (1994b). Equation 23 can be rewritten in matrix form as:

$$2\pi \begin{bmatrix} D_{11} & 0 & .. & 0 \\ D_{21} & D_{22} & .. & 0 \\ .. & .. & .. & .. \\ D_{n1} & D_{n2} & .. & D_{nn} \end{bmatrix} \begin{Bmatrix} K_{fs1} \\ K_{fs2} \\ .. \\ K_{fsn} \end{Bmatrix} = \begin{Bmatrix} Q_{t1} \\ Q_{t2} \\ .. \\ Q_{tn} \end{Bmatrix} \tag{27}$$

All coefficients in this matrix can be determined according to equations 24, 25, and 26. Solving the system of equations in 27 yields the conductivity of each layer.

Laboratory Methods

Soil Texture, Water Content, Bulk Density, and Porosity

Particle-size analyses were conducted by sieving the ≥2-mm fraction and the percent silt and clay was determined by pipette analysis (Gee and Bauder, 1982). Sediment samples that contained > 2% gravel were classified following (Folk, 1974) and those that contained ≤ 2% gravel were classified according to the U.S. Department of Agriculture (1975). Gravimetric- and volumetric-water content was determined by weighing and oven drying the samples at 105°C at 24-hr intervals until the weight change was less than 5%. Bulk density was calculated by dividing the weight of the oven-dried sample by the sample volume. Porosity (n) was calculated from the bulk density (ρ_b) data thus:

$$n = 1 - \rho_b/\rho_s \tag{28}$$

Particle density (ρ_s) was measured in 10 samples and ranged from 2.64 to 2.78 kg m^{-3}. Because these values are sufficiently close to 2.65 kg m^{-3}, the particle density of quartz, this value was used to calculate porosities.

Water Potential

Water potential was measured in the laboratory with two different instruments, a water activity meter (model CX-1) and a thermocouple psychrometer with sample changer (model SC-10), both manufactured by Decagon Devices, Inc., Pullman, WA. The water activity meter measures the water activity (Aw) of soil samples from 0.100 to 1.000 that corresponds to water potentials of –316 to 0 MPa with a resolution of ±0.003 water activity units across the range (Gee and others, 1992). The water activity (A_W) is converted to water potential using the Kelvin equation:

$$\psi = RT / M \ln(A_w) \tag{29}$$

where R is the ideal gas constant, T is temperature (K), and M is the molecular mass of water. The accuracy of the water activity meter was checked using saturated salt solutions before and after each set of samples. Soil samples were compressed in small plastic cups (4 mm diameter by 10 mm high) to a height of 5 mm using a no. 7 stopper and were analyzed immediately after taking them from the soil containers.

The Decagon SC-10 was calibrated using NaCl solutions that ranged in concentration from 0.05 M to saturated and corresponded to water potentials of –0.2 to –38 MPa at 20°C (Lang, 1967). Typical psychrometric output during evaporation shows that the plateau is stable. The 120 s microvolt output reading was used to calculate water potential. A set of 20 calibration solutions were prepared and measured initially to test the instrument, and the resulting regression line gave r^2 of 1.0 and a standard error of estimate of 0.06 MPa. Because water potentials from –0.01 to –10 MPa correspond to relative humidities from 93 to 100 percent, all measurements were conducted in a glove box lined with wet paper towels to minimize water loss from the samples. Temperature variations in the laboratory were minimal. During routine analyses, a set of six samples were placed in the sample changer; after 30 min of temperature- and vapor-pressure equilibration, the output was scanned to determine what bracketing standards should be run with the samples. The standards were then placed in the chamber and after another 30-min equilibration period, the samples and standards were measured. Least-squares linear regression was used to

calculate the sample water potential. Water potential measurements with the SC 10 thermocouple psychrometer were much more time consuming than those with the water activity meter because of the time required for calibration and temperature equilibration.

Field psychrometers were calibrated in the laboratory at three different temperatures (15°, 20°, and 25° C) and with 4 NaCl solutions (0.0 M, 0.5 M, 1.0 M, 1.5 M) and corresponded to water potentials of 0.0, –2.2, –4.6, and –7.0 MPa at 20°C (Lang, 1967). Calibration procedures similar to those outlined in Brown and Bartos (1982) were followed. The calibration data for all psychrometers were combined to develop the following general calibration equation using stepwise regression procedures (Meyn and White, 1972):

$$\psi = 0.0823 - 0.5000V + 0.0095VT \tag{30}$$

where ψ is water potential (MPa), V is voltage (μV), and T is temperature (°C). The general regression equation had an r^2 of 0.99 and a standard error of estimate of 0.025 MPa.

Voltage output from psychrometers increases with decreasing water potential down to a water potential of approximately –8, as represented by equation 30. Below this, the voltage output decreases with decreasing water potential (Brown and Bartos, 1982). Therefore, low voltage output from thermocouple psychrometers may correspond to very dry soil (beyond the calibration range of the psychrometers) or wet soil (Wiebe and others, 1971). To distinguish between dry and wet soil, 100 0.1-s readings were recorded to determine the evaporation curve for each psychrometer because the shape of the evaporation curve is narrow and spiked in the dry range and is flat and stable in the wet range. Psychrometer readings depend on the magnitude and duration of the cooling current. A Peltier cooling current of 5 milliamps (ma) and a 30-s cooling time are considered optimal (Brown and Bartos, 1982) and were used in this study. A water bath (Model 7011, Hart Scientific, Pleasant Grove, UT) equipped with a temperature control of 1×10^{-4}°C standard deviation was used to provide a constant temperature environment. Approximately 0.5 m of lead wire was submerged in the water bath during calibration to minimize heat conduction along the wires. Psychrometers were calibrated with the 100-ft- (30-m-) long cable lengths for field installation.

Meteoric Chloride

To determine chloride content, double-deionized water was added to the dried soil sample in a 3:1 ratio. Samples were agitated on a reciprocal shaker table for 4 hr. The supernatant was filtered through 0.45 μm filters. Chloride was then analyzed by ion chromatography or by potentiometric titration. Water fluxes were calculated for each depth interval from the chloride concentration data according to equation 4.

Cl/Br ratios were measured in 14 samples from the surface to 70 ft (21 m) depth from borehole. Both ions were analyzed using ion chromatography by HydroGeochem (Tucson, AZ).

Cosmogenic Chlorine-36

The $^{36}Cl/Cl$ ratios were measured by Tandem Accelerator Mass Spectrometry (TAMS) at Lawrence Livermore National Laboratory according to procedures outlined in Elmore and others (1984). Preparation of ^{36}Cl samples for analysis followed procedures outlined in Mattick and others (1987). Double-deionized water was added, and the mixture was stirred with an electric stirrer for approximately 12 hr. AgCl was precipitated from the chloride solution by addition of $AgNO_3$. Because ^{36}S interferes with ^{36}Cl analysis, $Ba(NO_3)_2$ was added to the solution to precipitate $BaSO_4$. In order to evaluate chemical contamination during sample preparation, a blank (Weeks Island halite from Louisiana, which contains no ^{36}Cl) was subjected to the same purification procedure as the soil samples. The AgCl samples were wrapped in aluminum foil to prevent reduction of Ag^+ to Ag prior to analysis. Uncertainties were calculated following Elmore and others (1984) and are reported as one standard deviation.

RESULTS

Soil Texture and Water Content

The predominant soil textures varied with geomorphic setting (table 2). Soil textures in Blanca Draw were predominantly clay and clay loam. Textures in the interstream setting were variable. Some of the profiles were primarily clay (YM14), whereas others were predominantly sandy clay loam to sandy loam (YM13). The fissured sediments were primarily loam, whereas the profiles 10 m distant from the fissure were primarily clay. Sediments beneath the borrow pit and in the adjacent profile ranged from clay to muddy gravel.

Spatial variability in water content was controlled primarily by variations in sediment grain size (table 2). Water contents in different geomorphic settings were variable (figs. 3, 4, 5, and 6). Water content in closely spaced boreholes in Blanca Draw was similar (fig. 3a, d, j, m, and p). Water contents were up to 2 times higher in the upper 27 to 33 ft (8 to 10 m) of fissured sediments than in the profile 33 ft (10 m) distant from the fissure (fig. 5, table 3). The highest water contents were measured in the profile in the borrow pit (fig. 6). Laboratory-measured water content in the profile in the borrow pit was up to 12 times higher than water content measured at the same elevation in a profile 33 ft (10 m) distant from the borrow pit. Both boreholes in and near the borrow pit were drilled after rainfall. Small changes in water content (0.02 to 0.04 m^3 m^{-3}) were monitored by the neutron probe down to a depth of 5 ft (1.5 m) in YM25 (sandy interstream site, fig. 7h) and in YM69 (Blanca Draw adjacent to the pseudo-fissure, fig. 7f). Much larger changes in water content (0.14 to 0.18 m^3 m^{-3}) were measured down to 5 ft (1.5 m) in neutron probe access tubes in Blanca Draw (YM58NP, fig. 7b) and in the fissure (YM55NP, fig. 7i). Water content monitored in a neutron probe access tube 33 ft (10 m) distant from the fissure was temporally invariant (YM56NP, fig. 7j). The calibration equation for the neutron probe was developed in silty loam soil and does not seem to apply to the coarse-textured soils in the borrow pit because the calculated volumetric water contents are extremely low. Water content monitored in the remainder of the neutron probe access tubes did not vary with time (fig. 7).

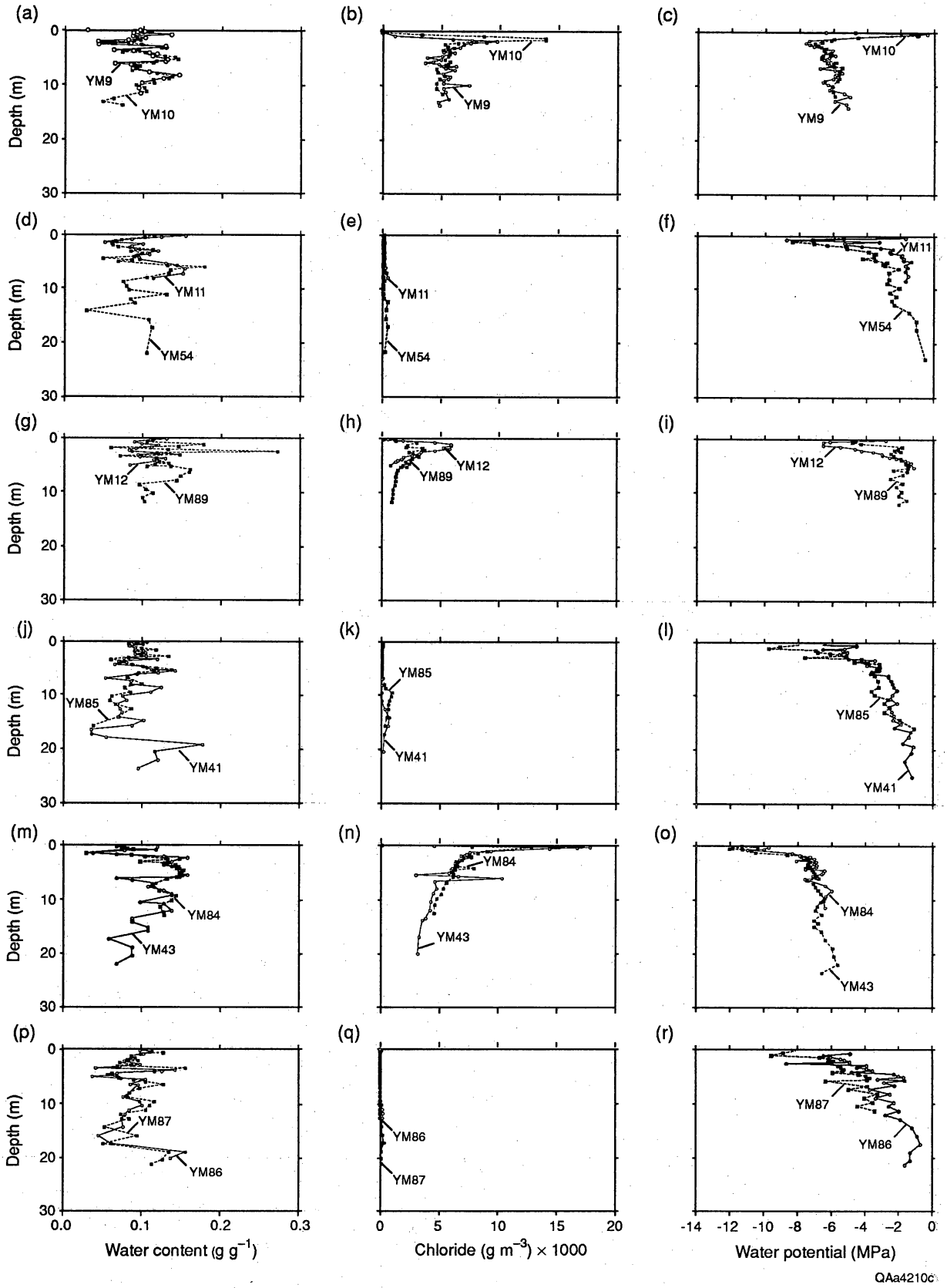

Figure 3. Profiles of gravimetric water content, chloride concentrations, and water potential for boreholes in Blanca Draw. For location of boreholes, see figure 1.

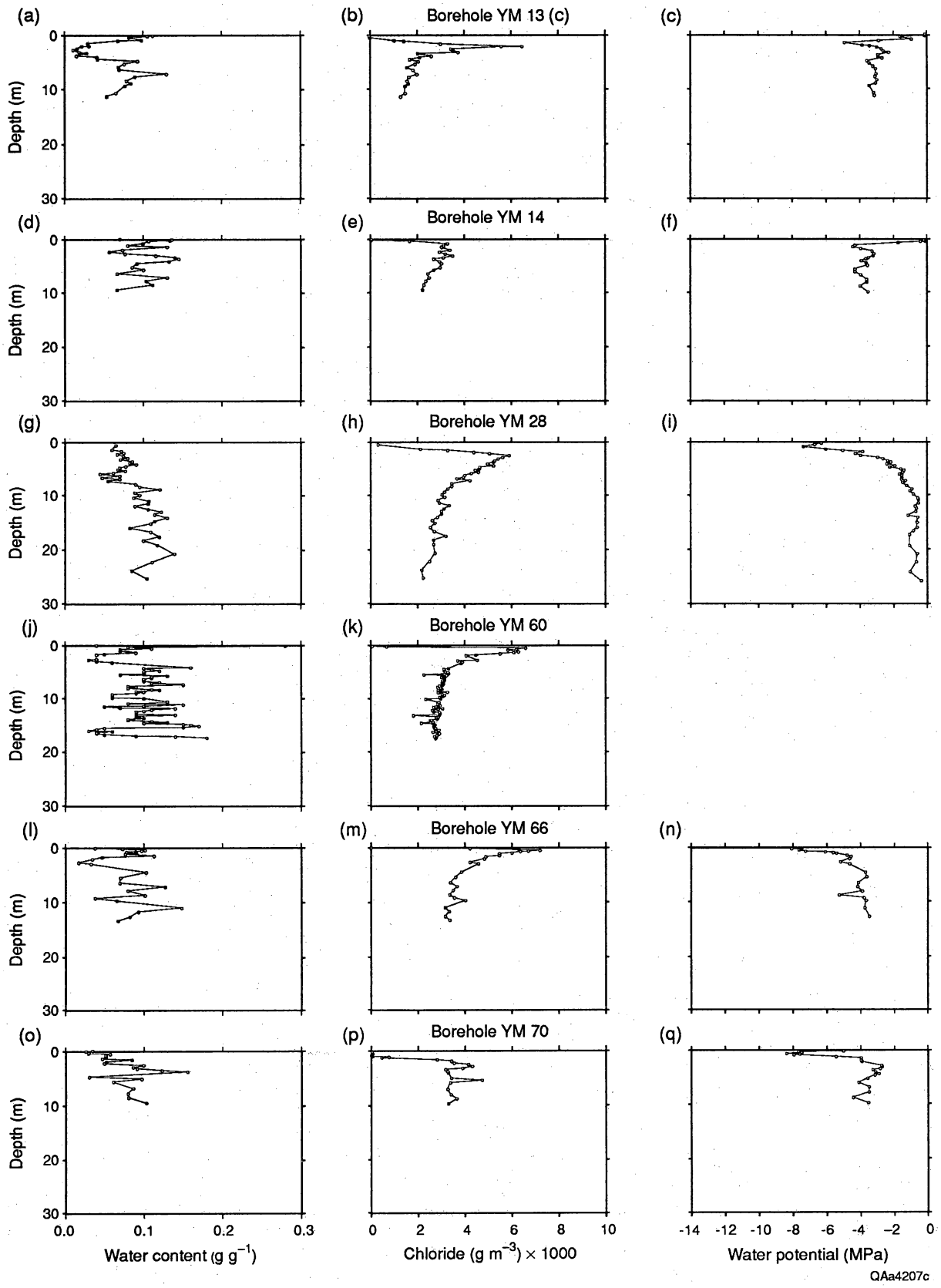

Figure 4. Profiles of gravimetric water content, chloride concentrations, and water potential for boreholes in the interstream setting. For location of boreholes, see figure 1. Water potential was not measured in soil samples from borehole YM 60. The lowest water potential (-44 MPa) measured in a soil sample from 0.05 m depth in YM 66 is not shown in fig. 4n.

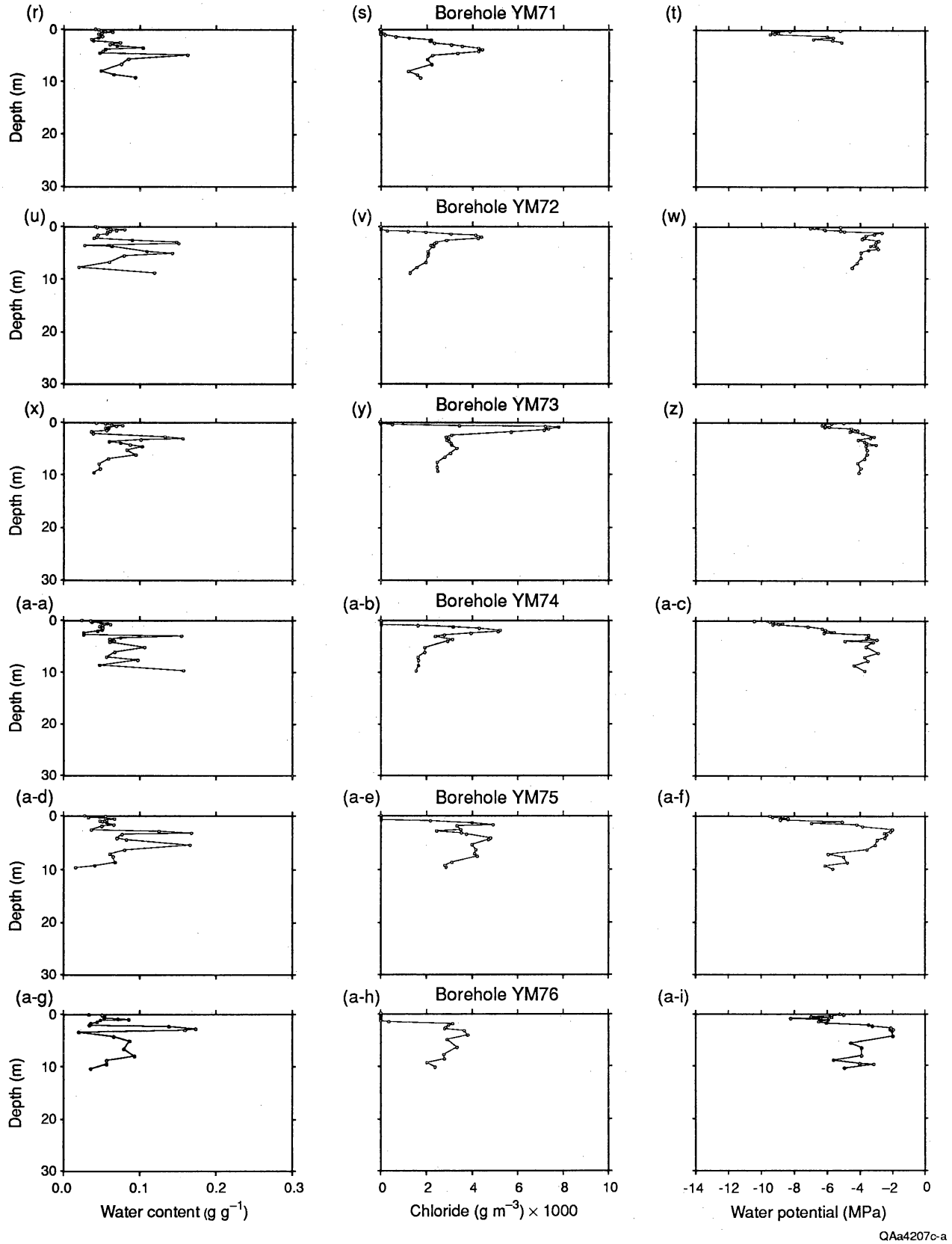

Figure 4. cont.

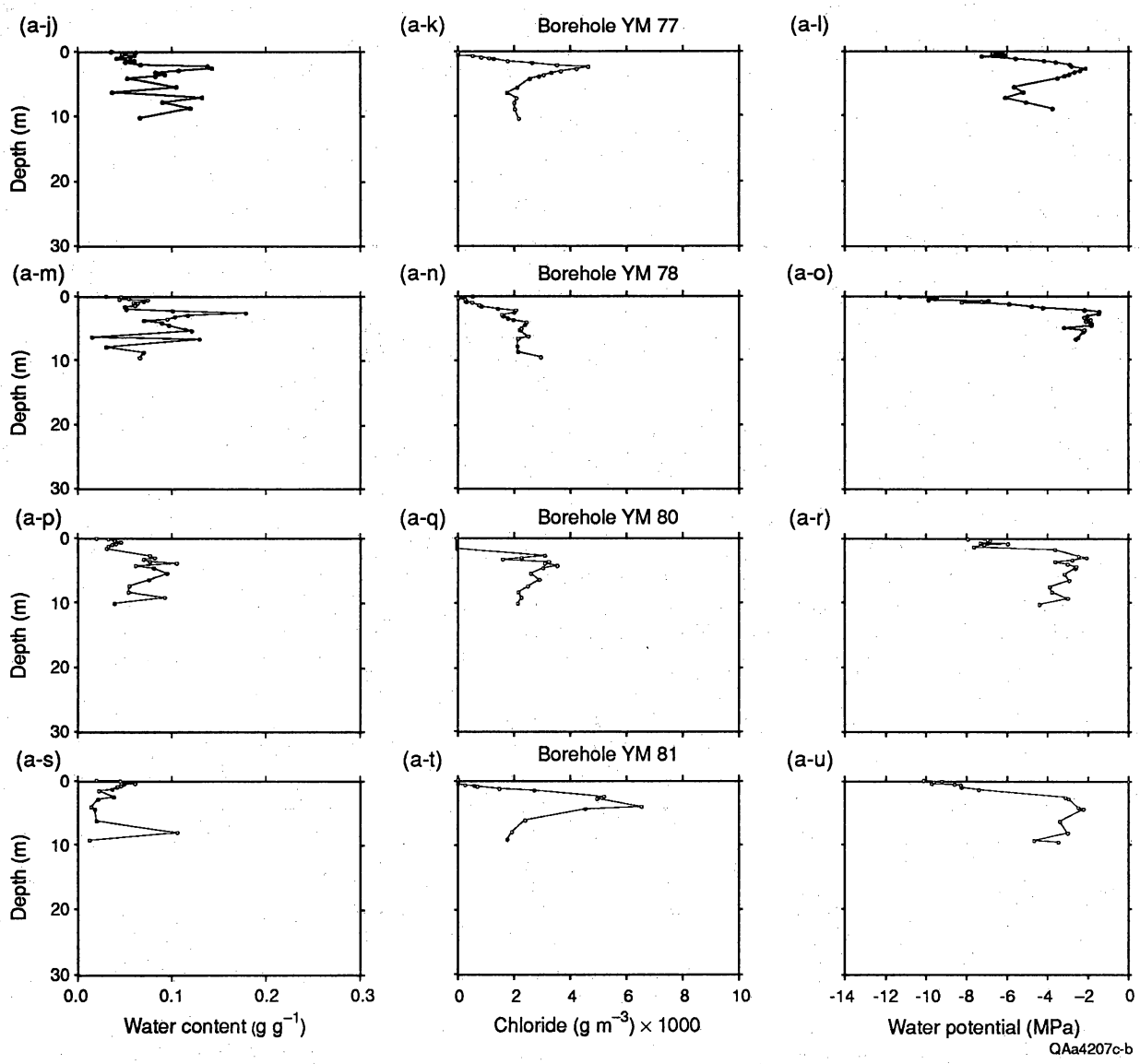

Figure 4. cont.

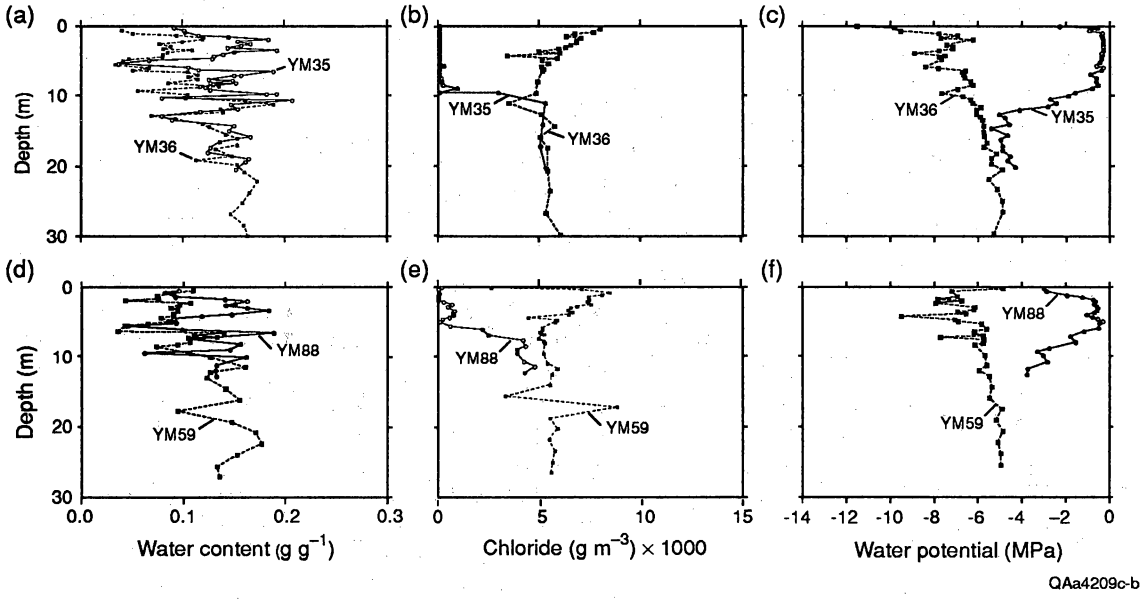

Figure 5. Profiles of gravimetric water content, chloride concentrations, and water potential for boreholes in fissured sediments. For location of boreholes, see figure 1.

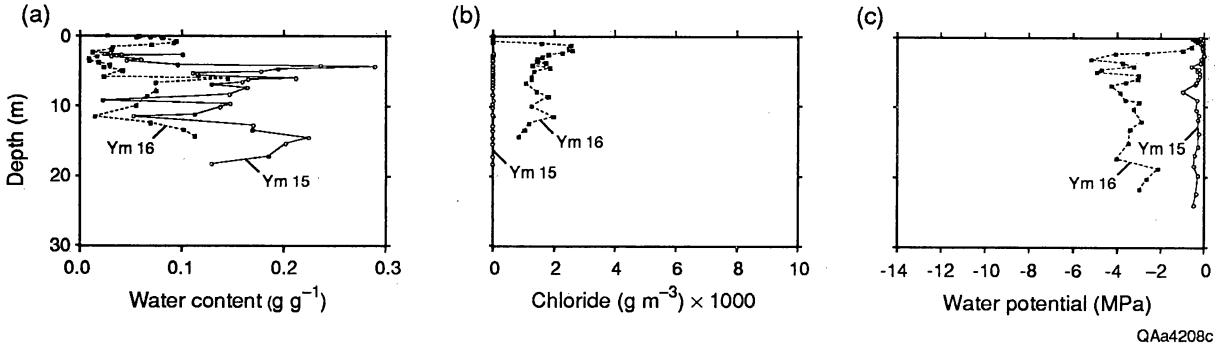

Figure 6. Profiles of gravimetric water content, chloride concentrations, and water potential for boreholes in a borrow pit. For location of boreholes, see figure 1.

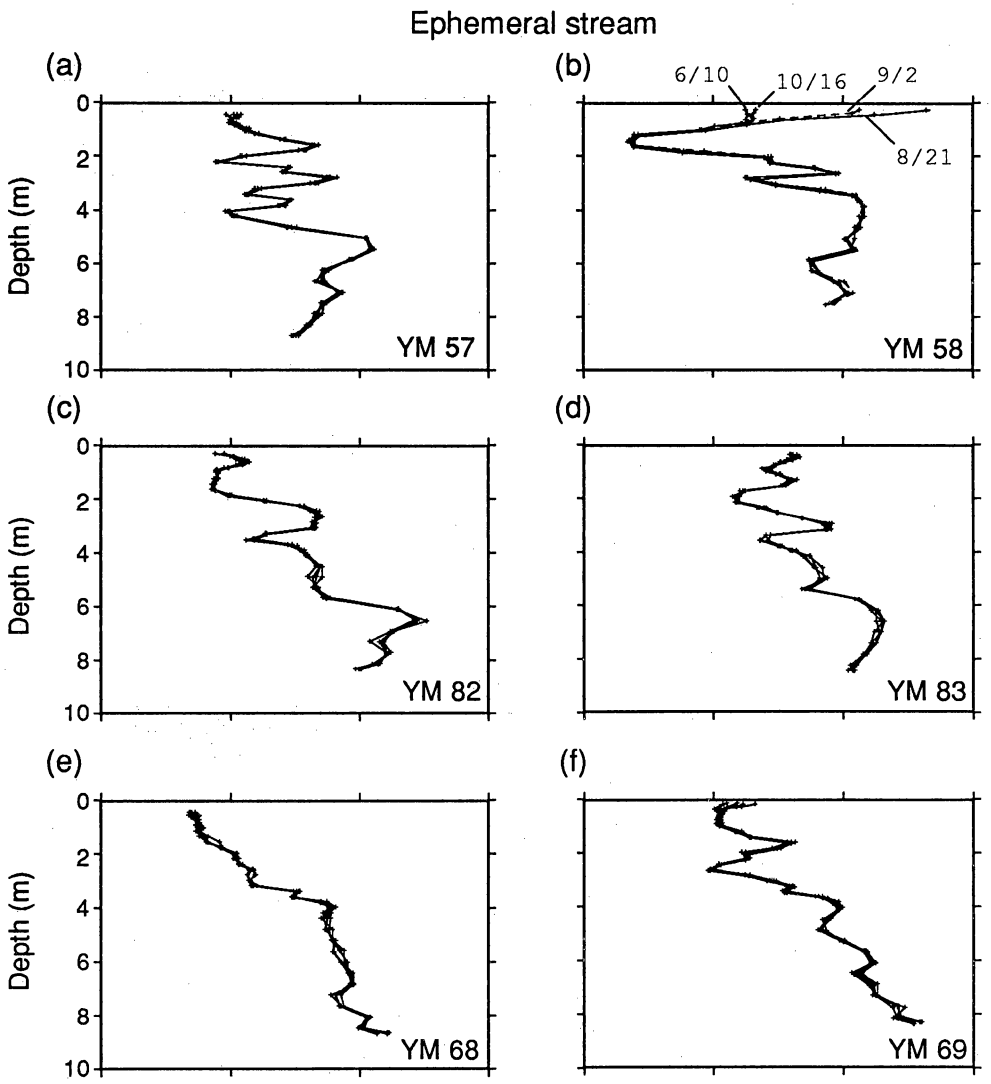

Figure 7. Variation in water content with depth and time in neutron probe access tubes. For location of access tubes, see figure 1.

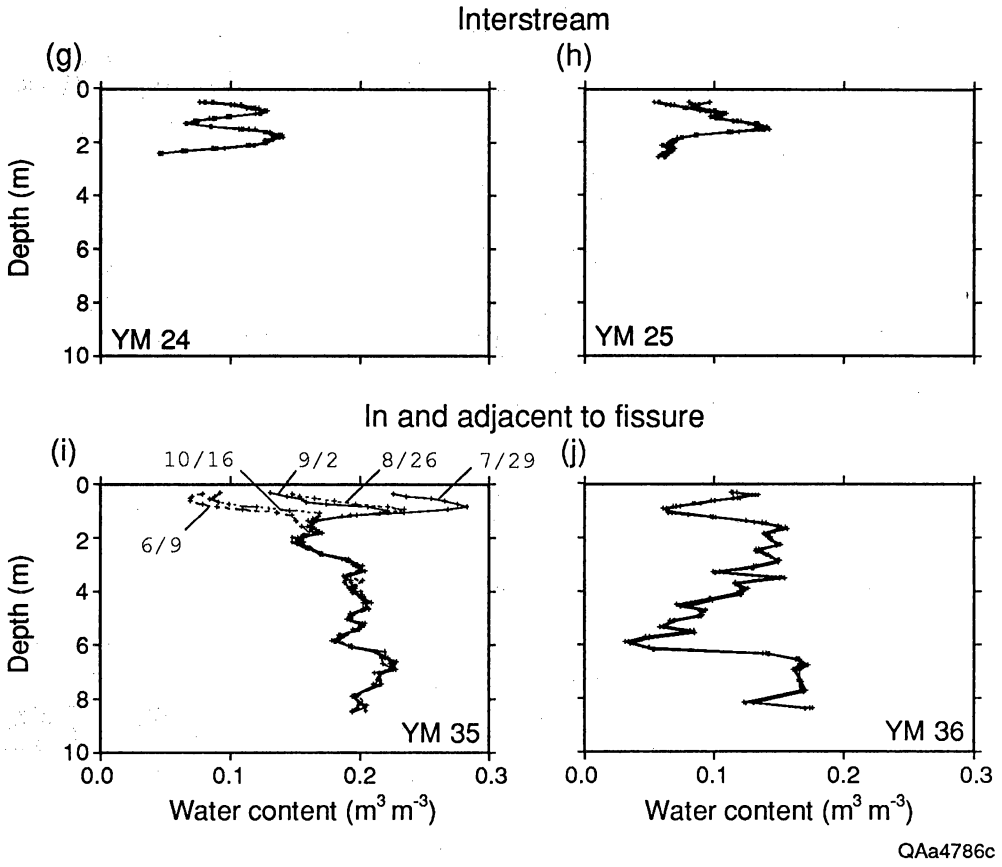

Figure 7. cont.

Table 3. Gravimetric water content, chloride concentration, water flux, water velocity, age, cumulative chloride, and cumulative water content of soil samples. BD 2 is below the detection limit of 2.0 gm^{-3} Cl in the supernatant measured by potentiometric titration and BD 0.1 is below the detection limit of 0.1 gm^{-3} Cl in the supernatant measured by ion chromatography.

Well number	Depth (m)	Interval thickness (m)	Gravimetric water content (g/g)	Chloride (mg Cl/kg soil)	Chloride (g Cl/m3 water)	Water flux (mm/yr)	Water velocity (mm/yr)	Age (yr)	Cumulative chloride (g/m2)	Cumulative H2O (m)
	0.08	0.08	0.087	3.5	40.4	1.88	14.32	6	0.44	0.01
	0.39	0.30	0.108	3.1	28.5	2.65	16.39	24	1.85	0.06
	1.10	0.72	0.087	97.0	1119.9	0.07	0.52	1401	106.04	0.15
	1.71	0.61	0.089	533.4	5973.8	0.01	0.09	7844	593.82	0.24
	1.76	0.05	0.094	715.5	7598.8	0.01	0.07	8493	642.89	0.24
	2.07	0.30	0.086	834.7	**9720.4**	0.01	0.05	15214	1151.71	0.29
	2.31	0.24	0.045	401.4	8840.9	0.01	0.09	17800	1347.46	0.32
	2.37	0.06	0.053	397.2	7484.1	0.01	0.10	18440	1395.89	0.32
	2.67	0.30	0.095	659.8	6939.8	0.01	0.06	23753	1798.10	0.38
	3.26	0.59	0.121	797.3	6614.1	0.01	0.05	36113	2733.72	0.52
	3.62	0.36	0.092	494.7	5385.6	0.01	0.08	40793	3088.04	0.59
	4.11	0.50	0.071	369.9	5227.3	0.01	0.10	45634	3454.47	0.66
	4.24	0.13	0.100	615.0	6165.1	0.01	0.06	47714	3611.93	0.68
	4.75	0.50	0.125	636.2	5108.7	0.01	0.06	56193	4253.84	0.81
	4.99	0.24	0.138	529.9	3853.3	0.02	0.07	59607	4512.28	0.88
9	5.37	0.38	0.142	706.5	4987.5	0.02	0.05	66719	5050.66	0.98
	5.74	0.37	0.114	495.7	4346.6	0.02	0.08	71510	5413.30	1.07
	5.95	0.21	0.110	404.9	3688.2	0.02	0.09	73792	5586.08	1.11
	6.20	0.24	0.085	411.1	4819.1	0.02	0.09	76441	5786.58	1.16
	6.62	0.43	0.093	485.5	5208.4	0.01	0.08	81915	6200.95	1.24
	6.65	0.03	0.089	556.3	6286.0	0.01	0.07	82363	6234.86	1.24
	6.99	0.34	0.089	477.8	5386.3	0.01	0.08	86595	6555.23	1.30
	7.32	0.34	0.083	512.9	6167.3	0.01	0.07	91138	6899.16	1.36
	7.93	0.61	0.115	592.6	5151.1	0.01	0.06	100682	7621.60	1.50
	8.54	0.61	0.134	773.1	5771.1	0.01	0.05	113133	8564.16	1.66
	8.83	0.29	0.130	724.9	5596.6	0.01	0.05	118678	8983.95	1.73
	9.17	0.34	0.110	574.6	5226.1	0.01	0.07	123768	9369.27	1.81
	9.70	0.53	0.112	586.5	5228.6	0.01	0.06	132033	9994.90	1.93
	10.05	0.35	0.088	649.7	7389.0	0.01	0.06	138050	10450.38	1.99
	10.69	0.64	0.099	517.7	5224.8	0.01	0.07	146805	11113.16	2.12
	11.25	0.56	0.102	549.5	5388.8	0.01	0.07	154992	11732.90	2.23
	12.64	1.39	0.060	339.2	5638.9	0.01	0.11	167419	12673.62	2.40
	13.17	0.53	0.046	218.4	4768.6	0.02	0.17	170497	12906.60	2.45
	13.82	0.65	0.071	345.3	4875.5	0.02	0.11	176391	13352.82	2.54

Table 3. cont.

Well number	Depth (m)	Interval thickness (m)	Gravimetric water content (g/g)	Chloride (mg Cl/kg soil)	Chloride (g Cl/m3 water)	Water flux (mm/yr)	Water velocity (mm/yr)	Age (yr)	Cumulative chloride (g/m2)	Cumulative H2O (m)
	0.01	0.01	0.027	1.6	59.4	1.27	31.86	0	0.02	0.00
	0.02	0.01	0.093	2.4	25.9	2.92	20.82	1	0.05	0.00
	0.16	0.14	0.095	2.1	21.8	3.48	24.30	7	0.50	0.02
	0.24	0.08	0.099	0.8	8.3	9.10	61.17	8	0.59	0.03
	0.31	0.08	0.090	1.2	13.8	5.47	40.72	10	0.73	0.04
	0.39	0.08	0.098	1.5	15.7	4.82	32.86	12	0.91	0.05
	0.50	0.11	0.085	4.2	49.9	1.52	11.92	22	1.63	0.07
	0.86	0.36	0.133	448.8	3367.1	0.02	0.11	3206	242.73	0.14
	1.14	0.27	0.084	724.4	8629.0	0.01	0.07	7144	540.80	0.18
	1.44	0.30	0.100	1387.0	**13850.0**	0.01	0.04	15521	1174.92	0.22
	1.74	0.30	0.078	1085.9	13842.4	0.01	0.05	22079	1671.39	0.26
	2.05	0.30	0.040	317.9	7957.5	0.01	0.12	24639	1865.17	0.28
	2.35	0.30	0.082	531.0	6465.2	0.01	0.07	28915	2188.89	0.33
	2.69	0.34	0.041	217.2	5340.3	0.01	0.17	30839	2334.54	0.36
	3.03	0.34	0.126	705.2	5582.7	0.01	0.05	37086	2807.44	0.44
10	3.27	0.24	0.127	773.6	6107.6	0.01	0.05	42070	3184.73	0.51
	3.67	0.40	0.060	308.4	5158.4	0.01	0.12	45299	3429.17	0.55
	3.88	0.21	0.085	489.5	5732.1	0.01	0.08	48059	3638.06	0.59
	4.21	0.34	0.105	601.0	5733.9	0.01	0.06	53383	4041.06	0.66
	4.49	0.27	0.115	660.5	5723.1	0.01	0.06	58170	4403.44	0.72
	4.76	0.27	0.109	608.4	5592.1	0.01	0.06	62579	4737.23	0.78
	5.45	0.69	0.128	678.6	5313.7	0.01	0.06	74874	5667.95	0.96
	5.75	0.30	0.126	727.6	5759.3	0.01	0.05	80734	6111.53	1.03
	6.13	0.38	0.062	345.7	5601.0	0.01	0.11	84213	6374.92	1.08
	6.41	0.27	0.082	440.3	5379.3	0.01	0.09	87404	6616.49	1.13
	7.08	0.67	0.084	387.7	4594.4	0.02	0.10	94272	7136.37	1.24
	7.69	0.61	0.105	497.3	4737.6	0.02	0.08	102281	7742.66	1.37
	8.33	0.64	0.143	757.1	5311.1	0.01	0.05	115084	8711.83	1.55
	8.85	0.52	0.123	603.3	4903.1	0.02	0.06	123343	9337.07	1.68
	9.76	0.91	0.096	444.3	4618.4	0.02	0.09	134076	10149.57	1.85
	10.71	0.94	0.092	426.2	4612.4	0.02	0.09	144715	10954.92	2.03
	11.65	0.94	0.094	480.4	5121.6	0.01	0.08	156707	11862.72	2.21
	0.22	0.22	0.154	5.1	33.1					
	0.53	0.30	0.123	3.4	27.2					

Table 3. cont.

Well number	Depth (m)	Interval thickness (m)	Gravimetric water content (g/g)	Chloride (mg Cl/kg soil)	Chloride (g Cl/m3 water)	Water flux (mm/yr)	Water velocity (mm/yr)	Age (yr)	Cumulative chloride (g/m2)	Cumulative H2O (m)
	0.86	0.34	0.086	2.8	32.4					
	1.14	0.27	0.065	1.8	27.2					
	1.44	0.30	0.052	0.7	12.7					
	2.11	0.30	0.086	2.1	24.3					
	2.39	0.27	0.083	0.6	7.7					
	2.78	0.40	0.091	0.4	4.9					
	3.09	0.30	0.119	6.0	50.6					
11	3.42	0.34	0.106	13.0	122.4					
	3.73	0.30	0.108	BD0.1	BD0.1					
	4.00	0.27	0.091	6.0	65.8					
	4.34	0.34	0.095	5.4	56.9					
	4.67	0.34	0.096	6.6	68.8					
	5.40	0.73	0.129	6.6	51.0					
	5.71	0.30	0.143	13.9	97.1					
	6.41	0.70	0.153	23.9	156.6					
	7.26	0.85	0.151	38.3	252.9					
	8.21	0.94	0.113	41.1	**363.2**					
	0.22	0.22	0.131	65.4	499.5	0.15	0.77	286	21.67	0.04
	0.46	0.24	0.110	197.3	1786.7	0.04	0.26	1240	93.85	0.08
	0.83	0.37	0.090	404.8	4479.2	0.02	0.12	4173	315.92	0.13
	1.15	0.32	0.099	584.7	**5878.0**	0.01	0.09	7881	596.62	0.18
	1.42	0.27	0.120	705.6	5868.1	0.01	0.07	11717	886.95	0.23
	1.81	0.38	0.112	587.5	5232.2	0.01	0.09	16152	1222.70	0.29
	2.10	0.29	0.092	530.9	5788.9	0.01	0.07	20213	1530.16	0.35
	2.40	0.30	0.083	374.9	4505.5	0.02	0.10	23233	1758.72	0.40
	2.69	0.29	0.087	288.3	3331.8	0.02	0.13	25439	1925.71	0.45
12	2.99	0.30	0.123	389.7	3158.1	0.02	0.10	28577	2163.26	0.52
	3.30	0.30	0.094	241.2	2560.7	0.03	0.16	30519	2310.28	0.58
	3.57	0.27	0.097	176.0	1821.7	0.04	0.22	31795	2406.86	0.63
	3.91	0.34	0.129	217.2	1687.0	0.04	0.17	33719	2552.52	0.72
	4.18	0.27	0.114	153.6	1345.6	0.06	0.25	34832	2636.79	0.78
	4.40	0.21	0.118	140.1	1185.9	0.06	0.27	35622	2696.55	0.83
	5.19	0.79	0.084	62.5	746.2	0.10	0.61	36931	2795.67	0.97
	0.08	0.08	0.111	1.2	10.8	7.00	42.06	2	0.15	0.01

Table 3. cont.

Well number	Depth (m)	Interval thickness (m)	Gravimetric water content (g/g)	Chloride (mg Cl/kg soil)	Chloride (g Cl/m3 water)	Water flux (mm/yr)	Water velocity (mm/yr)	Age (yr)	Cumulative chloride (g/m2)	Cumulative H2O (m)
	0.27	0.18	0.104	0.6	5.8	13.13	84.11	4	0.32	0.04
	0.51	0.24	0.081	1.4	16.8	4.50	37.00	11	0.81	0.07
	1.00	0.49	0.097	102.3	1058.0	0.07	0.49	1000	75.67	0.14
	1.14	0.14	0.066	98.4	1483.3	0.05	0.51	1267	95.92	0.16
	1.53	0.40	0.028	85.8	3041.5	0.02	0.59	1941	146.90	0.17
	2.02	0.49	0.030	193.1	**6495.8**	0.01	0.20	4429	335.26	0.20
	2.08	0.06	0.021	118.5	5609.3	0.01	0.32	4620	349.71	0.20
	2.51	0.43	0.015	53.3	3484.4	0.02	0.71	5220	395.18	0.22
	2.75	0.24	0.010	35.5	3560.1	0.02	1.07	5449	412.48	0.22
13	3.09	0.34	0.018	67.2	3768.0	0.02	0.56	6044	457.53	0.23
	3.39	0.30	0.027	54.4	2051.7	0.04	0.70	6482	490.71	0.25
	3.79	0.40	0.015	38.4	2646.6	0.03	0.99	6884	521.14	0.26
	4.09	0.30	0.040	85.1	2146.6	0.04	0.45	7569	572.98	0.29
	4.40	0.30	0.041	70.1	1714.5	0.04	0.54	8133	615.69	0.31
	4.84	0.44	0.092	191.1	2085.8	0.04	0.20	10365	784.64	0.39
	5.28	0.44	0.075	146.0	1952.4	0.04	0.26	12070	913.72	0.46
	5.86	0.58	0.068	109.9	1624.3	0.05	0.34	13752	1041.02	0.54
	6.35	0.49	0.068	127.2	1871.3	0.04	0.30	15391	1165.08	0.60
	7.23	0.88	0.128	260.7	2033.6	0.04	0.15	21479	1626.00	0.83
	7.72	0.49	0.088	150.3	1697.9	0.04	0.25	23416	1772.55	0.92
	8.39	0.67	0.077	125.2	1615.4	0.05	0.30	25633	1940.40	1.02
	8.94	0.55	0.093	155.9	1673.7	0.05	0.24	27893	2111.51	1.12
	9.40	0.46	0.076	115.4	1527.7	0.05	0.33	29287	2216.99	1.19
	10.71	1.31	0.065	97.9	1516.5	0.05	0.39	32675	2473.50	1.36
	11.29	0.58	0.052	69.9	1337.8	0.06	0.54	33744	2554.46	1.42
	0.01	0.01	0.070	1.8	25.8	2.94	28.08	0	0.02	0.00
	0.10	0.09	0.136	0.6	4.4	17.17	84.24	1	0.10	0.02
	0.19	0.09	0.133	2.1	15.8	4.80	24.08	5	0.39	0.04
	0.37	0.18	0.107	178.4	1668.7	0.05	0.28	652	49.33	0.07
	0.86	0.49	0.100	326.5	3279.1	0.02	0.15	3807	288.16	0.14
	1.17	0.30	0.080	250.0	3117.3	0.02	0.20	5317	402.46	0.18
	1.47	0.30	0.130	394.1	3022.4	0.03	0.13	7697	582.63	0.24
	1.99	0.52	0.073	248.2	3377.4	0.02	0.20	10245	775.52	0.29
	2.45	0.46	0.057	165.7	2932.3	0.03	0.23	12246	927.03	0.34

Table 3. cont.

Well number	Depth (m)	Interval thickness (m)	Gravimetric water content (g/g)	Chloride (mg Cl/kg soil)	Chloride (g Cl/m3 water)	Water flux (mm/yr)	Water velocity (mm/yr)	Age (yr)	Cumulative chloride (g/m2)	Cumulative H2O (m)
	2.81	0.37	0.077	244.2	3186.3	0.02	0.16	14606	1105.65	0.40
	3.15	0.34	0.116	406.6	**3512.9**	0.02	0.09	18207	1378.28	0.48
14	3.42	0.27	0.140	433.5	3097.9	0.02	0.09	21349	1616.11	0.56
	3.76	0.34	0.145	388.3	2685.0	0.03	0.10	24789	1876.50	0.65
	4.15	0.40	0.132	388.5	2933.4	0.03	0.10	28856	2184.41	0.76
	4.61	0.46	0.092	278.1	3024.2	0.03	0.14	32215	2438.70	0.84
	5.31	0.70	0.086	255.4	2964.8	0.03	0.15	36945	2796.76	0.96
	5.80	0.49	0.100	269.2	2689.9	0.03	0.14	40414	3059.38	1.06
	6.44	0.64	0.067	162.6	2438.7	0.03	0.23	43164	3267.48	1.15
	7.23	0.79	0.130	323.5	2494.8	0.03	0.12	49936	3780.16	1.35
	7.75	0.52	0.104	244.8	2363.9	0.03	0.15	53287	4033.83	1.46
	8.51	0.76	0.111	253.3	2275.7	0.03	0.15	58387	4419.86	1.63
	9.52	1.01	0.067	148.7	2234.3	0.03	0.25	62338	4718.99	1.76
	2.52	2.52	0.029	16.0	4.9					
	2.61	0.09	0.023	36.4	2.1					
	2.71	0.09	0.040	26.5	2.9					
	2.80	0.09	0.100	6.0	13.0					
	2.89	0.09	0.035	12.0	6.5					
	3.04	0.15	0.030	13.8	5.6					
	3.47	0.43	0.059	13.3	5.8					
	3.65	0.18	0.045	12.0	6.5					
	4.20	0.55	0.095	12.7	6.1					
	4.29	0.09	0.235	11.6	6.7					
	4.47	0.18	0.288	8.3	9.3					
15	5.39	0.91	0.110	4.9	15.8					
	5.55	0.17	0.114	5.2	14.8					
	5.74	0.18	0.115	5.5	14.2					
	6.07	0.34	0.211	2.7	28.6					
	6.29	0.21	0.164	2.9	26.5					
	6.62	0.34	0.158	2.6	**29.3**					
	6.96	0.34	0.128	4.7	16.5					
	7.48	0.52	0.163	6.0	12.9					
	8.34	0.87	0.146	3.9	19.9					
	9.24	0.90	0.022	18.4	4.2					

Table 3. cont.

Well number	Depth (m)	Interval thickness (m)	Gravimetric water content (g/g)	Chloride (mg Cl/kg soil)	Chloride (g Cl/m3 water)	Water flux (mm/yr)	Water velocity (mm/yr)	Age (yr)	Cumulative chloride (g/m2)	Cumulative H2O (m)
	9.76	0.52	0.147	7.9	9.8					
	10.25	0.49	0.137	6.1	12.7					
	11.24	0.99	0.112	8.0	9.7					
	11.53	0.29	0.052	16.3	4.8					
	12.82	1.30	0.169	11.2	6.9					
	13.62	0.79	0.168	6.6	11.7					
	14.65	1.04	0.223	5.4	14.4					
	15.52	0.87	0.201	3.0	26.0					
	17.26	1.74	0.184	7.0	11.1					
	18.33	1.07	0.128	7.0	11.1					
	0.01	0.01	0.026	0.4	13.7	5.51	141.12	0	0.00	0.00
	0.10	0.09	0.056	BD0.1	BD0.1	BD0.1	BD0.1	0	0.00	0.01
	0.19	0.09	0.054	BD0.1	BD0.1	BD0.1	BD0.1	0	0.00	0.02
	0.28	0.09	0.069	BD0.1	BD0.1	BD0.1	BD0.1	0	0.00	0.02
	0.37	0.09	0.080	BD0.1	BD0.1	BD0.1	BD0.1	0	0.00	0.04
	0.86	0.49	0.093	BD0.1	BD0.1	BD0.1	BD0.1	0	0.00	0.10
	1.14	0.27	0.090	146.7	1621.3	0.05	0.34	797	60.36	0.14
	1.38	0.24	0.069	179.3	**2586.8**	0.03	0.28	1663	125.93	0.17
	1.71	0.34	0.031	76.6	2507.2	0.03	0.66	2172	164.43	0.18
	2.02	0.30	0.030	78.9	2621.7	0.03	0.48	2807	212.53	0.20
	2.35	0.34	0.012	26.5	2266.7	0.03	1.43	3042	230.29	0.21
	2.66	0.30	0.026	48.3	1839.4	0.04	0.78	3431	259.74	0.22
	2.99	0.34	0.016	26.2	1639.5	0.05	1.44	3664	277.33	0.23
	3.27	0.27	0.008	11.5	1481.1	0.05	3.29	3747	283.64	0.24
16	3.57	0.30	0.008	12.3	1450.3	0.05	3.08	3846	291.13	0.24
	3.88	0.30	0.018	30.6	1742.1	0.04	1.24	4092	309.78	0.25
	4.18	0.30	0.029	37.5	1310.9	0.06	1.01	4394	332.64	0.27
	4.52	0.34	0.022	41.7	1884.8	0.04	0.91	4764	360.61	0.29
	5.04	0.52	0.041	56.1	1373.1	0.06	0.67	5532	418.77	0.33
	5.88	0.84	0.022	28.4	1266.1	0.06	1.33	6162	466.44	0.37
	6.13	0.26	0.144	183.8	1274.9	0.06	0.21	7420	561.71	0.44
	6.74	0.61	0.073	80.1	1091.0	0.07	0.47	8710	659.32	0.53
	7.96	1.22	0.074	107.5	1447.5	0.05	0.35	12172	921.42	0.71
	8.66	0.70	0.065	118.2	1825.0	0.04	0.32	14361	1087.12	0.80

Table 3. cont.

Well number	Depth (m)	Interval thickness (m)	Gravimetric water content (g/g)	Chloride (mg Cl/kg soil)	Chloride (g Cl/m3 water)	Water flux (mm/yr)	Water velocity (mm/yr)	Age (yr)	Cumulative chloride (g/m2)	Cumulative H2O (m)
	10.01	1.34	0.055	69.6	1276.2	0.06	0.54	16826	1273.76	0.95
	11.50	1.49	0.015	29.1	2001.0	0.04	1.30	17973	1360.59	0.99
	12.47	0.98	0.069	81.9	1190.6	0.06	0.46	20083	1520.27	1.13
	13.39	0.91	0.101	107.7	1066.9	0.07	0.35	22685	1717.25	1.31
	14.42	1.04	0.112	96.1	859.5	0.09	0.39	25315	1916.33	1.54
	0.53	0.53	0.064	21.3	330.6	0.23	2.37	225	17.02	0.05
	1.30	0.76	0.059	126.1	2129.7	0.04	0.40	2129	161.15	0.12
	1.60	0.30	0.071	232.4	3293.8	0.02	0.22	3533	267.42	0.15
	1.91	0.30	0.074	327.3	4428.1	0.02	0.15	5509	417.04	0.19
	2.21	0.30	0.066	332.9	5070.1	0.01	0.11	8190	620.01	0.23
	2.55	0.34	0.073	434.0	**5911.7**	0.01	0.09	12035	911.03	0.27
	2.85	0.30	0.079	448.8	5647.1	0.01	0.08	15649	1184.62	0.32
	3.15	0.30	0.070	383.4	5442.0	0.01	0.10	18736	1418.32	0.37
	3.46	0.30	0.085	450.6	5302.2	0.01	0.08	22365	1693.00	0.42
	3.76	0.30	0.082	432.3	5262.0	0.01	0.09	25846	1956.56	0.47
	4.07	0.30	0.090	448.4	5002.9	0.02	0.08	29457	2229.89	0.52
	4.40	0.34	0.077	401.1	5239.1	0.01	0.09	33010	2498.83	0.57
28	4.71	0.30	0.069	322.8	4663.1	0.02	0.12	35609	2695.60	0.62
	5.01	0.30	0.067	310.9	4630.3	0.02	0.12	38113	2885.14	0.66
	5.32	0.30	0.076	339.8	4462.0	0.02	0.11	40849	3092.30	0.70
	5.65	0.34	0.061	284.1	4623.0	0.02	0.13	43366	3282.79	0.74
	5.93	0.27	0.044	189.3	4315.0	0.02	0.20	44738	3386.66	0.77
	6.26	0.34	0.069	276.9	4018.5	0.02	0.14	47190	3572.32	0.81
	6.57	0.30	0.047	187.2	3960.6	0.02	0.20	48698	3686.42	0.84
	6.87	0.30	0.069	254.5	3681.8	0.02	0.15	50747	3841.58	0.89
	7.21	0.34	0.054	231.6	4257.9	0.02	0.16	52799	3996.86	0.92
	7.82	0.61	0.089	307.9	3473.9	0.02	0.12	57757	4372.21	1.03
	8.24	0.43	0.094	326.4	3477.1	0.02	0.12	61437	4650.81	1.11
	8.76	0.52	0.120	396.6	3315.7	0.02	0.10	66867	5061.85	1.23
	9.37	0.61	0.088	276.9	3164.7	0.02	0.14	71327	5399.49	1.34
	9.80	0.43	0.094	288.5	3061.0	0.02	0.13	74580	5645.71	1.42
	10.32	0.52	0.087	274.8	3169.1	0.02	0.14	78342	5930.49	1.51
	10.93	0.61	0.106	304.5	2877.3	0.03	0.12	83246	6301.75	1.64
	11.35	0.43	0.105	308.7	2931.4	0.03	0.12	86727	6565.23	1.73

Table 3. cont.

Well number	Depth (m)	Interval thickness (m)	Gravimetric water content (g/g)	Chloride (mg Cl/kg soil)	Chloride (g Cl/m3 water)	Water flux (mm/yr)	Water velocity (mm/yr)	Age (yr)	Cumulative chloride (g/m2)	Cumulative H2O (m)
	11.84	0.49	0.088	297.0	3372.2	0.02	0.13	90554	6854.93	1.82
	12.48	0.64	0.105	329.9	3133.7	0.02	0.11	96133	7277.27	1.95
	12.91	0.43	0.122	367.1	3016.5	0.03	0.10	100272	7590.61	2.05
	13.43	0.52	0.113	342.9	3035.3	0.02	0.11	104966	7945.96	2.17
	14.04	0.61	0.129	368.0	2859.3	0.03	0.10	110894	8394.68	2.33
	14.65	0.61	0.113	297.7	2636.4	0.03	0.13	115689	8757.66	2.47
	15.10	0.46	0.108	299.1	2763.2	0.03	0.13	119303	9031.20	2.57
	16.02	0.91	0.082	210.4	2560.1	0.03	0.18	124387	9416.06	2.72
	16.66	0.64	0.108	295.9	2733.6	0.03	0.13	129390	9794.84	2.85
	17.57	0.91	0.119	384.8	3230.8	0.02	0.10	138687	10498.60	3.07
	18.21	0.64	0.099	267.8	2708.1	0.03	0.14	143216	10841.44	3.20
	19.13	0.91	0.117	314.6	2692.3	0.03	0.12	150815	11416.70	3.41
	20.68	1.55	0.138	382.5	2763.2	0.03	0.10	166524	12605.83	3.84
	22.24	1.55	0.110	275.9	2516.3	0.03	0.14	177854	13463.52	4.18
	23.73	1.49	0.084	184.9	2204.5	0.03	0.20	185150	14015.88	4.43
	25.22	1.49	0.103	232.1	2249.1	0.03	0.16	194310	14709.30	4.74
	0.53	0.53	0.074	338.6	4562.3	0.02	0.15	3579	270.95	0.06
	0.87	0.34	0.070	531.4	**7577.9**	0.01	0.09	7110	538.21	0.04
32	1.30	0.43	0.088	592.8	6735.5	0.01	0.09	12123	917.68	0.06
	1.72	0.43	0.093	502.3	5422.4	0.01	0.10	16370	1239.21	0.06
	2.15	0.43	0.071	319.9	4484.6	0.02	0.12	19976	1512.19	0.06
	0.26	0.26	0.045	BD2	BD2	BD2	BD2	BD2	BD2	0.02
	0.59	0.34	0.038	BD2	BD2	BD2	BD2	BD2	BD2	0.02
34	1.36	0.76	0.075	339.7	**4534.2**	0.02	0.15	5130	388.30	0.09
	1.69	0.34	0.071	307.4	4312.7	0.02	0.16	7172	542.89	0.04
	2.09	0.40	0.087	354.8	4086.6	0.02	0.11	10886	824.05	0.07
	0.29	0.29	0.096	BD2	BD2					
	0.59	0.30	0.106	BD2	BD2					
	0.90	0.30	0.107	BD2	BD2					
	1.26	0.37	0.120	BD2	BD2					
	1.57	0.30	0.149	BD2	BD2					
	1.87	0.30	0.188	BD2	BD2					
	2.18	0.30	0.158	BD2	BD2					
	2.58	0.40	0.171	BD2	BD2					

Table 3. cont.

Well number	Depth (m)	Interval thickness (m)	Gravimetric water content (g/g)	Chloride (mg Cl/kg soil)	Chloride (g Cl/m3 water)	Water flux (mm/yr)	Water velocity (mm/yr)	Age (yr)	Cumulative chloride (g/m2)	Cumulative H2O (m)
	2.82	0.24	0.162	BD2	BD2					
	3.12	0.30	0.148	BD2	BD2					
	3.43	0.30	0.197	BD2	BD2					
	3.73	0.30	0.155	BD2	BD2					
	4.10	0.37	0.144	BD2	BD2					
35	4.37	0.27	0.135	BD2	BD2					
	4.68	0.30	0.133	BD2	BD2					
	4.95	0.27	0.072	BD2	BD2					
	5.41	0.46	0.042	BD2	BD2					
	5.93	0.52	0.110	21.6	196.4					
	6.23	0.30	0.120	BD2	BD2					
	6.54	0.30	0.193	BD2	BD2					
	7.03	0.49	0.162	3.0	18.6					
	7.09	0.06	0.155	BD2	BD2					
	7.70	0.61	0.130	9.9	75.7					
	7.76	0.06	0.153	BD2	BD2					
	8.15	0.40	0.132	3.0	22.7					
	8.21	0.06	0.157	18.0	114.7					
	8.67	0.46	0.122	19.4	158.4					
	8.73	0.06	0.127	BD2	BD2					
	9.10	0.37	0.132	118.1	892.9					
	9.16	0.06	0.131							
	9.68	0.52	0.187	BD2	BD2					
	9.71	0.03	0.197	568.8	2882.3					
	10.32	0.61	0.084							
	10.71	0.40	0.212							
	11.32	0.61	0.152	790.1	5205.3					
	11.84	0.52	0.158							
	12.27	0.43	0.122							
	12.88	0.61	0.084							
	13.40	0.52	0.094							
	14.31	0.91	0.155	784.6	5076.4					
	14.95	0.64	0.150							
	15.86	0.91	0.171							

Table 3. cont.

Well number	Depth (m)	Interval thickness (m)	Gravimetric water content (g/g)	Chloride (mg Cl/kg soil)	Chloride (g Cl/m3 water)	Water flux (mm/yr)	Water velocity (mm/yr)	Age (yr)	Cumulative chloride (g/m2)	Cumulative H2O (m)
	16.54	0.67	0.141							
	17.42	0.88	0.132	651.8	4945.4					
	18.09	0.67	0.129							
	18.91	0.82	0.169							
	19.46	0.55	0.166							
	20.47	1.01	0.157	823.9	**5255.0**					
	0.59	0.59	0.045	358.9	**7915.6**	0.01	0.14	4227	319.98	0.04
	1.05	0.46	0.056	428.3	7582.7	0.01	0.12	8107	613.72	0.08
	1.36	0.30	0.099	657.7	6670.1	0.01	0.08	12079	914.41	0.12
	1.66	0.30	0.125	780.4	6243.8	0.01	0.06	16793	1271.21	0.18
	1.97	0.30	0.124	859.6	6954.6	0.01	0.06	21985	1664.24	0.24
	2.27	0.30	0.104	704.6	6748.7	0.01	0.05	27658	2093.74	0.30
	2.58	0.30	0.082	554.0	6733.1	0.01	0.07	32119	2431.44	0.35
	2.91	0.34	0.093	604.6	6473.7	0.01	0.06	37475	2836.89	0.41
	3.22	0.30	0.086	532.5	6197.5	0.01	0.07	41764	3161.53	0.47
	3.52	0.30	0.113	663.4	5875.9	0.01	0.06	47106	3565.92	0.54
	3.83	0.30	0.090	437.0	4860.9	0.02	0.09	50625	3832.29	0.59
	4.13	0.30	0.086	509.9	5905.9	0.01	0.07	54731	4143.11	0.64
	4.47	0.34	0.085	283.9	3330.9	0.02	0.13	57245	4333.48	0.70
36	4.77	0.30	0.052	303.3	5782.8	0.01	0.12	59688	4518.37	0.73
	5.07	0.30	0.047	237.5	5046.8	0.02	0.16	61600	4663.13	0.76
	5.47	0.40	0.039	212.0	5383.9	0.01	0.18	63819	4831.13	0.79
	6.02	0.55	0.072	360.2	5012.0	0.02	0.11	69041	5226.39	0.87
	6.32	0.30	0.056	287.2	5119.7	0.01	0.13	71354	5401.49	0.91
	6.63	0.30	0.110	560.7	5083.4	0.01	0.07	75869	5743.28	0.97
	6.93	0.30	0.118							
	7.30	0.37	0.114							
	7.70	0.40	0.116							
	8.21	1.58	0.090	435.4	4840.2	0.02	0.09	94103	7123.57	1.26
	8.67	0.46	0.141							
	9.25	0.58	0.064							
	9.86	1.65	0.109	518.9	4745.8	0.02	0.07	116666	8831.64	1.62
	10.35	0.49	0.108							
	10.81	0.46	0.167							

Table 3. cont.

Well number	Depth (m)	Interval thickness (m)	Gravimetric water content (g/g)	Chloride (mg Cl/kg soil)	Chloride (g Cl/m3 water)	Water flux (mm/yr)	Water velocity (mm/yr)	Age (yr)	Cumulative chloride (g/m2)	Cumulative H2O (m)
	11.29	1.43	0.193	655.6	3405.4	0.02	0.06	141481	10710.11	2.17
	11.96	0.67	0.142							
	12.36	0.40	0.144							
	12.85	1.55	0.074	370.5	4996.1	0.02	0.10	156696	11861.90	2.40
	13.27	0.43	0.097							
	14.10	0.82	0.124							
	14.52	1.68	0.131	744.2	5663.2	0.01	0.05	189656	14356.97	2.84
	15.47	0.94	0.147							
	16.08	1.55	0.158	784.0	4967.3	0.02	0.05	221856	16794.48	3.33
	17.02	0.94	0.158							
	17.63	1.55	0.137	730.6	5314.0	0.01	0.05	251861	19065.86	3.76
	18.58	0.94	0.153							
	19.19	0.61	0.118							
	19.95	0.76	0.158							
	20.86	3.23	0.165	879.5	5335.4	0.01	0.04	326937	24749.13	4.82
	22.17	1.31	0.178							
	23.76	2.90	0.171	932.1	5448.3	0.01	0.04	398246	30147.21	5.81
	25.31	1.55	0.163							
	26.87	3.11	0.152	799.5	5263.9	0.01	0.05	463917	35118.53	6.76
	28.42	1.55	0.165							
	29.98	3.11	0.168	998.7	5946.3	0.01	0.04	545950	41328.44	7.80
	0.08	0.30	0.072	BD2	BD2					
	0.24	0.15	0.106	13.4	126.9					
	0.39	0.15	0.089	8.7	97.4					
	0.54	0.15	0.101	11.0	108.5					
	0.97	0.43	0.084	BD2	BD2					
	1.33	0.37	0.091	BD2	BD2					
	1.64	0.30	0.092	BD2	BD2					
	1.94	0.30	0.102	BD2	BD2					
	2.25	0.30	0.104	BD2	BD2					
	2.55	0.30	0.091	BD2	BD2					
	2.89	0.34	0.105	BD2	BD2					
	3.19	0.30	0.077	BD2	BD2					
	3.50	0.30	0.119	BD2	BD2					

Table 3. cont.

Well number	Depth (m)	Interval thickness (m)	Gravimetric water content (g/g)	Chloride (mg Cl/kg soil)	Chloride (g Cl/m3 water)	Water flux (mm/yr)	Water velocity (mm/yr)	Age (yr)	Cumulative chloride (g/m2)	Cumulative H2O (m)
41	3.80	0.30	0.070	BD2	BD2					
	4.08	0.27	0.080	BD2	BD2					
	4.44	0.37	0.065	BD2	BD2					
	4.75	0.30	0.100	BD2	BD2					
	5.05	0.30	0.106	BD2	BD2					
	5.36	0.30	0.112	BD2	BD2					
	5.63	0.27	0.142	BD2	BD2					
	6.00	0.37	0.120	BD2	BD2					
	6.30	0.30	0.093	BD2	BD2					
	7.00	0.69	0.053	BD2	BD2					
	7.55	0.56	0.086							
	8.16	0.61	0.085	BD2	BD2					
	8.77	0.61	0.124							
	9.62	0.85	0.111	BD2	BD2					
	10.36	0.73	0.075							
	11.18	0.82	0.080	BD2	BD2					
	11.91	0.73	0.068							
	12.73	0.82	0.072	19.4	267.7					
	13.37	0.64	0.074							
	14.29	0.91	0.069	45.8	**659.8**					
	14.93	0.64	0.102							
	15.84	0.91	0.087	50.2	575.1					
	16.54	0.70	0.035							
	17.40	0.64	0.036	7.7	216.3					
	18.04	1.49	0.054							
	19.26	1.86	0.177							
	20.60	1.34	0.116	19.3	166.7					
	22.15	1.55	0.120							
	23.71	1.55	0.095							
	0.08	0.08	0.067	6.7	100.5	0.75	7.55	11	0.84	0.01
	0.24	0.15	0.079	10.8	135.0	0.56	4.69	44	3.30	0.03
	0.39	0.15	0.081	370.1	4556.0	0.02	0.14	1161	87.91	0.05
	0.54	0.15	0.088	1570.5	**17821.0**	0.00	0.03	5904	446.92	0.07
	0.69	0.15	0.121	2020.6	16747.0	0.00	0.02	12006	908.83	0.09

Table 3. cont.

Well number	Depth (m)	Interval thickness (m)	Gravimetric water content (g/g)	Chloride (mg Cl/kg soil)	Chloride (g Cl/m3 water)	Water flux (mm/yr)	Water velocity (mm/yr)	Age (yr)	Cumulative chloride (g/m2)	Cumulative H2O (m)
	0.85	0.15	0.079	1142.7	14406.0	0.01	0.04	15456	1170.05	0.11
	1.27	0.43	0.038	361.1	9389.0	0.01	0.14	18510	1401.19	0.14
	1.58	0.30	0.069	524.9	7624.0	0.01	0.10	21680	1641.20	0.17
	1.88	0.30	0.131	955.4	7316.0	0.01	0.05	27450	2077.99	0.23
	2.19	0.30	0.156	1071.1	6853.0	0.01	0.04	36076	2730.93	0.32
	2.43	0.24	0.152	1168.6	7711.0	0.01	0.03	43604	3300.84	0.40
	2.83	0.40	0.136	918.1	6727.0	0.01	0.04	53215	4028.39	0.50
	3.13	0.30	0.126	840.0	6682.0	0.01	0.05	59980	4540.46	0.58
43	3.44	0.30	0.132	836.0	6335.0	0.01	0.05	66712	5050.07	0.66
	3.74	0.30	0.140	885.7	6347.0	0.01	0.04	73844	5590.01	0.75
	4.05	0.30	0.146	932.3	6402.0	0.01	0.04	81352	6158.33	0.84
	4.38	0.34	0.153	935.5	6125.0	0.01	0.04	89638	6785.62	0.94
	4.69	0.30	0.150	896.9	5976.0	0.01	0.04	96861	7332.36	1.03
	4.99	0.30	0.154	924.2	5998.0	0.01	0.04	104303	7895.75	1.12
	5.30	0.30	0.156	916.6	5859.0	0.01	0.04	111685	8454.54	1.22
	5.60	0.30	0.147	442.5	3011.0	0.03	0.09	115248	8724.26	1.31
	5.94	0.34	0.073	483.6	6615.0	0.01	0.08	119531	9048.52	1.36
	6.24	0.30	0.088	913.8	10347.0	0.01	0.04	126890	9605.59	1.41
	6.85	0.61	0.117	537.2	4593.0	0.02	0.07	135543	10260.60	1.55
	7.49	0.64	0.107							
	8.10	0.61	0.130	619.2	4778.0	0.02	0.06	155988	11808.30	1.88
	8.71	0.61	0.144							
	9.04	0.34	0.145	649.4	4490.0	0.02	0.06	172200	13035.51	2.15
	10.29	1.25	0.104							
	10.60	0.30	0.134	577.3	4295.0	0.02	0.07	195909	14830.34	2.57
	11.85	1.25	0.136							
	12.15	0.30	0.129	546.6	4245.0	0.02	0.07	218359	16529.77	2.97
	13.37	1.22	0.086							
	13.71	0.34	0.093	355.7	3810.0	0.02	0.11	232968	17635.70	3.26
	14.96	1.25	0.112							
	14.04	-0.91	0.088	310.1	3542.0	0.02	0.12	235715	17843.64	3.32
	15.60	1.55	0.110							
	17.15	1.55	0.063	207.7	3303.0	0.02	0.18	252777	19135.21	3.71
	18.71	1.55	0.091							

Table 3. cont.

Well number	Depth (m)	Interval thickness (m)	Gravimetric water content (g/g)	Chloride (mg Cl/kg soil)	Chloride (g Cl/m3 water)	Water flux (mm/yr)	Water velocity (mm/yr)	Age (yr)	Cumulative chloride (g/m2)	Cumulative H2O (m)
	20.26	1.55	0.086	272.1	3147.0	0.02	0.14	275129	20827.26	4.25
	21.82	1.55	0.068							
	0.22	0.22	0.115	6.4	56.1					
	0.53	0.30	0.102	BD2	BD2					
	0.92	0.40	0.073	BD2	BD2					
	1.32	0.40	0.067	BD2	BD2					
	1.62	0.30	0.060	BD2	BD2					
	1.93	0.30	0.062	BD2	BD2					
	2.23	0.30	0.068	BD2	BD2					
	2.87	0.64	0.113	BD2	BD2					
	3.18	0.30	0.084	BD2	BD2					
	3.48	0.30	0.099	BD2	BD2					
	3.79	0.30	0.093	6.2	66.5					
	4.09	0.30	0.089	6.5	73.5					
	4.43	0.34	0.050	BD2	BD2					
54	4.79	0.37	0.086	BD2	BD2					
	5.10	0.30	0.069	BD2	BD2					
	5.71	0.61	0.131	BD2	BD2					
	5.98	0.27	0.179	BD2	BD2					
	6.62	0.64	0.135	7.7	57.2					
	7.25	0.62	0.132	8.7	66.0					
	7.99	0.75	0.105	BD2	BD2					
	8.74	0.75	0.075	7.7	103.3					
	9.61	0.87	0.079	BD2	BD2					
	10.37	0.76	0.083	BD2	BD2					
	11.16	0.79	0.130	BD2	BD2					
	11.94	0.78	0.084	BD2	BD2					
	12.72	0.78	0.090	37.4	**416.1**					
	14.15	1.43	0.029	8.3	288.7					
	15.83	1.68	0.108	26.9	250.1					
	17.29	1.46	0.111	41.5	372.6					
	22.01	4.72	0.105	16.1	153.0					
	0.22	0.22	0.107	278.6	2593.0	0.03	0.18	1220	92.36	0.04
	0.53	0.30	0.088	623.5	7062.0	0.01	0.08	4986	377.41	0.08

Table 3. cont.

Well number	Depth (m)	Interval thickness (m)	Gravimetric water content (g/g)	Chloride (mg Cl/kg soil)	Chloride (g Cl/m3 water)	Water flux (mm/yr)	Water velocity (mm/yr)	Age (yr)	Cumulative chloride (g/m2)	Cumulative H2O (m)
	0.92	0.40	0.073	610.6	**8396.0**	0.01	0.08	9780	740.35	0.12
	1.29	0.37	0.073	590.2	8054.0	0.01	0.09	14057	1064.15	0.16
	1.56	0.27	0.042	309.7	7365.0	0.01	0.16	15741	1191.58	0.18
	1.90	0.34	0.105	779.9	7433.0	0.01	0.06	20922	1583.79	0.23
	2.20	0.30	0.094	688.8	7342.0	0.01	0.05	26469	2003.71	0.29
	2.60	0.40	0.086	643.9	7507.0	0.01	0.06	33210	2514.01	0.35
	2.84	0.24	0.093	633.0	6814.0	0.01	0.06	37288	2822.70	0.40
	3.15	0.30	0.093	601.7	6489.0	0.01	0.06	42134	3189.51	0.46
	3.45	0.30	0.088	562.1	6371.0	0.01	0.07	46660	3532.15	0.51
	3.76	0.30	0.088	579.7	6571.0	0.01	0.07	51328	3885.56	0.56
59	4.06	0.31	0.076	485.3	6418.0	0.01	0.08	55275	4184.33	0.61
	4.58	0.52	0.085	374.6	4429.0	0.02	0.10	60374	4570.28	0.70
	4.88	0.30	0.063	369.7	5848.0	0.01	0.10	63350	4795.62	0.74
	5.19	0.30	0.041	235.6	5748.0	0.01	0.16	65248	4939.26	0.76
	5.95	0.76	0.034	173.7	5138.0	0.01	0.22	68745	5204.03	0.81
	6.26	0.30	0.137	703.5	5125.0	0.01	0.05	74410	5632.87	0.90
	6.56	0.30	0.109	544.0	5014.0	0.02	0.07	78792	5964.52	0.96
	6.87	0.30	0.131	657.8	5038.0	0.02	0.06	84088	6365.49	1.04
	6.96	0.09	0.103	534.7	5215.0	0.01	0.07	85380	6463.27	1.06
	7.51	0.55	0.104	509.6	4906.0	0.02	0.07	92767	7022.46	1.17
	7.90	0.40	0.093	479.2	5169.0	0.01	0.08	97783	7402.21	1.25
	8.21	0.30	0.071	375.4	5266.0	0.01	0.10	100806	7631.03	1.29
	9.76	1.55	0.124	644.7	5182.0	0.01	0.06	127282	9635.28	1.68
	11.13	1.37	0.159	851.1	5368.0	0.01	0.04	158125	11970.03	2.11
	11.83	0.70	0.124	727.4	5874.0	0.01	0.05	171597	12989.86	2.29
	12.69	0.85	0.121	674.0	5568.0	0.01	0.06	186795	14140.35	2.49
	14.24	1.55	0.139	765.9	5510.0	0.01	0.05	218250	16521.56	2.93
	15.80	1.55	0.153	501.2	3286.0	0.02	0.08	238835	18079.79	3.40
	17.35	1.55	0.093	817.3	8804.0	0.01	0.05	272402	20620.83	3.69
	18.91	1.55	0.145	799.7	5512.0	0.01	0.05	305245	23107.08	4.14
	20.46	1.55	0.168	985.7	5861.0	0.01	0.04	345727	26171.53	4.66
	22.01	1.55	0.174	952.4	5475.0	0.01	0.04	384840	29132.40	5.20
	23.57	1.55	0.150	863.6	5753.0	0.01	0.04	420308	31817.32	5.67
	25.21	1.65	0.131	739.7	5642.0	0.01	0.05	452472	34252.16	6.10

Table 3. cont.

Well number	Depth (m)	Interval thickness (m)	Gravimetric water content (g/g)	Chloride (mg Cl/kg soil)	Chloride (g Cl/m3 water)	Water flux (mm/yr)	Water velocity (mm/yr)	Age (yr)	Cumulative chloride (g/m2)	Cumulative H2O (m)
	26.68	1.46	0.134	741.6	5550.0	0.01	0.05	481138	36422.14	6.49
	0.10	0.10	0.044	2.2	50.0	1.52	23.35	4	0.32	0.01
	0.30	0.20	0.285	187.2	658.0	0.12	0.27	739	55.97	0.09
	0.48	0.18	0.085	558.2	**6575.0**	0.01	0.09	2762	209.10	0.11
	0.69	0.21	0.108	667.5	6182.0	0.01	0.08	5584	422.72	0.15
	0.89	0.20	0.066	384.1	5820.0	0.01	0.10	7594	574.90	0.18
	1.17	0.27	0.065	408.5	6274.0	0.01	0.09	10555	799.03	0.21
	1.36	0.20	0.082	501.7	6097.0	0.01	0.08	13181	997.83	0.24
	1.56	0.20	0.089	492.1	5512.0	0.01	0.08	15757	1192.84	0.28
	1.76	0.20	0.053	235.4	4465.0	0.02	0.16	16990	1286.13	0.30
	1.96	0.20	0.040	164.0	4050.0	0.02	0.23	17848	1351.10	0.32
	2.72	0.76	0.042	190.2	4519.0	0.02	0.20	21678	1641.00	0.38
	2.92	0.20	0.031	116.3	3697.0	0.02	0.33	22286	1687.08	0.39
	3.12	0.20	0.036	140.6	3896.0	0.02	0.27	23022	1742.77	0.41
	3.31	0.20	0.060	230.5	3822.0	0.02	0.16	24229	1834.10	0.43
	4.27	0.96	0.160	526.9	3300.0	0.02	0.07	37593	2845.80	0.74
	4.47	0.20	0.095	296.8	3111.0	0.02	0.13	39147	2963.42	0.77
	4.67	0.20	0.110	341.3	3107.0	0.02	0.11	40933	3098.66	0.82
	4.87	0.20	0.119	378.9	3178.0	0.02	0.10	42917	3248.81	0.87
	5.07	0.20	0.104	340.3	3277.0	0.02	0.11	44698	3383.64	0.91
	5.27	0.20	0.098	323.2	3293.0	0.02	0.12	46390	3511.70	0.95
	5.46	0.20	0.104	232.1	2241.0	0.03	0.16	47605	3603.67	0.99
	5.66	0.20	0.065	210.2	3217.0	0.02	0.18	48705	3686.97	1.01
	5.83	0.17	0.128	407.3	3179.0	0.02	0.09	50509	3823.52	1.06
	6.03	0.20	0.109	326.3	3003.0	0.03	0.12	52217	3952.80	1.10
	6.23	0.20	0.113	355.2	3149.0	0.02	0.11	54076	4093.55	1.14
	6.42	0.20	0.098	305.8	3127.0	0.02	0.12	55677	4214.73	1.18
60	6.64	0.21	0.097	297.8	3059.0	0.02	0.13	57355	4341.80	1.22
	6.82	0.18	0.103	316.9	3082.0	0.02	0.12	58886	4457.69	1.26
	7.02	0.20	0.116	350.8	3018.0	0.03	0.11	60723	4596.70	1.31
	7.22	0.20	0.108	331.9	3071.0	0.02	0.11	62460	4728.22	1.35
	7.38	0.17	0.151	461.0	3060.0	0.02	0.08	64502	4882.79	1.40
	7.58	0.20	0.145	422.3	2910.0	0.03	0.09	66712	5050.10	1.46
	7.78	0.20	0.079	225.2	2840.0	0.03	0.17	67891	5139.33	1.49

Table 3. cont.

Well number	Depth (m)	Interval thickness (m)	Gravimetric water content (g/g)	Chloride (mg Cl/kg soil)	Chloride (g Cl/m3 water)	Water flux (mm/yr)	Water velocity (mm/yr)	Age (yr)	Cumulative chloride (g/m2)	Cumulative H2O (m)
	7.98	0.20	0.088	260.7	2962.0	0.03	0.19	68914	5216.80	1.52
	8.18	0.20	0.075	227.2	3016.0	0.03	0.22	69806	5284.30	1.54
	8.37	0.20	0.108	311.4	2873.0	0.03	0.16	71028	5376.84	1.57
	8.57	0.20	0.117	342.2	2920.0	0.03	0.15	72372	5478.52	1.61
	8.77	0.20	0.091	296.2	3251.0	0.02	0.17	73534	5566.55	1.63
	8.94	0.17	0.101	287.6	2861.0	0.03	0.18	74490	5638.88	1.66
	9.14	0.20	0.086	261.4	3034.0	0.03	0.19	75516	5716.57	1.68
	9.33	0.20	0.056	176.4	3142.0	0.02	0.29	76209	5768.99	1.70
	9.53	0.20	0.064	198.4	3082.0	0.02	0.25	76988	5827.97	1.72
	9.73	0.20	0.064	186.0	2912.0	0.03	0.27	77718	5883.23	1.74
	9.93	0.20	0.061	180.3	2964.0	0.03	0.28	78426	5936.81	1.76
	10.13	0.20	0.103	239.4	2323.0	0.03	0.21	79365	6007.96	1.79
	10.69	0.56	0.128	370.4	2889.0	0.03	0.14	83504	6321.25	1.89
	10.89	0.20	0.126	356.7	2823.0	0.03	0.11	85371	6462.61	1.95
	11.06	0.17	0.080	230.8	2891.0	0.03	0.16	86393	6539.98	1.97
	11.29	0.23	0.154	453.2	2949.0	0.03	0.08	89130	6747.16	2.04
	11.48	0.20	0.099	276.8	2790.0	0.03	0.14	90579	6856.85	2.08
	11.68	0.20	0.053	141.5	2660.0	0.03	0.27	91320	6912.91	2.10
	11.88	0.20	0.074	227.1	3069.0	0.02	0.17	92508	7002.87	2.13
	12.05	0.17	0.136	388.0	2852.0	0.03	0.10	94227	7132.96	2.18
	12.25	0.20	0.107	280.5	2621.0	0.03	0.13	95695	7244.10	2.22
	12.44	0.20	0.096	255.7	2672.0	0.03	0.15	97033	7345.41	2.26
	12.64	0.20	0.093	272.9	2927.0	0.03	0.14	98462	7453.56	2.29
	12.84	0.20	0.092	270.3	2938.0	0.03	0.14	99876	7560.65	2.33
	13.04	0.20	0.086	250.8	2926.0	0.03	0.15	101189	7660.02	2.37
	13.24	0.20	0.139	251.5	1813.0	0.04	0.15	102506	7759.68	2.42
	13.43	0.20	0.089	253.7	2853.0	0.03	0.15	103834	7860.22	2.46
	13.60	0.17	0.094	260.4	2768.0	0.03	0.15	104987	7947.51	2.49
	13.80	0.20	0.098	275.3	2822.0	0.03	0.14	106428	8056.58	2.53
	14.00	0.20	0.084	216.4	2575.0	0.03	0.17	107561	8142.33	2.56
	14.20	0.20	0.080	202.0	2516.0	0.03	0.19	108618	8222.36	2.59
	14.39	0.20	0.113	298.4	2636.0	0.03	0.13	110180	8340.60	2.64
	14.59	0.20	0.125	267.4	2132.0	0.04	0.14	111579	8446.54	2.69
	14.79	0.20	0.099	264.2	2673.0	0.03	0.14	112962	8551.22	2.72

Table 3. cont.

Well number	Depth (m)	Interval thickness (m)	Gravimetric water content (g/g)	Chloride (mg Cl/kg soil)	Chloride (g Cl/m3 water)	Water flux (mm/yr)	Water velocity (mm/yr)	Age (yr)	Cumulative chloride (g/m2)	Cumulative H2O (m)
	14.99	0.20	0.152	412.5	2721.0	0.03	0.12	114581	8673.81	2.77
	15.16	0.17	0.156	419.4	2684.0	0.03	0.12	115974	8779.26	2.81
	15.35	0.20	0.166	444.2	2678.0	0.03	0.11	117718	8911.28	2.86
	15.55	0.20	0.146	402.8	2754.0	0.03	0.13	119300	9030.98	2.90
	15.75	0.20	0.052	142.5	2723.0	0.03	0.35	119859	9073.33	2.92
	15.95	0.20	0.040	115.0	2901.0	0.03	0.44	120311	9107.51	2.93
	16.15	0.20	0.028	77.4	2783.0	0.03	0.65	120614	9130.52	2.94
	16.34	0.20	0.064	168.7	2642.0	0.03	0.30	121277	9180.64	2.96
	16.54	0.20	0.043	123.7	2909.0	0.03	0.31	121924	9229.67	2.97
	16.71	0.17	0.037	108.5	2899.0	0.03	0.35	122405	9266.06	2.99
	16.91	0.20	0.048	135.4	2809.0	0.03	0.28	123114	9319.73	3.00
	17.11	0.20	0.093	249.7	2696.0	0.03	0.15	124421	9418.67	3.04
	17.31	0.20	0.140	389.2	2783.0	0.03	0.10	126458	9572.86	3.10
	17.50	0.20	0.176	482.3	2738.0	0.03	0.08	128983	9763.98	3.17
	0.10	0.10	0.037							
	0.28	0.18	0.072	303.7	4227.0	0.02	0.12	1468	111.10	0.03
	0.43	0.15	0.100	630.7	6299.0	0.01	0.06	4007	303.33	0.06
	0.59	0.15	0.096	686.7	**7188.0**	0.01	0.06	6772	512.64	0.09
	0.74	0.15	0.088	587.2	6702.0	0.01	0.06	9136	691.60	0.12
	0.89	0.15	0.077	489.1	6362.0	0.01	0.08	11106	840.69	0.14
	1.04	0.15	0.089	531.1	5992.0	0.01	0.07	13244	1002.56	0.17
	1.20	0.15	0.075	411.2	5476.0	0.01	0.12	14486	1096.56	0.19
	1.50	0.30	0.112	612.7	5466.0	0.01	0.08	18186	1376.68	0.24
	1.81	0.30	0.046	223.0	4876.0	0.02	0.23	19533	1478.63	0.26
	2.11	0.30	0.033	161.2	4821.0	0.02	0.31	20506	1552.33	0.28
	2.75	0.64	0.016	69.3	4233.0	0.02	0.73	21385	1618.83	0.29
	3.03	0.28	0.032	148.0	4582.0	0.02	0.34	22211	1681.40	0.30
66	4.61	1.58	0.102	394.1	3860.0	0.02	0.13	34528	2613.79	0.55
	5.52	0.91	0.069	248.5	3612.0	0.02	0.20	39030	2954.56	0.64
	6.47	0.94	0.068	230.0	3383.0	0.02	0.16	44772	3389.26	0.77
	7.20	0.73	0.126	464.9	3678.0	0.02	0.08	53757	4069.38	0.95
	7.93	0.73	0.078	275.2	3509.0	0.02	0.14	59075	4472.01	1.07
	8.71	0.78	0.100	335.8	3358.0	0.02	0.11	65970	4993.95	1.22
	9.18	0.47	0.037	132.9	3557.0	0.02	0.28	67629	5119.48	1.26

Table 3. cont.

Well number	Depth (m)	Interval thickness (m)	Gravimetric water content (g/g)	Chloride (mg Cl/kg soil)	Chloride (g Cl/m3 water)	Water flux (mm/yr)	Water velocity (mm/yr)	Age (yr)	Cumulative chloride (g/m2)	Cumulative H2O (m)
	9.72	0.53	0.064	257.6	4022.0	0.02	0.15	71259	5394.31	1.33
	11.04	1.33	0.147	465.6	3166.0	0.02	0.08	87568	6628.89	1.72
	11.76	0.72	0.092	307.8	3342.0	0.02	0.12	93394	7069.89	1.85
	12.60	0.84	0.081	256.9	3170.0	0.02	0.15	99083	7500.60	1.99
	13.33	0.73	0.066	220.7	3362.0	0.02	0.17	103349	7823.49	2.08
	0.02	0.02	0.033	**1.5**	44.4	1.71	34.55	1	0.05	0.00
	0.18	0.15	0.025	**1.2**	47.6	1.59	41.73	4	0.33	0.01
	0.33	0.15	0.028	**2.3**	83.6	0.91	21.71	11	0.86	0.01
	0.48	0.15	0.028	**1.4**	51.0	1.48	35.34	16	1.18	0.02
	0.63	0.15	0.056	**1.3**	23.7	3.19	37.86	20	1.49	0.03
	0.78	0.15	0.050	**3.7**	73.7	1.03	13.66	31	2.33	0.04
	0.94	0.15	0.050	38.4	765.1	0.10	1.31	116	11.11	0.06
	1.12	0.18	0.051	23.8	466.0	0.16	1.59	231	19.83	0.07
	1.42	0.30	0.046	131.6	2846.8	0.03	0.29	1291	100.04	0.10
	1.73	0.30	0.083	285.8	3446.7	0.02	0.13	3592	274.26	0.15
	2.03	0.30	0.051	181.8	3553.3	0.02	0.21	5056	385.09	0.18
	2.34	0.30	0.048	200.6	4177.0	0.02	0.19	6672	507.38	0.21
	2.67	0.34	0.098	425.8	4327.1	0.02	0.09	10443	792.89	0.28
70	2.98	0.30	0.085	333.1	3917.7	0.02	0.11	13126	995.94	0.33
	3.28	0.30	0.090	287.5	3186.6	0.02	0.13	15441	1171.18	0.39
	3.59	0.30	0.122	402.1	3283.6	0.02	0.09	18679	1416.30	0.46
	3.89	0.30	0.154	507.1	3299.3	0.02	0.07	22762	1725.40	0.55
	4.84	0.94	0.029	98.9	3431.6	0.02	0.38	25232	1912.37	0.61
	5.14	0.30	0.096	456.6	**4740.9**	0.02	0.08	28909	2190.72	0.67
	5.60	0.46	0.060	201.0	3377.4	0.02	0.19	31336	2374.49	0.72
	6.85	1.25	0.085	279.6	3283.2	0.02	0.14	40569	3073.39	0.93
	7.83	0.98	0.078	264.7	3405.0	0.02	0.14	47390	3589.73	1.09
	8.53	0.70	0.079	289.3	3658.9	0.02	0.13	52748	3995.38	1.20
	9.47	0.94	0.102	339.2	3314.0	0.02	0.11	61215	4636.31	1.39
	0.02	0.02	0.041	**2.2**	54.6	1.39	17.00	1	0.10	0.00
	0.18	0.15	0.045	**1.8**	40.3	1.88	20.82	9	0.66	0.02
	0.33	0.15	0.048	**4.5**	95.2	0.80	11.15	22	1.69	0.03
	0.48	0.15	0.053	**2.4**	45.5	1.66	21.11	30	2.24	0.04
	0.63	0.15	0.063	**3.2**	50.3	1.50	15.97	39	2.96	0.05

Table 3. cont.

Well number	Depth (m)	Interval thickness (m)	Gravimetric water content (g/g)	Chloride (mg Cl/kg soil)	Chloride (g Cl/m3 water)	Water flux (mm/yr)	Water velocity (mm/yr)	Age (yr)	Cumulative chloride (g/m2)	Cumulative H2O (m)
	0.78	0.15	0.049	**3.9**	79.1	0.96	12.98	51	3.85	0.06
	0.94	0.15	0.045	**7.3**	164.2	0.46	6.87	73	5.53	0.07
	1.12	0.18	0.048	8.7	180.9	0.42	5.82	104	7.91	0.09
	1.42	0.30	0.050	33.3	664.8	0.11	1.52	305	23.11	0.11
	1.73	0.30	0.045	55.8	1252.3	0.06	0.90	642	48.62	0.13
	2.03	0.30	0.036	78.6	2209.4	0.03	0.64	1117	84.55	0.15
	2.34	0.30	0.038	81.9	2155.6	0.04	0.62	1611	121.99	0.16
	2.64	0.30	0.073	172.6	2354.9	0.03	0.22	3001	227.20	0.21
71	2.95	0.30	0.060	186.6	3121.0	0.02	0.20	4504	340.96	0.25
	3.25	0.30	0.069	248.2	3581.4	0.02	0.15	6503	492.26	0.29
	3.56	0.30	0.103	444.0	4311.7	0.02	0.09	10078	762.90	0.35
	3.86	0.30	0.054	242.6	**4466.2**	0.02	0.16	12032	910.80	0.38
	4.20	0.34	0.051	219.8	4306.7	0.02	0.17	13979	1058.17	0.42
	4.50	0.30	0.047	157.8	3389.6	0.02	0.24	15249	1154.34	0.45
	4.96	0.46	0.162	369.1	2271.7	0.03	0.10	19707	1491.81	0.59
	5.75	0.79	0.084	174.7	2068.9	0.04	0.22	23364	1768.69	0.73
	6.67	0.91	0.075	168.5	2249.1	0.03	0.22	27435	2076.84	0.87
	8.07	1.40	0.048	59.1	1226.9	0.06	0.64	29625	2242.63	1.00
	8.71	0.64	0.065	103.5	1602.3	0.05	0.37	31375	2375.12	1.08
	9.32	0.61	0.093	162.7	1745.3	0.04	0.23	33995	2573.44	1.20
	0.02	0.02	0.043	**2.5**	57.2	1.32	20.59	1	0.08	0.00
	0.18	0.15	0.045	**2.4**	52.2	1.45	16.07	11	0.80	0.02
	0.33	0.15	0.057	**2.8**	48.9	1.55	13.52	22	1.66	0.03
	0.48	0.15	0.063	**3.6**	57.6	1.31	10.47	36	2.76	0.05
	0.63	0.15	0.081	**3.5**	43.3	1.75	10.83	50	3.82	0.08
	0.78	0.15	0.070	19.5	278.3	0.27	1.94	78	9.76	0.10
	0.94	0.15	0.062	73.0	1186.7	0.06	0.52	373	32.02	0.12
	1.12	0.18	0.059	116.1	1975.6	0.04	0.33	933	74.47	0.14
	1.42	0.30	0.058	178.1	3091.2	0.02	0.21	2368	183.06	0.17
	1.73	0.30	0.046	192.0	4155.3	0.02	0.20	3914	300.13	0.20
	2.03	0.30	0.044	195.7	**4411.5**	0.02	0.19	5490	419.43	0.23
	2.34	0.30	0.041	174.3	4273.7	0.02	0.22	6894	525.71	0.25
	2.67	0.34	0.091	262.4	2893.7	0.03	0.14	9218	701.63	0.31
72	2.98	0.30	0.149	366.6	2455.2	0.03	0.10	12170	925.10	0.41

Table 3. cont.

Well number	Depth (m)	Interval thickness (m)	Gravimetric water content (g/g)	Chloride (mg Cl/kg soil)	Chloride (g Cl/m3 water)	Water flux (mm/yr)	Water velocity (mm/yr)	Age (yr)	Cumulative chloride (g/m2)	Cumulative H2O (m)
	3.28	0.30	0.152	357.4	2352.5	0.03	0.11	15048	1142.99	0.50
	3.59	0.30	0.029	62.8	2187.8	0.03	0.60	15554	1181.24	0.52
	3.89	0.30	0.064	147.8	2293.5	0.03	0.26	16744	1271.37	0.55
	4.84	0.94	0.110	227.3	2060.8	0.04	0.17	22418	1700.88	0.76
	5.14	0.30	0.143	296.7	2070.6	0.04	0.13	24807	1881.72	0.85
	5.60	0.46	0.080	164.8	2064.8	0.04	0.23	26798	2032.42	0.92
	6.85	1.25	0.061	118.7	1959.7	0.04	0.32	30718	2329.18	1.07
	7.83	0.98	0.021	32.6	1575.5	0.05	1.16	31559	2392.83	1.12
	8.91	1.08	0.120	152.4	1272.9	0.06	0.25	35916	2722.68	1.37
	0.02	0.02	0.043	**3.6**	83.6	0.91	10.52	2	0.16	0.00
	0.18	0.15	0.055	**4.6**	82.8	0.91	8.29	21	1.56	0.02
	0.33	0.15	0.064	**9.3**	146.3	0.52	4.07	58	4.39	0.04
	0.48	0.15	0.077	11.5	148.2	0.51	3.29	104	7.90	0.06
	0.63	0.15	0.069	35.7	515.6	0.15	1.06	144	18.77	0.08
	0.78	0.15	0.059	204.5	3459.1	0.02	0.19	967	81.11	0.10
	0.94	0.15	0.055	395.8	7248.3	0.01	0.10	2561	201.74	0.12
	1.12	0.18	0.059	464.7	**7831.3**	0.01	0.08	4806	371.70	0.14
	1.42	0.30	0.056	416.9	7383.1	0.01	0.12	7324	562.32	0.17
	1.73	0.30	0.037	264.3	7192.3	0.01	0.19	8920	683.16	0.18
	2.03	0.30	0.039	223.5	5742.8	0.01	0.23	10270	785.33	0.20
	2.67	0.64	0.133	418.1	3133.3	0.02	0.12	15573	1186.75	0.33
73	2.98	0.30	0.157	452.6	2882.7	0.03	0.11	18306	1393.69	0.40
	3.28	0.30	0.102	305.7	3002.6	0.03	0.17	20152	1533.44	0.45
	3.59	0.30	0.060	175.6	2926.9	0.03	0.29	21213	1613.73	0.47
	3.89	0.30	0.075	227.2	3026.9	0.03	0.22	22585	1717.61	0.51
	4.23	0.34	0.087	272.0	3117.3	0.02	0.19	24393	1854.42	0.55
	4.53	0.30	0.103	323.5	3138.7	0.02	0.16	26347	2002.35	0.60
	5.14	0.61	0.084	281.0	3355.9	0.02	0.18	29740	2259.25	0.68
	6.09	0.94	0.095	294.2	3087.7	0.02	0.13	37085	2815.23	0.86
	6.85	0.76	0.059	167.9	2825.7	0.03	0.23	40466	3071.16	0.95
	7.80	0.94	0.047	116.2	2492.2	0.03	0.33	43366	3290.68	1.03
	8.70	0.91	0.048	120.2	2497.4	0.03	0.31	46245	3508.65	1.12
	9.50	0.80	0.040	100.6	2530.2	0.03	0.38	48372	3669.66	1.19
	0.02	0.02	0.023	**3.5**	148.6	0.51	10.88	2	0.16	0.00

Table 3. cont.

Well number	Depth (m)	Interval thickness (m)	Gravimetric water content (g/g)	Chloride (mg Cl/kg soil)	Chloride (g Cl/m3 water)	Water flux (mm/yr)	Water velocity (mm/yr)	Age (yr)	Cumulative chloride (g/m2)	Cumulative H2O (m)
	0.18	0.15	0.035	**2.1**	58.8	1.29	18.34	10	0.79	0.01
	0.33	0.15	0.037	**6.6**	178.8	0.42	5.73	37	2.80	0.02
	0.48	0.15	0.048	**1.1**	22.7	3.34	35.01	41	3.13	0.04
	0.63	0.15	0.057	**1.2**	20.2	3.74	32.77	46	3.48	0.05
	0.78	0.15	0.061	**9.8**	162.1	0.47	3.86	86	6.47	0.07
	0.94	0.15	0.051	83.7	1625.2	0.05	0.45	422	31.98	0.09
	1.15	0.21	0.047	149.6	3172.9	0.02	0.25	1266	95.83	0.11
	1.46	0.30	0.051	218.6	4310.9	0.02	0.17	3026	229.10	0.14
	1.76	0.30	0.050	261.8	**5214.6**	0.01	0.14	5135	388.70	0.17
	2.07	0.30	0.044	227.5	5141.3	0.01	0.17	6967	527.37	0.20
	2.37	0.30	0.026	103.5	3932.0	0.02	0.37	7800	590.47	0.21
	2.71	0.34	0.026	71.8	2784.1	0.03	0.53	8436	638.64	0.23
74	3.01	0.30	0.154	368.4	2389.3	0.03	0.10	11403	863.24	0.33
	3.31	0.30	0.074							
	3.62	0.30	0.060	187.1	3135.0	0.02	0.20	14417	1091.39	0.40
	3.92	0.30	0.066	191.4	2905.1	0.03	0.20	15959	1208.09	0.44
	4.26	0.34	0.060							
	5.17	0.91	0.106	205.2	1930.2	0.04	0.18	22734	1720.97	0.70
	6.12	0.94	0.067	128.4	1925.1	0.04	0.29	25940	1963.66	0.83
	7.03	0.91	0.056	90.1	1614.1	0.05	0.42	28117	2128.46	0.93
	7.67	0.64	0.097	158.1	1632.4	0.05	0.24	30791	2330.92	1.06
	8.59	0.91	0.047	76.8	1649.8	0.05	0.49	32646	2471.32	1.14
	9.69	1.10	0.157	239.9	1531.6	0.05	0.16	39601	2997.80	1.48
	0.02	0.02	0.027	**1.7**	62.9	1.20	29.19	1	0.06	0.00
	0.18	0.15	0.054	**3.0**	55.8	1.36	16.89	10	0.74	0.01
	0.33	0.15	0.031	**3.0**	95.4	0.79	16.96	19	1.42	0.02
	0.48	0.15	0.054	**1.7**	31.3	2.42	29.76	24	1.81	0.03
	0.63	0.15	0.066	**1.7**	26.1	2.90	29.12	29	2.21	0.05
	0.78	0.15	0.056	**8.3**	146.8	0.52	6.09	54	4.10	0.06
	0.94	0.15	0.047	102.4	2165.3	0.03	0.49	309	27.51	0.07
	1.06	0.12	0.050							
	1.36	0.30	0.056	224.0	3990.2	0.02	0.17	2835	218.71	0.12
	1.67	0.30	0.065	320.4	**4922.0**	0.02	0.12	5415	414.00	0.16
	1.97	0.30	0.049	163.2	3330.4	0.02	0.23	6729	513.48	0.19

Table 3. cont.

Well number	Depth (m)	Interval thickness (m)	Gravimetric water content (g/g)	Chloride (mg Cl/kg soil)	Chloride (g Cl/m3 water)	Water flux (mm/yr)	Water velocity (mm/yr)	Age (yr)	Cumulative chloride (g/m2)	Cumulative H2O (m)
	2.61	0.64	0.036	125.3	3493.5	0.02	0.30	8847	673.83	0.23
75	2.92	0.30	0.124	301.2	2437.4	0.03	0.13	11273	857.44	0.31
	3.22	0.30	0.167	588.8	3526.0	0.02	0.06	16014	1216.40	0.41
	3.53	0.30	0.076	284.4	3757.2	0.02	0.13	18305	1389.79	0.46
	4.17	0.64	0.069	329.6	4809.5	0.02	0.11	23878	1811.67	0.55
	4.47	0.30	0.082	387.3	4731.0	0.02	0.10	26997	2047.79	0.60
	5.39	0.91	0.165	660.0	4000.9	0.02	0.06	42941	3254.75	0.90
	6.33	0.94	0.079	330.2	4163.9	0.02	0.11	51183	3878.67	1.05
	7.08	0.75	0.060	246.8	4118.7	0.02	0.15	56052	4247.25	1.14
	7.58	0.50	0.064	272.1	4221.0	0.02	0.14	59668	4520.96	1.20
	8.68	1.10	0.067	207.2	3102.8	0.02	0.18	65676	4975.77	1.35
	9.29	0.61	0.040	111.7	2805.0	0.03	0.34	67474	5111.90	1.40
	9.62	0.34	0.015	41.9	2869.2	0.03	0.90	67846	5140.02	1.41
	0.02	0.02	0.033	**2.0**	60.8	1.25	18.77	1	0.09	0.00
	0.18	0.15	0.051	**2.9**	56.4	1.34	13.06	13	0.98	0.02
	0.33	0.15	0.054	**3.2**	59.0	1.28	11.84	26	1.95	0.03
	0.48	0.15	0.054	**3.0**	55.6	1.36	12.60	38	2.87	0.05
	0.63	0.15	0.053	**2.7**	51.4	1.47	13.94	49	3.69	0.07
	0.78	0.15	0.072	**1.9**	26.8	2.83	19.51	57	4.28	0.09
	0.94	0.15	0.086	**4.9**	57.4	1.32	7.69	76	5.79	0.11
	1.12	0.18	0.048	**0.5**	10.0	7.59	78.53	79	5.96	0.13
	1.42	0.30	0.044	**0.2**	4.6	16.39	188.26	80	6.08	0.16
	1.73	0.30	0.036	12.8	359.3	0.21	2.96	103	13.88	0.18
	2.03	0.30	0.034	106.6	3165.3	0.02	0.36	961	78.86	0.20
76	2.34	0.30	0.138	413.2	2995.0	0.03	0.09	4289	330.75	0.28
	2.71	0.37	0.173	492.7	2851.6	0.03	0.08	9050	691.19	0.41
	3.01	0.30	0.159	445.0	2797.0	0.03	0.09	12634	962.47	0.51
	3.31	0.30	0.020	73.4	3662.5	0.02	0.52	13225	1007.19	0.52
	4.23	0.91	0.066	253.8	**3822.5**	0.02	0.15	19356	1471.37	0.64
	4.99	0.76	0.087	253.9	2918.9	0.03	0.15	24468	1858.30	0.77
	6.55	1.55	0.079	267.2	3368.5	0.02	0.14	35442	2689.08	1.02
	7.98	1.43	0.093	259.6	2778.3	0.03	0.15	45270	3433.00	1.29
	8.74	0.76	0.057	160.5	2794.4	0.03	0.24	48502	3677.68	1.38
	9.50	0.76	0.057	115.9	2023.1	0.04	0.33	50836	3854.34	1.46

Table 3. cont.

Well number	Depth (m)	Interval thickness (m)	Gravimetric water content (g/g)	Chloride (mg Cl/kg soil)	Chloride (g Cl/m3 water)	Water flux (mm/yr)	Water velocity (mm/yr)	Age (yr)	Cumulative chloride (g/m2)	Cumulative H2O (m)
	10.29	0.79	0.036	86.1	2381.7	0.03	0.44	52639	3990.89	1.52
	0.02	0.02	0.033	**1.6**	49.7	1.52	22.97	1	0.08	0.00
	0.18	0.15	0.060	**2.9**	48.8	1.55	13.01	13	0.96	0.02
	0.33	0.15	0.045	**1.0**	21.7	3.50	51.76	16	1.19	0.03
	0.48	0.15	0.045	**5.7**	126.8	0.60	8.88	33	2.48	0.04
	0.63	0.15	0.058	31.4	539.6	0.14	1.61	95	9.66	0.05
	0.78	0.15	0.054	45.3	843.0	0.09	1.12	231	20.00	0.07
	0.94	0.15	0.043	47.7	1101.9	0.07	1.06	375	30.90	0.08
	1.12	0.18	0.039	50.2	1286.6	0.06	1.00	557	44.68	0.09
	1.42	0.30	0.058	103.5	1774.8	0.04	0.49	1183	92.01	0.11
	1.73	0.30	0.048	125.9	2628.8	0.03	0.30	2196	168.73	0.14
	2.03	0.30	0.065	228.5	3519.7	0.02	0.17	4036	308.02	0.18
77	2.34	0.30	0.137	633.7	**4632.9**	0.02	0.06	9139	694.34	0.27
	2.67	0.34	0.142	599.8	4227.7	0.02	0.06	14453	1096.56	0.36
	2.98	0.30	0.106	390.6	3668.0	0.02	0.10	17598	1334.69	0.43
	3.28	0.30	0.081	268.6	3327.4	0.02	0.14	19762	1498.44	0.47
	3.59	0.30	0.091	277.7	3054.5	0.02	0.14	21998	1667.71	0.53
	3.89	0.30	0.081	233.9	2883.6	0.03	0.16	23881	1810.27	0.58
	4.23	0.34	0.051	129.4	2541.5	0.03	0.29	25027	1897.02	0.61
	5.51	1.28	0.103	219.3	2123.8	0.04	0.17	32444	2458.50	0.88
	6.39	0.88	0.034	60.2	1758.8	0.04	0.63	33850	2564.91	0.94
	7.19	0.79	0.131	274.5	2096.3	0.04	0.14	39598	3000.03	1.15
	7.95	0.76	0.088	175.6	2001.8	0.04	0.22	43133	3267.63	1.28
	8.89	0.94	0.118	239.9	2025.3	0.04	0.16	49121	3720.93	1.50
	10.29	1.40	0.064	137.6	2153.0	0.04	0.28	54219	4106.82	1.68
	0.02	0.02	0.030	**2.6**	87.9	0.86	14.37	2	0.12	0.00
	0.18	0.15	0.046	24.6	530.2	0.14	1.54	101	7.61	0.02
	0.33	0.15	0.054	**4.3**	80.0	0.95	8.79	69	8.93	0.03
	0.48	0.15	0.044	**2.3**	53.2	1.42	16.28	69	9.63	0.05
	0.63	0.15	0.074	18.0	244.5	0.31	2.10	142	15.13	0.07
	0.78	0.15	0.070	18.0	257.5	0.29	2.11	214	20.60	0.09
	0.94	0.15	0.059	18.7	318.3	0.24	2.03	289	26.29	0.11
	1.12	0.18	0.063	31.3	494.2	0.15	1.21	440	37.75	0.13
	1.42	0.30	0.061	46.0	760.6	0.10	0.82	811	65.81	0.17

Table 3. cont.

Well number	Depth (m)	Interval thickness (m)	Gravimetric water content (g/g)	Chloride (mg Cl/kg soil)	Chloride (g Cl/m3 water)	Water flux (mm/yr)	Water velocity (mm/yr)	Age (yr)	Cumulative chloride (g/m2)	Cumulative H2O (m)
	1.73	0.30	0.050	41.3	834.6	0.09	0.92	1144	90.99	0.20
	2.03	0.30	0.052	74.2	1425.0	0.05	0.51	1741	136.21	0.23
78	2.34	0.30	0.101	207.1	2042.9	0.04	0.18	3409	262.46	0.29
	2.67	0.34	0.178	354.8	1991.5	0.04	0.11	6552	500.38	0.41
	2.98	0.30	0.117	181.8	1548.7	0.05	0.21	8016	611.22	0.48
	3.28	0.30	0.103	164.2	1599.1	0.05	0.23	9339	711.34	0.54
	3.59	0.30	0.095	168.8	1778.6	0.04	0.22	10698	814.22	0.60
	3.89	0.30	0.070	136.2	1959.5	0.04	0.28	11795	897.26	0.64
	4.23	0.34	0.089	217.1	2442.0	0.03	0.17	13718	1042.85	0.70
	4.53	0.30	0.097	232.0	2381.3	0.03	0.16	15586	1184.25	0.76
	5.14	0.61	0.114	256.3	2255.4	0.03	0.15	19714	1496.77	0.90
	5.45	0.30	0.121	265.9	2190.2	0.03	0.14	21856	1658.89	0.98
	6.39	0.94	0.015	38.0	2509.0	0.03	1.00	22804	1730.70	1.00
	6.70	0.30	0.129	276.6	2138.9	0.04	0.14	25032	1899.34	1.08
	7.95	1.25	0.030	63.2	2109.4	0.04	0.60	27118	2057.21	1.16
	8.71	0.76	0.070	149.9	2147.7	0.04	0.25	30135	2285.63	1.26
	9.65	0.94	0.066	192.5	**2937.8**	0.03	0.20	34940	2649.38	1.39
	0.02	0.02	0.019	**6.9**	365.5	0.21	5.48	4	0.32	0.00
	0.18	0.15	0.032	**2.4**	74.5	1.02	21.40	11	0.85	0.01
	0.33	0.15	0.038	**2.5**	65.9	1.15	20.22	19	1.43	0.02
	0.48	0.15	0.039	**1.9**	47.9	1.58	26.93	24	1.85	0.03
	0.63	0.15	0.045	**1.6**	34.9	2.17	32.44	29	2.21	0.04
	0.78	0.15	0.040	**1.3**	31.3	2.42	40.12	33	2.50	0.05
	0.94	0.15	0.036	**1.7**	47.9	1.58	29.12	38	2.89	0.05
	1.24	0.30	0.032	**1.3**	39.3	1.93	29.90	48	3.66	0.07
	1.55	0.30	0.030	**1.3**	43.5	1.74	28.93	59	4.46	0.09
	2.64	1.10	0.076	239.6	3141.8	0.02	0.16	6946	530.29	0.26
80	2.95	0.30	0.081	185.4	2296.9	0.03	0.20	8439	643.33	0.31
	3.25	0.30	0.069	113.8	1650.8	0.05	0.33	9356	712.67	0.35
	3.56	0.30	0.076	251.4	3290.9	0.02	0.15	11380	865.93	0.40
	3.86	0.30	0.104	326.8	3144.5	0.02	0.12	14011	1065.13	0.46
	4.20	0.34	0.061	220.5	**3595.6**	0.02	0.17	15964	1212.97	0.50
	4.50	0.30	0.080	246.1	3085.0	0.02	0.15	17946	1362.99	0.55
	5.42	0.91	0.094	246.7	2635.3	0.03	0.15	23906	1814.17	0.72

Table 3. cont.

Well number	Depth (m)	Interval thickness (m)	Gravimetric water content (g/g)	Chloride (mg Cl/kg soil)	Chloride (g Cl/m3 water)	Water flux (mm/yr)	Water velocity (mm/yr)	Age (yr)	Cumulative chloride (g/m2)	Cumulative H2O (m)
	6.36	0.94	0.075	220.4	2952.4	0.03	0.17	29408	2230.69	0.86
	7.31	0.94	0.054	137.7	2535.8	0.03	0.27	32846	2490.89	0.96
	8.22	0.91	0.053	117.6	2207.3	0.03	0.32	35686	2705.87	1.06
	9.17	0.94	0.092	211.5	2310.4	0.03	0.18	40965	3105.54	1.23
	10.08	0.91	0.038	83.2	2162.9	0.03	0.46	42975	3257.67	1.31
	0.00									
	0.02	0.02	0.020	**4.8**	242.8	0.31	7.86	3	0.22	0.00
	0.18	0.15	0.045	**2.6**	57.6	1.31	14.65	13	1.01	0.01
	0.33	0.15	0.051	**4.3**	84.2	0.90	8.80	31	2.32	0.03
	0.48	0.15	0.061	**9.5**	155.9	0.49	4.00	69	5.20	0.05
	0.63	0.15	0.049	**3.4**	69.3	1.09	11.12	82	6.24	0.06
	0.78	0.15	0.046	11.8	258.6	0.29	3.21	48	9.83	0.08
	0.94	0.15	0.043	24.3	570.8	0.13	1.56	145	17.23	0.09
	1.12	0.18	0.041	28.4	685.0	0.11	1.33	282	27.61	0.11
	1.42	0.30	0.036	53.5	1466.6	0.05	0.71	713	60.20	0.13
	1.73	0.30	0.023	61.5	2721.7	0.03	0.82	1084	88.32	0.14
	2.67	0.94	0.038	199.9	5199.4	0.01	0.25	4827	371.64	0.19
	2.98	0.30	0.022	106.5	4949.7	0.02	0.47	5470	420.33	0.20
81	4.23	1.25	0.014	93.3	**6529.7**	0.01	0.54	7780	595.15	0.23
	4.53	0.30	0.019	84.0	4527.9	0.02	0.60	8287	633.54	0.24
	6.38	1.84	0.020	47.4	2382.0	0.03	1.07	10017	764.52	0.29
	8.19	1.81	0.105	201.7	1912.6	0.04	0.25	17266	1313.29	0.58
	9.35	1.16	0.013	22.3	1750.5	0.04	2.26	17778	1352.03	0.60
	0.22	0.22	0.077	9.2	120.0	0.63	5.46	41	3.07	0.03
	0.53	0.30	0.084	648.8	7757.0	0.01	0.06	5265	398.57	0.08
	0.66	0.13	0.092	1176.2	**12833.0**	0.01	0.03	9291	703.31	0.10
	1.32	0.66	0.032	291.8	9059.0	0.01	0.13	14401	1090.18	0.14
	1.62	0.30	0.089	738.6	8269.0	0.01	0.05	20349	1540.43	0.20
	1.93	0.30	0.106	801.6	7530.0	0.01	0.05	26804	2029.09	0.26
	2.23	0.30	0.133	1026.2	7739.0	0.01	0.04	35068	2654.68	0.34
	2.54	0.30	0.135	948.9	7033.0	0.01	0.04	42710	3233.13	0.43
	2.87	0.34	0.100	697.5	6949.0	0.01	0.05	48889	3700.86	0.49
	3.18	0.30	0.134	865.2	6434.0	0.01	0.04	55856	4228.28	0.57
84	3.48	0.30	0.145	943.7	6508.0	0.01	0.04	63456	4803.59	0.66

Table 3. cont.

Well number	Depth (m)	Interval thickness (m)	Gravimetric water content (g/g)	Chloride (mg Cl/kg soil)	Chloride (g Cl/m3 water)	Water flux (mm/yr)	Water velocity (mm/yr)	Age (yr)	Cumulative chloride (g/m2)	Cumulative H2O (m)
	3.79	0.30	0.149	958.4	6439.0	0.01	0.04	71174	5387.84	0.75
	4.10	0.31	0.147	965.7	6578.0	0.01	0.04	79144	5991.23	0.85
	4.43	0.33	0.155	1231.4	7930.0	0.01	0.03	89804	6798.18	0.95
	4.73	0.30	0.153	970.8	6359.0	0.01	0.04	97622	7390.00	1.04
	5.04	0.30	0.152	929.8	6117.0	0.01	0.04	105110	7956.80	1.13
	5.34	0.30	0.153	951.1	6204.0	0.01	0.04	112769	8536.59	1.23
	5.65	0.31	0.147	899.9	6139.0	0.01	0.04	120197	9098.88	1.32
	5.95	0.30	0.134	826.1	6148.0	0.01	0.05	126683	9589.88	1.40
	7.14	1.19	0.116	651.6	5636.0	0.01	0.06	147147	11139.06	1.67
	8.15	1.01	0.124	664.7	5351.0	0.01	0.06	164812	12476.31	1.92
	9.09	0.94	0.146	755.8	5189.0	0.01	0.05	183681	13904.62	2.20
	10.01	0.91	0.140	670.8	4802.0	0.02	0.06	199887	15131.47	2.45
	11.19	1.19	0.126	580.1	4612.0	0.02	0.07	218107	16510.68	2.75
	12.75	1.55	0.131	595.1	4543.0	0.02	0.06	242549	18360.94	3.16
	0.22	0.22	0.092	BD2	BD2					
	0.53	0.30	0.082	BD2	BD2					
	0.83	0.30	0.084	9.5	114.2					
	1.32	0.49	0.099	BD2	BD2					
	1.62	0.30	0.118	BD2	BD2					
	1.93	0.30	0.090	BD2	BD2					
	2.23	0.30	0.103	BD2	BD2					
	2.55	0.31	0.098	BD2	BD2					
	2.87	0.33	0.133	BD2	BD2					
	3.18	0.30	0.082	BD2	BD2					
85	3.48	0.30	0.060	BD2	BD2					
	3.79	0.30	0.077	BD2	BD2					
	4.14	0.35	0.070	BD2	BD2					
	4.49	0.35	0.087	BD2	BD2					
	4.79	0.30	0.101	BD2	BD2					
	5.10	0.30	0.118	BD2	BD2					
	5.40	0.30	0.137	BD2	BD2					
	5.72	0.31	0.115	BD2	BD2					
	5.98	0.27	0.095	BD2	BD2					
	6.90	0.91	0.081	10.4	128.7					

Table 3. cont.

Well number	Depth (m)	Interval thickness (m)	Gravimetric water content (g/g)	Chloride (mg Cl/kg soil)	Chloride (g Cl/m3 water)	Water flux (mm/yr)	Water velocity (mm/yr)	Age (yr)	Cumulative chloride (g/m2)	Cumulative H2O (m)
	8.05	1.16	0.099	20.4	205.2					
	8.79	0.73	0.077	25.5	330.6					
	9.61	0.82	0.085	75.3	**884.3**					
	10.34	0.73	0.061	52.0	857.3					
	11.16	0.82	0.059	38.9	664.2					
	11.89	0.73	0.066	37.6	573.1					
	12.72	0.82	0.086	48.2	562.1					
	14.27	1.55	0.070	30.2	429.6					
	15.83	1.55	0.037	10.3	276.2					
	0.22	0.22	0.099	BD2	BD2					
	0.53	0.30	0.114	21.6	189.2					
	0.98	0.46	0.103	BD2	BD2					
	1.35	0.37	0.087	BD2	BD2					
	1.65	0.30	0.088	BD2	BD2					
	1.96	0.30	0.082	BD2	BD2					
	2.26	0.30	0.079	BD2	BD2					
	2.90	0.64	0.099	BD2	BD2					
	3.21	0.30	0.073	BD2	BD2					
	3.51	0.30	0.043	BD2	BD2					
86	3.82	0.30	0.143	BD2	BD2					
	4.06	0.24	0.127	BD2	BD2					
	4.46	0.40	0.070	BD2	BD2					
	4.76	0.30	0.067	BD2	BD2					
	5.07	0.30	0.038	BD2	BD2					
	5.37	0.30	0.075	BD2	BD2					
	5.68	0.31	0.106	BD2	BD2					
	6.53	0.85	0.087	BD2	BD2					
	6.63	0.10	0.097	BD2	BD2					
	8.08	1.46	0.086	BD2	BD2					
	8.82	0.73	0.078	BD2	BD2					
	9.64	0.82	0.098	6.6	66.8					
	10.37	0.73	0.101	16.0	157.4					
	11.19	0.82	0.085	18.3	215.8					
	11.93	0.73	0.080	22.1	274.8					

Table 3. cont.

Well number	Depth (m)	Interval thickness (m)	Gravimetric water content (g/g)	Chloride (mg Cl/kg soil)	Chloride (g Cl/m3 water)	Water flux (mm/yr)	Water velocity (mm/yr)	Age (yr)	Cumulative chloride (g/m2)	Cumulative H2O (m)
	12.75	0.82	0.076	14.9	196.1					
	14.33	1.58	0.078	13.3	171.0					
	15.86	1.52	0.046	11.3	246.2					
	17.41	1.55	0.063	24.5	**390.9**					
	18.98	1.57	0.157	20.0	127.5					
	20.22	1.23	0.137	18.0	131.2					
	0.71	0.71	0.129	BD2	BD2					
	0.98	0.27	0.100	BD2	BD2					
	1.29	0.30	0.088	BD2	BD2					
	1.59	0.30	0.092	BD2	BD2					
	1.90	0.30	0.084	BD2	BD2					
	2.20	0.30	0.097	BD2	BD2					
	2.51	0.30	0.073	BD2	BD2					
	2.84	0.34	0.088	BD2	BD2					
	3.15	0.30	0.070	BD2	BD2					
	3.45	0.30	0.157	BD2	BD2					
	4.03	0.58	0.118	BD2	BD2					
	4.40	0.37	0.063	BD2	BD2					
87	4.70	0.30	0.058	BD2	BD2					
	5.01	0.30	0.070	BD2	BD2					
	5.31	0.30	0.072	BD2	BD2					
	5.59	0.27	0.091	BD2	BD2					
	5.95	0.37	0.106	BD2	BD2					
	6.50	0.55	0.129	BD2	BD2					
	7.20	0.70	0.098	BD2	BD2					
	8.02	0.82	0.085	BD2	BD2					
	8.76	0.73	0.083	BD2	BD2					
	9.58	0.82	0.117	BD2	BD2					
	10.31	0.73	0.111	BD2	BD2					
	11.13	0.82	0.106	BD2	BD2					
	11.86	0.73	0.074	BD2	BD2					
	12.69	0.82	0.085	BD2	BD2					
	14.24	1.55	0.053	9.1	170.7					
	15.80	1.55	0.095	21.6	228.5					

Table 3. cont.

Well number	Depth (m)	Interval thickness (m)	Gravimetric water content (g/g)	Chloride (mg Cl/kg soil)	Chloride (g Cl/m3 water)	Water flux (mm/yr)	Water velocity (mm/yr)	Age (yr)	Cumulative chloride (g/m2)	Cumulative H2O (m)
	17.35	1.55	0.051	11.6	225.4					
	18.91	1.55	0.136	17.3	126.8					
	20.46	1.55	0.127	13.7	108.1					
	21.28	0.82	0.113	12.8	112.8					
	0.22	0.22	0.093	15.1	162.1					
	0.53	0.30	0.080	BD2	BD2					
	1.10	0.58	0.090	BD2	BD2					
	1.41	0.30	0.138	BD2	BD2					
	1.71	0.30	0.160	BD2	BD2					
	2.02	0.30	0.148	BD2	BD2					
	2.34	0.32	0.139	37.0	266.7					
	2.66	0.32	0.160	104.8	653.6					
	2.96	0.30	0.181	79.6	438.9					
	3.57	0.61	0.145	112.3	774.0					
	3.89	0.32	0.116	80.7	694.6					
	4.21	0.32	0.089	65.0	733.0					
88	4.52	0.30	0.090	47.9	532.2					
	4.82	0.30	0.091	19.4	214.3					
	5.13	0.30	0.044	BD2	BD2					
	5.77	0.64	0.096	55.1	572.1					
	6.29	0.52	0.186	401.3	2160.5					
	7.06	0.78	0.105	256.5	2453.4					
	7.84	0.78	0.153	636.5	4157.2					
	8.59	0.75	0.143	612.6	4272.2					
	9.15	0.56	0.060	231.0	3870.4					
	9.73	0.58	0.159	616.5	3867.4					
	10.95	1.22	0.130	544.4	4195.0					
	11.65	0.70	0.129	614.9	**4753.3**					
	12.50	0.85	0.130	552.2	4244.2					
	0.22	0.22	0.114	12.8	112.0	0.68	2.95	75	5.66	0.05
	0.53	0.30	0.112	130.6	1163.5	0.07	0.29	1127	85.28	0.12
	0.83	0.30	0.106	313.2	2950.8	0.03	0.12	3649	276.23	0.18
	1.35	0.52	0.177	388.1	2187.2	0.03	0.10	8962	678.43	0.37
	1.65	0.30	0.146	302.6	2072.6	0.04	0.13	11399	862.88	0.46

Table 3. cont.

Well number	Depth (m)	Interval thickness (m)	Gravimetric water content (g/g)	Chloride (mg Cl/kg soil)	Chloride (g Cl/m3 water)	Water flux (mm/yr)	Water velocity (mm/yr)	Age (yr)	Cumulative chloride (g/m2)	Cumulative H2O (m)
	1.96	0.30	0.060	205.5	3437.6	0.02	0.18	13054	988.16	0.49
	2.26	0.30	0.132	476.1	**3601.0**	0.02	0.08	16888	1278.39	0.57
	2.66	0.40	0.272	626.3	2302.1	0.03	0.06	23445	1774.75	0.79
	2.90	0.24	0.118	311.8	2636.5	0.03	0.12	25453	1926.81	0.85
	3.21	0.30	0.148	432.3	2930.0	0.03	0.09	28935	2190.35	0.94
89	3.51	0.30	0.072	224.2	3117.0	0.02	0.17	30740	2327.02	0.98
	3.82	0.30	0.117	297.4	2536.0	0.03	0.13	33135	2508.29	1.05
	4.46	0.64	0.122	243.1	1999.7	0.04	0.16	37245	2819.48	1.21
	4.76	0.30	0.134	309.5	2316.0	0.03	0.12	39738	3008.14	1.29
	5.07	0.30	0.116	206.9	1781.9	0.04	0.18	41404	3134.29	1.36
	5.37	0.30	0.106	162.3	1535.4	0.05	0.23	42711	3233.21	1.42
	5.40	0.03	0.136	290.3	2131.3	0.04	0.13	42945	3250.91	1.43
	6.01	0.61	0.161	211.9	1314.2	0.06	0.18	46357	3509.21	1.63
	6.53	0.52	0.159	191.8	1208.2	0.06	0.20	48983	3708.01	1.79
	7.23	0.70	0.149	176.8	1189.1	0.06	0.21	52257	3955.83	2.00
	8.08	0.85	0.144	170.4	1186.4	0.06	0.22	56098	4246.65	2.25
	8.76	0.67	0.096	104.9	1091.7	0.07	0.36	57957	4387.35	2.38
	9.64	0.88	0.105	101.0	966.3	0.08	0.37	60317	4565.97	2.56
	10.36	0.72	0.113	107.7	949.7	0.08	0.35	62354	4720.22	2.72
	11.19	0.84	0.100	89.0	890.4	0.09	0.43	64325	4869.43	2.89
	11.93	0.73	0.102	87.3	852.4	0.09	0.43	66013	4997.22	3.04

Porosities of sediments estimated from bulk densities of samples collected in and adjacent to the area of the proposed repository ranged from 29 to 54% and averaged 43% in the upper 7 ft (2 m), whereas porosities ranged from 15 to 32% and averaged 26% in the 7 to 82 ft (2 to 25 m) depth interval. On the basis of porosity and water content data, saturation of the sediments in the top 2 m ranged from 20 to 40%, whereas saturation of the sediments from 7 to 82 ft (2 to 25 m) depth was ≥ 70%.

Water Potential

Water potentials measured with the Decagon SC10 thermocouple psychrometer and the water activity meter were similar (fig. 8). In the remainder of the results section we will present the water potentials measured with the Decagon SC10. Water potential measured by thermocouple psychrometers is the sum of matric and osmotic potential. The osmotic potentials were generally less than –1 MPa (table 4). The minimum osmotic potential was –2.2 MPa and corresponded to the highest chloride concentration (17,821 g m^{-3}) in YM43. Osmotic potentials generally constituted ≤15% of the water potential. The profile for YM28 is an exception in that osmotic potentials constituted 1 to 74% of the water potential. The gravitational potential is estimated from the elevation above the water table and was relatively uniform in the shallow unsaturated zone (maximum range 0.3 MPa in YM36; table 4).

Typical water potential profiles measured in the laboratory had low potentials in the upper 7 ft (2 m) (–12 to –2 MPa) that increased with depth below the minimum to maximum values that ranged from –6 to –0.4 MPa in different profiles (table 4). The low water potentials indicate that the sediments are dry; the upward decrease in water potentials indicates an upward driving force for water flow. Boreholes drilled after rainfall had high water potentials near the surface that decreased sharply at the base of the wetting front (table 4).

Profiles in Blanca Draw sampled after long dry periods had low water potentials near surface (–10 to –12 MPa in YM43; fig. 3o, table 4). Many of the profiles in the ephemeral stream setting,

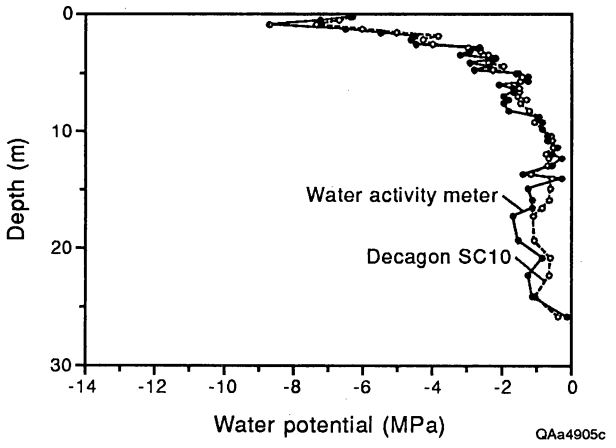

Figure 8. Comparison of water potential measured with a Decagon SC10 sample changer and water activity meter in soil samples from borehole YM28.

Table 4. Gravitational, water, total, and osmotic potentials of soil samples.

Borehole number	Depth (m)	Gravitational potential (MPa)	Water potential (MPa)	Total potential (MPa)	Depth (m)	Osmotic Potential (MPa)
	0.04	2.11	-6.49	-4.38	0.08	-0.01
	0.34	2.10	-0.56	1.55	0.39	0.00
	0.95	2.10	-4.63	-2.54	1.10	-0.15
	1.56	2.09	-7.45	-5.36	1.71	-0.75
	2.03	2.09	-7.65	-5.56	1.76	-0.96
	2.24	2.09	-7.48	-5.39	2.07	-1.22
	2.33	2.08	-7.41	-5.33	2.31	-1.11
	2.64	2.08	-7.21	-5.13	2.37	-0.94
	3.32	2.08	-6.11	-4.04	2.67	-0.87
	3.69	2.07	-6.20	-4.12	3.26	-0.83
	3.92	2.07	-6.20	-4.13	3.62	-0.68
	4.27	2.07	-5.96	-3.89	4.11	-0.66
	4.69	2.06	-6.28	-4.22	4.24	-0.78
YM9	5.00	2.06	-6.63	-4.57	4.75	-0.65
	5.52	2.05	-6.37	-4.31	4.99	-0.49
	5.65	2.05	-6.47	-4.41	5.37	-0.63
	5.96	2.05	-6.29	-4.24	5.74	-0.55
	6.25	2.05	-6.04	-3.99	5.95	-0.47
	6.63	2.04	-6.85	-4.80	6.20	-0.61
	7.01	2.04	-5.97	-3.93	6.62	-0.66
	7.04	2.04	-5.77	-3.73	6.59	-0.79
	7.50	2.03	-5.56	-3.53	6.99	-0.68
	7.68	2.03	-5.92	-3.88	7.32	-0.78
	7.96	2.03	-5.99	-3.96	7.93	-0.65
	8.21	2.03	-5.80	-3.77	8.54	-0.73
	8.56	2.02	-6.08	-4.06	8.83	-0.71
	8.87	2.02	-6.58	-4.55	9.17	-0.66
	9.11	2.02	-6.69	-4.67	9.70	-0.66
	9.56	2.01	-6.37	-4.35	10.05	-0.93
	10.00	2.01	-6.12	-4.11	10.69	-0.66
	10.50	2.00	-6.30	-4.29	11.25	-0.68
	11.10	2.00	-5.44	-3.44	12.64	-0.71
	11.70	1.99	-5.08	-3.09	13.17	-0.60
	12.60	1.98	-5.97	-3.99	13.82	-0.62
	13.20	1.98	-5.33	-3.35		
	13.90	1.97	-5.19	-3.22		
	0.05	2.11	-4.80	-2.69	0.01	-0.01
	0.12	2.11	-2.12	-0.01	0.02	0.00
	0.20	2.11	-1.56	0.54	0.16	0.00
	0.27	2.11	-1.33	0.77	0.24	0.00
	0.35	2.10	-1.19	0.92	0.31	0.00
	0.43	2.10	-1.06	1.04	0.39	0.00
	0.56	2.10	-1.12	0.98	0.50	-0.01
	0.91	2.10	-4.61	-2.51	0.86	-0.43
	1.18	2.10	-6.04	-3.94	1.14	-1.08
	1.49	2.09	-6.19	-4.10	1.44	-1.73

Table 4. cont.

Borehole number	Depth (m)	Gravitational potential (MPa)	Water potential (MPa)	Total potential (MPa)	Depth (m)	Osmotic Potential (MPa)
YM10	1.79	2.09	-6.72	-4.63	1.74	-1.73
	2.10	2.09	**-7.16**	-5.07	2.05	-1.00
	2.40	2.08	-6.96	-4.88	2.35	-0.81
	2.74	2.08	-6.77	-4.69	2.69	-0.67
	3.03	2.08	-6.51	-4.43	3.03	-0.70
	3.32	2.08	-6.60	-4.52	3.27	-0.77
	3.71	2.07	-6.55	-4.48	3.67	-0.65
	3.92	2.07	-6.25	-4.18	3.88	-0.72
	4.26	2.07	-6.71	-4.64	4.21	-0.72
	4.53	2.06	-6.75	-4.69	4.49	-0.72
	4.81	2.06	-6.77	-4.71	4.76	-0.71
	5.48	2.05	-5.91	-3.86	5.75	-0.73
	5.80	2.05	-6.05	-4.00	6.13	-0.71
	6.18	2.05	-6.05	-4.00	6.41	-0.68
	6.45	2.04	-5.57	-3.52	7.08	-0.58
	7.10	2.04	-5.68	-3.65	7.69	-0.60
	7.73	2.03	-5.77	-3.74	8.33	-0.67
	8.37	2.03	-5.71	-3.68	8.85	-0.62
	8.89	2.02	-5.84	-3.82	9.76	-0.58
	9.81	2.01	-6.14	-4.12	10.71	-0.58
	10.80	2.00	-6.09	-4.09	11.65	-0.65
	11.70	1.99	-5.98	-3.98		
	0.27	2.11	-1.69	0.42	0.22	0.00
	0.57	2.10	**-8.72**	-6.62	0.53	0.00
	0.91	2.10	-3.24	-1.14	0.86	0.00
	1.18	2.10	-5.28	-3.18	1.14	0.00
	1.49	2.09	-5.25	-3.16	1.44	0.00
	1.85	2.09	-4.29	-2.20	1.81	0.00
	2.16	2.09	-3.17	-1.08	2.11	0.00
	2.43	2.08	-2.43	-0.34	2.39	0.00
	2.83	2.08	-2.61	-0.53	2.78	0.00
	3.13	2.08	-2.54	-0.46	3.09	-0.01
YM11	3.47	2.07	-1.86	0.22	3.42	-0.02
	3.77	2.07	-1.92	0.16	3.73	0.00
	4.05	2.07	-1.77	0.30	4.00	-0.01
	4.38	2.06	-1.79	0.28	4.34	-0.01
	4.72	2.06	-1.33	0.74	4.67	-0.01
	5.45	2.05	-1.67	0.39	5.40	-0.01
	5.75	2.05	-1.54	0.51	5.71	-0.01
	6.45	2.04	-1.66	0.39	6.41	-0.02
	7.31	2.04	-1.51	0.53	7.26	-0.03
	8.25	2.03	-1.68	0.34	8.21	-0.05
	0.26	2.11	-2.85	-0.75	0.22	-0.07
	0.53	2.10	-6.15	-4.04	0.46	-0.23
	0.59	2.10	-6.52	-4.41	0.83	-0.57

Table 4. cont.

Borehole number	Depth (m)	Gravitational potential (MPa)	Water potential (MPa)	Total potential (MPa)	Depth (m)	Osmotic Potential (MPa)
	1.19	2.10	-6.55	-4.45	1.15	-0.74
	1.46	2.09	-5.51	-3.42	1.42	-0.74
	1.83	2.09	-4.66	-2.57	1.81	-0.66
	2.12	2.09	-4.26	-2.17	2.10	-0.73
	2.42	2.08	-3.56	-1.48	2.40	-0.57
	2.71	2.08	-3.06	-0.97	2.69	-0.42
	3.02	2.08	-3.03	-0.95	2.99	-0.40
YM12	3.32	2.08	-2.60	-0.52	3.30	-0.33
	3.61	2.07	-2.22	-0.15	3.57	-0.23
	3.93	2.07	-1.68	0.39	3.91	-0.22
	4.22	2.07	-1.53	0.53	4.18	-0.17
	4.43	2.06	-1.32	0.74	4.40	-0.15
	5.27	2.06	-1.16	0.90	5.19	-0.10
	0.04	2.11	-0.07	2.03	0.08	0.00
	0.23	2.11	-0.10	2.00	0.27	0.00
	0.47	2.10	-1.55	0.56	0.51	0.00
	1.00	2.10	-0.91	1.19	1.00	-0.14
	1.18	2.10	-2.84	-0.74	1.14	-0.19
	1.58	2.09	-4.87	-2.77	1.53	-0.39
	2.07	2.09	-3.80	-1.71	2.02	-0.82
	2.16	2.09	-3.38	-1.30	2.08	-0.71
	2.40	2.08	-2.94	-0.86	2.51	-0.44
YM13	2.80	2.08	-2.68	-0.60	2.75	-0.45
	3.13	2.08	-2.55	-0.48	3.09	-0.48
	3.40	2.07	-2.24	-0.17	3.39	-0.26
	3.83	2.07	-2.88	-0.81	3.79	-0.34
	4.20	2.07	-2.89	-0.83	4.09	-0.27
	4.44	2.06	-2.66	-0.60	4.40	-0.22
	4.88	2.07	-3.54	-1.47	4.84	-0.27
	5.33	2.06	-3.43	-1.37	5.28	-0.25
	5.90	2.05	-3.20	-1.15	5.86	-0.21
	6.40	2.05	-3.02	-0.98	6.35	-0.24
	7.28	2.04	-2.99	-0.96	7.23	-0.26
	7.76	2.03	-3.06	-1.03	7.72	-0.22
	8.43	2.03	-2.95	-0.92	8.39	-0.21
	8.98	2.02	-3.03	-1.01	8.94	-0.22
	9.44	2.02	-3.41	-1.39	9.40	-0.20
	10.80	2.00	-3.14	-1.14	10.71	-0.20
	11.30	2.00	-3.13	-1.13	11.29	-0.17
	0.05	2.11	-0.23	1.88	0.01	0.00
	0.15	2.11	-0.17	1.94	0.10	0.00
	0.24	2.11	-0.41	1.69	0.19	0.00
	0.42	2.10	-1.74	0.36	0.37	-0.21
	0.91	2.10	-4.31	-2.21	0.86	-0.42
	1.25	2.10	-4.43	-2.33	1.17	-0.40

Table 4. cont.

Borehole number	Depth (m)	Gravitational potential (MPa)	Water potential (MPa)	Total potential (MPa)	Depth (m)	Osmotic Potential (MPa)
	1.52	2.09	-3.96	-1.87	1.47	-0.38
	2.04	2.09	-3.32	-1.23	1.99	-0.43
	2.49	2.08	-3.18	-1.10	2.45	-0.37
	2.86	2.08	-3.22	-1.14	2.81	-0.41
YM14	3.19	2.08	-3.52	-1.44	3.15	-0.45
	3.47	2.07	-3.67	-1.60	3.42	-0.39
	3.80	2.07	-3.94	-1.87	3.76	-0.34
	4.20	2.07	-3.67	-1.60	4.15	-0.37
	4.66	2.06	-3.58	-1.52	4.61	-0.38
	5.36	2.06	-4.33	-2.27	5.31	-0.38
	5.85	2.05	-4.31	-2.26	5.80	-0.34
	6.48	2.04	-3.96	-1.92	6.44	-0.31
	7.28	2.04	-3.63	-1.59	7.23	-0.32
	7.80	2.03	-3.63	-1.60	7.75	-0.30
	8.56	2.02	-3.99	-1.97	8.51	-0.29
	9.56	2.01	-3.52	-1.51	9.52	-0.29
	0.04	2.11	-0.19	1.91	2.52	0.00
	0.13	2.11	-0.06	2.04	2.61	0.00
	0.41	2.10	-0.12	1.99	2.71	0.00
	0.50	2.10	-0.11	1.99	2.80	0.00
	0.56	2.10	-0.21	1.90	2.89	0.00
	0.59	2.10	-0.08	2.02	3.04	0.00
	0.99	2.10	-0.12	1.98	3.47	0.00
	1.17	2.10	-0.06	2.04	3.65	0.00
	1.72	2.09	-0.05	2.04	4.20	0.00
	1.81	2.09	-0.09	2.00	4.29	0.00
	1.98	2.09	-0.15	1.94	4.47	0.00
YM15	2.40	2.08	-0.20	1.89	5.39	0.00
	2.74	2.08	-0.61	1.47	5.55	0.00
	2.98	2.08	-0.29	1.79	5.74	0.00
	3.12	2.08	-0.36	1.72	6.07	0.00
	3.35	2.08	-0.23	1.85	6.29	0.00
	3.68	2.07	-0.24	1.83	6.62	0.00
	3.90	2.07	-0.30	1.77	6.96	0.00
	4.23	2.07	-0.37	1.70	7.48	0.00
	4.39	2.06	-0.44	1.62	8.34	0.00
	5.08	2.06	-1.02	1.04	9.24	0.00
	5.95	2.05	-0.35	1.70	9.76	0.00
	6.85	2.04	-0.39	1.65	10.25	0.00
	7.37	2.04	-0.26	1.77	11.24	0.00
	7.86	2.03	-0.29	1.74	11.53	0.00
	7.81	2.03	-0.30	1.74	12.82	0.00
	9.14	2.02	-0.26	1.76	13.62	0.00
	10.40	2.01	-0.31	1.70	14.65	0.00
	11.20	2.00	-0.47	1.52	15.52	0.00

Table 4. cont.

Borehole number	Depth (m)	Gravitational potential (MPa)	Water potential (MPa)	Total potential (MPa)	Depth (m)	Osmotic Potential (MPa)
	12.30	1.99	-0.50	1.49	17.26	0.00
	13.10	1.98	-0.32	1.66	18.33	0.00
	14.90	1.96	-0.38	1.59		
	16.00	1.95	-0.50	1.45		
	0.05	2.11	-0.60	1.51	0.01	0.00
	0.15	2.11	-0.48	1.62	0.10	0.00
	0.24	2.11	-0.41	1.70	0.19	0.00
	0.33	2.10	-0.32	1.78	0.28	0.00
	0.42	2.10	-0.25	1.85	0.37	0.00
	0.91	2.10	-0.62	1.48	0.86	0.00
	1.18	2.10	-1.02	1.08	1.14	-0.21
	1.43	2.09	-2.65	-0.56	1.38	-0.33
	1.52	2.09	-4.10	-2.00	1.71	-0.32
	2.07	2.09	-5.23	-3.14	2.02	-0.33
	2.40	2.08	-3.79	-1.71	2.35	-0.29
	2.71	2.08	-3.28	-1.19	2.66	-0.24
	3.04	2.08	-4.74	-2.66	2.99	-0.21
	3.32	2.08	-4.92	-2.85	3.27	-0.19
	3.62	2.07	-3.04	-0.97	3.57	-0.19
	3.92	2.07	-3.07	-1.00	3.88	-0.22
YM16	4.23	2.07	-3.61	-1.54	4.18	-0.17
	4.56	2.06	-4.27	-2.21	4.52	-0.24
	5.18	2.06	-3.89	-1.83	5.04	-0.18
	5.92	2.05	-3.65	-1.60	5.88	-0.16
	6.18	2.05	-2.98	-0.93	6.13	-0.16
	6.79	2.04	-3.27	-1.23	6.74	-0.14
	8.01	2.03	-2.93	-0.90	7.96	-0.19
	8.71	2.02	-3.41	-1.38	8.66	-0.23
	10.10	2.01	-3.49	-1.48	10.01	-0.16
	11.50	1.99	-4.06	-2.07	11.50	-0.26
	12.50	1.99	-2.13	-0.15	12.47	-0.15
	13.40	1.98	-2.68	-0.71	13.39	-0.14
	14.50	1.97	-2.98	-1.02	14.42	-0.11
	0.23	2.11	-6.31	-4.20	0.53	-0.04
	0.53	2.10	-6.71	-4.60	1.30	-0.28
	0.90	2.10	-7.37	-5.27	1.60	-0.42
	1.27	2.10	-6.05	-3.95	1.91	-0.56
	1.57	2.09	-5.03	-2.94	2.21	-0.64
	1.86	2.09	-3.84	-1.75	2.55	-0.75
	2.18	2.09	-4.28	-2.20	2.85	-0.71
	2.55	2.08	-3.98	-1.90	3.15	-0.69
	2.85	2.08	-2.97	-0.89	3.46	-0.67
	3.16	2.08	-2.63	-0.56	3.76	-0.66
	3.46	2.07	-2.38	-0.31	4.07	-0.63
	3.76	2.07	-2.18	-0.11	4.40	-0.66

Table 4. cont.

Borehole number	Depth (m)	Gravitational potential (MPa)	Water potential (MPa)	Total potential (MPa)	Depth (m)	Osmotic Potential (MPa)
	4.10	2.07	-2.40	-0.33	4.71	-0.59
	4.40	2.06	-1.95	0.12	5.01	-0.59
	4.71	2.06	-2.26	-0.20	5.32	-0.56
	5.01	2.06	-1.61	0.45	5.65	-0.58
	5.32	2.06	-1.42	0.64	5.93	-0.55
	5.65	2.05	-1.48	0.57	6.26	-0.51
	5.99	2.05	-1.66	0.39	6.57	-0.50
	6.29	2.05	-1.51	0.54	6.87	-0.47
	6.60	2.04	-1.50	0.54	7.21	-0.54
	6.90	2.04	-1.56	0.49	7.82	-0.44
	7.24	2.04	-1.31	0.73	8.24	-0.44
	7.57	2.03	-1.47	0.57	8.76	-0.42
	8.18	2.03	-1.23	0.80	9.37	-0.40
	8.73	2.02	-0.93	1.09	9.80	-0.39
	9.16	2.02	-1.06	0.96	10.30	-0.40
	9.77	2.01	-0.84	1.17	10.90	-0.37
	10.40	2.01	-0.58	1.43	11.40	-0.37
	10.70	2.00	-0.55	1.45	11.80	-0.43
YM28	11.40	2.00	-0.55	1.45	12.50	-0.40
	12.00	1.99	-0.75	1.24	12.90	-0.39
	12.30	1.99	-0.66	1.33	13.40	-0.39
	12.90	1.98	-0.69	1.29	14.00	-0.37
	13.60	1.97	-1.16	0.81	14.60	-0.34
	14.00	1.97	-0.57	1.40	15.10	-0.35
	15.00	1.96	-0.61	1.35	16.00	-0.33
	15.90	1.95	-0.64	1.31	16.70	-0.35
	16.50	1.95	-0.85	1.10	17.60	-0.41
	17.30	1.94	-1.10	0.84	18.20	-0.35
	19.30	1.92	-1.07	0.84	19.10	-0.35
	20.80	1.90	-0.62	1.29	20.70	-0.35
	22.30	1.89	-0.65	1.24	22.20	-0.32
	24.10	1.87	-1.03	0.84	23.70	-0.28
	25.80	1.85	-0.39	1.46	25.20	-0.29
	0.23	2.11	-2.28	-0.17	0.29	0.00
	0.53	2.10	-0.58	1.53	0.59	0.00
	0.84	2.10	-0.93	1.17	0.90	0.00
	1.20	2.10	-0.35	1.75	1.26	0.00
	1.51	2.09	-0.37	1.72	1.57	0.00
	1.81	2.09	-0.35	1.74	1.87	0.00
	2.12	2.09	-0.31	1.78	2.18	0.00
	2.52	2.08	-0.33	1.75	2.58	0.00
	2.76	2.08	-0.30	1.78	2.82	0.00
	3.06	2.08	-0.30	1.78	3.12	0.00
	3.37	2.07	-0.31	1.76	3.43	0.00
	3.67	2.07	-0.31	1.76	3.73	0.00

Table 4. cont.

Borehole number	Depth (m)	Gravitational potential (MPa)	Water potential (MPa)	Total potential (MPa)	Depth (m)	Osmotic Potential (MPa)
	4.04	2.07	-0.38	1.69	4.10	0.00
	4.31	2.07	-0.36	1.70	4.37	0.00
	4.62	2.06	-0.41	1.66	4.68	0.00
	4.89	2.06	-0.38	1.68	4.95	0.00
	5.35	2.06	-0.45	1.60	5.41	0.00
	5.87	2.05	-0.61	1.44	5.93	-0.03
	6.17	2.05	-0.33	1.72	6.23	0.00
	6.48	2.04	-0.40	1.64	6.54	0.00
	7.03	2.04	-0.88	1.16	7.03	0.00
	7.70	2.03	-0.64	1.39	7.09	0.00
	8.15	2.03	-0.62	1.40	7.76	0.00
	8.67	2.02	-0.54	1.48	8.15	0.00
YM35	9.10	2.02	-0.81	1.21	8.21	-0.02
	9.71	2.01	-1.60	0.41	8.67	-0.02
	10.30	2.01	-1.90	0.10	9.10	-0.12
	10.70	2.00	-2.72	-0.72	9.68	0.00
	11.30	2.00	-2.44	-0.45	11.32	-0.66
	11.80	1.99	-2.84	-0.85	14.31	-0.64
	12.20	1.99	-4.11	-2.12	17.42	-0.63
	12.80	1.98	-5.04	-3.06	20.47	-0.66
	13.30	1.98	-4.80	-2.82		
	14.20	1.97	-4.58	-2.62		
	15.80	1.95	-4.65	-2.70		
	16.50	1.95	-5.00	-3.05		
	14.90	1.96	-5.41	-3.45		
	17.40	1.94	-4.89	-2.95		
	18.00	1.93	-4.89	-2.95		
	18.90	1.92	-4.54	-2.62		
	19.40	1.92	-4.68	-2.76		
	20.40	1.91	-4.32	-2.41		
	0.23	2.11	-11.50	-9.42	0.59	-1.00
	0.53	2.10	-9.79	-7.68	1.05	-0.95
	0.99	2.10	-9.52	-7.42	1.36	-0.84
	1.30	2.10	-7.77	-5.68	1.66	-0.79
	1.60	2.09	-6.92	-4.82	1.97	-0.88
	1.91	2.09	-7.69	-5.60	2.27	-0.85
	2.21	2.09	-6.22	-4.13	2.58	-0.85
	2.85	2.08	-7.41	-5.33	3.22	-0.78
	3.15	2.08	-7.16	-5.09	3.52	-0.74
	3.46	2.07	-7.14	-5.07	3.83	-0.61
	3.76	2.07	-7.79	-5.72	4.13	-0.74
	4.07	2.07	-8.90	-6.84	4.47	-0.42
	4.40	2.06	-7.49	-5.42	4.77	-0.73
	4.71	2.06	-7.78	-5.72	5.07	-0.64
	5.01	2.06	-7.65	-5.59	5.47	-0.68

Table 4. cont.

Borehole number	Depth (m)	Gravitational potential (MPa)	Water potential (MPa)	Total potential (MPa)	Depth (m)	Osmotic Potential (MPa)
	5.96	2.05	-8.41	-6.36	6.32	-0.65
	6.26	2.05	-7.82	-5.77	6.63	-0.64
	6.57	2.04	-6.56	-4.52	8.21	-0.61
	6.87	2.04	-6.73	-4.68	9.86	-0.60
	7.24	2.04	-6.66	-4.62	11.30	-0.43
	7.64	2.03	-6.61	-4.58	12.80	-0.63
	8.15	2.03	-6.35	-4.33	14.50	-0.71
	8.61	2.02	-6.18	-4.16	16.10	-0.63
	9.19	2.02	-6.95	-4.93	17.60	-0.67
	9.80	2.01	-7.74	-5.73	20.90	-0.67
	10.30	2.01	-6.69	-4.68	23.80	-0.69
	10.70	2.00	-6.35	-4.35	26.90	-0.66
	11.20	2.00	-6.26	-4.26	30.00	-0.75
	11.90	1.99	-5.81	-3.81		
	12.30	1.99	-6.06	-4.07		
	12.80	1.98	-6.08	-4.10		
YM36	13.20	1.98	-5.83	-3.85		
	13.70	1.97	-5.81	-3.83		
	14.50	1.97	-5.76	-3.79		
	15.40	1.96	-5.74	-3.79		
	16.00	1.95	-5.70	-3.75		
	17.00	1.94	-5.59	-3.64		
	17.60	1.94	-5.74	-3.81		
	18.50	1.93	-5.18	-3.25		
	19.10	1.92	-5.40	-3.48		
	19.90	1.91	-5.41	-3.49		
	20.80	1.90	-4.90	-2.99		
	22.10	1.89	-5.52	-3.63		
	23.50	1.88	-5.12	-3.24		
	25.30	1.86	-4.90	-3.04		
	26.80	1.85	-4.88	-3.03		
	29.90	1.81	-5.27	-3.46		
	0.04	2.11	-6.30	-4.20	0.08	0.00
	0.19	2.11	-6.46	-4.35	0.24	-0.02
	0.34	2.11	-4.52	-2.41	0.39	-0.01
	0.50	2.11	-4.52	-2.41	0.54	-0.01
	0.92	2.12	-5.23	-3.12	0.97	0.00
	1.07	2.12	-6.51	-4.39	1.33	0.00
	1.38	2.12	-5.34	-3.21	1.94	0.00
	1.68	2.12	-5.05	-2.93	2.25	0.00
	1.99	2.13	-5.53	-3.40	2.55	0.00
	2.84	2.14	-4.96	-2.82	2.89	0.00
	3.15	2.14	-3.44	-1.30	3.19	0.00
	3.45	2.14	-4.01	-1.87	3.50	0.00
	3.76	2.14	-3.79	-1.65	3.80	0.00

Table 4. cont.

Borehole number	Depth (m)	Gravitational potential (MPa)	Water potential (MPa)	Total potential (MPa)	Depth (m)	Osmotic Potential (MPa)
	4.03	2.15	-3.87	-1.72	4.08	0.00
	4.40	2.15	-3.24	-1.09	4.44	0.00
	4.70	2.15	-3.32	-1.17	4.75	0.00
	5.01	2.16	-3.16	-1.00	5.05	0.00
	5.31	2.16	-3.62	-1.46	5.36	0.00
	5.59	2.16	-3.67	-1.51	5.63	0.00
	5.95	2.17	-2.61	-0.45	6.00	0.00
	6.26	2.17	-2.61	-0.44	6.30	0.00
	6.96	2.18	-2.44	-0.26	7.00	0.00
	7.51	2.18	-2.39	-0.20	7.55	0.00
	8.12	2.19	-2.29	-0.10	8.16	0.00
YM41	8.73	2.19	-2.10	0.09	9.62	0.00
	9.58	2.20	-2.37	-0.17	11.18	0.00
	10.31	2.21	-2.50	-0.30	12.73	-0.04
	11.13	2.22	-2.09	0.13	14.29	-0.09
	11.86	2.22	-2.56	-0.34	15.84	-0.08
	12.69	2.23	-2.41	-0.18	17.40	-0.03
	13.39	2.24	-2.30	-0.06	20.60	-0.02
	14.24	2.25	-2.32	-0.07		
	14.94	2.25	-1.86	0.40		
	15.77	2.26	-2.27	-0.01		
	16.47	2.27	-1.28	0.99		
	17.35	2.28	-1.41	0.87		
	18.59	2.29	-1.75	0.54		
	19.21	2.30	-1.12	1.17		
	20.46	2.31	-1.23	1.08		
	22.01	2.32	-1.65	0.68		
	24.88	2.35	-1.21	1.14		
	0.04	2.11	-11.10	-8.98	0.08	-0.01
	0.19	2.11	-9.76	-7.65	0.24	-0.02
	0.34	2.10	-11.90	-9.78	0.39	-0.58
	0.50	2.10	-12.20	-10.10	0.54	-2.22
	0.65	2.10	-11.10	-8.97	0.69	-2.09
	0.80	2.10	-10.40	-8.26	0.85	-1.80
	1.23	2.10	-9.94	-13.20	1.27	-1.18
	1.53	2.09	-9.72	-7.63	1.58	-0.96
	1.84	2.09	-7.23	-5.14	1.88	-0.92
	2.14	2.09	-6.12	-4.04	2.19	-0.86
	2.39	2.08	-6.81	-4.73	2.43	-0.97
	2.78	2.08	-5.71	-3.63	2.83	-0.85
	3.09	2.08	-5.53	-3.46	3.13	-0.84
	3.39	2.07	-5.58	-3.50	3.44	-0.80
	3.70	2.07	-5.36	-3.29	3.74	-0.80
	4.00	2.07	-5.77	-3.70	4.05	-0.81
	4.34	2.07	-5.21	-3.14	4.38	-0.77

Table 4. cont.

Borehole number	Depth (m)	Gravitational potential (MPa)	Water potential (MPa)	Total potential (MPa)	Depth (m)	Osmotic Potential (MPa)
	4.64	2.06	-5.12	-3.06	4.69	-0.75
	4.95	2.06	-4.98	-2.92	4.99	-0.76
	5.25	2.06	-4.96	-2.90	5.30	-0.74
	5.56	2.05	-4.81	-2.75	5.60	-0.38
	5.89	2.05	-4.61	-2.56	5.94	-0.83
	6.20	2.05	-5.61	-3.56	6.24	-1.30
	6.81	2.04	-5.09	-3.05	6.85	-0.58
	7.45	2.03	-4.28	-2.25	8.10	-0.60
YM43	8.05	2.03	-3.70	-1.67	9.04	-0.57
	8.66	2.02	-3.21	-1.19	10.60	-0.54
	9.52	2.01	-2.43	-0.41	12.20	-0.54
	10.20	2.01	-3.31	-1.30	13.70	-0.48
	11.10	2.00	-3.94	-1.94	14.00	-0.45
	11.80	1.99	-4.27	-2.28	17.20	-0.42
	12.60	1.98	-3.11	-1.13	20.30	-0.40
	13.60	1.97	-4.52	-2.55		
	14.20	1.97	-3.87	-1.90		
	14.90	1.96	-4.57	-2.61		
	15.70	1.95	-3.21	-1.26		
	17.30	1.94	-4.02	-2.09		
	18.80	1.92	-3.44	-1.52		
	20.40	1.91	-3.34	-1.43		
	22.00	1.89	-3.00	-1.10		
	23.50	1.88	-4.30	-2.43		
	0.27	2.11	-5.32	-3.22	0.22	-0.01
	0.57	2.10	-7.15	-5.05	0.53	0.00
	0.97	2.10	-8.35	-6.25	0.92	0.00
	1.36	2.09	-7.07	-4.97	1.32	0.00
	1.67	2.09	-6.32	-4.22	1.62	0.00
	1.97	2.09	-5.19	-3.10	1.93	0.00
	2.28	2.09	-5.15	-3.06	2.23	0.00
	2.92	2.08	-3.84	-1.76	2.87	0.00
	3.22	2.08	-3.41	-1.34	3.18	0.00
	3.53	2.07	-3.54	-1.46	3.48	0.00
	3.83	2.07	-3.55	-1.48	3.79	-0.01
	4.14	2.07	-4.22	-2.15	4.09	-0.01
	4.47	2.06	-3.45	-1.38	4.43	0.00
	4.84	2.06	-2.77	-0.71	4.79	0.00
	5.14	2.06	-2.98	-0.93	5.10	0.00
	5.45	2.05	-2.88	-0.83	5.71	0.00
	6.03	2.05	-2.07	-0.02	5.98	0.00
	6.68	2.04	-2.65	-0.61	6.62	-0.01
YM54	8.04	2.03	-2.65	-0.62	7.99	0.00
	8.79	2.02	-2.77	-0.75	8.74	-0.01
	9.65	2.01	-2.01	0.00	9.61	0.00

Table 4. cont.

Borehole number	Depth (m)	Gravitational potential (MPa)	Water potential (MPa)	Total potential (MPa)	Depth (m)	Osmotic Potential (MPa)
	10.40	2.01	-2.59	-0.59	10.40	0.00
	11.20	2.00	-2.24	-0.24	11.20	0.00
	12.00	1.99	-2.49	-0.50	11.90	0.00
	12.80	1.98	-2.35	-0.36	12.70	-0.06
	14.20	1.97	-1.42	0.55	14.20	-0.04
	15.90	1.95	-1.03	0.93	15.80	-0.03
	17.30	1.94	-1.01	0.93	17.30	-0.05
	22.80	1.88	-0.46	1.42	22.00	-0.02
	0.27	2.11	-4.87	-2.77	0.22	-0.33
	0.57	2.10	-7.15	-5.05	0.53	-0.89
	1.33	2.09	-6.89	-4.79	1.29	-1.01
	1.61	2.09	-7.76	-5.67	1.56	-0.93
	1.94	2.09	-6.68	-4.60	1.90	-0.93
	2.25	2.09	-7.88	-5.79	2.20	-0.42
	2.89	2.08	-6.13	-4.05	2.84	-0.93
	3.19	2.08	-6.15	-4.08	3.15	-0.86
	3.50	2.07	-6.90	-4.82	3.45	-0.90
	3.80	2.07	-6.51	-4.44	3.76	-0.86
	4.12	2.07	-9.41	-7.34	4.06	-0.93
	4.63	2.06	-7.01	-4.95	4.58	-0.86
	4.93	2.06	-6.86	-4.80	4.88	-0.97
	5.24	2.06	-5.82	-3.76	5.19	-1.15
	6.00	2.05	-5.58	-3.53	5.95	-1.38
	6.30	2.05	-6.11	-4.07	6.26	-0.22
	6.61	2.04	-6.16	-4.11	6.56	-0.21
	6.91	2.04	-5.74	-3.70	6.87	-0.68
	7.17	2.04	-7.65	-5.61	6.96	-0.66
	7.55	2.03	-5.70	-3.66	7.51	-0.81
YM59	7.95	2.03	-5.72	-3.69	7.90	-0.73
	8.25	2.03	-6.11	-4.08	8.21	-0.88
	9.81	2.01	-5.67	-3.65	9.76	-0.49
	11.20	2.00	-5.57	-3.57	11.10	-0.31
	11.90	1.99	-5.93	-3.94	11.80	-0.66
	12.70	1.98	-5.47	-3.49	12.70	-0.88
	14.30	1.97	-5.35	-3.38	14.20	-0.66
	15.80	1.95	-5.47	-3.52	15.80	-0.56
	17.40	1.94	-4.91	-2.97	17.40	-1.04
	19.00	1.92	-5.18	-3.26	18.90	-0.44
	20.50	1.91	-4.86	-2.95	20.50	-0.61
	22.10	1.89	-5.08	-3.19	22.00	-0.60
	23.60	1.88	-4.93	-3.06	23.60	-0.83
	25.30	1.86	-4.93	-3.07	25.20	-0.88
	0.00				26.70	-0.81
	0.05	2.11	-43.61	-41.50	0.10	0.00
	0.21	2.11	-8.04	-5.93	0.28	-0.54

Table 4. cont.

Borehole number	Depth (m)	Gravitational potential (MPa)	Water potential (MPa)	Total potential (MPa)	Depth (m)	Osmotic Potential (MPa)
	0.36	2.11	-7.47	-5.35	0.43	-0.79
	0.51	2.11	-7.62	-5.51	0.59	-0.90
	0.66	2.11	-7.23	-5.12	0.74	-0.84
	0.82	2.12	-6.07	-3.95	0.89	-0.80
	0.97	2.12	-5.61	-3.49	1.04	-0.76
	1.12	2.12	-5.39	-3.27	1.20	-0.69
	1.43	2.12	-4.77	-2.65	1.50	-0.69
	2.04	2.13	-4.64	-2.51	1.81	-0.62
YM66	2.68	2.13	-5.17	-3.03	2.11	-0.61
	2.98	2.14	-4.64	-2.50	2.75	-0.54
	1.73	2.12	-4.53	-2.41	3.03	-0.58
	4.54	2.15	-3.69	-1.54	4.61	-0.49
	5.45	2.16	-3.62	-1.46	5.52	-0.46
	6.44	2.17	-4.13	-1.96	6.47	-0.43
	7.14	2.18	-4.15	-1.97	7.20	-0.47
	7.99	2.19	-3.91	-1.72	7.93	-0.45
	8.76	2.19	-5.24	-3.05	8.71	-0.43
	9.24	2.20	-3.78	-1.58	9.18	-0.45
	9.76	2.20	-3.64	-1.43	9.72	-0.51
	11.08	2.22	-3.75	-1.53	11.04	-0.40
	12.63	2.23	-3.47	-1.24	12.60	-0.40
	0.10	2.11	-5.04	-2.93	0.02	0.00
	0.25	2.11	-7.67	-5.56	0.18	0.00
	0.40	2.11	-7.48	-5.37	0.33	0.00
	0.56	2.11	-8.34	-6.23	0.48	0.00
	0.71	2.11	-7.59	-5.48	0.63	0.00
	0.86	2.12	-7.94	-5.82	0.78	0.00
	1.17	2.12	-5.45	-3.33	0.94	-0.10
	1.47	2.12	-3.97	-1.85	1.12	-0.06
	1.78	2.13	-3.95	-1.82	1.42	-0.36
	2.08	2.13	-3.92	-1.79	1.73	-0.44
	2.72	2.13	-2.75	-0.62	2.34	-0.53
YM70	3.03	2.14	-2.71	-0.57	2.67	-0.55
	3.33	2.14	-2.82	-0.68	2.98	-0.50
	3.64	2.14	-3.26	-1.12	3.28	-0.41
	3.94	2.15	-3.12	-0.97	3.59	-0.42
	4.28	2.15	-2.93	-0.78	3.89	-0.42
	4.58	2.15	-3.17	-1.01	4.84	-0.44
	5.19	2.16	-3.59	-1.43	5.14	-0.60
	5.83	2.16	-4.10	-1.94	5.60	-0.43
	6.74	2.17	-3.52	-1.34	6.85	-0.42
	7.69	2.18	-3.52	-1.34	7.83	-0.43
	8.60	2.19	-4.43	-2.23	8.53	-0.46
	9.55	2.20	-3.55	-1.34	9.47	-0.42
	0.10	2.11	-5.19	-3.08	0.02	0.00

Table 4. cont.

Borehole number	Depth (m)	Gravitational potential (MPa)	Water potential (MPa)	Total potential (MPa)	Depth (m)	Osmotic Potential (MPa)
	0.25	2.11	-8.29	-6.18	0.18	0.00
	0.40	2.11	-9.35	-7.24	0.33	0.00
	0.56	2.11	-8.99	-6.87	0.48	0.00
	0.71	2.11	-9.24	-7.12	0.63	0.00
YM71	0.86	2.12	-9.50	-7.39	0.78	-0.02
	1.17	2.12	-6.02	-3.90	1.12	-0.02
	1.47	2.12	-5.65	-3.52	1.42	-0.09
	1.78	2.13	-6.85	-4.72	1.73	-0.16
	2.08	2.13	-5.69	-3.56	2.03	-0.28
	2.39	2.13	-5.12	-2.99	2.34	-0.28
					2.64	-0.30
					2.95	-0.40
					3.25	-0.45
					3.56	-0.55
					3.86	-0.57
					4.20	-0.55
					4.50	-0.43
					4.96	-0.29
					5.75	-0.26
					6.67	-0.29
					8.07	-0.16
					8.71	-0.21
					9.32	-0.22
	0.10	2.11	-5.20	-3.09	0.02	0.00
	0.25	2.11	-6.81	-4.70	0.18	0.00
	0.40	2.10	-7.02	-4.92	0.33	0.00
	0.56	2.10	-6.19	-4.08	0.48	0.00
	0.71	2.10	-6.14	-4.04	0.63	0.00
	0.86	2.10	-5.20	-3.10	0.79	-0.04
	1.01	2.10	-4.97	-2.87	0.94	-0.16
	1.20	2.10	-2.67	-0.58	1.12	-0.26
	1.50	2.09	-3.16	-1.07	1.42	-0.39
	1.81	2.09	-3.66	-1.57	1.73	-0.53
	2.11	2.09	-3.76	-1.67	2.03	-0.56
	2.42	2.08	-3.88	-1.80	2.34	-0.54
	2.75	2.08	-2.89	-0.81	2.67	-0.37
	3.06	2.08	-3.04	-0.96	2.98	-0.32
YM72	3.36	2.07	-3.09	-1.02	3.28	-0.30
	3.67	2.07	-3.37	-1.30	3.59	-0.28
	3.97	2.07	-2.99	-0.92	3.89	-0.30
	4.27	2.07	-2.91	-0.85	4.84	-0.27
	4.61	2.06	-3.52	-1.46	5.14	-0.27
	5.07	2.06	-3.97	-1.91	5.60	-0.27
	6.01	2.05	-3.96	-1.92	6.85	-0.25
	6.93	2.04	-4.22	-2.18	7.83	-0.21

Table 4. cont.

Borehole number	Depth (m)	Gravitational potential (MPa)	Water potential (MPa)	Total potential (MPa)	Depth (m)	Osmotic Potential (MPa)
	7.90	2.03	-4.51	-2.48	8.91	-0.17
	0.10	2.11	-4.97	-2.86	0.02	0.00
	0.25	2.11	-5.74	-3.63	0.18	-0.01
	0.41	2.10	-6.21	-4.10	0.33	0.00
	0.56	2.10	-6.31	-4.21	0.48	0.00
	0.71	2.10	-6.10	-4.00	0.63	-0.07
	0.86	2.10	-5.89	-3.79	0.79	-0.44
	1.02	2.10	-6.15	-4.06	0.94	-0.91
	1.20	2.10	-4.52	-2.43	1.12	-0.98
	1.50	2.09	-4.14	-2.04	1.42	-0.93
	1.78	2.09	-4.59	-2.50	1.73	-0.90
	2.11	2.09	-3.82	-1.73	2.03	-0.72
	2.75	2.08	-3.11	-1.03	2.67	-0.40
YM73	3.06	2.08	-3.36	-1.29	2.98	-0.37
	3.36	2.07	-4.07	-2.00	3.28	-0.38
	3.67	2.07	-3.70	-1.62	3.59	-0.37
	3.97	2.07	-3.59	-1.52	3.89	-0.39
	4.31	2.07	-3.00	-0.93	4.23	-0.40
	4.61	2.06	-3.60	-1.54	4.53	-0.40
	5.22	2.06	-3.53	-1.47	5.14	-0.43
	6.17	2.05	-3.54	-1.50	6.09	-0.39
	6.93	2.04	-3.68	-1.64	6.85	-0.36
	7.84	2.03	-4.11	-2.08	7.80	-0.32
	8.76	2.02	-3.93	-1.91	8.70	-0.32
	9.58	2.01	-4.05	-2.03	9.50	-0.33
	0.10	2.11	-10.43	-8.33	0.02	0.00
	0.25	2.11	-9.47	-7.36	0.18	0.00
	0.40	2.11	-9.29	-7.17	0.33	0.00
	0.56	2.11	-8.69	-6.58	0.48	0.00
	0.71	2.11	-8.95	-6.84	0.63	0.00
	0.86	2.12	-9.29	-7.17	0.78	0.00
	1.23	2.12	-7.15	-5.03	1.15	-0.40
	1.53	2.12	-6.31	-4.19	1.46	-0.55
	1.84	2.13	-6.12	-3.99	1.76	-0.66
	2.14	2.13	-5.57	-3.44	2.07	-0.65
	2.45	2.13	-6.17	-4.04	2.37	-0.50
YM74	2.78	2.14	-3.44	-1.31	2.71	-0.35
	3.09	2.14	-3.45	-1.31	3.01	-0.31
	3.39	2.14	-3.56	-1.42	3.62	-0.40
	3.70	2.14	-2.96	-0.81	3.92	-0.37
	4.00	2.15	-4.88	-2.74	5.17	-0.25
	4.18	2.15	-3.20	-1.05	6.12	-0.25
	5.10	2.16	-3.63	-1.47	7.03	-0.21
	6.20	2.17	-2.87	-0.70	7.67	-0.21
	7.11	2.18	-3.69	-1.52	8.59	-0.21

Table 4. cont.

Borehole number	Depth (m)	Gravitational potential (MPa)	Water potential (MPa)	Total potential (MPa)	Depth (m)	Osmotic Potential (MPa)
	7.75	2.18	-3.52	-1.34	9.69	-0.20
	8.66	2.19	-4.35	-2.16		
	9.76	2.20	-3.68	-1.48		
	0.10	2.11	-9.47	-7.36	0.02	0.00
	0.25	2.11	-8.73	-6.62	0.18	0.00
	0.40	2.11	-9.35	-7.24	0.33	0.00
	0.56	2.11	-8.41	-6.29	0.48	0.00
	0.71	2.11	-8.41	-6.29	0.63	0.00
	0.86	2.12	-8.85	-6.73	0.78	0.00
	1.14	2.12	-5.10	-2.98	1.36	-0.51
	1.44	2.12	-6.97	-4.85	1.67	-0.62
	1.74	2.12	-4.18	-2.06	1.97	-0.42
	2.05	2.13	-3.86	-1.73	2.61	-0.44
	2.69	2.13	-2.02	0.12	2.92	-0.31
YM75	2.99	2.14	-2.15	-0.01	3.22	-0.45
	3.30	2.14	-2.53	-0.39	3.53	-0.48
	3.60	2.14	-2.37	-0.22	4.17	-0.61
	4.24	2.15	-2.48	-0.33	4.47	-0.60
	4.55	2.15	-2.94	-0.79	5.39	-0.51
	5.46	2.16	-3.06	-0.89	6.33	-0.53
	6.41	2.17	-3.58	-1.41	7.08	-0.52
	7.19	2.18	-5.94	-3.76	7.58	-0.53
	7.66	2.18	-5.01	-2.83	8.68	-0.39
	8.76	2.19	-4.79	-2.59	9.29	-0.36
	9.36	2.20	-6.14	-3.94	9.62	-0.37
	10.01	2.21	-5.69	-3.48		
	0.10	2.11	-5.21	-3.10	0.02	0.00
	0.25	2.11	-4.97	-2.86	0.18	0.00
	0.40	2.11	-5.72	-3.61	0.33	0.00
	0.56	2.11	-6.97	-4.86	0.48	0.00
	0.71	2.11	-5.72	-3.60	0.63	0.00
	0.86	2.12	-6.39	-4.27	0.78	0.00
	1.01	2.12	-8.22	-6.10	0.94	0.00
	1.20	2.12	-5.92	-3.80	1.12	0.00
	1.50	2.12	-6.50	-4.38	1.42	0.00
	1.81	2.13	-6.04	-3.92	1.73	-0.05
	2.11	2.13	-3.44	-1.31	2.03	-0.40
	2.40	2.13	-3.24	-1.11	2.34	-0.38
YM76	2.75	2.13	-2.10	0.04	2.71	-0.36
	3.06	2.14	-2.13	0.01	3.01	-0.36
	3.15	2.14	-1.95	0.19	3.31	-0.46
	3.36	2.14	-2.03	0.11	4.23	-0.48
	4.31	2.15	-1.97	0.18	4.99	-0.37
	5.68	2.16	-4.55	-2.39	6.55	-0.43
	6.62	2.17	-3.90	-1.73	7.98	-0.35

Table 4. cont.

Borehole number	Depth (m)	Gravitational potential (MPa)	Water potential (MPa)	Total potential (MPa)	Depth (m)	Osmotic Potential (MPa)
	8.05	2.19	-3.88	-1.69	8.74	-0.36
	8.82	2.19	-5.60	-3.41	9.50	-0.26
	9.58	2.20	-4.00	-1.79	10.29	-0.30
	9.73	2.20	-3.17	-0.96		
	10.37	2.21	-4.93	-2.72		
	0.25	2.11	-6.08	-3.97	0.18	0.00
	0.40	2.11	-6.68	-4.57	0.33	0.00
	0.56	2.11	-6.14	-4.02	0.48	0.00
	0.71	2.11	-6.08	-3.96	0.63	-0.07
	0.86	2.12	-7.24	-5.12	0.78	-0.11
	1.20	2.12	-5.56	-3.44	1.12	-0.17
	1.50	2.12	-4.15	-2.03	1.42	-0.23
	1.81	2.13	-3.57	-1.44	1.73	-0.34
	2.11	2.13	-2.89	-0.76	2.03	-0.45
	2.42	2.13	-2.81	-0.67	2.34	-0.59
	2.75	2.13	-2.10	0.03	2.67	-0.54
	3.97	2.15	-3.13	-0.98	2.98	-0.46
YM77	3.06	2.14	-2.38	-0.25	3.28	-0.42
	3.36	2.14	-2.66	-0.52	3.59	-0.39
	3.67	2.14	-2.93	-0.79	3.89	-0.37
	4.31	2.15	-3.49	-1.34	4.23	-0.32
	5.59	2.16	-5.62	-3.46	5.51	-0.27
	6.47	2.17	-5.17	-3.00	6.39	-0.23
	7.26	2.18	-6.08	-3.90	7.19	-0.27
	8.02	2.19	-5.07	-2.88	7.95	-0.26
	8.97	2.20	-3.75	-1.56	8.89	-0.26
	0.10	2.11	-11.33	-9.22	0.18	-0.07
	0.25	2.11	-9.48	-7.37	0.33	0.00
	0.40	2.11	-9.56	-7.45	0.48	0.00
	0.56	2.11	-9.90	-7.78	0.63	-0.03
	0.71	2.11	-6.90	-4.79	0.78	-0.03
	0.86	2.12	-7.28	-5.16	0.94	-0.04
	1.01	2.12	-8.23	-6.12	1.12	-0.06
	1.20	2.12	-5.91	-3.79	1.42	-0.10
	1.50	2.12	-4.78	-2.65	1.73	-0.11
	1.81	2.13	-4.23	-2.10	2.03	-0.18
	2.11	2.13	-2.19	-0.06	2.34	-0.26
	2.42	2.13	-1.44	0.69	2.67	-0.26
YM78	2.75	2.13	-1.47	0.66	2.98	-0.20
	3.06	2.14	-2.01	0.13	3.28	-0.21
	3.36	2.14	-2.17	-0.03	3.59	-0.23
	3.67	2.14	-1.88	0.26	3.89	-0.25
	3.97	2.15	-2.08	0.07	4.23	-0.31
	4.31	2.15	-1.81	0.34	4.53	-0.30
	4.61	2.15	-1.83	0.32	5.14	-0.29

Table 4. cont.

Borehole number	Depth (m)	Gravitational potential (MPa)	Water potential (MPa)	Total potential (MPa)	Depth (m)	Osmotic Potential (MPa)
	4.91	2.16	-3.19	-1.03	5.45	-0.28
	5.22	2.16	-2.19	-0.03	6.39	-0.32
	5.52	2.16	-2.23	-0.06	6.70	-0.27
	6.47	2.17	-2.51	-0.34	7.95	-0.27
	6.77	2.17	-2.62	-0.45		
	0.10	2.11	-7.98	-5.87	0.02	0.00
	0.25	2.11	-6.99	-4.88	0.18	0.00
	0.40	2.11	-6.88	-4.77	0.33	0.00
	0.56	2.11	-6.92	-4.81	0.48	0.00
	0.71	2.11	-7.35	-5.23	0.63	0.00
	0.86	2.12	-5.98	-3.86	0.78	0.00
	1.01	2.12	-7.16	-5.04	0.94	0.00
	1.36	2.12	-7.67	-5.55	1.24	0.00
	1.62	2.12	-3.67	-1.54	1.55	0.00
	3.03	2.14	-2.08	0.05	2.64	-0.40
	3.33	2.14	-2.82	-0.67	2.95	-0.29
	3.64	2.14	-3.66	-1.52	3.25	-0.21
	2.72	2.13	-2.51	-0.37	3.56	-0.42
YM80	3.94	2.15	-3.05	-0.90	3.86	-0.40
	4.28	2.15	-2.61	-0.46	4.20	-0.46
	4.58	2.15	-2.64	-0.49	4.50	-0.39
	5.49	2.16	-3.21	-1.04	5.42	-0.34
	6.44	2.17	-2.96	-0.79	6.36	-0.38
	7.38	2.18	-3.91	-1.73	7.31	-0.32
	8.30	2.19	-3.81	-1.62	8.22	-0.28
	9.24	2.20	-3.03	-0.83	9.17	-0.30
	10.16	2.21	-4.43	-2.22	10.08	-0.28
	0.10	2.11	-10.20	-8.05	0.02	0.00
	0.25	2.11	-9.27	-7.16	0.18	0.00
	0.40	2.10	-9.66	-7.56	0.33	0.00
	0.56	2.10	-9.74	-7.64	0.48	0.00
	0.71	2.10	-8.63	-6.53	0.63	0.00
	0.86	2.10	-8.31	-6.21	0.79	-0.03
	1.20	2.10	-8.28	-6.18	1.12	-0.09
YM81	1.50	2.09	-7.45	-5.35	1.42	-0.19
	2.75	2.08	-3.16	-1.08	2.67	-0.66
	3.06	2.08	-2.99	-0.91	2.98	-0.63
	4.31	2.07	-2.54	-0.47	4.23	-0.82
	4.61	2.06	-2.24	-0.18	4.53	-0.57
	6.45	2.04	-3.40	-1.36	6.38	-0.31
	8.27	2.03	-3.04	-1.01	8.19	-0.25
	9.43	2.02	-4.69	-2.68	9.35	-0.23
	9.70	2.01	-3.50	-1.49		
	0.27	2.11	-8.83	-6.73	0.22	-0.02
	0.57	2.10	-9.21	-7.11	0.53	-0.98

Table 4. cont.

Borehole number	Depth (m)	Gravitational potential (MPa)	Water potential (MPa)	Total potential (MPa)	Depth (m)	Osmotic Potential (MPa)
	0.69	2.10	-10.60	-8.53	0.66	-1.61
	1.35	2.09	-6.81	-4.72	1.32	-1.14
	1.67	2.09	-6.21	-4.11	1.62	-1.04
	1.98	2.09	-5.32	-3.23	1.93	-0.95
	2.28	2.09	-5.01	-2.92	2.23	-0.97
	2.61	2.08	-6.52	-4.43	2.54	-0.88
	2.92	2.08	-4.83	-2.75	2.87	-0.87
	3.22	2.08	-5.01	-2.93	3.18	-0.81
	3.53	2.07	-4.78	-2.71	3.48	-0.82
	3.83	2.07	-4.81	-2.74	3.79	-0.81
YM84	4.16	2.07	-5.74	-3.67	4.10	-0.83
	4.47	2.06	-4.12	-2.06	4.43	-1.00
	4.78	2.06	-4.23	-2.17	4.73	-0.80
	5.08	2.06	-4.34	-2.29	5.04	-0.77
	5.39	2.06	-5.09	-3.03	5.34	-0.78
	5.72	2.05	-4.72	-2.66	5.65	-0.77
	6.03	2.05	-5.76	-3.71	5.95	-0.78
	7.22	2.04	-4.05	-2.01	7.14	-0.71
	8.19	2.03	-3.52	-1.49	8.15	-0.68
	9.14	2.02	-4.01	-1.99	9.09	-0.66
	10.10	2.01	-4.16	-2.15	10.00	-0.61
	11.20	2.00	-4.05	-2.05	11.20	-0.58
					12.70	-0.57
	0.27	2.11	-7.86	-5.75	0.22	0.00
	0.57	2.11	-9.04	-6.92	0.53	0.00
	0.98	2.12	-9.68	-7.56	0.83	-0.02
	1.36	2.12	-6.93	-4.81	1.32	0.00
	1.67	2.12	-6.80	-4.67	1.62	0.00
	1.97	2.13	-6.08	-3.95	1.93	0.00
	2.28	2.13	-5.09	-2.96	2.23	0.00
	2.61	2.13	-7.55	-5.42	2.55	0.00
	2.92	2.14	-4.20	-2.07	2.87	0.00
	3.22	2.14	-4.20	-2.06	3.18	0.00
	3.53	2.14	-4.65	-2.50	3.48	0.00
	3.83	2.15	-3.15	-1.00	3.79	0.00
	4.47	2.15	-3.10	-0.94	4.49	0.00
	4.78	2.15	-3.19	-1.04	4.79	0.00
YM85	5.08	2.16	-3.31	-1.15	5.10	0.00
	5.39	2.16	-3.55	-1.38	5.40	0.00
	6.03	2.17	-3.42	-1.25	5.98	0.00
	6.94	2.18	-3.22	-1.04	6.90	-0.02
	8.10	2.19	-3.17	-0.98	8.05	-0.03
	8.83	2.19	-3.62	-1.43	8.79	-0.04
	9.65	2.20	-3.44	-1.24	9.61	-0.11
	10.39	2.21	-2.82	-0.61	10.34	-0.11

Table 4. cont.

Borehole number	Depth (m)	Gravitational potential (MPa)	Water potential (MPa)	Total potential (MPa)	Depth (m)	Osmotic Potential (MPa)
	11.21	2.22	-2.66	-0.44	11.16	-0.09
	11.94	2.22	-2.85	-0.63	11.89	-0.08
	12.79	2.23	-4.29	-2.05	14.27	-0.06
	14.32	2.25	-1.95	0.30	15.83	-0.04
	15.87	2.26	-1.08	1.18		
	0.27	2.11	-8.10	-5.99	0.22	0.00
	0.57	2.10	-8.85	-6.75	0.53	-0.03
	1.03	2.10	-9.51	-7.41	0.98	0.00
	1.39	2.09	-6.71	-4.61	1.35	0.00
	1.70	2.09	-6.16	-4.07	1.65	0.00
	2.00	2.09	-5.88	-3.79	1.96	0.00
	2.31	2.09	-6.21	-4.13	2.26	0.00
	2.95	2.08	-5.64	-3.56	2.90	0.00
	3.25	2.08	-5.42	-3.35	3.21	0.00
	3.56	2.07	-5.29	-3.22	3.51	0.00
	3.86	2.07	-5.36	-3.29	3.82	0.00
	4.11	2.07	-5.94	-3.87	4.06	0.00
	4.50	2.06	-4.39	-2.33	4.46	0.00
	4.81	2.06	-4.00	-1.93	4.76	0.00
	5.11	2.06	-3.75	-1.69	5.07	0.00
	5.42	2.05	-3.90	-1.84	5.37	0.00
	5.75	2.05	-6.34	-4.29	5.68	0.00
	6.67	2.04	-3.91	-1.87	6.53	0.00
	7.30	2.04	-5.00	-2.96	6.63	0.00
	8.13	2.03	-3.27	-1.25	8.08	0.00
YM86	8.86	2.02	-4.06	-2.04	8.82	0.00
	9.69	2.01	-3.54	-1.53	9.64	-0.01
	10.40	2.01	-4.46	-2.45	10.37	-0.02
	11.20	2.00	-3.44	-1.44	11.19	-0.03
					11.93	-0.04
					12.75	-0.03
					14.33	-0.02
					15.86	-0.03
					17.41	-0.05
					18.98	-0.02
					20.22	-0.02
	0.75	2.10	-4.89	-2.79	14.20	-0.02
	1.03	2.10	-6.47	-4.38	15.80	-0.03
	1.33	2.09	-6.03	-3.94	17.40	-0.03
	1.64	2.09	-5.46	-3.37	18.90	-0.02
	1.94	2.09	-5.26	-3.17	20.50	-0.01
	2.25	2.09	-4.95	-2.86	21.30	-0.02
	2.55	2.08	-8.66	-6.58		
	2.89	2.08	-3.96	-1.88		
	3.19	2.08	-4.51	-2.43		

Table 4. cont.

Borehole number	Depth (m)	Gravitational potential (MPa)	Water potential (MPa)	Total potential (MPa)	Depth (m)	Osmotic Potential (MPa)
	3.50	2.07	-3.95	-1.88		
	3.80	2.07	-3.60	-1.53		
	4.08	2.07	-4.82	-2.76		
	4.44	2.06	-2.35	-0.28		
	4.75	2.06	-2.07	-0.01		
	5.05	2.06	-1.74	0.32		
	5.36	2.06	-3.30	-1.25		
	5.63	2.05	-1.70	0.35		
	6.00	2.05	-2.92	-0.88		
	6.55	2.04	-2.30	-0.25		
	7.25	2.04	-3.76	-1.73		
	8.07	2.03	-2.55	-0.52		
YM87	8.80	2.02	-3.39	-1.37		
	9.62	2.01	-2.31	-0.30		
	10.40	2.01	-2.66	-0.65		
	11.20	2.00	-2.02	-0.02		
	11.90	1.99	-2.83	-0.84		
	12.70	1.98	-1.95	0.03		
	14.30	1.97	-1.28	0.69		
	15.80	1.95	-0.97	0.98		
	17.40	1.94	-0.76	1.18		
	19.00	1.92	-1.39	0.53		
	20.50	1.91	-1.37	0.53		
	21.30	1.90	-1.68	0.22		
	0.27	2.11	-3.03	-0.92	0.22	-0.02
	0.57	2.10	-2.90	-0.80	0.53	0.00
	1.15	2.10	-2.00	0.10	1.10	0.00
	1.46	2.09	-1.30	0.80	1.41	0.00
	1.76	2.09	-0.80	1.29	1.71	0.00
	2.07	2.09	-0.73	1.35	2.02	0.00
	2.39	2.08	-0.75	1.33	2.34	-0.04
	2.71	2.08	-0.64	1.45	2.66	-0.09
	3.01	2.08	-0.63	1.45	2.96	-0.06
	3.32	2.08	-0.63	1.44	3.57	-0.10
	3.62	2.07	-0.75	1.32	3.89	-0.09
	3.92	2.07	-1.11	0.96	4.21	-0.10
	4.26	2.07	-0.85	1.21	4.52	-0.07
	4.56	2.06	-0.62	1.45	4.82	-0.03
	4.87	2.06	-0.40	1.66	5.13	0.00
	5.17	2.06	-0.54	1.52	5.77	-0.08
YM88	5.81	2.05	-0.59	1.47	6.29	-0.28
	6.33	2.05	-1.23	0.82	7.06	-0.32
	7.05	2.04	-1.84	0.20	7.84	-0.53
	7.89	2.03	-1.61	0.43	8.59	-0.54
	8.63	2.02	-2.79	-0.77	9.15	-0.49

Table 4. cont.

Borehole number	Depth (m)	Gravitational potential (MPa)	Water potential (MPa)	Total potential (MPa)	Depth (m)	Osmotic Potential (MPa)
	9.20	2.02	-3.32	-1.30	9.73	-0.49
	9.78	2.01	-3.06	-1.05	10.90	-0.53
	10.70	2.00	-2.86	-0.85	11.70	-0.60
	11.70	1.99	-3.74	-1.75	12.50	-0.54
	12.60	1.98	-3.79	-1.81		
	0.27	2.11	-4.61	-2.50	0.22	-0.01
	0.57	2.10	-4.83	-2.73	0.53	-0.15
	0.88	2.10	-4.30	-2.20	0.83	-0.38
	1.39	2.09	-1.88	0.22	1.35	-0.28
	1.70	2.09	-2.10	0.00	1.65	-0.27
	2.00	2.09	-2.34	-0.25	1.96	-0.44
	2.31	2.09	-1.96	0.13	2.26	-0.46
	2.64	2.08	-2.52	-0.44	2.66	-0.30
	2.95	2.08	-2.39	-0.31	2.90	-0.34
	3.25	2.08	-2.37	-0.29	3.21	-0.37
	3.56	2.07	-1.96	0.12	3.51	-0.40
	3.86	2.07	-1.90	0.17	3.82	-0.33
	4.50	2.06	-1.64	0.42	4.46	-0.26
	4.81	2.06	-1.44	0.62	4.76	-0.30
	5.11	2.06	-1.52	0.54	5.07	-0.23
	5.42	2.05	-1.53	0.53	5.37	-0.20
	5.75	2.05	-2.38	-0.33	5.40	-0.28
YM89	6.06	2.05	-1.54	0.51	6.01	-0.17
	6.58	2.04	-1.82	0.23	6.53	-0.16
	7.28	2.04	-2.58	-0.54	7.23	-0.16
	8.16	2.03	-1.81	0.22	8.08	-0.16
	8.80	2.02	-2.21	-0.18	8.76	-0.14
	9.69	2.01	-1.92	0.09	9.64	-0.13
	10.40	2.01	-2.06	-0.05	10.40	-0.12
	11.20	2.00	-1.61	0.39	11.20	-0.12
	12.00	1.99	-2.06	-0.06	11.90	-0.11

however, were sampled after rainfall and had high water potentials near the surface (up to –0.6 MPa, YM9) that decreased sharply at the base of the wetting front (fig. 3c). Maximum water potentials measured at the base of the profiles in Blanca Draw ranged from –6.0 MPa (fig. 3c, YM10) to –0.5 MPa (fig. 3f, YM54). Water potentials in closely spaced profiles were similar.

In the interstream setting, water potentials were also generally low in the shallow subsurface and increased with depth (fig. 4, table 3). The lowest water potential was measured in a soil sample from YM66 (–44 MPa) at 0.16 ft (0.05 m) depth (table 3). Maximum water potentials measured at depths ≥ 26 ft (8 m) ranged from –3 to –5 MPa with the exception of YM28, which had maximum water potentials ≥ –1 MPa (fig. 4i). The monitoring record for the in situ psychrometers was insufficient to evaluate long-term fluctuations in water potential. A vertical profile based on data collected on August 13, 1993, showed water potentials as low as –6 MPa at 1 ft (0.3 m) depth, which increased to a maximum value of –2 MPa at 60.7 ft (18.5 m) depth (fig. 9). Deviations from the typical profiles were found in the fissured sediments and beneath the borrow pit (figs. 5 and 6). The fissured sediments had much higher water potentials in the upper 43 ft (13 m) than the sediments adjacent to the fissure (fig. 5). Within the fissure, water potentials were uniformly high (≥ –1 MPa) from 3 to 30 ft (1 to 9 m) depth in profile YM35 and decreased to –5 MPa from 30 to 43 ft (9 to 13 m) depth (fig. 5c). The general trend in the water potential profile 10 m distant (YM36) was an increase in water potential from –11.5 MPa near the surface to –5 MPa at 98-ft (30-m) depth. The relationship between water potentials in the other pair of profiles (YM88 and YM59; fig. 5f) in and adjacent to the fissure was similar to that described for profiles YM35 and YM36. Water potentials were generally greater than –0.5 MPa in the borrow pit, whereas water potentials in the profile drilled 10 m distant from the borrow pit (YM16) ranged from –5 to –2 MPa below the wetting front (YM16) (fig. 6c).

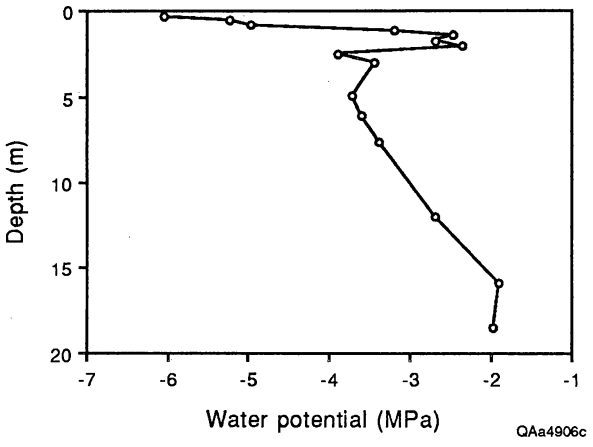

Figure 9. Profile of water potentials monitored by in situ psychrometers on August 13, 1993.

Permeameter Tests

Results of the K_{fs} estimates that neglected the unsaturated effect (equation 10) were analyzed to determine if soil heterogeneity in the test hole had a greater effect on the calculated hydraulic conductivities than the three different methods (equations 11, 12, and 16) of evaluating the C coefficient (table 5). The effect of soil heterogeneity was evaluated by comparing the K_{fs} estimates for the two ponding depths within each test hole. If the soil is homogenous, these K_{fs} estimates should be similar. For each test hole, K_{fs} values based on H_1 were compared with those based on H_2 to evaluate the effect of heterogeneity (F heterog) and K_{fs} values based on each equation were compared to evaluate the effect of the different equations (F method). Analysis of variance showed that in 73 % of the tests the different methods of calculating the C coefficient had a greater effect on the estimated K_{fs} values than soil heterogeneity. K_{fs}^{R} values based on equation 12 (Reynolds and others, 1983) were 9 to 38% higher than K_{fs}^{G} based on equation 11 (Glover, 1953) and K_{fs}^{X} values based on equation 16 (Xiang, 1994a) were 45 to 64% higher than K_{fs}^{G} based on equation 11. The results based on the new solution (K_{fs}^{X}, equation 16) are thought to be the most accurate because this pressure solution most closely approximates the actual pressure distribution.

The unsaturated effect was also included in the analysis of the permeameter data according to equation 18 (table 6). Inclusion of the unsaturated effect, which considers some of the water as capillary flow, generally results in lower K_{fs} values than when the unsaturated effect is neglected. Calculated matric flux potentials estimated from equation 18 were negative for all three methods of evaluating the C coefficient (equations 11, 12, and 16; GP2, GP4, GP12, GP15, GP21, and GP26; table 6) when K_{fs} values based on equation 10 (which ignores the unsaturated effect) were greater for the larger ponding depth (H_2) than for the smaller ponding depth (H_1) (table 5). Conversely, calculated K_{fs} values based on equation 18 were negative when K_{fs} values estimated from H_2 were much less than those from H_1 (GP22, tables 5 and 6). Therefore, equation (18)

Table 5. Calculated field saturated hydraulic conductivity (*Kfs*) values based on the permeameter data. These values were calculated using equation 10, which ignores the unsaturated effect.

No	D_b (m)	A (m^2)	H_1 (m)	Q_1 x10^{-6} (m/s)	H_2 (m)	Q_2 x10^{-6} (m/s)	Q_2/Q_1	K_{fs1}^G (m/s)	K_{fs2}^G (m/s)	K_{fs1}^R (m/s)	K_{fs2}^R (m/s)	K_{fs1}^X (m/s)	K_{fs2}^X (m/s)	F method	F heter.
GP1	0.25	0.003509	0.1	0.538	0.15	0.754	1.4	9.56E-06	7.73E-06	1.15E-05	9.97E-06	1.51E-05	1.18E-05	25.88	16.48
GP2	0.4	0.003509	0.15	0.143	0.25	0.394	2.76	1.46E-06	1.91E-06	1.89E-06	2.65E-06	2.23E-06	2.77E-06	27.77	40.14
GP3	0.25	0.003509	0.05	0.427	0.1	1.181	2.77	1.73E-05	2.10E-05	1.89E-05	2.53E-05	2.83E-05	3.32E-05	79.45	40.98
GP4	0.45	0.000215	0.05	0.071	0.1	0.155	2.18	2.86E-06	2.75E-06	3.13E-06	3.33E-06	4.70E-06	4.36E-06	44	0.28
GP5	0.25	0.003509	0.05	4.386	0.1	7.018	1.6	1.77E-04	1.25E-04	1.94E-04	1.51E-04	2.91E-04	1.97E-04	12.8	16.07
GP6	0.25	0.003509	0.05	5.556	--	--	--	2.25E-04	-	2.45E-04	-	3.69E-04	-	-	-
GP7	0.25	0.003509	0.05	0.643	0.15	1.135	1.77	2.60E-05	1.16E-05	2.84E-05	1.50E-05	4.27E-05	1.77E-05	3.4	22.49
GP8	0.25	0.003509	0.05	1.439	0.1	2.468	1.72	5.82E-05	4.38E-05	6.35E-05	5.30E-05	9.55E-05	6.94E-05	16.46	13.15
GP9	0.25	0.003509	0.05	4.187	0.1	5.954	1.42	1.69E-04	1.06E-04	1.85E-04	1.28E-04	2.78E-04	1.67E-04	9.09	20.3
GP10	0.25	0.003509	0.05	0.819	0.1	2.193	2.68	6.93E-05	5.21E-05	7.57E-05	6.30E-05	1.14E-04	8.25E-05	16.05	13.04
GP11	0.25	0.003509	0.05	0.55	0.1	0.819	1.49	2.22E-05	1.45E-05	2.43E-05	1.76E-05	3.65E-05	2.30E-05	10.59	19.25
GP12	0.25	0.003509	0.05	0.521	0.1	0.55	1.06	3.31E-05	3.89E-05	3.62E-05	4.71E-05	5.44E-05	6.17E-05	76.38	27.95
GP13	0.25	0.000215	0.05	0.039	0.1	0.072	1.85	1.59E-06	1.27E-06	1.74E-06	1.54E-06	2.62E-06	2.01E-06	19.25	9.58
GP14	0.25	0.003509	0.05	0.585	0.1	0.994	1.7	2.37E-05	1.77E-05	2.58E-05	2.13E-05	3.88E-05	2.80E-05	16.4	13.96
GP15	0.25	0.000215	0.05	0.018	0.1	0.057	3.17	7.25E-07	1.02E-06	7.91E-07	1.23E-06	1.19E-06	1.61E-06	48.91	72.53
GP16	0.25	0.003509	0.05	0.643	0.1	1.462	2.27	2.60E-05	2.60E-05	2.84E-05	3.14E-05	4.27E-05	4.11E-05	50.37	0.12
GP17	0.25	0.000215	0.05	<0.001	0.1	<0.002	--	<1.0E-7	<1.0E-7	<1.0E-7	<1.0E-7	< 1.0E-7	<1.0E-7	-	-
GP18	0.25	0.003509	0.05	0.234	0.1	0.526	2.25	9.46E-06	9.35E-06	1.03E-05	1.13E-05	1.55E-05	1.48E-05	48.21	0.02
GP19	0.25	0.003509	0.05	0.339	0.1	0.702	2.07	1.37E-05	1.25E-05	1.50E-05	1.51E-05	2.25E-05	1.97E-05	32.99	2.4
GP20	0.25	0.000215	0.05	0.022	0.1	0.05	2.27	8.99E-07	8.91E-07	9.81E-07	1.08E-06	1.47E-06	1.41E-06	49	0.05
GP21	0.25	0.003509	0.05	0.147	0.1	0.374	2.54	5.96E-06	6.65E-06	6.51E-06	8.03E-06	9.78E-06	1.05E-05	71.82	12.91
GP22	0.25	0.003509	0.05	1.714	0.1	2.936	1.71	2.11E-05	9.76E-06	2.30E-05	1.18E-05	3.46E-05	1.55E-05	5.05	28.27
GP23	0.25	0.003509	0.05	0.14	0.1	0.316	2.26	5.68E-06	5.61E-06	6.20E-06	6.78E-06	9.32E-06	8.88E-06	48.66	0.01
GP24	0.3	0.003509	0.05	1.205	0.1	2.164	1.8	4.87E-05	3.84E-05	5.32E-05	4.64E-05	8.00E-05	6.08E-05	19.32	10.75
GP25	0.3	0.003509	0.05	0.468	0.1	1.082	2.31	1.89E-05	1.92E-05	2.07E-05	2.32E-05	3.11E-05	3.04E-05	55.41	0.55
GP26	0.3	0.003509	0.05	0.573	0.1	1.491	2.6	2.32E-05	2.65E-05	2.53E-05	3.20E-05	3.80E-05	4.19E-05	74.93	19.56

A is the cross sectional area of the water column in the permeameter, Q_1 and Q_2 are the measured flow rates, H_1 and H_2 are the hydraulic hydraulic heads, and D_b is the borehole depth, subscripts 1 and 2 refer to estimates of K_{fs} using H_1 and H_2, superscript G refers to Glover's 1953 solution, superscript R refers to Reynolds and others, 1983 solution, and superscript X refers to the new Xiang (1994a) solution, F_{method} and $F_{heter.}$ are the F values obtained from the two variable analysis of variance analysis for method effect and heterogeneity (H_1 and H_2) effect, respectively.

Table 6. Calculated field saturated hydraulic conductivity (K_{fs}) values based on permeameter data.

No	A (m^2)	H_1 (m)	Q_1 x10^{-6} (m/s)	H_2 (m)	Q_2 x10^{-6} (m/s)	Q_2/Q_1	K_{fs}^G (m/s)	K_{fs}^R (m/s)	K_{fs}^X (m/s)	ϕ_m^R (1/m)	ϕ_m^G (1/m)	ϕ_m^X (1/m)
GP1	0.003509	0.1	0.538	0.15	0.754	1.4	3.84E-06	6.57E-06	4.30E-06	5.30E-07	6.02E-07	1.18E-06
GP2	0.003509	0.15	0.143	0.25	0.394	2.76	2.61E-06	3.85E-06	3.64E-06	-3.07E-07	-1.77E-07	-2.20E-07
GP3	0.003509	0.05	0.427	0.1	1.181	2.77	2.53E-05	3.29E-05	3.96E-05	-8.00E-07	-4.51E-07	-6.91E-07
GP4	0.000215	0.05	0.071	0.1	0.155	2.18	2.62E-06	3.56E-06	3.91E-06	-2.46E-08	1.35E-08	4.85E-08
GP5	0.003509	0.05	4.386	0.1	7.018	1.6	6.36E-05	1.01E-04	7.45E-05	5.32E-06	6.43E-06	1.33E-05
GP6	0.003509	0.05	5.556	–	–	–	–	–	–	–	–	–
GP7	0.003509	0.05	0.643	0.15	1.135	1.77	3.34E-06	7.22E-06	1.62E-06	1.21E-06	1.28E-06	2.53E-06
GP8	0.003509	0.05	1.439	0.1	2.468	1.72	2.72E-05	4.07E-05	3.52E-05	1.31E-06	1.75E-06	3.71E-06
GP9	0.003509	0.05	4.187	0.1	5.954	1.42	3.21E-05	6.15E-05	2.27E-05	7.06E-06	7.75E-06	1.57E-05
GP10	0.003509	0.05	0.819	0.1	2.193	2.68	3.23E-05	4.83E-05	4.17E-05	1.57E-06	2.09E-06	4.43E-06
GP11	0.003509	0.05	0.55	0.1	0.819	1.49	5.64E-06	9.79E-06	5.40E-06	8.28E-07	9.37E-07	1.91E-06
GP12	0.003509	0.05	0.521	0.1	0.55	1.06	4.57E-05	5.97E-05	7.12E-05	-1.34E-06	-7.09E-07	-1.04E-06
GP13	0.000215	0.05	0.039	0.1	0.072	1.85	9.01E-07	1.30E-06	1.23E-06	2.51E-08	3.92E-08	8.55E-08
GP14	0.003509	0.05	0.585	0.1	0.994	1.7	1.07E-05	1.61E-05	1.37E-05	5.55E-07	7.31E-07	1.54E-06
GP15	0.000215	0.05	0.018	0.1	0.057	3.17	1.36E-06	1.74E-06	2.16E-06	-5.41E-08	-3.57E-08	-6.00E-08
GP16	0.003509	0.05	0.643	0.1	1.462	2.27	2.59E-05	3.48E-05	3.90E-05	-3.64E-07	7.47E-09	2.28E-07
GP17	0.000215	0.05	<0.001	0.1	<0.002	–	< 1.0E-7	< 1.0E-7	<1.0E-7	–	–	–
GP18	0.003509	0.05	0.234	0.1	0.526	2.25	9.21E-06	1.24E-05	1.38E-05	-1.18E-07	1.42E-08	1.04E-07
GP19	0.003509	0.05	0.339	0.1	0.702	2.07	1.10E-05	1.51E-05	1.61E-05	-9.23E-09	1.53E-07	3.96E-07
GP20	0.000215	0.05	0.022	0.1	0.05	2.27	8.82E-07	1.19E-06	1.33E-06	-1.17E-08	9.62E-10	9.18E-09
GP21	0.003509	0.05	0.147	0.1	0.374	2.54	7.44E-06	9.79E-06	1.15E-05	-1.88E-07	-8.34E-08	-1.05E-07
GP22	0.003509	0.05	1.714	0.1	2.936	1.71	-3.30E-06	-1.17E-06	-9.52E-06	1.38E-06	1.38E-06	2.71E-06
GP23	0.003509	0.05	0.14	0.1	0.316	2.26	5.53E-06	7.44E-06	8.30E-06	-7.11E-08	8.53E-09	6.25E-08
GP24	0.003509	0.05	1.205	0.1	2.164	1.8	2.65E-05	3.86E-05	3.58E-05	8.37E-07	1.26E-06	2.72E-06
GP25	0.003509	0.05	0.468	0.1	1.082	2.31	1.95E-05	2.62E-05	2.96E-05	-3.14E-07	-3.48E-08	9.15E-08
GP26	0.003509	0.05	0.573	0.1	1.491	2.6	3.03E-05	3.97E-05	4.70E-05	-8.24E-07	-4.01E-07	-5.50E-07

should not be used for evaluation of K_{fs} and/or matric flux potential when the soil is obviously heterogeneous.

The conductivities evaluated using equations 12 (K_{fs}^{R}); Reynolds and others, 1983) and 16 (K_{fs}^{X}, the new solution, Xiang, 1994a) were similar in many of the tests (table 6). This similarity can be explained by examining the C coefficients and the ponding depths H_1 and H_2 for each test. The difference in estimated K_{fs} values calculated by the two methods (equations 12 and 16) depends on the ratio of the coefficient difference (ΔC_1) from the two solutions for the first ponding depth (H_1) and the coefficient difference from the two solutions (ΔC_2) for the second ponding depth (H_2). If the following relationship exists,

$$\frac{\Delta C_1}{\Delta C_2} \approx \frac{H_1}{H_2}\frac{Q_{t2}}{Q_{t1}} \tag{31}$$

where $\Delta C_i = C_i - C_i^{**}$ (C is calculated by equation 12 and C_i^{**} is calculated by equation 16), then equations 12 (Reynolds and others, 1983) and 16 (Xiang, 1994a) provide similar results. When the ratio of the flow rates (Q_2/Q_1) changes greatly, however, equation (31) does not hold and the conductivities estimated by equations 12 (K_{fs}^{R}) and 16 (K_{fs}^{X}) differ, as shown by results from GP2, GP5, GP7, GP9, and GP11 (table 6).

In cases where K_{fs} or ϕ_m were negative (table 6), the estimated results using equation 10 that neglected the unsaturated effect ($\phi_m = 0$) should be used (table 5). K_{fs} based on the Guelph permeameter data ranged from $\leq 10^{-7}$ to 10^{-4} m s^{-1} (tables 5 and 6). Hydraulic conductivities were highest in the borrow pit (GP5, GP6; table 6, fig. 2). Sediments at this site are sandy and loosely consolidated. Hydraulic conductivities were lowest in Blanca Draw (GP7, GP13, GP15, GP17, and GP20, fig. 2). The hydraulic conductivity in GP17, which was in Blanca Draw, was extremely low and was estimated to be $\leq 10^{-7}$ m s^{-1}.

Constant-Head Borehole Infiltration Tests

Analysis of the constant-head borehole infiltration tests was limited to evaluation of the field saturated flow component of the hydraulic conductivity (table 7). Only one head measurement was used because of potential problems related to soil heterogeneity. Preliminary analysis showed that neglecting flow out of the bottom of the borehole resulted in errors of less than 1%; therefore, equation 9 was used in the final analysis, which neglects flow out of the bottom of the borehole.

Results from the constant-head borehole infiltration tests showed that when the ratio H/a was large, conductivities based on equations 12 (Reynolds and others, 1983) and 21 (the new solution) were almost identical and were up to 60% higher than those based on equation 11 (Glover, 1953). Glover's solution overestimates the pressure on the top of the borehole, which results in the low hydraulic conductivities. The range in K_{fs} estimated by the new solution was approximately two orders of magnitude (10^{-8} to 10^{-6} m s^{-1}). Hydraulic conductivities did not seem to vary systematically with geomorphic setting. The lowest (YM78: 10^{-8} m s^{-1}) and highest (YM80: 10^{-6} m s^{-1}) hydraulic conductivities were measured in the interstream setting.

Multistep Constant-Head Borehole Infiltration Tests

The unsaturated effect was neglected in estimating the hydraulic conductivity of layered soils. In order to consider the unsaturated effect, two boreholes of different radii are required; however, all boreholes drilled in the study area had the same radius. Equation 27 was used to calculate K_{fs}. The conductivities of layered soils, evaluated by the computer code LAYERK, are shown in table 8. Because the backfilled sediments were generally loose and had a high conductivity, their effect on the flow from the borehole was not included.

Results indicate that the hydraulic conductivity of individual layers varied up to three orders of magnitude (YM80 and YM84, table 8). Information on vertical variability in hydraulic conductivity is important for evaluation of flow and contaminant transport. In general, the geometric average conductivity obtained from the multistep constant-head borehole infiltration test

Table 7. Calculated field saturated hydraulic conductivity (K_{fs}) values for deep soil using the constant head borehole infiltration tests.

BN	H (m)	H/a	Q (m^3/s)	C^G	K_{fs}^G(m/s)	C^R	K_{fs}^R(m/s)	C^X	K_{fs}^X(m/s)
YM21	8.69	85.5	1.325E-04	4.153	1.16E-06	6.944	1.94E-06	7.016	1.96E-06
YM34	2.71	26.7	8.330E-06	3.015	5.43E-07	4.716	8.49E-07	4.792	8.63E-07
YM45	10.08	99.21	9.042E-05	4.300	6.09E-07	7.235	1.02E-06	7.303	1.03E-06
YM46	9.47	93.21	4.542E-05	4.239	3.41E-07	7.112	5.73E-07	7.183	5.79E-07
YM47	7.32	72	1.051E-05	3.984	1.24E-07	6.609	2.07E-07	6.683	2.09E-07
YM48	4.15	40.8	6.151E-05	3.426	1.95E-06	5.514	3.14E-06	5.600	3.19E-06
YM51	10.39	102.3	6.308E-06	4.331	4.02E-08	7.295	6.78E-08	7.365	6.84E-08
YM54	23.65	232.8	4.100E-05	5.148	6.00E-08	8.918	1.04E-07	8.993	1.04E-07
YM78	10.42	102.6	1.577E-06	4.334	1.00E-08	7.300	1.69E-08	7.367	1.70E-08
YM80	8.36	82.29	7.570E-05	4.116	7.09E-07	6.869	1.18E-06	6.958	1.19E-06
YM84	13.23	130.2	3.375E-04	4.570	1.40E-06	7.769	2.38E-06	7.837	2.40E-06

Table 8. Calculated field saturated hydraulic conductivity (K_{fs}) values for deep soil using the multistep constant head borehole infiltration test and code LAYERK.

BN.	Layer	Q (Cub.m/s)	H (m)	H* (m)	Layer bottom (m)	Layer Top (m)	K (m/s)
YM21	1	8.2008E-05	6.49	6.49	8.69	2.20	1.98E-6
	2	1.3248E-04	8.70	8.69	2.20	0.00	1.36E-6
	Backfilled		0.00			Average	1.82E-6
YM45	1	4.2051E-06	2.11	2.72	11.95	9.23	4.30E-7
	2	2.3656E-05	4.27	4.88	9.23	7.08	2.95E-6
	3	6.5186E-05	7.40	8.02	7.08	3.93	1.14E-7
	4	9.0419E-05	9.47	10.08	3.93	1.87	2.36E-7
	Backfilled		0.61			Average	8.31E-07
YM46	1	9.4625E-06	3.26	5.43	9.48	4.05	3.09E-7
	2	4.5420E-05	7.32	9.48	4.05	0.00	1.74E-6
	Backfilled		2.16			Average	9.22E-7
YM51	1	-	2.75	6.04	10.40	4.36	< 1.00E-8
	2	-	4.84	8.13	4.36	2.27	< 1.00E-8
	3	-	6.25	9.54	2.27	0.86	< 1.00E-8
	4	6.3083E-06	7.10	10.40	0.86	0.00	3.80E-6
	Backfilled		3.29				–
YM54	1	3.6798E-06	6.56	14.00	23.65	9.65	2.35E-8
	2	8.6214E-06	12.03	19.47	9.65	4.18	1.15E-7
	3	4.1004E-05	16.22	23.65	4.18	0.00	2.19E-6
	Backfilled		7.44			Average	4.27E-7
YM78	1	-	1.80	4.70	10.42	5.72	< 1.00E-8
	2	-	3.63	6.53	5.72	3.90	< 1.00E-8
	3	-	5.52	8.42	3.90	2.00	< 1.00E-8
	4	1.5771E-06	7.52	10.42	2.00	0.00	2.64E-7
	Backfilled		2.90				–
YM80	1	2.6285E-06	1.69	6.05	10.39	4.34	7.14E-8
	2	9.4625E-06	2.84	7.19	4.26	3.19	4.77E-6
	3	7.5700E-05	4.00	8.36	3.19	2.03	4.29E-5
	Backfilled		4.43			Average	6.69E-6
84	1	1.5771E-06	3.47	9.83	13.53	3.70	1.87E-8
	2	3.3750E-04	6.86	13.23	3.70	0.30	3.53E-5
	Backfilled		6.36			Average	9.10E-6

differed from the conductivity estimated from the constant-head borehole infiltration test that was conducted in the same borehole.

Chloride/Bromide Ratios, Meteoric Chloride, and Cosmogenic Chlorine-36

Chloride/bromide ratios in soil water samples from YM61 ranged from 86 to 150. These values are typical of meteoric water and suggest that the chloride is of meteoric origin and that there is no rock component, which is as expected in these terrigenous deposits. Typical chloride profiles in the study area are bulge shaped and have low chloride concentrations near the surface, generally less than 100 g m^{-3}, which increase to maximum concentrations of approximately 3,000 to 18,000 g m^{-3} at depths of 1.7 to 17 ft (0.5 to 5 m) and decrease gradually below the peak to concentrations of 1,000 to 6,000 g m^{-3} (table 3). Soil water fluxes are inversely proportional to chloride concentrations because a uniform chloride deposition rate was assumed throughout the study area; therefore, water fluxes were highest near the surface, decreased to a minimum at the chloride peak, and increased with depth below the chloride peak. Water fluxes decreased to less than 1 mm yr^{-1} within the top meter of soil (table 3). Water flux estimates for profiles in Blanca Draw were a minimum because chloride in runon and runoff was neglected. Water fluxes were not calculated in areas where chloride was leached, such as in areas of Blanca Draw, the borrow pit, and the fissure.

Deviations from the typical profile were found in some areas of Blanca Draw where chloride was leached (fig. 3e, k, and q). YM86 was located in a pseudo-fissure and YM87 was located 33 ft (10 m) distant from the pseudo-fissure (fig. 1). The highest peak chloride concentration was found in YM43, which is in Blanca Draw (figs. 1 and 3n). High maximum chloride concentrations were found in both profiles in the flank of Blanca Draw and were up to 9,720 to 13,850 g m^{-3} in YM9 and YM10, respectively (fig. 3b).

Chloride profiles in the interstream setting were also quite variable. The chloride profiles in the area of the proposed repository were low in the upper meter and increased to a maximum with

depth. The leached zone in these profiles probably results from high infiltration in sandy surface soils. Chloride profiles in the fissure were leached (fig. 5b and e, table 3). The profile YM35 had low chloride concentrations in the upper 30 ft (9 m). Below 30 ft (9 m), chloride concentrations increased sharply to 5,200 g m^{-3} within a 7 ft (2 m) depth interval. Chloride concentrations remained high below this depth. The chloride profile 33 ft (10 m) from the fissure had highest concentrations near the surface (8,000 g m^{-3}) and concentrations decreased to 5,000 to 6,000 g m^{-3} at depths from 39 to 98 ft (12 to 30 m). A low chloride spike (reduction of approximately 1,500 g m^{-3}) was found at the same depth interval that the sharp increase in chloride was found in the fissure. The other pair of profiles in and adjacent to the fissure (YM59 and YM88) had similar characteristics. In YM 88 low chloride concentrations were found in the upper 20 ft (6 m) in the fissure, and chloride concentrations increased to 4272 g m^{-3} from 20 to 28 ft (6 to 8.6 m) depth. The chloride profile adjacent to the fissure had variable concentrations that were much higher than those in the fissure in the upper 20 ft (6 m) but were similar to those in the fissure below this depth. Chloride was also leached in the profile in the borrow pit ($\leq$ 50 g m^{-3}) whereas chloride concentrations in the profile 33 ft (10 m) distant reached a maximum value of 2,621 g m^{-3} and decreased to 860 g m^{-3} at 47 ft (14.4 m) depth (fig. 6b, table 3).

Ratios of $^{36}Cl/Cl$ ranged from 4.57×10^{-13} to 5.09×10^{-13} in the 6 to 37.1 ft (1.8 to 11.3 m) depth interval. The average $^{36}Cl/Cl$ ratio was 4.90×10^{-13} and was similar to the background $^{36}Cl/Cl$ ratio found in the Hueco Bolson (4.7×10^{-13} below 4.1 ft [1.25 m]). These $^{36}Cl/Cl$ ratios agree with the predicted natural fallout of 5×10^{-14} for this latitude. There was no systematic variation in $^{36}Cl/Cl$ ratios with depth, which suggests that the secular variation in ^{36}Cl production is not preserved in the subsurface. The most likely explanation is that the variation is reduced by diffusion.

DISCUSSION

Water Content and Water Potential

Spatial variability in water content is controlled primarily by variations in sediment grain size. Discontinuities in water content across different soil types indicate that water-content variations with depth cannot be used to determine the direction of water movement. Temporal variations in water content were restricted to sandy interstream sites, fissured sediments, and some areas in Blanca Draw. The maximum depth of water penetration in these areas was 5 ft (1.5 m). The absence of temporal variations in water content monitored in the remainder of the neutron probe access tubes indicates that water pulses did not move through these areas. Because a constant flux could result in temporally invariant water content, the absence of such variations does not preclude water movement.

The low measured water potentials indicate that the unsaturated system is very dry and water fluxes are expected to be minimal. Except in the upper meter after rainfall, the water-potential gradients indicate an upward driving force for water movement, probably controlled by evapotranspiration. The length of the monitoring period (June to October 1993) was insufficient to evaluate long-term fluctuations in water potential. Long-term monitoring of water potentials at the Hueco Bolson can be used to evaluate temporal variations in water potential in a similar setting (Appendix B). These data showed that water infiltrated to greater depth in sandy soils ($\leq$ 2.7 ft [0.8 m]) than in clay loam soils ($\leq$ 1 ft [0.3 m]). Infiltration and redistribution of water occurred in response to abnormally high winter precipitation in 1992 and 1993. The progressive increase in water potentials with depth during infiltration and redistribution suggests piston flow. Comparison of field- and laboratory-measured water potentials in nearby profiles showed that the general shape of the two profiles was similar; however, water potentials measured at the same depth differed by up to 6 MPa in coarse-grained sediments and by up to 2 MPa in fine-grained sediments. The lower water potentials measured by the laboratory psychrometers are attributed to drying during sample collection and analysis.

Meteoric Chloride

Many assumptions are used to estimate water fluxes from chloride data, and the validity of these assumptions in this study area needs to be examined. The assumption of one-dimensional vertical flow is considered valid because all chloride profiles are from topographically flat areas having slopes of less than 1%. The direction of water flux is assumed to be downward. If the water flux were in fact upward, the highest chloride concentrations would occur at the land surface, as seen in chloride profiles from the Sahara (Fontes, 1986). Maximum chloride concentrations typically found at depths of 1.7 to 17 ft (0.5 to 5 m) indicate that the net water flux is downward in this interval of the unsaturated zone. Precipitation is assumed to be the only source of chloride; there are no chloride sources or sinks below the root zone. The sediments in this study area are terrigenous and do not contain any chloride of marine origin. The low Cl/Br ratios are also consistent with the chloride being of meteoric origin.

The piston-flow assumption is more difficult to assess. The applicability of piston flow depends on the temporal and spatial scales being considered. Near the soil surface where desiccation cracks develop, nonpiston flow may be dominant. Higher water fluxes based on ground-water chloride relative to those based on chloride concentration in the unsaturated zone in many areas have been attributed to nonpiston flow or bypass of the matrix with low-chloride water (Peck and others, 1981; Sharma and Hughes, 1985; Johnston, 1987). Chloride profiles in these areas are generally smooth, which indicates that the smoothness of the profiles does not help discriminate between piston and nonpiston flow. Flow along preferential pathways that bypasses the matrix is used to explain the reduction in chloride concentrations below the peak in some profiles (Sharma and Hughes, 1985). Many profiles characterized by a large amount of preferential flow are from wetter regions (precipitation 800 to 1,200 mm yr^{-1} [Sharma and Hughes, 1985; Johnston, 1987]) than the Eagle Flat area (precipitation 320 mm yr^{-1}). The water potentials (matric and osmotic potentials) in the Eagle Flat area are very low except in the fissured sediments and beneath the borrow pits; therefore, in most areas water is adsorbed onto grain surfaces and is

unlikely to move along larger openings or root channels. Long-term water potential monitoring in the Hueco Bolson also suggests piston flow (Appendix B).

The long time period represented by chloride profiles in this study spans paleoclimatic variations and may invalidate the steady-state subsurface flow assumption (table 3). The decrease in soil water chloride concentrations below the peak may represent temporally varying environmental conditions (Allison and others, 1985). Previous work in the Hueco Bolson suggested higher water fluxes prior to 6,000 to 9,000 yr, which is consistent with paleoclimatic data that suggest that the climate during the late Wisconsinan and early Holocene (22,000 to 8,000 yr) was much wetter than middle to late Holocene (8,000 yr to present) (van Devender and Spaulding, 1979). In addition to higher precipitation rates in the past, the seasonality of the precipitation is also thought to differ, winter frontal storms being dominant before 8,000 yr, whereas summer convective storms are more typical of the climate since 8,000 yr (van Devender and Spaulding, 1979), which would further reduce the water flux from 8,000 yr to the present. This is the most plausible cause of the reduction in chloride below the peak in profiles from the Eagle Flat site.

Numerical Modeling

Because of the limited duration of monitoring at the Eagle Flat site, numerical simulations of unsaturated flow were based on long-term monitoring data at the Hueco Bolson test area. These simulations are described in Appendix A. The main aspects of the modeling study are described in this section. The objective of the modeling study was to evaluate and explain liquid and vapor fluxes in the shallow unsaturated zone in response to an annual climate cycle. We made no attempt to calibrate the model. The initial conditions for the simulation were based on water potential and temperature monitored by in situ psychrometers that were installed in an ephemeral stream setting in the Hueco Bolson. The range in water potentials at the Hueco Bolson site is similar to that measured at the Eagle Flat site. The upper boundary condition was based on hourly climatic data

from October 1, 1989, to September 30, 1990, monitored at the meteorologic station. The total precipitation for that year was 8.15 in (207 mm), which is lower than the long-term average annual precipitation at Eagle Flat (12.60 in [320 mm]) but within the range of variability of annual precipitation at Eagle Flat. Soil textures for the model domain were based on grain size analyses that ranged from clay to muddy sandy gravel. Material properties were assigned to these soil textures on the basis of laboratory retention data for soils of similar texture. Sediments in the upper 5 ft (1.5 m) of the profile modeled are finer grained (silty clay to clay) than sediments found in this depth interval in the area near the proposed Eagle Flat repository (sandy loam, YM13 and YM14). The gravel lens at depths of 5 to 23 ft (1.5 to 7 m) is similar to that found in YM13 and YM16 at the Eagle Flat site.

There was remarkable consistency between the simulated water potentials and the available field measured water potentials (Appendix A). The simulated seasonal changes of temperature were also in good agreement with the field measurements. Measured and simulated values both showed the well-known extinction and phase shift of the annual surface temperature wave with depth. Below 1 ft (0.3 m) depth, the attenuation and phase shift of water potentials with depth were similar to those of temperature. This similarity suggests that the water potential changes were driven primarily by the temperature changes, with water content remaining relatively constant. This was confirmed by the similarity between modeled water potentials and those computed using temperature changes alone. Temperature is likely to be the main control on seasonal water potential fluctuations below the shallow subsurface active zone in many arid sites.

The changes in water storage associated with individual rainfall events were confined mainly to the top 1 ft (0.3 m) of the soil. This was consistent with the field measured water potential variations. The maximum depth of penetration of water would probably be greater at the proposed Eagle Flat repository because the surface sediments have more sand. The deeper penetration of water in coarser textured sites is shown by water potential monitoring data from the field psychrometers at 77P at the Hueco Bolson site (Appendix B).

A detailed analysis of water fluxes in this near-surface layer revealed that the dominant process for downward water movement was liquid flow. Very close to the surface, upward isothermal vapor fluxes were significant. Below 1 ft (0.3 m) depth, water fluxes varied relatively little and were dominated by thermal vapor flux, which varied with season and depth following the temperature gradient. In the annual mean, its downward values in summer outweighed the upward values in winter, giving cumulative annual downward thermal vapor fluxes. Thermal vapor flux was essentially unbalanced by the other water fluxes in the simulation. Comparison of numerical modeling results with chemical tracer data showed that downward vapor flux below the evaporation front (0.27 ft [0.08 m]) based on the numerical simulations agreed with the deeper penetration of bomb ^{3}H (volatile) relative to that of bomb ^{36}Cl (nonvolatile). The simulated average downward vapor flux from 0.27 to 4.7 ft (0.08 to 1.4 m) depth (1.1 mm yr^{-1}) is within the same order of magnitude as that based on the relative distribution of ^{3}H and $^{36}Cl/Cl$ (5.6 mm yr^{-1}).

Conceptual Flow Model

The hydrologic data were integrated to develop a conceptual flow model of the vadose zone in the Eagle Flat study area. Profiles in the ephemeral stream setting are characterized by variable water content, low water potentials, upward water potential gradients below the shallow subsurface after rainfall, and variable chloride profiles. The generally low water potentials and upward water potential gradients suggest dry soils and an upward driving force for water movement under present conditions. Low chloride concentrations in some of the profiles in Blanca Draw indicate that at some time in the past the chloride was leached, probably when these sites were ponded. The typical profiles in the interstream setting have variable water contents, low water potentials, upward water potential gradients, and high maximum chloride concentrations. In this setting the water potential data suggest upward driving forces for liquid flow, and the chloride data suggest very low fluxes for thousands of years. In the borrow pit, the sediments are disturbed and ponded water occurs for long periods, which results in downward water movement as indicated by

high water potentials and low chloride concentrations. The fissured sediments also have ponded water after rainfall. High water potentials and low chloride concentrations in the upper 20 to 30 ft (6 to 9 m) of the fissured sediments indicate downward fluxes to this depth. Water content monitoring data showed downward movement of water to 5 ft (1.5 m) depth after rainfall. The sharp decrease in water potentials and increase in chloride at 20 to 30 ft (6 to 9 m) may occur because the fissure has not been present long enough for water to move deeper or may mark the location of a clay zone.

Long-term water potential monitoring data from the Hueco Bolson provide valuable information on unsaturated zone processes in response to climatic variations. These data indicate that the penetration depth of the wetting front after rainfall is greater in coarse textured soils (2.7 ft [0.8 m] in sand) than in fine textured soils (1 ft [0.3 m] in clay loam). The progressive increase in water potentials with depth during infiltration and redistribution suggests piston flow.

The soil physics and chemical data for the area of the proposed Eagle Flat repository both suggest negligible fluxes. Long-term net water fluxes estimated from the soil water chloride concentrations were downward and were less than 1 mm yr^{-1} below the top meter of soil. The upward decrease in water potentials indicates an upward driving force for water movement under present climatic conditions.

CONCLUSIONS

Soil textures in the study area varied with geomorphic setting. Sediments beneath Blanca Draw were fine grained and ranged from clay to clay loam. In the interstream setting, some profiles were predominantly clay whereas others were primarily clay loam and sandy loam. Sediments beneath the borrow pit and adjacent profile were coarse grained and ranged from clay to muddy gravel. The fissured sediments were primarily loam whereas those adjacent to the fissure were predominantly clay.

Spatial variability in water content is controlled primarily by variations in sediment grain size. Discontinuities in water content across different soil types indicate that water-content variations with depth cannot be used to determine the direction of water movement. Temporal variations in water content were restricted to the fissured sediments and some areas in Blanca Draw. The maximum depth of penetration of a water pulse in these areas was 5 ft (1.5 m). The absence of temporal variations in water content monitored in the remainder of the neutron probe access tubes indicates that water pulses did not move through these areas. Because a constant flux could result in temporally invariant water content, the absence of such variations does not preclude water movement.

Typical water potential profiles at the site, which is located in an interstream setting, were low in the upper 7 ft (2 m) (~–12 to –2 MPa) and increase with depth below the minimum to maximum values of –6 to –0.4 MPa in different profiles. The monitoring record for the in situ psychrometers was insufficient to evaluate long-term fluctuations in water potential. A vertical profile based on data collected on August 13, 1993, showed low water potentials at 1 ft (0.3 m) depth (-6 MPa), which increased to a maximum value of –2 MPa at 60.7 ft (18.5 m) depth. The low water potentials indicate that the sediments are dry and the upward water potential gradients indicate an upward driving force for liquid flow. Boreholes drilled after rainfall had high water potentials in the surficial sediments which decreased sharply at the base of the wetting front. Exceptions to this typical profile were found in the profile in the fissured sediments and beneath the borrow pit. The fissured sediments had much higher water potentials in the upper 43 ft (13 m) than the sediments 33 ft (10 m) distant from the fissure. Water potentials in soil samples from the borrow pit were much higher than those in soil samples from the profile 33 ft (10 m) distant from the borrow pit.

In addition to water potential data, information on hydraulic conductivity is also required to calculate water fluxes. K_{fs} based on the Guelph permeameter data ranged from $\leq 10^{-7}$ to 10^{-4} m s^{-1}. Hydraulic conductivities were highest in the coarse grained sediments beneath the borrow pit and were lowest in fine grained sediments in Blanca Draw. The range in K_{fs} values for the

constant-head borehole tests was 10^{-8} to 10^{-6} m s^{-1}. Hydraulic conductivities estimated from the constant-head borehole tests did not vary systematically with geomorphic setting, and the lowest and highest hydraulic conductivities were measured interstream setting. The results of multistep constant-head borehole infiltration tests indicated that the hydraulic conductivity of individual layers within a borehole varied up to three orders of magnitude. Geometric average conductivities based on the multistep constant-head borehole tests differed from conductivities based on the regular constant-head tests by up to two orders of magnitude. Hydraulic conductivities based on the regular constant-head borehole tests depend on the location of the high-conductivity zone. When the high-conductivity zone is located in the upper portion of the borehole, the calculated hydraulic conductivity based on the constant-head borehole test is lower than the average hydraulic conductivity, whereas when the high-conductivity zone is located in the lower portion of the borehole, the calculated hydraulic conductivity based on the constant-head borehole test is higher than the average hydraulic conductivity.

Typical chloride profiles in the study area are bulge shaped and have low chloride concentrations near the surface, generally less than 100 g m^{-3}, which increase to maximum concentrations of 3,000 to 18,000 g m^{-3} at depths of generally between 1.6 and 16 ft (0.5 and 5 m) and gradually decrease with depth below the peak to concentrations of 1,000 to 6,000 g m^{-3}. Calculated water fluxes are inversely proportional to chloride concentrations in the soil water because a constant chloride deposition rate was assumed throughout the study area. Water fluxes estimated from the chloride data were highest at the surface and decreased to less than 1 mm yr^{-1} within the top meter. Flux estimates for profiles in the ephemeral stream were a minimum because chloride in runon and runoff was neglected. Deviations from the typical profiles were found in parts of Blanca Draw where maximum chloride concentrations in some profiles were less than 400 to 900 g m^{-3} whereas chloride in other profiles in Blanca Draw reached maximum concentrations of 17,821 g m^{-3}. Chloride was leached in the upper 20 to 30 ft (6 to 9 m) depth in the fissure whereas chloride concentrations in profiles 33 ft (10 m) distant from the fissure were much higher in this zone. Below 20 to 30 ft (6 to 9 m), chloride concentrations in the fissure increased to concentrations similar to those found in samples at the same depth in the profiles 33 ft (10 m) from

the fissure. Chloride concentrations in the profile in the borrow pit were less than 50 g m^{-3}, whereas the profile 33 ft (10 m) distant from the borrow pit had maximum chloride concentrations of 2,621 g m^{-3}.

Because of the limited monitoring data at the Eagle Flat site, numerical simulations of unsaturated flow were based on long-term monitoring data at the Hueco Bolson site. These simulations were conducted to evaluate unsaturated zone processes. The results from these simulations are considered applicable to the Eagle Flat study area because the range in water potentials is similar at both sites. The sediments in the upper 5 ft (1.5 m) of the model domain (silty clay to clay) are finer grained than sediments found in this depth interval in the area of the proposed Eagle Flat repository (sandy loam). The gravel lens at depths of 5 ft to 23 ft (1.5 to 7 m) is similar to that found in some of the profiles at the Eagle Flat site. Precipitation for the one year simulated (October 1, 1989, to September 30, 1990; 8.15 in [207 mm]) is lower than the long-term average annual precipitation at Eagle Flat (12.60 in [320 mm]) but is within the range of variability of annual precipitation at Eagle Flat. Analysis of water fluxes in the upper 1 ft (0.3 m) revealed that the dominant process for downward water movement was liquid flow. Below a 1 ft (0.3 m) depth, water fluxes varied relatively little and were dominated by net downward thermal vapor flux.

The hydrologic data were integrated to develop a conceptual flow model of the vadose zone in the Eagle Flat study area. Profiles in the ephemeral stream setting are characterized by variable water content, low water potentials, and upward water potential gradients except in the shallow subsurface immediately after rainfall, and variable chloride profiles. The generally low water potentials and upward water potential gradients suggest dry soils and an upward driving force for water movement under present conditions. Low chloride concentrations in some of the profiles in Blanca Draw indicate that at some time in the past the chloride was leached, probably when these sites were ponded. The typical profiles in the interstream setting have variable water contents, low water potentials, upward water potential gradients, and high maximum chloride concentrations. In this setting the water potential data suggest upward driving forces for liquid flow, and the chloride data suggest very low fluxes for thousands of years. In the borrow pit, the sediments are disturbed and ponded water occurs for long periods, which results in downward water movement as

and ponded water occurs for long periods, which results in downward water movement as indicated by high water potentials and low chloride concentrations. The fissured sediments also have ponded water after rainfall. High water potentials and low chloride concentrations in the upper 20 to 30 ft (6 to 9 m) of the fissured sediments indicate downward fluxes to this depth. Water content monitoring data showed downward movement of water to 5 ft (1.5 m) depth after rainfall. The sharp decrease in water potentials and increase in chloride at 20 to 30 ft (6 to 9 m) may occur because the fissure has not been present long enough for water to move deeper or may mark the location of a clay zone. Long-term water potential monitoring data from the Hueco Bolson provide valuable information on unsaturated zone processes in response to climatic variations. These data indicate that the penetration depth of the wetting front after rainfall is greater in coarse textured soils (2.67 ft [0.8 m] in sand) than in fine textured soils (1 ft [0.3 m] in clay loam). The progressive increase in water potentials with depth during infiltration and redistribution suggests piston flow. The soil physics and chemical data for the area of the proposed Eagle Flat repository are consistent and suggest negligible fluxes. Long-term net water fluxes estimated from the soil water chloride concentrations were less than 1 mm yr^{-1} below the top meter of soil. The upward decrease in water potentials indicates an upward driving force for water movement.

ACKNOWLEDGMENTS

This report was prepared for the Texas Low-Level Radioactive Waste Disposal Authority under Interagency Contract Number IAC(92-93)-0910. The conclusions of the authors are neither endorsed nor approved by the Authority. Illustrations were prepared under the supervision of Richard L. Dillon. Word processing was by Susan Lloyd, editing by Amanda R. Masterson, and layout by Margaret L. Evans.

REFERENCES

Ababou, R., McLaughin, D., Gelhar, L. W., and Tompson, F. B., 1987, Numerical simulation of three-dimensional saturated flow in randomly heterogeneous porous media: paper submitted to the Journal of Transport in Porous Media.

Allison, G. B., Stone, W. J., and Hughes, M. W., 1985, Recharge in karst and dune elements of a semi-arid landscape as indicated by natural isotopes and chloride: Journal of Hydrology, v. 76, p. 1–26.

Bentley, H. W., Phillips, F. M., and Davis, S. N., 1986, ^{36}Cl in the terrestrial environment, *in* Fritz, P., and Fontes, J.-C., Handbook of environmental isotope geochemistry: New York, Elsevier Science, p. 422–475.

Bresler, E., 1973, Simultaneous transport of solutes and water under transient unsaturated flow conditions: Water Resources Research, v. 9, p. 975–986.

Brown, R. W., and Bartos, D. L., 1982, A calibration model for screen-caged Peltier thermocouple psychrometers: USDA, Intermtn. For. Range Exp. Stn., Ogden, Utah, Report 293, 155 p.

Campbell, G. S., 1985, Soil physics with BASIC: transport models for soil-plant systems: New York, Elsevier, 150 p.

Darling, B. K., and Hibbs, B. J., 1993, Ground-water hydrology and hydrochemistry of Eagle Flat and surrounding area: The University of Texas at Austin, Bureau of Economic Geology, final report prepared for the Texas Low-Level Radioactive Waste Disposal Authority, 122 p.

de Marsily, G., 1986, Quantitative hydrogeology: London, Academic Press, 440 p.

Elmore, D., Conard, N. J., Kubik, P. W., and Fabryka-Martin, J., 1984, Computer controlled isotope ratio measurements and data analysis: Nucl. Inst. Meth. Phys. Res., v. B5, p. 233–237.

Elmore, D., Fulton, B. R., Clover, M. R., Marsden, J. R., Gove, H. E., Naylor, H., Purser, K. H., Kilius, L. R., Beukens, R. P., and Litherland, A. E., 1979, Analysis of ^{36}Cl in environmental water samples using an electrostatic accelerator: Nature, v. 227, p. 22–25.

Enfield, C. G., Hsieh, J. J. C., and Warrick, A. W., 1973, Evaluation of water flux above a deep water table using thermocouple psychrometers: Soil Science Society of America Proceedings, v. 37, p. 968–970.

Folk, R. L., 1974, Petrology of sedimentary rocks: Austin, Hemphill, 182 p.

Fontes, J. C., Yousfi, M., and Allison, G. B., 1986, Estimation of long-term, diffuse ground-water discharge in the Northern Sahara using stable isotope profiles in soil water: Journal of Hydrology, p. 315–327.

Gaudet, J. P., Jegat, H., and Vachaud, G., 1977, Methodes de mesure permettant de caracterizer l'ecoulement de l'eau et de solute dans la zone non-saturee: Symposium on Hydrodynamic diffusion and dispersion in porous media: Pavia, Italy, International Association for Hydraulic Research.

Gee, G. W., and Bauder, J. W., 1982, Particle-size analysis, *in* Page, A. L., ed., Methods of soil analysis, part 2, chemical and mineralogical methods: Madison, Wisconsin, American Society of Agronomists, p. 383–410.

Gee, G. W., Campbell, M. D., Campbell, G. S., and Campbell, J. H., 1992, Rapid measurement of low soil water potentials using a water activity meter: Soil Science Society of America Journal, v. 56, p. 1068–1070.

Gee, G. W., and Heller, P. R., 1985, Unsaturated water flow at the Hanford site: a review of literature and annotated bibliography: Richland, Washington, Pacific Northwest Laboratory, Report PNL-5428, 42 p.

Gee, G. W., and Hillel, D., 1988, Ground-water recharge in arid regions: review and critique of estimation methods: Hydrological Proceedings, v. 2, p. 255–266.

Gile, L. H., Hawley, J. W., and Grossman, R. B., 1981, Soils and geomorphology in the Basin and Range area of Southern New Mexico—Guidebook to the Desert Project: New Mexico Bureau of Mines and Mineral Resources, Memoir 39, 222 p.

Glover, R. E., 1953, Flow from a test-hole located above ground-water level, *in* Zangar, C. N., ed., Theory and problems of water percolation: U.S. Dept. of Interior, Bureau of Reclamation, Engineering Monograph 8, p. 69–71.

Hudson, D. B., and Wierenga, P. J., 1988, Agronomy Abstracts, Neutron probe standard counts, Madison, Wisconsin, American Society of Agronomy, p. 184–185.

Isaacson, R. E., Brownell, L. E., Nelson, R. W., and Roetman, E. L., 1974, Soil-moisture transport in arid site vadose zones: Atlantic Richfield Hanford Company, Richland, Washington, Report ARH-2983, 90 p.

Jackson, M. L. W., Langford, R. P., and Whitelaw, M. J., 1993, Basin-fill stratigraphy, Quaternary history, and paleomagnetics of the Eagle Flat study area, southern Hudspeth County, Texas: The University of Texas at Austin, Bureau of Economic Geology, final report prepared for the Texas Low-Level Radioactive Waste Disposal Authority, 137 p.

Johnston, C. D., 1987, Distribution of enviromental chloride in relation to subsurface hydrology: Journal Hydrology, v. 94, p. 67–88.

Lang, A. R. G., 1967, Osmotic coefficients and water potentials of sodium chloride solutions from 0 to 40°C: Australian Journal of Chemistry, v. 20, p. 2017–2023.

Langford, R. P., 1993, Landscape evolution of Eagle Flat and Red Light Basins, Chihuahuan Desert, south-central Trans-Pecos Texas: The University of Texas at Austin, Bureau of Economic Geology, final report prepared for the Texas Low-Level Radioactive Waste Disposal Authority, 153 p.

Larkin, T. J., and Bomar, G. W., 1983, Climatic atlas of Texas: Austin, Texas, Department of Water Resources, Publication LP-192, 151 p.

Mattick, J. L., Duval, T. A., and Phillips, F. M., 1987, Quantification of ground-water recharge rates in New Mexico using bomb ^{36}Cl, bomb ^{3}H and chloride as soil-water

tracers: Las Cruces, New Mexico, New Mexico Water Resources Research Institute, Report 220, 184 p.

Mazaud, A., Laj, C., Bard, E., Arnold, M., and Trice, E., 1991, Geomagnetic field control of ^{14}C production over the last 80 ky: implications for radiocarbon time-scale: Geophysical Research Letters, 18, 1885–1888.

Meyn, R. L., and White, R. S., 1972, Calibration of thermocouple psychrometers: a suggested procedure for development of a reliable predictive model: Logan, Utah, Utah State University, Utah Agricultural Experiment Station, Psychrometry in water relations research, p. 56–63.

Montazer, P., and Wilson, W. E., 1985, Conceptual hydrologic model of flow in unsaturated zone, Yucca Mountain, Nevada: U.S. Geolological Survey Water-Resources Investigations, Report 84-4345.

Nichols, W. D., 1987, Geohydrology of the unsaturated zone at the burial site for low-level radioactive waste near Beatty, Nye County, Nevada: U.S. Geological Survey Water Supply Paper 2312, 57 p.

Peck, A. J., Johnston, C. D., and Williamson, D. R., 1981, Analyses of solute distributions in deeply weathered soils: Agricultural Water Management, v. 4, p. 83–102.

Phillips, F. M., Mattick, J. L., and Duval, T. A., 1988, Chlorine-36 and tritium from nuclear weapons fallout as tracers for long-term liquid movement in desert soils: Water Resources Research, v. 24, p. 1877–1891.

Phillips, F. M., and Stone, W. J., 1985, Chemical considerations in ground-water recharge: Symposium on Water and Science, Socorro, New Mexico, New Mexico Water Resources Research Institute, p. 109–125.

Rawlins, S. L., and Campbell, G. S., 1986, Water potential: thermocouple psychrometry, *in* Klute, A., ed., Methods of soil analysis, part 1, physical and mineralogical methods: , Madison, American Society of Agronomy, Wisconsin, p. 597–617.

Reynolds, W. D., and Elrick, D. E., 1985, In situ measurement of field-saturated hydraulic conductivity, sorptivity, and the alpha-parameter using the Guelph permeameter: Soil Science, 140, p. 292–302.

Reynolds, W. D., and Elrick, D. E., 1986, A method for simultaneous in situ measurement in the vadose zone of field-saturated hydraulic conductivity and the conductivity-pressure head relationship: Ground Water Monitoring Review, v. 6, p. 84–95.

Reynolds, W. D., Elrick, D. E., and Topp, G. C., 1983, A reexamination of the constant-head well permeameter method for measuring saturated hydraulic conductivity above the water table: Soil Science, v. 136, p. 250–268.

Robinson, R. A., and Stokes, R. H., 1959, Electrolyte solutions: London, Butterworths Publishing, 571 p.

Rose, C. W., Stern, W. R., and Drummond, J. E., 1965, Determination of hydraulic conductivity as a function of depth and water content for soil in situ: Aust. J. Soil Res., v. 3, p. 1–9.

Scanlon, B. R., 1991, Evaluation of moisture flux from chloride data in desert soils, Journal of Hydrology, v. 128, p. 137–156.

Scanlon, B. R., 1992a, Evaluation of liquid and vapor flow in desert soils based on chlorine-36 and tritium tracers and nonisothermal flow simulations: Water Resources Research, v. 28, p. 285–297.

Scanlon, B. R., 1992b, Moisture and solute flux along preferred pathways characterized by fissured sediments in desert soils: Journal of Contaminant Hydrology, v. 10, p. 19–46.

Scanlon, B. R., Wang, F. P., and Richter, B. C., 1991, Field studies and numerical modeling of unsaturated flow in the Chihuahuan Desert, Texas: The University of Texas at Austin, Bureau of Economic Geology, Report of Investigations No. 199, 56 p.

Schlemon, R. J., and LaChapelle, W. A., 1992, Pseudo earth fissures in the Lancaster area, Antelope Valley, California: Association of Engineering Geologists 35th Annual meeting, p. 165–169.

Sharma, M. L., and Hughes, M. W., 1985, Ground-water recharge estimation using chloride, deuterium and oxygen-18 profiles in the deep coastal sands of western Australia: Journal of Hydrology, v. 81, p. 93–109.

Stephens, D. B., and Knowlton, R. J., 1986, Soil water movement and recharge through sand at a semiarid site in New Mexico: Water Resources Research, v. 22, p. 881–889.

Tyler, S. W., McKay, W. A., Hess, J. W., Jacobson, R. L., and Taylor, K., 1986, Effects of surface collapse structures on infiltration and moisture redistribution: Desert Research Institute, Report 45045, 48 p.

U.S. Department of Agriculture, 1975, Soil taxonomy: Washington, D.C., Soil Conservation Service, 754 p.

van de Pol, R. M., Wierenga, P. J., and Nielsen, D. R., 1977, Solute movement in a field soil: Soil Science Society of America Journal, v. 41, p. 10–13.

van Devender, T. R., and Spaulding, W. G., 1979, Development of vegetation and climate in the Southwestern United States: Science, v. 204, p. 701–710.

Van Genuchten, M. T., 1980, A closed-form equation for predicting the hydraulic conductivity of unsaturated soils: Soil Science of America Journal, v. 44, p. 892–898.

Wiebe, H. H., Campbell, G. S., Gardner, W. H., Rawlins, S. L., Cary, J. W., and Brown, R. W., 1971, Measurement of plant and soil water status: Utah Agricultural Experiment Station.

Winograd, I. J., 1981, Radioactive waste disposal in thick unsaturated zones: Science, v. 212, p. 1457–1464.

Xiang, J., 1994a, A new solution for the constant-head borehole permeameter test: paper submitted to *Water* Resources Research.

Xiang, J., 1994b, A single borehole test for conductivity measurements of layered soils or rocks: Water Resources Research.

Xiang, J., and Chen, L., 1994, A solution for the constant-head borehole test: Water Resources Research.

Zreda, M. G., Phillips, F. M., Elmore, D., Kubik, P. W., Sharma, P., and Dorn, R. I., 1991, Cosmogenic chlorine-36 production rates in terrestrial rocks: Earth and Planetary Science Letters, v. 105, p. 94–109.

APPENDIX A. WATER AND HEAT FLUXES IN DESERT SOILS 2. NUMERICAL SIMULATIONS

Bridget R. Scanlon
Bureau of Economic Geology
W. L. Fisher, Director
The University of Texas at Austin
Austin, Texas

P. C. D. Milly
U.S. Geological Survey
Geophysical Fluid Dynamics Laboratory / NOAA
Princeton, New Jersey

ABSTRACT

Transient one-dimensional fluxes of soil water (liquid and vapor) and heat in response to one year of atmospheric forcing were simulated numerically for a site in the Chihuahuan Desert of Texas. The model was initialized and evaluated using the monitoring data presented in a companion paper. Soil hydraulic and thermal properties were estimated a priori from a combination of laboratory measurements, models, and other published information. In the first simulation, the main drying curves were used to describe soil water retention, and hysteresis was ignored. Remarkable consistency was found between computed and measured water potentials and temperatures. Attenuation and phase shift of the seasonal cycle of water potentials below the shallow subsurface active zone (0.3 m) were similar to those of temperatures, suggesting that water potential fluctuations may be driven primarily by temperature changes. Water fluxes in the upper 0.3 m were dominated by downward and upward liquid fluxes that resulted from infiltration of rain and subsequent evaporation from the surface. Only in the top several millimeters of the soil during evaporation periods was upward flux vapor-dominated. Below 0.3 m, water fluxes varied slowly and were dominated by downward thermal vapor flux that decreased with depth, causing a net accumulation of water. In a second simulation, nonhysteretic water retention was instead described by the estimated main wetting curves; the resulting differences in fluxes were attributed to lower initial water contents (given fixed initial water potentials) and lower unsaturated hydraulic conductivities in the second simulation. Below 0.3 m, the thermal vapor fluxes dominated and were similar to those in the first simulation. Two other simulations were performed, differing from the first only in the prescription of different (wetter) initial water potentials. These three simulations converged in the upper 0.2 m after infiltration of summer rain; however, the various initial water potentials were preserved throughout the year at greater depths. Comparison of all four simulations showed that the predominantly upward liquid fluxes below 0.2 m were very sensitive to the differences in water retention curves and initial water potentials among simulations, because these strongly affected hydraulic conductivities. Comparison of numerical modeling results with chemical tracer data showed that values of downward vapor flux below the surface evaporation

zone were of the same order of magnitude as those previously estimated by analysis of depth distributions of bomb ^{3}H (volatile) and bomb ^{36}Cl (nonvolatile).

INTRODUCTION

The complexity of flow in the shallow unsaturated zone of desert soils requires the use of numerical models to evaluate flow processes and to analyze interactions and feedback mechanisms between various controlling parameters. Most numerical modeling studies focus on isothermal liquid flow and neglect the effect of vapor flow. However, vapor flow may be important, particularly near the soil surface in arid systems, where the soils are very dry and where temperature gradients are steep. Numerical models of varying complexity have been used to simulate nonisothermal liquid and vapor flow. Development of these models has been motivated by problems such as evaluation of shallow unsaturated zones, geothermal reservoirs, and nuclear waste disposal sites. This study is concerned primarily with the "weakly" nonisothermal systems of *Pruess* (1987), in which temperatures remain below the boiling point of water. Models of these weakly nonisothermal systems are generally based on the equations of *Philip and de Vries* (1957). Application of these numerical models to evaluate subsurface water flux has been limited by lack of appropriate field data. Although field studies were conducted to evaluate the numerical model developed by *Sophocleous* (1979), test cases representing dry conditions were hypothetical because of problems with field psychrometric measurements. Only water content data were available to evaluate results of heat and water flux simulations conducted by *Baca et al.* (1978) because temperature and water potential were not monitored.

Previous simulations of nonisothermal liquid and vapor flow in the shallow unsaturated zone of an area within the Chihuahuan Desert of Texas were restricted to 5-day periods in the summer and winter and showed that below the evaporation front, downward vapor fluxes in the summer were much greater than generally upward vapor fluxes in the winter (*Scanlon*, 1992a). The results suggested an annual net downward vapor flux that is consistent with the observed deeper penetration of ^{3}H (volatile) relative to that of ^{36}Cl (nonvolatile).

The objective of this study was to evaluate and explain liquid and vapor fluxes in the shallow unsaturated zone of the Chihuahuan site in response to an annual climate cycle. Our approach was to use numerical simulations to interpret observed field data. In contrast to previous simulations (*Scanlon*, 1992a) that considered short-term precipitation-free periods, the full annual cycle includes alternating periods of precipitation and evaporation. The long-term monitoring record of subsurface temperatures and water potentials in this study provided initial conditions for the model and data to test model results. Because of the complexity of the system and the numerical model, there were considerable uncertainties in the soil physical properties. We made no attempt to calibrate the model, but did use sensitivity runs to understand the physical factors that control water movement.

One major difference between this and previous studies of nonisothermal flow systems is that flow in the natural system was evaluated in this study, whereas many previous studies evaluated subsurface flow after an initial period of artificial saturation (*Hanks et al.*, 1967; *Rose*, 1968). In addition, the one-year period simulated is much longer than the periods (hours to days) simulated in previous studies (*Sophocleous*, 1979; *van de Griend et al.*, 1985; *de Silans et al.*, 1989); this gives a more comprehensive view of flow processes with reduced dependence on initial conditions.

GOVERNING EQUATIONS

Water and heat flux were simulated with a one-dimensional numerical model, SPLaSHWaTr (*Milly*, 1982). SPLaSHWaTr is based on the formulation of water and heat flux by *Philip and de Vries* (1957) and *de Vries* (1958), as generalized by *Milly* (1982). Two features of SPLaSHWaTr are critical for this study and distinguish this code from many other codes that simulate nonisothermal flow in the unsaturated zone. The first is the use of matric potential rather than water content as one of the dependent variables; this allows simulation of flow in heterogeneous, variably saturated systems. The second critical feature is the specification of the upper boundary condition in terms of atmospheric forcing. Model assumptions include (1) no

uptake of water by plants, (2) local hydraulic and thermal equilibrium among solid particles, air, and water, and (3) a static air phase (*Milly and Eagleson*, 1982). The lack of water uptake by plants is appropriate for the study area because hydraulic parameters were monitored in bare soil. The assumption of local hydraulic and thermal equilibrium only breaks down at high infiltration rates in coarse soil (*Milly*, 1982); therefore, this assumption is reasonable for the study area, which is characterized by fine-grained surficial sediments. The effect of the static air phase assumption on simulation results will be discussed in a later section.

It is well known that the relation between matric potential and water content of soils exhibits hysteresis. In this study, however, we assume that the water content is a unique function of matric potential and temperature at any time. This neglect of hysteresis is a definite limitation of this study. The SPLaSHWaTr code permits hysteresis but fails to consider the entire wetting and drying history in an internally consistent way (*Milly and Eagleson,* 1980). We judged that it was better to neglect hysteresis altogether in this study than to use a questionable parameterization of it. Furthermore, we were not aware of any comparable model with a valid description of hysteresis, we did not have the resources to develop one, and we felt that meaningful results could be obtained without considering hysteresis. The slight hysteresis in the dependence of hydraulic conductivity on water content is also ignored here.

The SPLaSHWaTr code is fully documented by *Milly and Eagleson* (1980) and *Milly* (1982; 1984); however, the governing equations are provided here for convenience. The governing equation for water is given by *Milly* (1982):

$$\left[\left(1-\frac{\rho_v}{\rho_l}\right)\frac{\partial\theta}{\partial\psi}\bigg|_T+\frac{\theta_a}{\rho_l}\frac{\partial\rho_v}{\partial\psi}\bigg|_T\right]\frac{\partial\psi}{\partial t}+\left[\left(1-\frac{\rho_v}{\rho_l}\right)\frac{\partial\theta}{\partial T}\bigg|_\psi+\frac{\theta_a}{\rho_l}\frac{\partial\rho_v}{\partial T}\bigg|_\psi\right]\frac{\partial T}{\partial t}$$

$$=\frac{\partial}{\partial z}\left[\left(K+D_{\psi v}\right)\frac{\partial\psi}{\partial z}+\left(D_{Tv}+D_{Ta}\right)\frac{\partial T}{\partial z}\right]+\frac{\partial K}{\partial z} \qquad (1)$$

where ρ_v is density of water vapor in the air-filled portion of the pore space, ρ_l is density of liquid water, θ is volumetric liquid water content, ψ is matric potential, θ_a is volumetric air content, T is temperature, t is time, K is hydraulic conductivity, z is vertical space coordinate, $D_{\psi v}$ is isothermal

vapor diffusivity, D_{Tv} is thermal vapor diffusivity, and D_{Ta} is transport coefficient for adsorbed liquid flow due to thermal gradients, which is ignored in this study because we believe it is negligible in comparison with D_{Tv} at the study site. $D_{\psi v}$ and D_{Tv} are given by *Milly* (1982) and *Milly and Eagleson* (1980):

$$D_{\psi v} = \frac{D_{atm}}{\rho_l}\alpha\theta_a \left.\frac{\partial \rho_v}{\partial \psi}\right|_T = \frac{D_{atm}}{\rho_l}\alpha\theta_a \frac{g\rho_v}{RT}$$

and

$$D_{Tv} = \frac{D_{atm}}{\rho_l} f\zeta \left.\frac{\partial \rho_v}{\partial T}\right|_\psi$$

$$= \frac{D_{atm}}{\rho_l} f\zeta\left(h\frac{\partial \rho_{vs}}{\partial T} - \frac{g\rho_v \psi}{RT^2}\right)$$

in which D_{atm} is molecular diffusivity of water vapor in air, α is tortuosity factor, g is acceleration due to gravity, R is gas constant for water vapor,

$$f = \begin{cases} n & \theta \le \theta_k \\ \theta_a + \dfrac{\theta_a}{n-\theta_k}\theta & \theta_k < \theta \end{cases}$$

in which n is porosity, θ_k is highest water content at which unsaturated hydraulic conductivity (K_u) is much lower than $D_{\psi v}$, $\zeta = (\nabla T)_a / \nabla T$, $(\nabla T)_a$ being average temperature gradient in the air phase, h is relative humidity, ρ_{vs} is saturated vapor density, and T is absolute temperature (°K).

The heat equation as given by *Milly* (1982) is the following:

$$\left(C + H_1 \left.\frac{\partial \rho_v}{\partial T}\right|_\psi + H_2 \left.\frac{\partial \theta}{\partial T}\right|_\psi\right)\frac{\partial T}{\partial t} + \left(H_1 \left.\frac{\partial \rho_v}{\partial \psi}\right|_T + H_2 \left.\frac{\partial \theta}{\partial \psi}\right|_T\right)\frac{\partial \psi}{\partial t}$$

$$= \frac{\partial}{\partial z}\left[\lambda\frac{\partial T}{\partial z} + \rho_l\left(LD_{\psi v} + gTD_{Ta}\right)\frac{\partial \psi}{\partial z} - c_l(T - T_0)q\right] \qquad (2)$$

where

$$H_1 = \left[L_0 + c_p(T - T_0)\right]\theta_a$$

$$H_2 = \left(c_l\rho_l - c_p\rho_v\right)(T - T_0) - \rho_l W - \rho_v L_0$$

and C is volumetric heat capacity of the soil, λ is effective thermal conductivity, L is latent heat of vaporization of water, c_l is specific heat of liquid water, L_0 is the value of L at an arbitrary reference temperature T_0, q is total water flux, c_p is specific heat of water vapor at constant pressure, and W is differential heat of wetting of the soil. The volumetric heat capacity of the soil is a weighted mean of the capacities of its components (*de Vries*, 1963). The effective thermal conductivity of the soil and ζ were calculated according to *de Vries* (1963), and the differential heat of wetting was calculated according to *Groenevelt and Kay* (1974).

The effects of temperature enter directly through the temperature gradients in equations 1 and 2 and indirectly through the temperature dependence of the matric potential, hydraulic conductivity, and vapor diffusivity. The temperature dependence of the matric potential was calculated by introducing the variable Ψ, in essence, a temperature corrected potential, which is assumed to be a function of water content only (*Milly,* 1984):

$$\Psi(\theta) = \psi \exp\left[-C_\psi (T - T_0)\right] \tag{3a}$$

where

$$C_\psi = \frac{1}{\psi}\frac{\partial \psi}{\partial T}\bigg|_\theta \tag{3b}$$

T is temperature, and T_0 is an arbitrary reference temperature. The surface tension model generally underestimates observed values of C_ψ (*Wilkinson and Klute*, 1962; *Nimmo and Miller*, 1986). In an early application of SPLaSHWaTr, *Milly* (1984) assigned a value of –0.0068 $°K^{-1}$ to C_ψ (*Milly*, 1984); this value is approximately three times that predicted by the surface tension model (*Philip and de Vries*, 1957). *Milly's* (1984) value was retained for simulations in this study. The temperature dependence of the hydraulic conductivity (K) is given by

$$K = K_s K_r(\theta)\nu(T_0) / \nu(T) \tag{4}$$

where K_s is saturated hydraulic conductivity at the reference temperature T_0, K_r is relative hydraulic conductivity (which is a function of water content [θ]), and ν is kinematic viscosity (*Milly*, 1984). In fact, this approach may underestimate the sensitivity of K to T by a factor of 2 or 3 (*Giakoumakis and Tsakiris*, 1991).

If the surface does not become saturated, then the surface boundary condition associated with the water flux is:

$$(q/\rho_l)_{z=0} = P - E \tag{5a}$$

where P is precipitation and E is evaporation (*Milly*, 1984). The evaporation rate is defined by the aerodynamic diffusion relation (*Milly*, 1984). When the surface becomes saturated, the boundary condition can be shown by:

$$\psi|_{z=0} = 0 \tag{5b}$$

where the depth of ponded water at the surface is negligible. In that situation, the model determines the surface influx, and any excess precipitation produces runoff. This surface boundary condition fails to allow for infiltration of runoff produced upstream of our ephemeral channel site. Such runoff events are rare and short lived. Furthermore, they would tend to occur when the model predicts surface saturation and maximum possible infiltration, in which case the additional water available from upstream could not infiltrate.

The surface boundary condition associated with the heat flux equation is (*Milly*, 1984):

$$q_h|_{z=0} = -(1-A)I_s - \varepsilon\left[I_{ld} - \sigma\left(T|_{z=0} + 273\right)^4\right] + \rho_l\left[L + c_l\left(T|_{z=0} - T_0\right)\right]E - \rho_l c_l\left(T_a - T_0\right)P + H \tag{6}$$

where q_h is soil heat flux, A is albedo, I_s is incoming solar radiation, ε is emissivity, I_{ld} is incoming atmospheric radiation, σ is Stefan-Boltzman constant, T is temperature (°C), $T+273$ is absolute temperature (°K), and H is turbulent diffusion of sensible heat into the atmosphere.

The one-dimensional forms of the governing partial differential water and heat equations are solved by the Galerkin finite element method in SPLaSHWaTr. The resulting nonlinear system of ordinary differential equations is solved by finite differencing and Picard iteration at each time step. The water and heat equations are solved alternately to maintain the tridiagonal nature of the matrix. Convergence and mass-conservation problems are sometimes cited as problems in ψ-based numerical models; such problems were eliminated in SPLaSHWaTr by introduction of a new numerical technique (*Milly*, 1985) and by automatic control of the time step size, allowing high

accuracy to be achieved without excessive use of computing time. The code was implemented on a MicroVax computer workstation.

NUMERICAL SIMULATIONS

Overview

We performed four 1-year (October 1989-September 1990) simulations of water and heat fluxes in response to atmospheric forcing. Hysteresis in the soil hydraulic properties was ignored in all simulations in this study. Simulation NHD (nonhysteretic drying) employed the measured main drying data to describe nonhysteretic water retention; NHW (nonhysteretic wetting) used the main wetting data estimated from the measured main drying data. The purpose of running both NHD and NHW was to obtain some insight into the sensitivity of long-time simulations to differences in water retention curves and associated differences in relative hydraulic conductivity, which was derived from the retention curve. (Comparison of NHD and NHW may also give some crude estimate of the importance of hysteresis, though such inferences would be tenuous, because the computed variables in NHD and NHW do not necessarily bound the variables that would be computed with the consistent hysteretic soil.) Both NHD and NHW were initialized with field measurements of water potential and temperature. Two other simulations, WP/5 and WP/10, were identical to NHD, except that the initial values of water potential inferred from field measurements were increased by dividing initial water potentials by 5 and 10. The purpose of these additional simulations was to provide an understanding of the sensitivity of the simulation to the initial condition.

Further details on initial conditions, boundary conditions, water retention, and hydraulic conductivity are provided in the remainder of this section.

Initial and Boundary Conditions

Initial conditions (Fig. 1) were based on water potential and temperature monitored by in situ psychrometers that were installed in an ephemeral stream setting (20P and P, Fig. 1, *Scanlon*, this

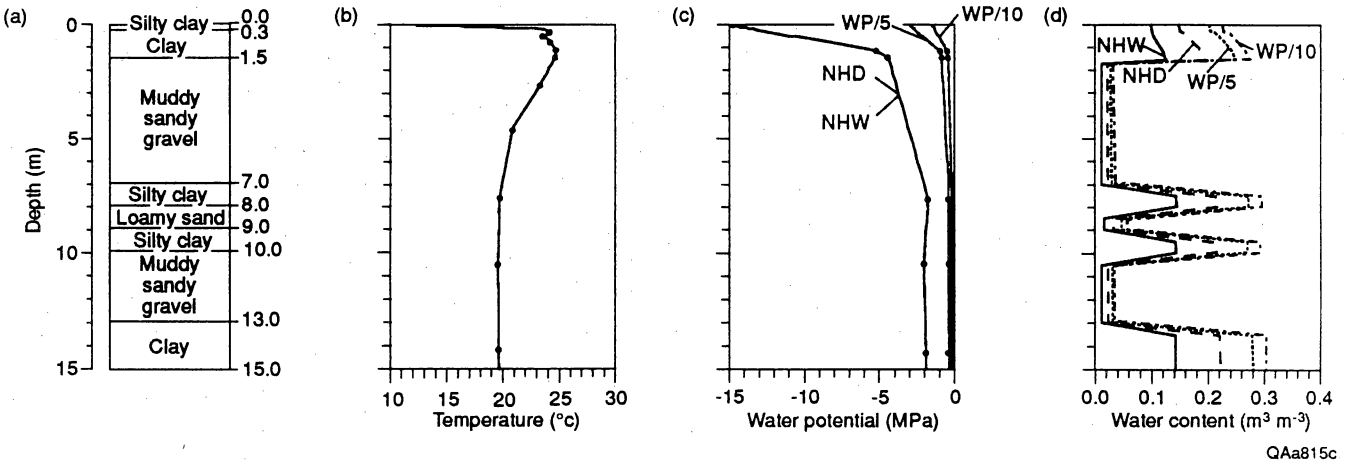

Figure 1. Variations in soil texture from borehole 50S (Fig. 1, *Scanlon*, this issue) with depth for simulated region. Water potential and temperature profiles measured by in situ psychrometers (P and 20P; Fig. 1, *Scanlon*, this issue) on October 1, 1989. These profiles constitute the initial conditions for the one–year simulations. The corresponding water content profiles for the nonhysteretic simulations were estimated from the measured water potential data using the main drying (NHD) and main wetting (NHW) curves for the materials at each depth. The WP/5 and WP/10 profiles represent the water content profiles calculated with the main drying function from initial water potentials that were divided by 5 and 10.

issue). Water potentials were out of range of the in situ psychrometers in the upper 0.8 m of the soil; therefore, the initial surface water potential (for NHD and NHW) was assigned a value of −15 MPa, which is approximately equal to the lowest water potential measured in the laboratory on soil sampled from the field site. Rainfall data were mostly obtained from the R_E gauge which is located approximately 2 km east-northeast of the psychrometers 20P and P (Fig. 1, *Scanlon*, this issue). The R_E gauge malfunctioned in September and December 1989 and in August 1990 and data for these months were obtained from the other gauges (R_W gauge September, 1989; R_C gauge December 1989 and August 1990; Fig. 1, *Scanlon*, this issue). Rainfall of 207 mm for the year simulated (October 1, 1989 – September 30, 1990) (Fig. 2) was lower than the long-term (1966–1987) mean annual rainfall of 280 mm for the Fort Hancock observation station situated 18 km southwest of the study area. Rainfall occurred primarily from July through September 1990. The initial temperature at the soil surface was approximated by the soil temperature measured at 0.01 m depth. The upper boundary conditions were based on hourly averages of air temperature, solar radiation, wind speed, and absolute humidity measured from October 1, 1989, through September 30, 1990, 2 m above the soil surface at a meteorological station approximately 1.6 km northeast of 20P and P (Fig. 1, *Scanlon*, this issue). Daily averages of these parameters were plotted to evaluate seasonal fluctuations (Fig. 2). Air temperature and solar radiation were highest in the summer. Wind speed was characterized by large short-term fluctuations. The absolute humidity was highest in the summer of 1990, when rainfall and temperature were highest. Incoming longwave radiation was calculated according to *Milly and Eagleson* (1982). Values of albedo for dry (0.2) and wet (0.1) silt loam (*Milly and Eagleson*, 1982) were assigned to the surficial sediments. A surface roughness value of 25 mm, based on previous analyses (*Scanlon*, 1992a), was used in the simulations and is a reasonable value for bare soil.

Zero gradients of water potential and temperature were assigned as the lower boundary (15 m depth) conditions. At this depth, temperature fluctuations are known to be negligible, and water flow is assumed to be controlled by gravity. Nodal spacing ranged from 0.25 mm near the soil surface to 500 mm at depth; the 15-m section of the unsaturated zone was represented by 57

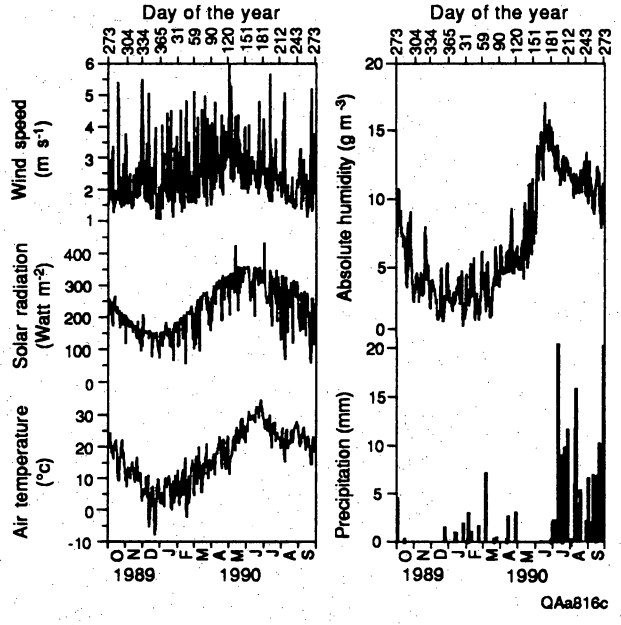

Figure 2. Daily rainfall and daily mean air temperature, solar radiation, wind speed, and absolute humidity for October, 1, 1989 through September, 30 1990. Rainfall based on east stn oct 89 no rain nov. center dec east Jan to Jul 1990 Aug center to 8/10 and then east and east in sept 90. only used center when east malfunctioned. Chose east stn because closest to A&M and problems with A&M data I presume.

elements. Previous simulations showed that increases and decreases in grid size did not affect the output (*Scanlon*, 1992a). The time step size was controlled automatically so that temperature would not change by more than 0.1°C or water content by more than 0.001 $m^3\ m^{-3}$ during a time step.

Hydraulic parameter estimation methods

Soil textures for the model domain were based on grain-size analyses of soil samples from borehole 50 (Fig. 1, *Scanlon*, this issue). Material properties were assigned to these soil textures on the basis of laboratory retention data for soils of similar texture that ranged from clay to muddy sandy gravel (Fig. 1, Table 1). Experimental data on soil-water desorption were fitted to determine a main drying curve, $\theta_d(\Psi)$, described by the following function (*Brooks and Corey*, 1964; *Milly and Eagleson*, 1980) (Fig. 3, Table 1):

$$\theta_d(\Psi) = \min\left\{\theta_u, \theta_u\left[(\Psi / a)^b - (-10^5 / a)^b\right] + c\left[5 - \log(-\Psi)\right]\right\} \quad (7)$$

where Ψ is in m, θ_u is the water content obtained upon rewetting and is taken to be 90% to 95% of the porosity following *Mualem* (1974) because of air entrapment, and a, b, and c are fitting parameters. This water retention function was employed to describe nonhysteretic soil water retention in the NHD simulation. For the NHW simulation, the main wetting curve, $\theta_w(\Psi)$, was used instead. The main wetting curve was estimated from the measured main drying data by the independent domain theory (*Mualem*, 1977):

$$\theta_d(\Psi) = \left[2 - \theta_u^{-1}\theta_w(\Psi)\right]\theta_w(\Psi) \quad (8)$$

Data on saturated hydraulic conductivity were obtained from field and laboratory measurements (Table 1) as described in Scanlon (this issue). The unsaturated hydraulic conductivity (Fig. 4) was calculated by numerical integration of the following (*Mualem*, 1976):

$$K_u(\theta) = \left(\sqrt{S_e}\left[\int_0^{S_e} \frac{dS}{\Psi(S)}\right]^2 \left[\int_0^1 \frac{dS}{\Psi(S)}\right]^{-2}\right) K_s \quad (9)$$

where S_e is the effective saturation

$$S_e = \frac{\theta - \theta_k}{\theta_u - \theta_k}$$

Table 1. Hydraulic parameters for soil textures used in the simulations.

Soil texture	clay	silty clay	loamy sand	muddy sandy gravel
K_S (cm s^{-1})	2.70×10^{-6}	3.20×10^{-6}	3.70×10^{-3}	2.60×10^{-3}
porosity	0.51	0.47	0.45	0.41
θ_u	0.48	0.42	0.41	0.37
a^d	–80	–50	–2	–1
a^w	–80	–50	–2	–1
b^d	–2.632	–2.067	–0.430	–0.560
b^w	–3.856	–1.808	–0.562	–0.664
c^d	0.08149	0.07875	0.00898	0.0078
c^w	0.0522	0.0526	0.0051	0.0041
$\theta_k{}^d$	0.13	0.11	0.034	0.029
$\theta_k{}^w$	0.12	0.11	0.021	0.019

Superscripts d and w refer to main drying and main wetting curves.

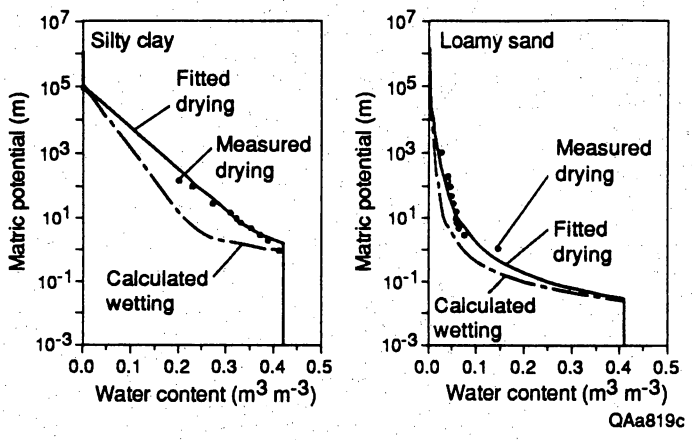

Figure 3. Measured main drying water retention data; fitted analytic function (*Brooks and Corey*, 1964; *Milly and Eagleson,* 1980) ; estimated main wetting water retention data (*Mualem*, 1977) and fitted analytic function (*Brooks and Corey*, 1964; *Milly and Eagleson,* 1980).

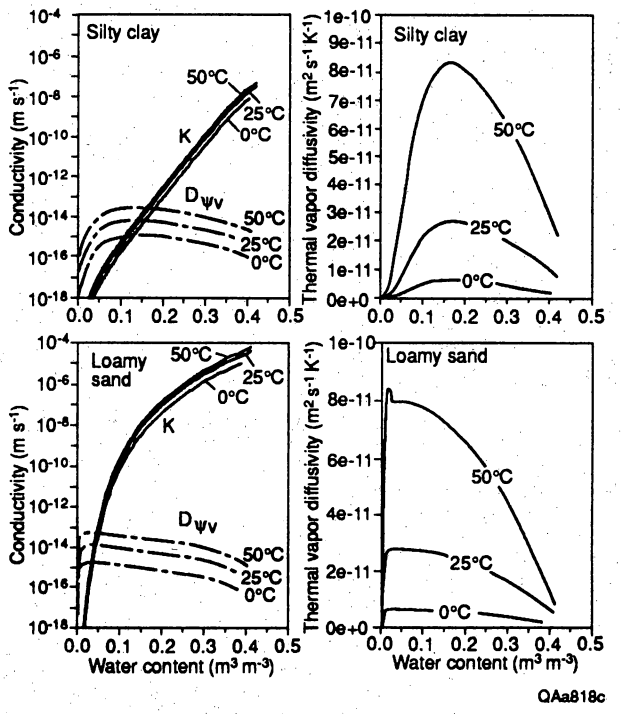

Figure 4. Liquid hydraulic conductivity (K) and isothermal ($D_{\psi v}$) and thermal (D_{Tv}) vapor diffusivity as a function of water content and temperature for representative soil textures.

θ_k is the value of water content at which liquid flow becomes negligible (specified as the water content at which isothermal vapor diffusivity is an order of magnitude greater than unsaturated hydraulic conductivity [*Milly and Eagleson*, 1982]) and S is a dummy integration variable for S_e.

The percent quartz, other minerals, and organic matter were input for soil thermal conductivity, which was calculated according to the method of *de Vries* (1963) (*Milly*, 1984). Isothermal and thermal vapor diffusivities were calculated according to *Milly* (1982) and *Milly and Eagleson* (1980). The temperature and water content dependencies of liquid hydraulic conductivity and of isothermal and thermal vapor diffusivities for representative soil textures are shown in Figure 4.

RESULTS AND DISCUSSION

Comparison of NHD Simulation with Measurements

There is remarkable consistency between the NHD simulated water potentials and the available field measurements. Figure 5 shows simulated and measured water potentials at 0900 hr, for the 1-year period, at depths of 0.3, 0.5, 0.8, 1.1, 1.4, and 10.5 m. Computed water potentials at 10.5 m depth were temporally invariant, and were similar to measured water potentials at that depth. At depths of 1.4 and 1.1 m, the measured and simulated seasonal changes in water potentials were very similar; however, the simulated values were somewhat higher than the measured values throughout the 1-year period, and had somewhat smaller seasonal variations. Water potentials at 0.3, 0.5, and 0.8 m depths were below the measurement range of the in situ psychrometers (< -7 to -8 MPa) for most of the monitoring period; computed water potentials were also less than -8 MPa. Measured water potentials increased to ≥ -7 MPa at 0.3 m depth in September 1990 after summer rain, and this change in water potentials was reproduced by the simulation.

The NHD simulation of seasonal changes of temperature at 0900 hr is also in good agreement with the field measurements (Fig. 6). Measured and simulated values both show the well-known

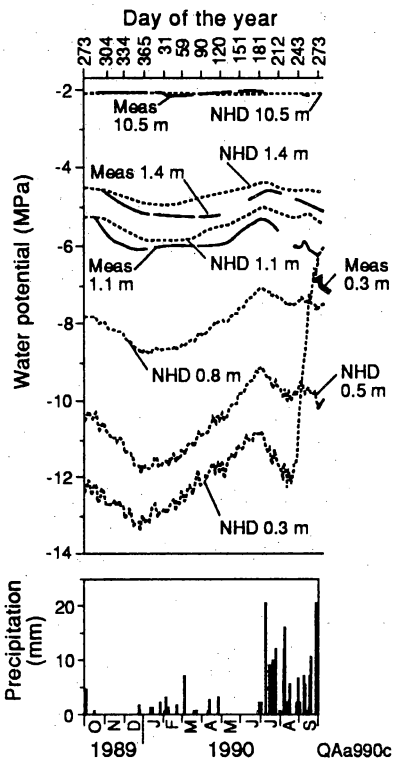

Figure 5. Comparison of time evolution of daily (0900 hr) measured and computed (NHD) water potentials.

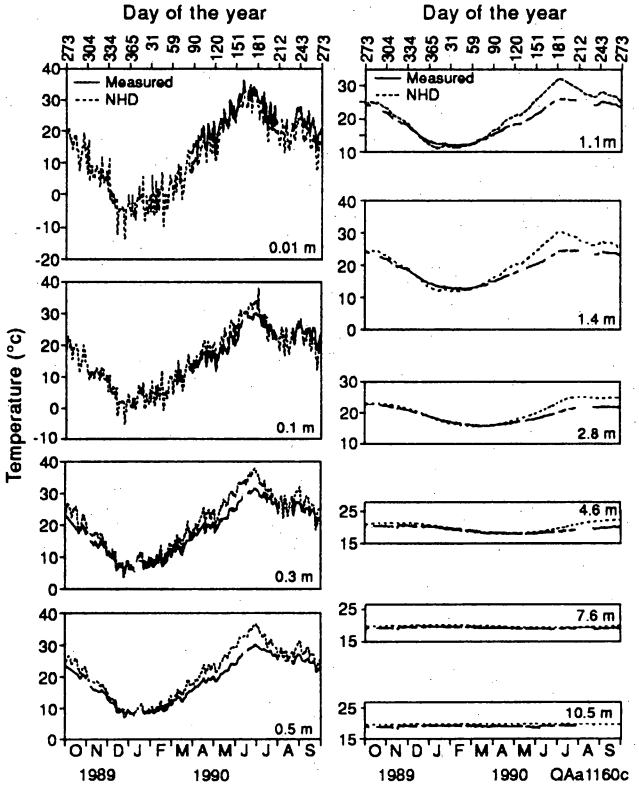

Figure 6. Comparison of time evolution of daily (0900 hr) measured and computed (NHD) temperatures.

extinction and phase-shift of the annual surface temperature wave with depth. There is a positive error in simulated peak temperatures at depths of 0.3 m and below, despite a relatively accurate simulation of the temperature at 0.01 and 0.1 m depths. This can be attributed to errors in the prescribed (and uncalibrated) thermal properties of the soil.

The similarity between Figures 5 and 6 suggests an explanation for the measured depth and time dependencies of water potential and their faithful reproduction in the simulation, which was achieved despite gross uncertainties in hydraulic properties. Ignoring the effect of the surface water input in the summer of 1990, we can see that the attenuation and phase shift of water potentials with depth are similar to those of temperature. We propose that the water potential changes are driven primarily by the temperature changes, with water content remaining relatively constant, according to (3a). For the model simulation, this hypothesis is confirmed by Figures 7a and b, which compare modeled potentials at depths of 1.1 and 1.4 m with those computed from (3a) using the modeled soil temperatures and the initial values of Ψ. Figures 7c and d compare the potentials computed from (3a), using field-measured temperatures and $C_\psi = -0.0068\ °K^{-1}$, with the field measured water potentials. The computed potentials change considerably less than the measured values. However; it should be kept in mind that the true value of C_ψ is quite uncertain, and may vary with depth and time. A value of $C_\psi = -0.015\ °K^{-1}$ provides much better, but still far from perfect, agreement between water potentials computed using (3a) and field measurements except after June 1990. Thus, the field data are generally consistent with the proposed hypothesis if one accepts an average field-inferred value for C_ψ of about $-0.015\ °K^{-1}$.

Consistent with the time and depth behaviors of water potential noted above, the changes in water storage associated with individual rainfall events were confined mainly to the top 0.3 m of soil. Water potential data for this upper layer are not available for comparison with simulated results. Simulated water potentials in this zone ranged from 0 to –387 MPa. The dominant effect of rainfall in the summer of 1990 is shown by substantial increases in computed water potentials and water content at this time (Figs. 8 and 9).

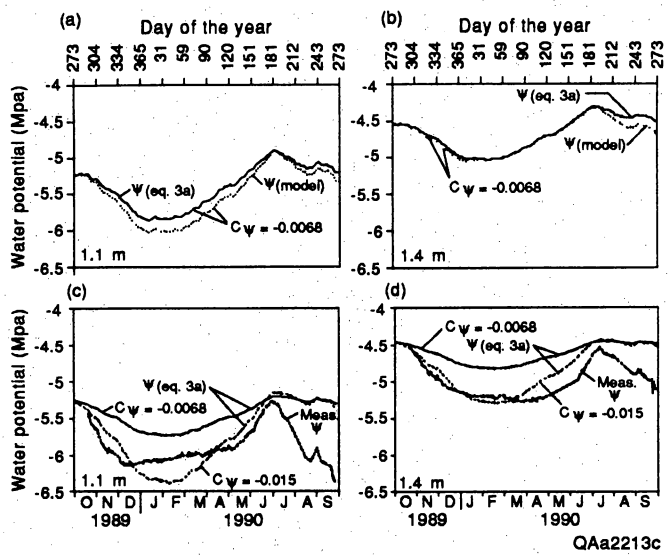

Figure 7. Comparison of modeled water potentials at 1.1 m (a) and 1.4 m (b) depth with those computed from (3a) using the modeled soil temperatures and initial values of Ψ; comparison of field-measured water potentials at (c) 1.1 m and (d) 1.4 m depths with those computed from (3a) using field measured temperatures and values of C_ψ = -0.0068°K^{-1} and of C_ψ = -0.015°K^{-1}.

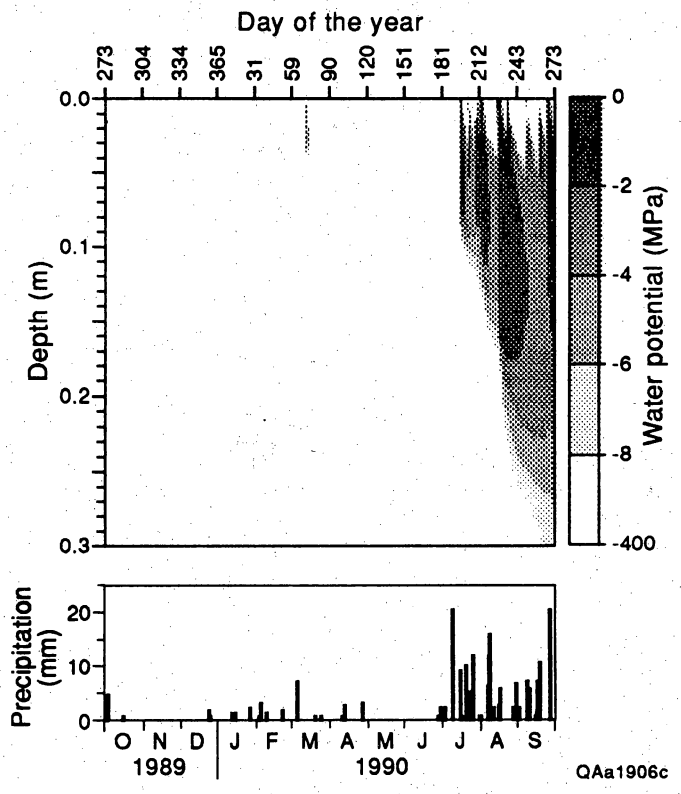

Figure 8. Time evolution of computed water potentials based on daily 0900 hr output from NHD and daily precipitation. Water potential output from the simulation was for 20 depths that range from 0.0025 m near surface to 0.2 m intervals at depth; water potentials in between these levels were interpolated linearly and are shown on a linear scale as gray tones.

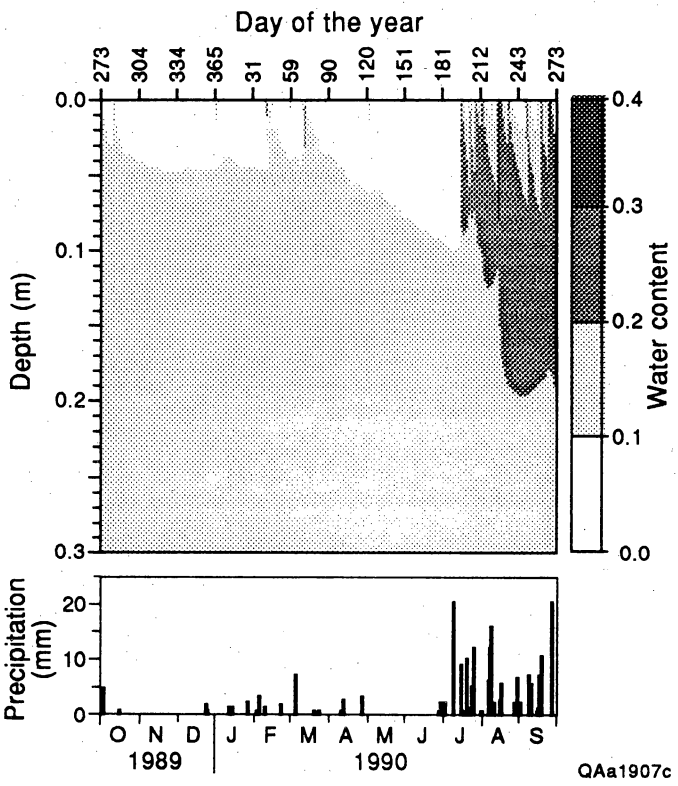

Figure 9. Time evolution of computed water contents based on daily 0900 hr output from NHD and daily precipitation. See Figure 7.

Another important feature of the measurements, which is present also in the simulation, is the vertical gradient in water potential. The measured annual mean water potential decreased from –2.1 MPa at 10.5 m depth to –4.7 MPa at 1.4 m depth and –5.4 MPa at 1.1 m depth; this indicates a driving force for upward liquid water flow. The reproduction of this gradient in the simulation could be attributed to its specification in the initial condition; such a possibility cannot be eliminated without knowing how long the effective "memory" of the system is. This issue is discussed in the next section.

The water balance computed for the simulated year is summarized in Table 2; the accumulation of this balance over time is shown in Figure 10. A total precipitation of 207 mm was balanced by 162 mm evaporative loss to the atmosphere, 10 mm surface runoff due to surface saturation during storms, and an increase of storage in the modeled soil (0 to 15 m depth) of 35 mm. The efflux from the bottom of the modeled soil was negligible. Measurements of evaporation are not available for comparison. Analysis of stream gauge data for the site suggests that 0.2% to 2% of precipitation runs off (S. Akhter, pers. comm., 1990), which would result in 0.4 to 4 mm runoff for the simulated year. These values are slightly lower than the simulated runoff of 10 mm. Rainfall in summer was approximately seven times higher than that in winter and resulted in high surface runoff, evaporation, and storage change in the summer.

Mechanisms of Water Transport in the Model

In this section, we discuss the simulation results in terms of the various fluxes. Vertical fluxes of water can be decomposed into fluxes of liquid $\left(-K\frac{\partial \psi}{\partial z}\right)$, which are driven by water potential gradients, and diffusive fluxes of vapor, which are driven by vapor pressure gradients that are in turn caused by water potential gradients (isothermal vapor flux, $\left(-D_{\psi v}\frac{\partial \psi}{\partial z}\right)$) and temperature gradients (thermal vapor flux, $\left(-D_{Tv}\frac{\partial T}{\partial z}\right)$). The sign convention for subsurface fluxes is that upward fluxes are positive and downward fluxes are negative.

Table 2. Soil-water balance.

	P (mm)	E (mm)	R_S (mm)	ΔS (mm)	Deep drainage (mm)
NHD (1 Oct 89–30 Sep 90)	207	162	9.9	35.2	-4.8×10^{-3}
NHD (21 Jun 90–21 Sep 90)	138	109	5.5	23.3	-1.2×10^{-3}
NHD (21 Dec 89–21 Mar 90)	19	17	0.00	1.6	-1.2×10^{-3}
NHW (1 Oct 89–30 Sep 90)	207	156	19.3	32.1	-1.8×10^{-4}
NHW (21 Jun 90–21 Sep 90)	138	105	12.3	20.0	-4.5×10^{-5}
NHW (21 Dec 89–21 Mar 90	19	17	0.0	2.0	-7.9×10^{-4}
WP/5 (1 Oct 89–30 Sep 90)	207	174	10.2	22.9	-1.3×10^{-1}
WP/10 (1 Oct 89–30 Sep 90)	207	182	10.4	14.8	-5.5×10^{-1}

P is precipitation; E is evaporation; R_S is surface runoff; ΔS is storage change; NHD and NHW are nonhysteretic drying and wetting simulations, respectively; WP/5 and WP/10 are similar to NHD except that the initial water potentials have been increased.

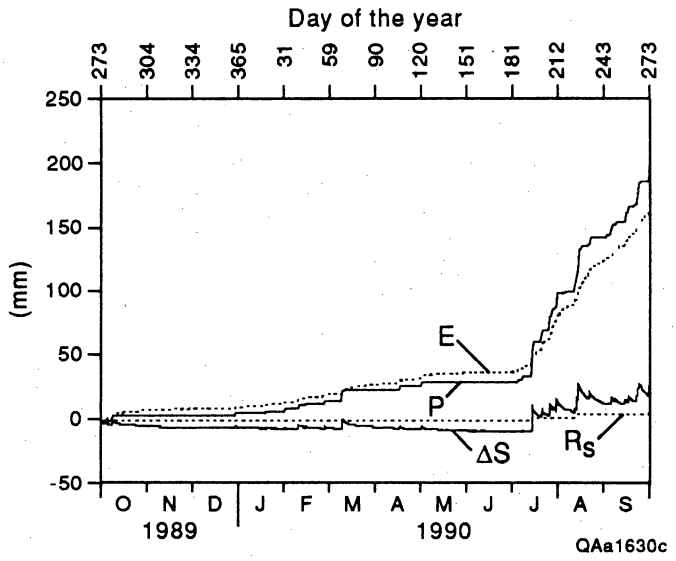

Figure 10. Measured cumulative precipitation, computed cumulative evaporation (E), surface runoff (R_s), and storage change (ΔS) for NHD.

In the upper 0.3 m of the soil, the direction, magnitude, and mechanism of water fluxes vary in response to the intermittent wetting and drying by weather events discussed earlier. As a consequence, it is not easy to characterize them succinctly. A detailed analysis of water fluxes in this near-surface layer revealed that the dominant process for downward water movement was liquid flow (Fig. 11a). Very close to the surface, upward isothermal vapor fluxes were significant. The annual evaporation of 162 mm may be compared to mean annual isothermal vapor fluxes of 128, 86, 35, and 16 mm at depths of 1.25, 7.5, 25, and 55 mm. Cumulative downward liquid flux in summer penetrated to a much greater depth (0.3 m) than downward liquid flux in winter (0.05 m) because of high summer rain (Fig. 12).

Below 0.3 m depth, water fluxes varied relatively little. The dominant term was the thermal vapor flux, which varied with season and depth following the temperature gradient. In the annual mean, its downward values in summer outweighed the upward values in winter (Fig. 12), giving cumulative annual downward thermal vapor fluxes of 1.5, 0.9, 0.65, and 0.17 mm yr^{-1} at depths of 0.5, 1.0, 2.0, and 5.0 m (Fig. 11). Thermal vapor flux was essentially unbalanced by the other water fluxes in the simulation. As a result, there was a net convergence of total water flux and hence an accumulation of water at all depths below the near surface layer. The associated rate of change of water content was 0.0018, 0.0003, 0.0003, and 0.0001 $m^3\ m^{-3}\ yr^{-1}$ at depths of 0.5, 1.0, 2.0, and 5.0 m. The low water flux throughout most of the domain confirms the earlier suggestion that the preservation of the initial water potential distribution was a major factor in the simulation.

Possible Causes of Lack of Equilibrium in the Model

We have shown that simulated thermal vapor flux convergence in NHD was unbalanced by other water fluxes below 0.3 m. It is important to consider whether such a situation is likely to occur in the field. On the basis of sensitivity simulations and approximate calculations, it appears that the sign and magnitude of the net annual convergence of thermally driven vapor flux is realistic, robust, and persistent through the years, as long as the soil below 0.3 m does not become

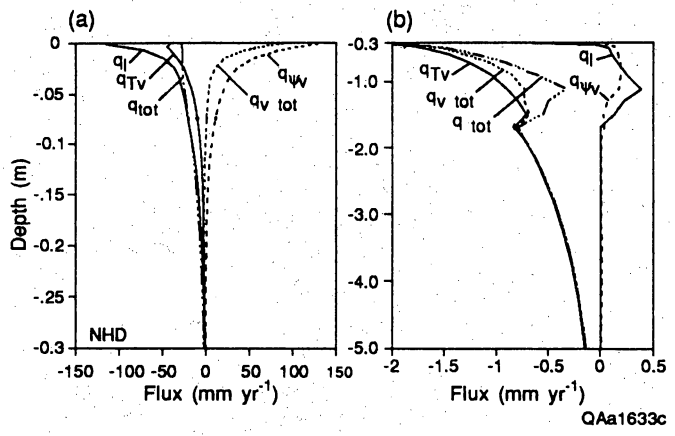

Figure 11. Variations in annual cumulative liquid (q_l), isothermal vapor ($q_{v\,iso}$), thermal vapor ($q_{v\,th}$), total vapor ($q_{v\,tot}$), and total (liquid + vapor; q_{tot}) flux for the upper 0.3 m (a) and for 0.3 to 5 m (b) for NHD.

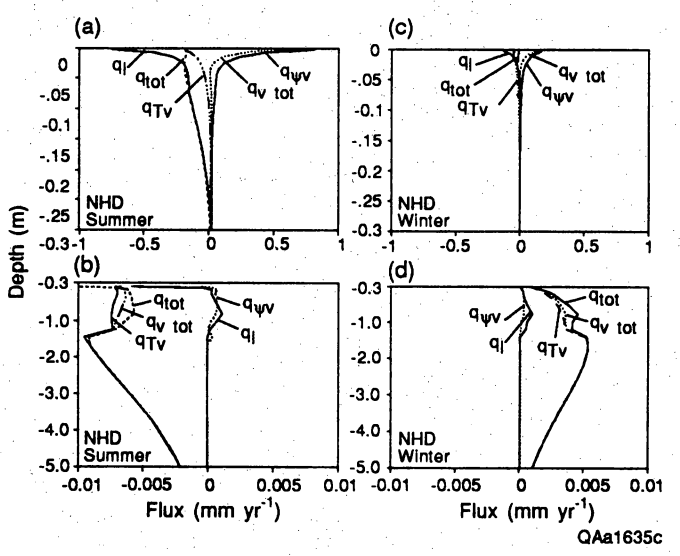

Figure 12. Variations in liquid (q_l), isothermal vapor ($q_{v\,iso}$), thermal vapor ($q_{v\,th}$), total vapor ($q_{v\,tot}$), and total (liquid + vapor; q_{tot}) flux for the upper 0.3 m (a and c) and for 0.3 to 5 m (b and d) for summer (June 21 to September, 21; a and b) and winter (December 21 to March 21; c and d) for NHD.

so dessicated (potential of approximately -10^4 m [−100 MPa] or lower) that the relative humidity of soil air drops far below saturation. Furthermore, the isothermal vapor flux appears to be too small to balance the thermal vapor flux. This implies that there is an annual mean source of liquid water below 0.3 m (and a related sink near the surface), which must be balanced by some combination of changes in liquid storage and divergences of liquid flux.

In the short term, annual storage changes could balance vapor convergence below 0.3 m, but in the long term liquid flux divergence would have to occur. In our simulation, values of hydraulic conductivity were far too small for such liquid flow compensation to occur, and storage changes resulted instead. If the same forcing had been continued through many annual cycles, the soil would have eventually moistened to the point where the source term was balanced in the annual mean, by liquid efflux, either upward or downward, from the source region.

The question naturally arises as to whether the source was balanced by storage change or liquid flux divergence in the field during the year that we simulated. If hydraulic conductivity values were actually greater than those computed from (9), then a return flow of liquid toward the surface, driven by the observed hydraulic gradient, could have balanced the thermal vapor flux. Indeed, the necessary increase in conductivity values would be within the known range of errors of equations such as (9). The compensating upward liquid return flow would imply in situ values of hydraulic conductivity on the order of 3.4×10^{-14}, 6.0×10^{-13}, and 3.0×10^{-13} m s^{-1} at depths of 1, 2, and 3 m. The alternative hypothesis is that the liquid fluxes were indeed negligible in the field, and that storage increases occurred instead, as in the model. Such behavior might be expected if the year under consideration were somehow anomalous relative to the preceding years; if prolonged drying of the soil below 0.3 m had occurred in recent history, then the model-inferred positive trend in water content could represent a recovery from the dry period. There are insufficient data available to determine whether the net downward thermal vapor flux was balanced by storage change or liquid flux in the field.

Model Sensitivity to Water Retention Function

Simulations NHD and NHW used the same initial profiles of water potential and temperature. However, initial water contents were much lower in NHW than in NHD because soil holds less water at a given potential when it is wetting than when it is drying (Fig. 1). Differences between main wetting and drying curves at the prevailing water potentials were greater for fine-textured soils than for coarse-textured soils (Fig. 3). Thermal properties of the soils were minimally affected by the difference in initial soil-water content. At depths greater than 0.3 m, the agreement between measured and simulated water potentials and temperatures found in NHD was present also in NHW. This insensitivity to soil hydraulic properties, within the range considered here, is consistent with our hypothesis that the measured and simulated water potential fluctuations below the near-surface zone are controlled primarily by temperature variations. However, it should be kept in mind that these results were obtained in a model whose hydraulic conductivity, we have argued, may be too low.

The annual water balance for NHW is given in Table 2; differences between NHD and NHW are relatively small. The difference in hydraulic properties apparently changes the ability of the soil to absorb the heaviest rainfalls, with decreased infiltration occurring in the NHW case. This loss of input is compensated by reductions in water accumulation and evaporation relative to those in NHD. The relative magnitudes of cumulative liquid and vapor fluxes in the near-surface layer in NHW (Fig. 13) were similar to those in NHD (Fig. 11).

The uncompensated thermal vapor flux convergences below 0.5 m depth found in NHD were present also in NHW (Figs. 11 and 13). Magnitudes of thermal vapor fluxes were nearly the same for NHD and NHW; mean annual values differed by less than 10% at most depths. Because of the lower water contents in NHW, the hydraulic conductivities and associated upward liquid fluxes below the 0.3 m depth were even smaller in NHW than in NHD. Liquid fluxes were typically reduced by factors of 10 in the coarse-grained sediments and by factors of 30 in the fine-grained sediments. The NHW simulation thus confirmed that the deeper liquid fluxes are highly sensitive

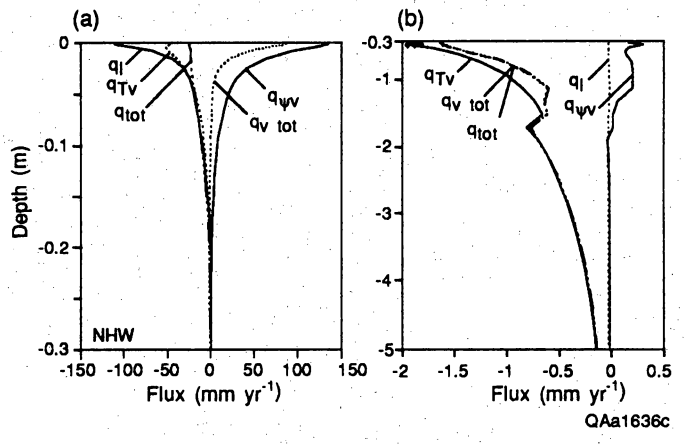

Figure 13. Variations in annual cumulative liquid (q_l), isothermal vapor ($q_{v\ iso}$), thermal vapor ($q_{v\ th}$), total vapor ($q_{v\ tot}$), and total (liquid + vapor; $q_{\ tot}$) flux for the upper 0.3 m (a) and for 0.3 to 5 m (b) for NHW.

to the assumed hydraulic properties. This is a consequence of the fact that the profile of water potential remains almost frozen at its initial shape for the entire simulation.

Model Sensitivity to Initial Water Potentials

In simulations WP/5 and WP/10, only the initial conditions differ from NHD. Differences in initial water potential among NHD (–15 to –2 MPa), WP/5 (–3 to –0.4 MPa), and WP/10 (–1.5 to –0.2 MPa) are much greater than the standard error associated with psychrometer calibration (± 0.2 MPa). Because the three simulations differed only in their initial water potentials, simulations for these three cases would be expected to converge to the same solution at sufficiently large time. Water potentials for the three simulations converged in the upper 0.2 m after infiltration of summer rain (Fig. 14). At depths greater than 0.2 m, the relaxation time greatly exceeded one year, and the higher initial water potentials in WP/5 and WP/10 were preserved through the simulation.

The water balances for WP/5 and WP/10 are given in Table 2. Because the water balance is determined mainly by the upper soil layers, and because NHD, WP/5, and WP/10 converge within a year in these upper layers, the difference in 1-year water balances is mainly attributable to the difference in initial storage of water in the soil and is insensitive to increased hydraulic conductivities associated with increased initial water potentials. WP/10, with the highest initial storage, experiences the smallest storage increase. The difference in storage changes of about 20 mm between NHD and WP/10 is approximately equal to the initial difference in storage within the top 0.3-m silty clay.

In the layers below 0.2 m, the effect of higher initial water potentials is opposite in sign, but otherwise similar, to the effect of changing from NHD to NHW. From about 0.2 to 2 m, the hydraulic conductivities are large enough in WP/10 to make computed upward liquid fluxes comparable to net downward thermal vapor fluxes on an annual basis (Fig. 15). The sensitivity of fluxes to variations in initial water potential suggests that accurate information on initial water potentials is important, particularly below the shallow subsurface active zone. These results differ

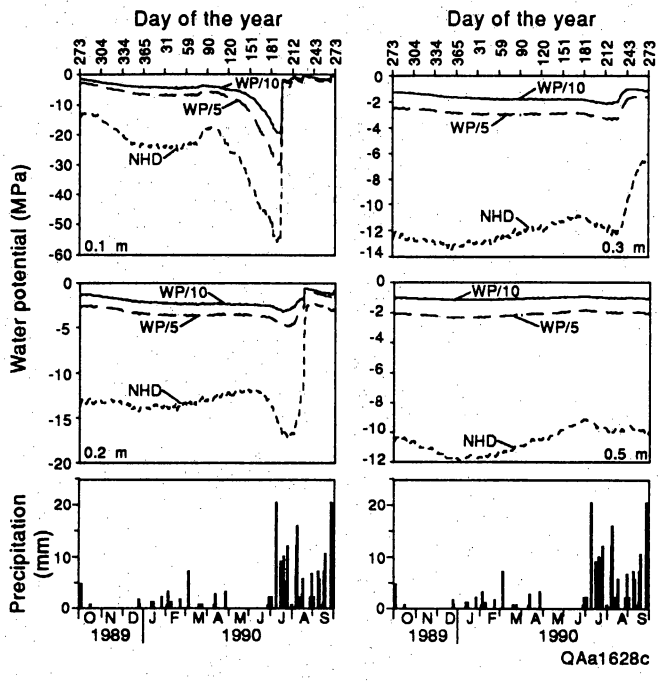

Figure 14. Time evolution of water potentials for NHD, WP/5, and WP/10 for selected depths.

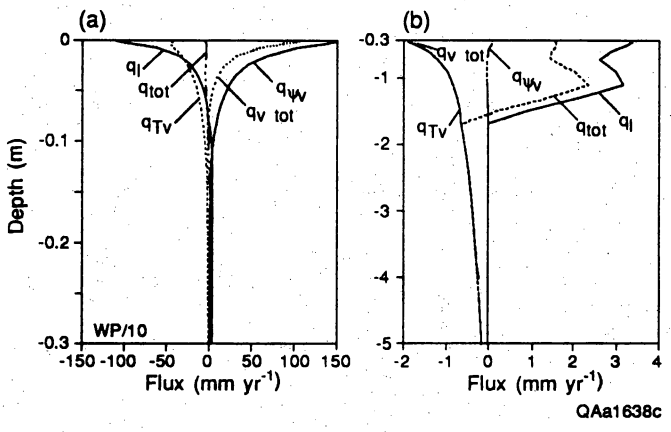

Figure 15. Variations in annual cumulative liquid (q_l), isothermal vapor ($q_{v\,iso}$), thermal vapor ($q_{v\,th}$), total vapor ($q_{v\,tot}$), and total (liquid + vapor; q_{tot}) flux for the upper 0.3 m (a) and for 0.3 to 5 m (b) for WP/10.

from those of isothermal liquid flow simulations using the computer code TRACR3D (*Scanlon et al.*, 1991; *Scanlon*, 1992b). Isothermal liquid flux in these simulations were insensitive to variations in initial water potentials except at very high values (> –0.1 MPa).

Comparison with Chemical Tracer Data

Chloride is nonvolatile and is restricted to liquid phase flow, whereas tritiated water is volatile and can move in both liquid and vapor phases. The $^{36}Cl/Cl$ peak was measured at a depth of 0.5 m and suggested a liquid flux of 1.4 mm yr^{-1} based on a 35-yr period since peak fallout and an average water content of 0.1 m^3 m^{-3} in the top 0.5 m of the unsaturated zone (*Scanlon*, 1992a). The ^3H profile was multipeaked and the peak at 1.4 m depth was assumed to represent the 1963–1964 bomb pulse. The resultant water (liquid + vapor) flux was 7 mm yr^{-1} based on a 25-year period since peak fallout and an average water content in the upper 1.4 m of 0.13 m^3 m^{-3}. The relative distribution of the two tracers suggests a vapor flux of 5.6 mm yr^{-1}. The previous 5-day summer and winter simulations suggested an annual net downward vapor flux that was consistent with the chemical tracer data (*Scanlon*, 1992a). Because of the limited time of the simulations (5 days), the magnitude of the simulated fluxes was not compared with that suggested by the chemical tracers. The 1-year simulation in this study also suggests cumulative downward vapor flux except in the upper 0.08 m. The average value of downward vapor flux (NHD 1.1 mm yr^{-1}; NHW 0.9 mm yr^{-1}) from 0.08 to 1.4 m depth (the depth of the ^3H peak) is the same order of magnitude as the 5.6 mm yr^{-1} vapor flux estimated from the relative distribution of the ^3H and $^{36}Cl/Cl$ tracers.

The vapor fluxes estimated from the tracer data and from the model differ by a factor of 5 or 6. If the flow system is not in equilibrium, then the simulated year could be nonrepresentative of the period since bomb fallout began. However, it would seem to be very difficult to explain the noted discrepancy in terms of any interannual variability of the factors driving vapor flux, at least within the diffusion theory applied here. As already mentioned, the thermal vapor flux calculations appear to be relatively robust. An alternative explanantion is that the apparent vapor transport

inferred from the tracer data is attributable to the strong seasonality of the thermal vapor flux. Seasonal thermal vapor fluxes are much larger than the annual means, yet this factor was not considered in the simple steady-advection estimates of vapor flux from the tracer data. Further evaluation of this issue would be facilitated by the use of a transport model having seasonally varying liquid and vapor flux profiles.

Sources of Uncertainty

One of the greatest sources of uncertainty in these simulations is the estimated hydraulic conductivity function ($K(\theta)$). The $K(\theta)$ function is much more nonlinear than the $D_{\psi v}(\theta)$ or the $D_{Tv}(\theta)$ functions (Fig. 4). Because the $K(\theta)$ function is estimated from the water retention function and saturated hydraulic conductivity (K_s), inaccuracies in the $K(\theta)$ function result from inaccuracies in the water retention functions, the K_s data, and especially in the estimation procedure. *Luckner et al.* (1989) discuss many possible sources of error in K_s measurements and suggest that the unsaturated hydraulic conductivity at a water content slightly less than saturation be used as a matching point rather than K_s. Uncertainties in the $K(\theta)$ function make it difficult to assess the relative importance of liquid and vapor transport in arid systems. Some ongoing studies are examining different procedures to obtain direct measurements of the $K(\theta)$ function (Hopmans, pers. comm. 1992; *Hudson*, 1992). These laboratory measurements should provide data to evaluate various $K(\theta)$ estimation procedures. If the hypothesis advanced herein concerning balance of upward liquid and downward thermal vapor fluxes is correct, then it may be possible to estimate in situ hydraulic conductivity values from measurements of water potentials in the field in arid environments.

Simulations in this study demonstrate that most of the variations in hydraulic parameters and fluxes were found in the top 0.3 m; however, instrumentation has not been developed to monitor water potential variations in this zone. In situ thermocouple psychrometers do not work well in these shallow sediments because of steep temperature gradients. The lack of detailed measurements

of water potential in the upper 0.3 m makes it impossible to evaluate the simulation results in this zone.

The conceptual model used for this study neglected hysteresis in the water retention functions. Although main wetting and main drying water retention curves bound hysteretic scanning curves, simulated liquid fluxes based on main curves do not necessarily bracket those based on hysteretic curves. There are many problems with simulating water retention hysteresis. Different procedures to estimate the main wetting function from the main drying function (*Mualem*, 1977; *Kool and Parker*, 1987) result in substantial differences in the estimated main wetting functions; this indicates that the main wetting and drying functions should be based on measured data. Even if measurements and an accurate model of water retention hysteresis are available, the saturation history of the profile must be determined, such as whether the system is initially drying or wetting, or whether sections of the profile are drying or wetting before the natural system can be simulated. The present analysis suggests that this is a serious concern, at least in principle, for the deeper soil horizons in an arid setting.

One of the assumptions in this study is that the air phase is static; however, in the unsaturated zone, the air phase is generally not static and the ability of the air phase to remain close to atmospheric pressure is attributed to the air phase being much more mobile than the water phase (*Hillel*, 1980). Air pressure may affect both liquid and vapor fluxes. The effect on liquid flux should be negligible because air pressure gradients are small relative to water potential gradients, and air permeabilities should be sufficiently high to allow, without much pressure buildup, the needed air displacement with the computed water fluxes from the simulations. Air movement may also result in water movement in the vapor phase. Our model assumed that vapor phase transport simply results from diffusion relative to a static air phase. In fact, the air moves both as a result of displacement by a dynamic liquid phase and, more importantly, as a result of atmospheric pressure fluctuations, from wind gusts to synoptic-scale weather systems. The net effect is to increase the effective diffusion coefficient in the upper layers by a pumping action; that is, the air is breathed in

and out. The effect of a separate air phase is thought to be greatest during individual storm events and should be relatively minor over the long time considered in these simulations.

CONCLUSIONS

Good agreement was found between NHD-(nonhysteretic drying water retention function) simulated and field-measured water potentials and temperatures. Below 0.3 m, attenuation and phase shift of water potentials and temperatures were similar and suggest that water potential variations may be controlled by temperature fluctuations, with little influence from changes of water content. Water balance data indicated that of the 207 mm of precipitation, 162 mm was evaporation, 10 mm was runoff, and 25 mm was increased soil water storage. Simulated surface runoff values (10 mm) were slightly higher than estimated values (0.4 to 4 mm) based on stream gauge data. Rainfall was much higher in summer than in winter, and summer infiltration dominated annual cumulative subsurface fluxes in the upper 0.3 m. Below this zone, downward thermal vapor fluxes were dominant and were not balanced by other fluxes. This annual cumulative downward water flux indicates that the model is not in equilibrium with its atmospheric forcing. This could indicate true disequilibrium in the field, or it may be attributable to inaccuracies in hydraulic conductivities, which may underestimate upward liquid fluxes.

Sensitivity of model results to use of the nonhysteretic wetting water retention function was examined in the NHW simulation. Use of the main wetting data resulted in much lower initial saturation distribution relative to that in NHD. Thermal properties of soil were negligibly affected by differences in initial water content. Computed water potentials and temperatures based on NHD and NHW were similar below 0.3 m, which supports the explanation that water potential variations are controlled by temperature fluctuations. Increased surface runoff in NHW relative to that in NHD was compensated by reduced water accumulation and evaporation in NHW. Below 0.3 m, smaller upward liquid fluxes in NHW relative to those in NHD suggest that liquid fluxes in this zone are sensitive to the water retention functions that enter the calculations of hydraulic conductivity.

Simulations WP/5 and WP/10 differed from NHD in that the initial water potentials were increased by dividing by 5 and 10. Water potentials in the upper 0.2 m in all three simulations converged after infiltration of summer rain; however, initial water potentials at greater depths were preserved throughout the year. Below 0.2 m, the initial water distribution remains almost unchanged for 1 year, and the increased upward liquid fluxes associated with increased initial water potential are attributed to increased unsaturated hydraulic conductivity. The water balance is determined mainly in the shallow subsurface ($\leq$ 0.3 m). Differences in water balance among the three simulations can be explained by variations in initial soil water storage and are negligibly affected by differences in unsaturated hydraulic conductivity associated with variations in initial water potential.

Comparison of numerical model results with chemical tracer data shows that simulated downward vapor flux below the evaporation front (0.08 m) based on these numerical simulations agrees with the deeper penetration of bomb ^{3}H (volatile) relative to that of bomb ^{36}Cl (nonvolatile). The simulated average downward vapor flux from 0.08 to 1.4 m depth (NHD 1.1 mm yr^{-1}; NHW 0.9 mm yr^{-1}) is within the same order of magnitude as that based on the relative distribution of ^{3}H and $^{36}Cl/Cl$ (5.6 mm yr^{-1}).

This simulation research provides a greater understanding of unsaturated zone processes in desert soils. Agreement between computed and measured parameters is attributed to the robustness of the thermal calculations. These simulations also indicate some of the main sources of uncertainty, particularly in the estimated hydraulic conductivities.

ACKNOWLEDGMENTS

This project was funded by the Texas Low-Level Radioactive Waste Disposal Authority under contract IAC(88-89)0932. Publication of this manuscript was authorized by the Director, Bureau of Economic Geology, The University of Texas at Austin. A. J. Avakian, J. E. Constantz, A. Fryar, and R. W. Healy provided very helpful reviews. The manuscript was edited by A. R. Masterson and B. S. Duncan. Drafting was by J. L. Lardon and S. Krepps under the direction of R. L. Dillon.

REFERENCES

Baca, R. G., King, I. P., and Norton, W. R., Finite element models for simultaneous heat and moisture transport in unsaturated soils, in *Finite Elements in Water Resources*, by C. A. Brebbia, W. G. Gray, and G. F. Pinder *(Eds.)*, pp. 1.19–1.35, Pentech Press, Lond., 1978.

Brooks, R. H., and Corey, A. T., Hydraulic properties of porous media, *Hydrol. Papers*, Colorado State Univ., 27 pp., 1964.

de Silans, A. P., Bruckler, L., Thony, J. L., and Vauclin, M., Numerical modeling of coupled heat and water flows during drying in a stratified bare soil-comparison with field observations, *J. Hydrol.*, 105, 109–138, 1989.

de Vries, D. A., Simultaneous transfer of heat and moisture in porous media, *Trans. AGU*, 39, 909–916, 1958.

de Vries, D. A., Thermal properties of soils. In van Wijk, W.R. (Ed.) *Physics of Plant Environment*, North-Holland, Amsterdam, 1963.

Giakoumakis, S. G., and Tsakiris, G. P., Eliminating the effect of temperature from unsaturated soil hydraulic functions: *J. Hydrol.*, 129, 109–125, 1991.

Groenevelt, P. H., and Kay, B. D., On the interaction of water and heat transport in frozen and unfrozen soils: II. The liquid phase, *Soil Sci. Soc. Am. Proc.*, 38, 400–404, 1974.

Hanks, R. J., Gardner, H. R., and Fairbourn, M. L., Evaporation of water from soils as influenced by drying with wind or radiation, *Soil Sci. Soc. Am. Proc.*, 31, 593–598, 1967.

Hillel, D., ***Fundamentals of Soil Physics***, 413 pp., Academic Press, London, 1980.

Hudson, D. B., A transient method for estimating the hydraulic properties of dry unsaturated soil cores. Ph.D. dissertation, 294 pp., New Mexico State Univ., Las Cruces, 1992.

Kool, J. B., and Parker, J. C., Development and evaluation of closed-form expressions for hysteretic soil hydraulic properties, *Water Resour. Res.*, 23, 105–114, 1987.

Luckner, L., van Genuchten, M. Th., and Nielsen, D. R., A consistent set of parametric models for the two-phase flow of immiscible fluids in the subsurface, *Water Resour. Res.*, 25, 2187–2193, 1989.

Milly, P. C. D., Moisture and heat transport in hysteretic, inhomogeneous porous media: a matric head-based formulation and a numerical model, *Water Resour. Res.*, 18, 489–498, 1982.

Milly, P. C. D., A simulation analysis of thermal effects on evaporation from soil, *Water Resour. Res.*, 20, 1087–1098, 1984.

Milly, P. C. D., A mass-conservative procedure for time-stepping in models of unsaturated flow, *Adv. Water Resour.*, 8, 32–36, 1985.

Milly, P. C. D., and Eagleson, P. S., The coupled transport of water and heat in a vertical soil column under atmospheric excitation, *Rep. 258*, 234 pp., Ralph M. Parsons Lab., Mass. Inst. Technol., Cambridge, 1980.

Milly, P. C. D., and Eagleson, P. S., Parameterization of moisture and heat fluxes across the land surface for use in atmospheric general circulation models, *Rep. 279*, 226 pp., Ralph M. Parsons Lab., Mass. Inst. Technol., Cambridge, 1982.

Mualem, Y., A conceptual model of hysteresis: *Water Resour. Res.*, 10, 514–520, 1974.

Mualem, Y., A new model for predicting the hydraulic conductivity of unsaturated porous media: *Water Resour. Res.*, 12, 513–521, 1976.

Mualem, Y., Extension of the similarity hypothesis used for modeling the soil water characteristics, *Water Resour. Res.*, 13, 773–780, 1977.

Nimmo, J. R., and Miller, E. E., The temperature dependence of isothermal moisture vs. potential characteristics of soils, *Soil Sci. Soc. Am. J.*, 50, 1105–1113, 1986.

Philip, J. R., and de Vries, D. A., Moisture movement in porous materials under temperature gradients, *Trans. AGU*, 38, 222–232, 1957.

Pruess, K., TOUGH user's guide, *Rep. NUREG/CR-4645*, 78 pp., U.S. Nucl. Reg. Comm., Washington, D.C., 1987.

Rose, C. W., Water transport in soil with a daily temperature wave I. Theory and experiment, *Aust. J. Soil Res.*, 6, 31–44, 1968.

Scanlon, B.R., Moisture flux in desert soils 1. Field studies. *Water Resour. Res.*, this issue.

Scanlon, B. R., Evaluation of liquid and vapor flow in desert soils based on chlorine-36 and tritium tracers and nonisothermal flow simulations, *Water Resour. Res.*, 28, 285–297, 1992a.

Scanlon, B. R., Moisture and solute flux along preferred pathways characterized by fissured sediments in desert soils, *J. Contam. Hydrol.*, 10, 19–46, 1992b.

Scanlon, B. R., Wang, F. P., and Richter, B. C., Field studies and numerical modeling of unsaturated flow in the Chihuahuan Desert, Texas, Rep. Invest. 199, 55 pp. Bur. Econ. Geol., Univ. of Texas., Austin, 1991.

Sophocleous, M., Analysis of water and heat flow in unsaturated-saturated porous media, *Water Resour. Res.*, 15, 1195–1206, 1979.

van de Griend, A. A., Camillo, P. J., and Gurney, R. J., Discrimination of soil physical parameters, thermal inertia, and soil moisture from diurnal surface temperature fluctuations, *Water Resour. Res.*, 21, 997–1009, 1985.

Wilkinson, G. E., and Klute, A., The temperature effect on the equilibrium energy status of water held by porous media, *Soil Sci. Soc. Am. Proc.*, 26, 326–329, 1962.

APPENDIX B. ANALYSIS OF LONG-TERM WATER POTENTIAL MONITORING DATA

ANALYSIS OF LONG TERM WATER POTENTIAL MONITORING DATA TO EVALUATE UNSATURATED ZONE PROCESSES IN AN ARID REGION UNDER NATURAL CONDITIONS

ABSTRACT

The use of thermocouple psychrometry to evaluate unsaturated flow processes under natural conditions in a semiarid site in the Chihuahuan Desert of Texas was examined. Water potential and temperature were monitored by thermocouple psychrometers installed in the bed of an ephemeral stream from 0.3 m to 24.1 m depth from April 1990 through June 1993. Soil texture in the upper 8.4 m ranged from gravely muddy sand to sand and below 8.4 m was clay. Water potentials were also measured in the laboratory on soil samples collected in a nearby borehole. Infiltration and redistribution of water was monitored by psychrometers in the upper 1.4 m during 1992 and 1993 as a result of abnormally high winter precipitation. The wetting front penetrated to a maximum depth of 0.8 m. The wetting front penetration depth monitored by another set of psychrometers in the Hueco Bolson was much less (0.3 m) because the surficial sediments were finer grained (clay loam). Water moved down by piston flow as evidenced by the progressive increase in water potentials with depth. The soil, particularly in the upper 0.8 m dried within a short time as indicated by the short lag between water potential changes in psychrometers at different depths. The short time required for drying the soil can be explained by roots effectively removing water from various depths at approximately the same time. Seasonal fluctuations in water potential were monitored at depths of 2.3 to 7.4 m. The magnitude of the water potential fluctuations decreased with depth and the phase of the wave shifted with depth similar to those of temperature fluctuations. These seasonal water potential variations are attributed to seasonal temperature fluctuations and probably do not reflect changes in water content. The general shape of the laboratory and field measured water potential profiles was similar. Below the zone of active circulation, water

potentials measured at the same depth differed by up to 6 MPa in the coarse grained sediments and by up to 2 MPa lower in the fine grained sediments. The lower water potentials measured by the laboratory psychrometer are attributed to sample drying during collection and analysis. Water potential profiles based on the field monitored data suggest an upward driving force for liquid and isothermal vapor movement except in the zone of active water circulation. A sharp increase in field monitored water potentials was found from 5.9 to 7.4 m depth and marks the sand clay contact. This corresponds to a chloride mass balance age of 13 kyr and may reflect transient conditions and increased recharge in the Pleistocene when vegetation was mesic. Comparison of water potential data from the Hueco Bolson with those from other desert sites in the southwest shows that water potentials are low and gradients are generally upward except in the shallow subsurface after rainfall. Water potential monitoring data from the Hueco Bolson have important implications for waste disposal in arid sites and emphasize the importance of fine grained surficial sediments and revegetation of trench caps to minimize subsurface water movement.

INTRODUCTION

Although much of the previous work on unsaturated zone processes in arid regions has concentrated on flow in the shallow zone in response to agricultural irrigation (Gaudet et al., 1977; van de Pol et al., 1977), more recent interest in desert soils has developed because of their suitability as repositories of radioactive materials (Enfield et al., 1973; Gee and Heller, 1985; Montazer et al., 1985; Nichols, 1987; Winograd, 1981). Water fluxes under natural conditions in desert soils are generally very low and difficult to estimate. Various methods have been used to quantify water fluxes in arid settings. Although the water balance approach may be suitable in irrigated agricultural regions, it is generally unsuitable in natural arid systems because evapotranspiration comprises a large component of the water balance and techniques for measuring actual evapotranspiration in partly

vegetated desert regions are highly inaccurate. Weighing lysimeters have been used to measure directly evapotranspiration and drainage (Gee and Jones, 1985); however, disturbance of the natural soil and artificial boundary conditions may affect flow. Monitoring water content with a neutron probe may not be sufficiently accurate to detect the small fluxes that move through the unsaturated zone. In addition, water content is discontinuous across different lithologies and variations in water content with depth do not indicate the direction of water movement.

In contrast to water content data, under steady state conditions energy potential is continuous across different soil types and is typically used to infer the flow direction. The energy potential consists of matric, gravitational, temperature, and osmotic components. Steep temperature gradients are generally restricted to the upper meter of the unsaturated zone and osmotic potential gradients are generally negligible. In dry soils, matric potential gradients are dominant.

Thermocouple psychrometers are used to measure water (matric and osmotic) potential and temperature of dry soils both in the field and in the laboratory. The theory of thermocouple psychrometry is described in Rawlins and Campbell (1986). Thermocouple psychrometers measure the relative humidity (p/p_o) of the soil atmosphere, which is proportional to water potential (ψ in MPa) according to the Kelvin equation:

$$\psi = RT / M \ln(p / p_0) \qquad (1)$$

where R is the ideal gas constant, M is the molecular mass of water (R/M is 0.462 MPa K^{-1}), and T is temperature (K).

The use of thermocouple psychrometers in previous hydrologic studies has been very limited because these instruments are small and easily broken, and individual psychrometric calibration is time consuming and expensive. Psychrometers may also lose calibration in the field (Merrill and Rawlins, 1972). Much of the psychrometric data in the literature is questionable because of poor installation procedures and lack of sophisticated data loggers for recording water potentials accurately (Montazer, et al., 1985).

Purpose

The objective of this study was to examine the use of thermocouple psychrometry to evaluate hydrologic processes in the shallow unsaturated zone of a natural semiarid system. Thermocouple psychrometers provide information on water potential and temperature gradients which are the driving forces for liquid and vapor flow. Examination of temporal and spatial variations in these parameters helps us understand the controls on unsaturated flow processes. Water potential data from the Hueco Bolson and from other arid and semiarid regions were compared. Analysis of long-term monitoring data provides insights that can be used to optimize the design of future monitoring programs in similar settings.

Study Area

The study area (31° 25'N, 105° 40'W) is located in the Hueco Bolson, a 200-m-thick sediment-filled basin within the Chihuahuan Desert of Texas (Fig. 1). Groundwater ranges from 110 to 150 m deep within the study area (Mullican et al., 1989). The unsaturated zone consists of 0 to 15 m of clay to gravel of the Tertiary/Quaternary Camp Rice Formation and 140 to 200 m of clay containing interbedded silts and sands of the underlying Tertiary Fort Hancock Formation. Extreme textural variations from clay to gravel were found in trenches dug to a depth of 7 m. A discontinuous layer of caliche lies approximately 2 m deep. The present surface of the Hueco Bolson is an alluvial plain that slopes 1 to 1.5% toward the Rio Grande. The elevation of the study area is approximately 1,300 m. Modern ephemeral streams that drain the alluvial plain lack well-defined channels (maximum relief is 0.6 m) and drain into arroyos that border the study area. In general both streams and arroyos are dry except after rainfall. Shrubs such as native grasses, creosote (Larrea tridentata) and mesquite (Prosopis glandulosa) with rooting depths of 1 to 5 m are common.

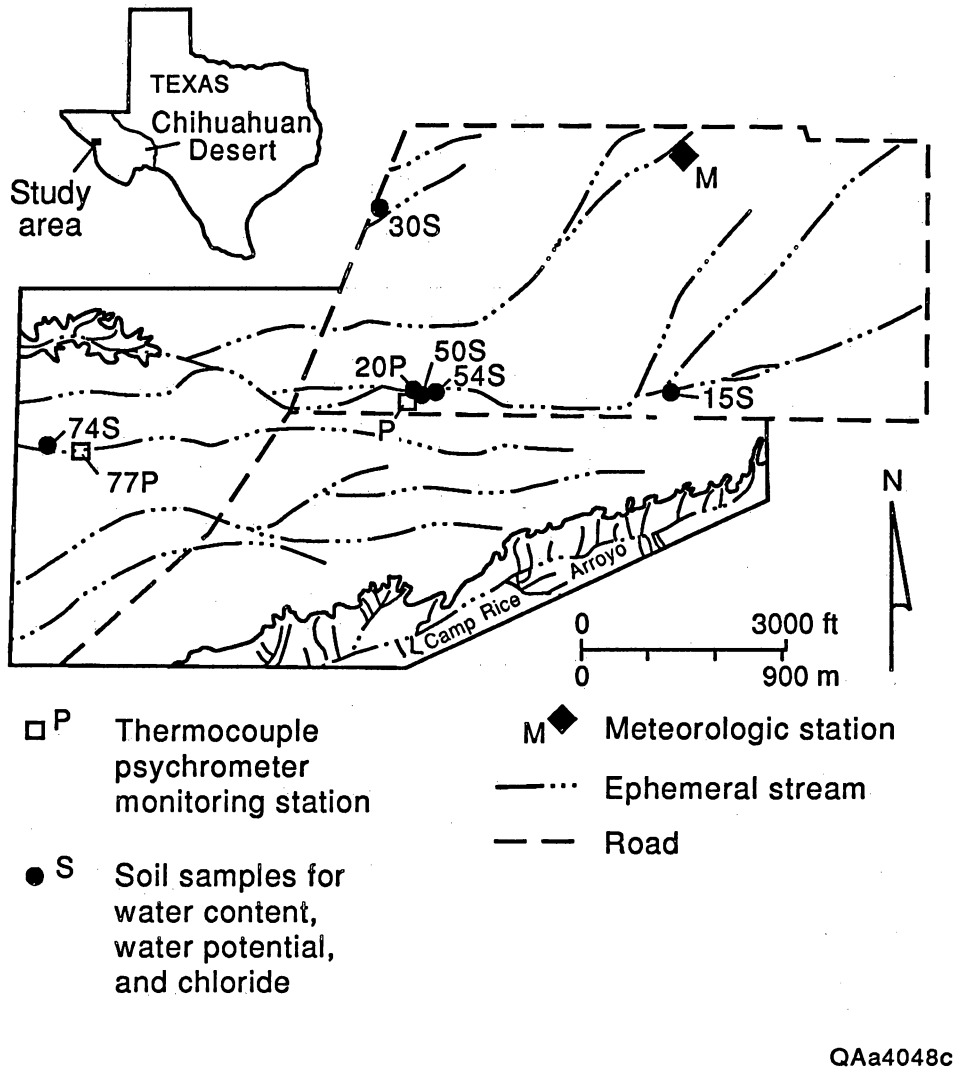

Figure 1. Location of sampled boreholes and thermocouple psychrometer monitoring stations in the study area.

The regional climate is subtropical arid (Larkin and Bomar, 1983). Long-term meteorological data were based on a 22 yr record (1967 to 1991, excluding 1971, 1983, and 1989) from Fort Hancock, which is 18 km southwest of the study area. Monitoring at the Fort Hancock station was discontinued in May, 1992. Long-term mean annual precipitation is 296 mm and exhibits large interannual variations (from 115 mm in 1967 to 433 mm in 1970). Analysis of the 22 yr record indicates that 63% of the precipitation falls from June through September (Fig. 2). Most of this rain falls as local intense, short duration convective storms, when temperature and evaporation are highest. Minor winter frontal storms are of longer duration. Mean annual class-A pan evaporation is approximately seven times mean annual precipitation. Mean monthly air temperatures based on data from 1966 to 1987 at Fort Hancock range from 5°C in December to 28°C in July.

METHODS

Field psychrometric measurements were conducted with Peltier- or Spanner-type psychrometers that use a cooling current (the Peltier effect), to condense water below the dew point on the thermocouple (Spanner, 1951). These psychrometers can be used for laboratory and field measurements; they operate in the range of approximately –0.2 to –8 MPa because the Peltier effect cannot condense water at potentials of less than approximately –8 MPa. Laboratory psychrometric measurements were made with a Richards-type psychrometer which uses a drop of water that is added mechanically to the thermocouple and spans a much larger range in water potential (–0.2 to –300 MPa) (Rawlins and Campbell, 1986). After water is added or condensed onto the thermocouple, this water evaporates and results in a temperature depression that is translated into output voltage. The output voltage changes rapidly initially and then stabilizes at a plateau value before final reduction to the reference voltage level.

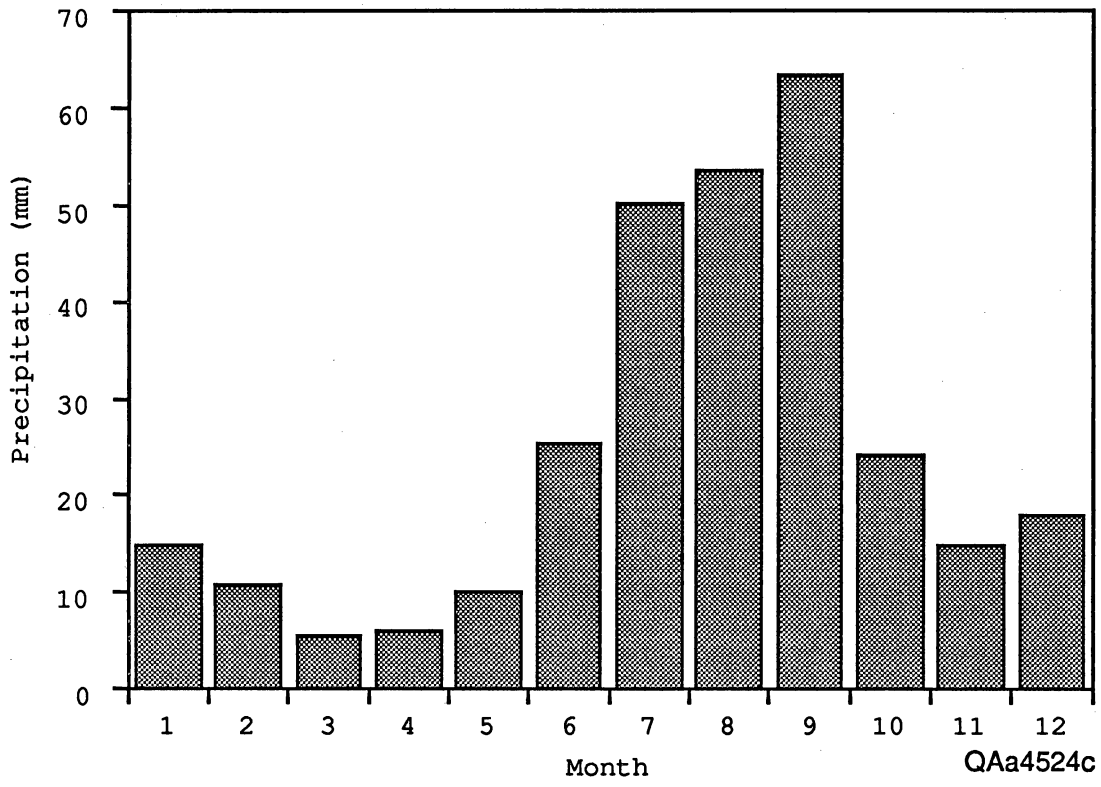

Figure 2. Long-term average monthly precipitation based on 22 yr of data from Fort Hancock.

Temperature gradients, whether in laboratory systems or near the soil surface, are critical because a 1K temperature difference between the dry bulb and the sample at 20°C can result in a measurement error of approximately 13 MPa (Rawlins and Campbell, 1986). Temperature gradients can be inferred in Spanner-type psychrometers from the null output (Brown and Bartos, 1982). The null output is the temperature difference between the reference and measuring junctions before Peltier cooling and should be zero under isothermal conditions. For example, a null output of +60 mV indicates that the sensing junction is approximately 1°C cooler than the reference junction.

Because psychrometers are manufactured manually, each has a slightly different geometry which results in a unique relationship between water potential and emf output. Psychrometers are generally calibrated individually because of their unique characteristics. Fifty screen-caged, single junction, Peltier (Spanner, 1951) thermocouple psychrometers (Model PST-55, Wescor, Logan, UT) were calibrated with four NaCl solutions (0.0, 0.5, 1.0, and 1.5 molal [M]) which correspond to water potentials of 0.0, -2.2, -4.6, and -7.0 MPa at 20°C (Lang, 1967). Calibration procedures similar to those outlined in Brown and Bartos (1982) were followed. A constant temperature water bath provided temperatures of 15, 20 and 25°C ± 0.01°C for calibration. A Peltier cooling current of 5 ma and a 30-s cooling time are considered optimal (Brown and Bartos, 1982) and were used in calibration and monitoring. Psychrometers were calibrated with the required cable lengths for field installation (30 m). A datalogger (Model CR7, Campbell Scientific, Inc., Logan, UT) supplied the cooling current to the psychrometers and recorded psychrometer output. The calibration data for all psychrometers were combined to develop the following general calibration equation using stepwise regression procedures (Meyn and White, 1972):

$$\psi = 0.0345 - 0.4176V + 0.0073VT \qquad (1)$$

where ψ is water potential (MPa), V is voltage (microvolts) and T is temperature (°C). The general regression equation had a coefficient of determination (r^2) of 0.96 and a standard error of estimate of 0.49 MPa. Most of the error occurs in the dry range. When

the readings from the 1.5 M solution were excluded from the calibration equation, the r^2 increased to 0.98 and the standard error of estimate reduced to 0.25 MPa.

Voltage output from psychrometers increases with decreasing water potential down to a water potential of approximately -7 to -8 MPa as represented by equation (1). Below this, the voltage output decreases with decreasing water potential (Brown and Bartos, 1982). Therefore, low voltage output from thermocouple psychrometers may correspond to very dry soil (beyond the calibration range of the psychrometers) or wet soil (Wiebe et al., 1971). To distinguish between very dry and wet soil 100 0.1-s readings were recorded to determine the evaporation curve for each psychrometer because the shape of the evaporation curve is narrow and spiked in the dry range and is flat and stable in the wet range. Because the plateau voltage is very short in Spanner type psychrometers in the dry range a representative voltage is not readily determined. Comparison of different methods to obtain the voltage endpoint including 2 s and 5 s readings and extrapolation of the plateau voltage to the beginning of evaporation showed that extrapolation of the plateau gave the most consistent results (Savage and Wiebe, 1987). An algorithm was used to estimate the plateau voltage region and to extrapolate the plateau voltage to zero time using linear regression (Kurzmack, pers. comm. 1990).

Psychrometers were installed in an ephemeral stream setting to determine the water potential gradient to 24.1 m depth and to evaluate temporal variations in water potential (Fig. 1). Duplicate psychrometers were placed in holes (13-mm diameter, 0.5 m length) drilled horizontally into a vertical face exposed by digging a trench to 1.7-m depth. The horizontal installation minimized the effect of temperature gradients on psychrometer output (Rawlins and Campbell, 1986). The trench was backfilled with the original sediments after psychrometer installation. At depths of 2 to 24.1 m, duplicate psychrometers were installed in a borehole that was drilled using a solid-stem auger. Epoxy (DER324/DEH24) was used to prevent preferential water or air flow between psychrometer stations within the borehole and to form a seal at the surface that would preclude surface drainage into the

borehole. Epoxy was chosen because it does not introduce water into the system. Epoxy properties (curing time, viscosity, and exothermic curing temperature) were tested in the laboratory before field use to ensure that the epoxy would not become viscous while being poured down the tremie pipe. Sand was poured down a separate tremie pipe immediately after the epoxy to form a sand/epoxy column that reduced the reaction temperature to 80°C. The small diameter of the borehole (50 mm) was designed to minimize psychrometer equilibration time. Water potentials were monitored daily in the field at 0900 hr because temperature gradients in the shallow subsurface should be minimal at this time.

Soil samples were collected from boreholes 15S, 30S, 54S and 74S for laboratory measurement of water potential with a Decagon psychrometer SC-10A sample changer (Decagon Devices, Incorporated, Pullman, WA) that was calibrated using NaCl solutions that ranged from 0.05 M to saturated and corresponded to osmotic potentials (ψ_π) of -0.2 to -38 MPa at 20°C (Lang, 1967). The 1-s readings were recorded with a data logger for 120 s. The plateau output voltage from Richard's type psychrometers is fairly stable over a wide range in water potentials and the 120 s microvolt reading is generally used to calculate the water potential (Jones et al., 1990) and was used in this study. Because water potentials from –0.01 to –10 MPa correspond to relative humidities from 93 to 100 percent, all measurements were conducted in a glove box lined with wet paper towels to minimize water loss from the samples. Temperature variations in the laboratory were minimal. A set of 20 calibration solutions were prepared and measured initially to test the instrument, and the resulting regression gave an r^2 of 1.0 and a standard error of estimate of 0.06 MPa.

RESULTS

Laboratory Measured Water Potential Profile

Sediments from borehole 74 were uniformly coarse grained (gravelly muddy sand to sand) in the upper 8.4 m and fine grained (clay) below this depth (Fig. 3a). Gravimetric water content was low in the coarse grained sediments and high in the fine grained sediments (Fig. 3b). An increase in water content of 0.22 g g^{-1} was found at the contact between the sand and the underlying clay.

Although water potential measured by thermocouple psychrometers is the sum of matric and osmotic potential, psychrometers at this site essentially measured the matric potential because the osmotic potential was negligible (0.0 to -0.8 MPa). Total (matric + osmotic + gravitational) potential is generally used to indicate the direction of liquid water flow. Variations in gravitational potential were estimated from the elevation of the sample point above the water table and were small ($\leq$ 0.14 MPa within a profile). Laboratory measured water potentials in samples from borehole 74 ranged from -11.5 to -2.6 MPa (Fig. 3c). Water potentials in surficial sediments were low (-7.9 MPa at the surface to -4.6 MPa at 0.26 m depth) and suggest that these sediments were dry. The upward water potential gradient in this zone reflects evapotranspiration. The downward water potential gradient from 0.26 (-4.6 MPa) to 1.3 m (-11.5 MPa) probably resulted from a previous infiltration event. Below 1.3 m the overall water potential gradient was upward. . Under equilibrium conditions, the sum of the water and gravitational potentials is zero and the water potential at the soil surface is equal to the water table depth (-110 m or -1.08 MPa at this site) (Koorevaar et al., 1983). Water potentials plotted to the right of equilibrium line indicate downward flow, whereas those plotted to the left indicate upward flow under equilibrium conditions. The position of the water potential profile to the left of the equilibrium line and the upward water potential gradients both indicate an upward driving

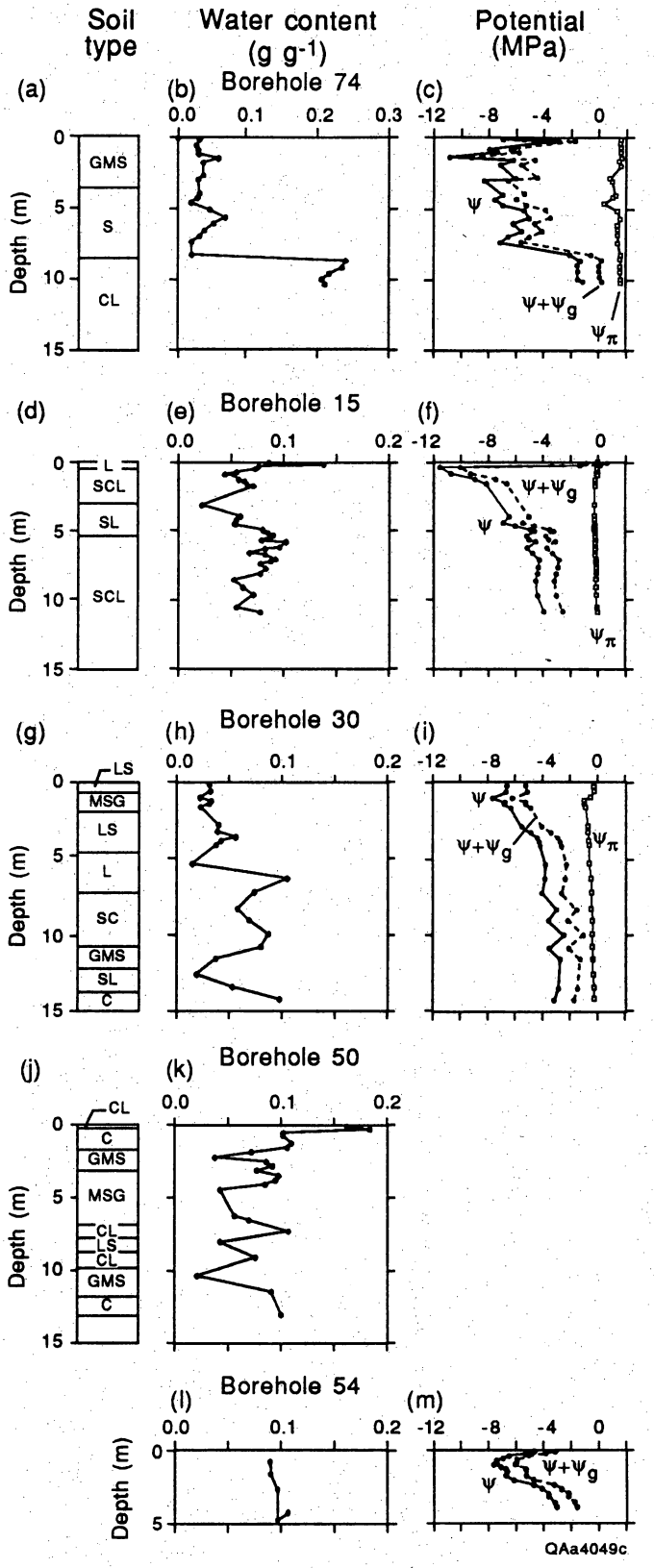

Figure 3. Profiles of soil texture, water content, water potential (ψ), osmotic potential ($\psi\pi$), and total potential ($\psi+\psi_\gamma$) for boreholes 74, 15, and 30, soil texture and water content for borehole 50, and water potential for borehole 54. Soil textures: GMS, gravelly muddy sand; S, sand; LS, loamy sand; SL, sandy loam; SCL, sandy clay loam; LS, loamy sand; L, loam; and CL, clay loam. Sediment samples that contained gravel were classified according to Folk (1974), and those that did not contain gravel were classified according to the U.S. Department of Agriculture (1975).

force for water movement. A sharp increase in water potentials from -8 to -3.4 MPa was found from 7.4 to 8.4 m depth. This water potential increase corresponds to the soil textural change from sand to clay and to the water content increase of 0.22 g g^{-1}. At depths ≥ 8.4 m, water potentials were uniformly high and ranged from -2.6 to -3.4 MPa.

The range and general trend in water potentials in soil samples from borehole 74S were similar to those in soil samples from other boreholes in the study area (Fig. 3). Water potentials in near surface sediments varied depending on the time of sampling relative to rainfall events. The existence of sharp wetting fronts after rainfall events is shown in the profiles from borehole 15. Water potentials from approximately 3 to 7.5 m depth in borehole 74 were lower than those in the other profiles. The soils in this zone were generally coarser grained than soils from the same depth interval in the other boreholes. This low water potential zone in profile 74 may be partly an artifact of a greater effect of drying during sample collection and analysis on water potentials in coarse grained sand than in fine grained sediments. Coarse grained sediments in the other profiles generally have a fine matrix such as clay or silt which would not lose water during sampling and analysis as readily as the sand from borehole 74S. Water potentials in the clay below 8.4 m depth in borehole 74 were similar to water potentials at similar depths in the other boreholes.

Field Monitored Water Potentials

Generally good agreement was found between water potentials monitored by duplicate psychrometers installed in the trench face from depths of 0.3 to 1.4 m. Only one (7.4 m) of the 14 pairs of psychrometers at greater depths showed good agreement. One can readily determine which of the duplicates was operating correctly because in most cases water potentials monitored by one of the duplicates was fairly stable whereas water potentials recorded by the other duplicate migrated toward 0 (Fig. 4). Some drifted to 0

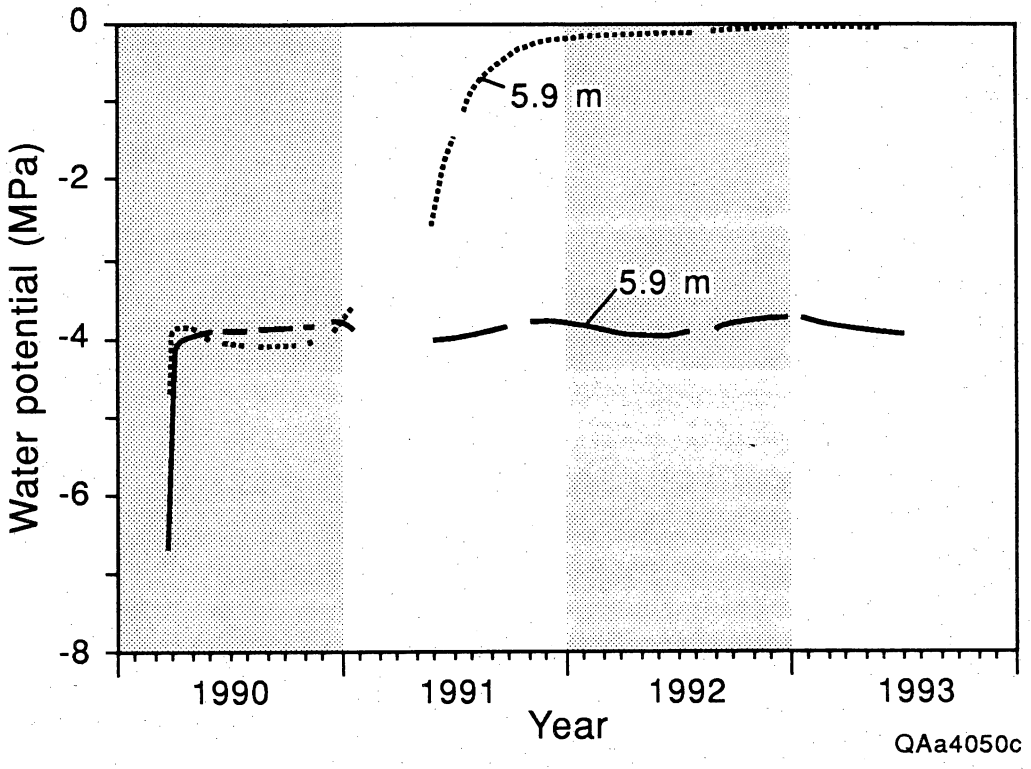

Figure 4. Temporal variations in water potential measured at 0900 hr by duplicate psychrometers at 5.9 m depth in borehole 77P.

immediately after installation whereas others drifted toward 0 within the first year. This phenomenon cannot readily be explained.

The monitoring record for the psychrometers is discontinuous. Data are not available from January to June, 1991 because the monitoring program was shut down. Loss of data at other times resulted from problems with downloading the data loggers. The shallow in situ psychrometers (≤ 1.7 m depth) which were installed in a pit in close contact with the surrounding sediments, equilibrated within a day of installation, whereas the deeper borehole psychrometers (2.3 to 24.1 m depth) required from 30 to 120 days to equilibrate. The rate of equilibration decreased with time. Water potentials increased during equilibration because the backfill sediments that dried while being stored during drilling recovered water from subsurface sediments after psychrometer installation.

Water infiltration and redistribution occurred to a depth of 1.4 m. Water potentials from 0.5 to 1.4 m depth were much higher in the latter half of 1991 than in 1990 as seen in the water potential data for 1.4 m depth in Fig. 5. The lack of water potential data for the first 5 months of 1991 makes it difficult to determine how this increase occurred. The increase probably resulted from high rainfall that was recorded from July through September in 1990 (223 mm) and in January 1991 (75 mm) (Fig. 5). The greatest increase in water potentials was recorded in the beginning of 1992. Precipitation in December (1991) and in June (1992) was 4.8 and 3.5 times long term average for these months respectively (Fig. 2). Water potentials increased by up to 4 to 4.5 MPa at 0.5 and 0.8 m depths (Fig. 6). The increase in water potentials was very rapid (0.2 to 0.3 MPa d^{-1}). The water potential increase was attenuated with depth with maximum water potential increases of 2.4 MPa at 1.1 m depth and 1.6 MPa at 1.4 m depth. The phase of the wave also shifted with depth. A lag of 30 d occurred between water potential increases recorded at depths of 0.5 m and 0.8 m which suggests a water velocity of 0.01 m d^{-1}. Water potentials remained close to 0 for 120 to 70 d at depths of 0.3 and 0.8 m respectively although rainfall was low for much of this period. Water potential variations at depths of

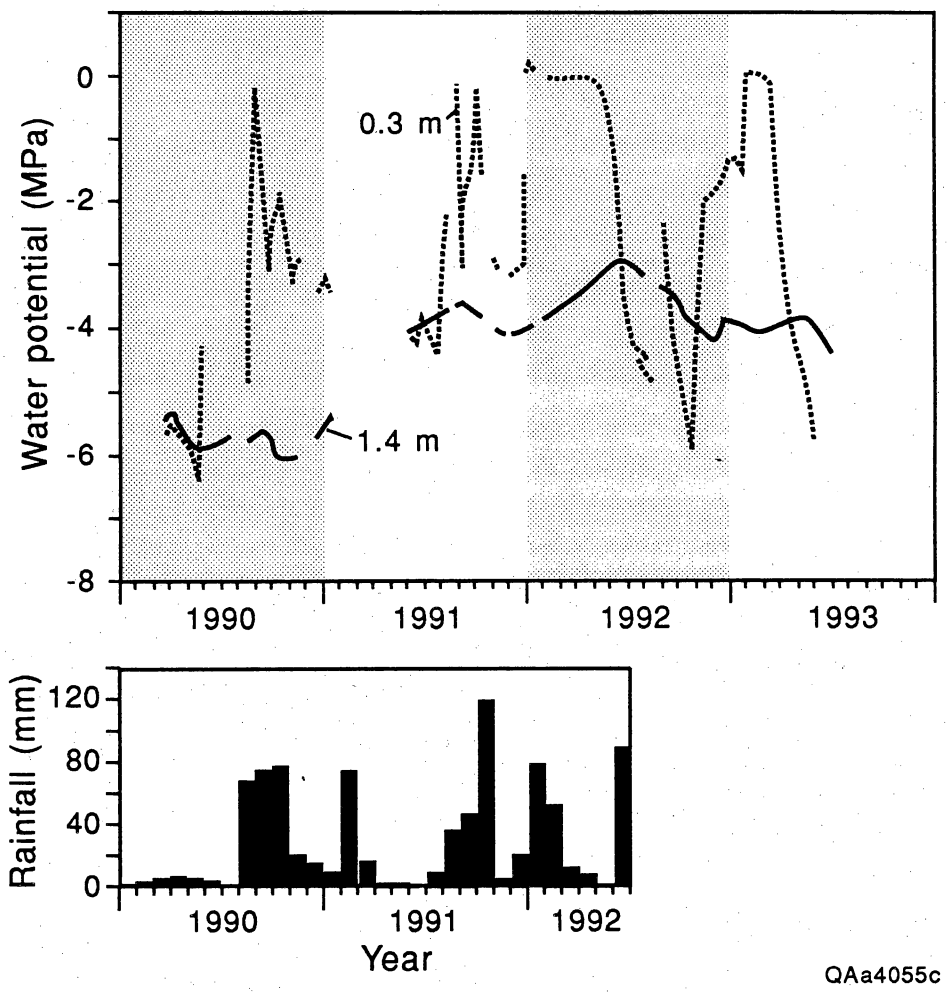

Figure 5. Temporal variations in water potential monitored by psychrometers at 0.3 and 1.4 m depth. Monthly precipitation was recorded at the Fort Hancock station.

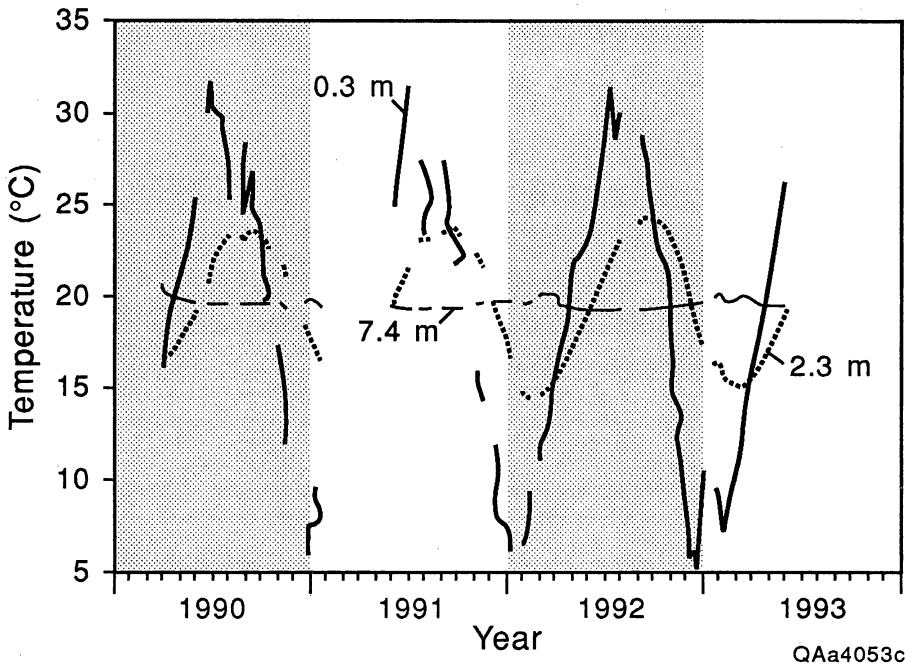

Figure 6. Seasonal temperature fluctuations monitored by psychrometers at depths of 0.3, 2.3, and 7.4 m in borehole 77P and adjacent trench.

0.3 to 0.8 m resembled a square wave whereas water potentials at depths of 1.1 and 1.4 m peaked and decreased in a short period. During the drying phase water potentials decreased rapidly (-0.07 MPa d^{-1} at 0.5 and 0.8 m). The lag between water potential decreases at 0.3 to 0.8 m depth was much less during the drying phase than during the wetting phase. Rainfall during May 1992 was high (90 mm); however, water potentials continued to decline. This lack of response to rainfall may have occurred because of saturation of surficial sediments and rainfall runoff. Psychrometers also recorded an infiltration event in the fall and winter of 1992 to 1993. This infiltration event did not penetrate as deep as that in the beginning of 1992. Many of the features found in the first infiltration event can also be seen in the second event such as attenuation and phase shift of the water potential increase with depth and very little lag between water potential decreases at different depths during the drying phase. There are no precipitation records for this period as monitoring at the NOA station in Fort Hancock station was discontinued in May, 1992.

Seasonal fluctuations in water potential were monitored at depths of 2.3 to 7.4 m (Fig. 7). The magnitude of the seasonal water potential variations decreased from approximately 1 MPa at 2.3 m depth to approximately 0.2 MPa at 7.4 m depth. At 2.3 m depth maximum water potentials occurred in the summer and minimum water potentials in the winter. The phase of the wave shifted with depth such that at 7.4 m depth the seasonal maxima and minima were reversed and maximum water potentials occurred in the winter instead of the summer. The seasonal water potential variations were generally in phase with seasonal temperature fluctuations at each depth (Fig. 8). Seasonal variations in null output were also recorded and ranged from -3 to 2 μV at 2.3 m depth to -0.5 to 0.5 μV at 7.4 m depth (Fig. 9). These null output fluctuations also followed temperature fluctuations. Psychrometer readings were corrected in the data logger for variations in null output. Water potential variations monitored by psychrometers at depths greater than 7.4 m were negligible (Fig. 10).

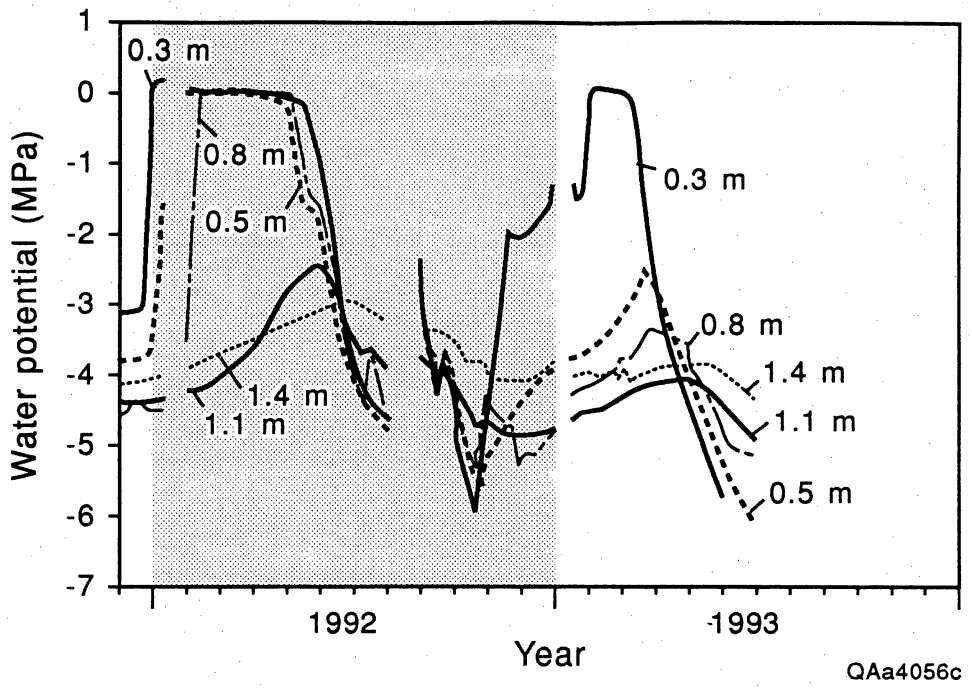

Figure 7. Variations in water potential that show infiltration and redistribution of water at depths of 0.3 to 1.4 m.

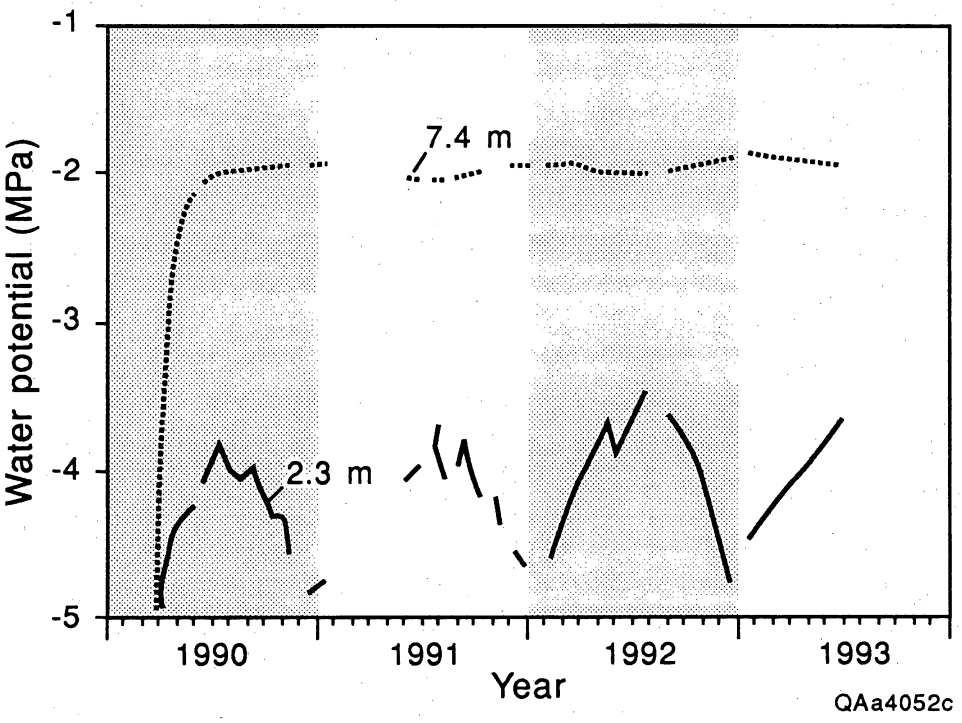

Figure 8. Seasonal fluctuations in water potential monitored by psychrometers at 2.3 and 7.4 m depth.

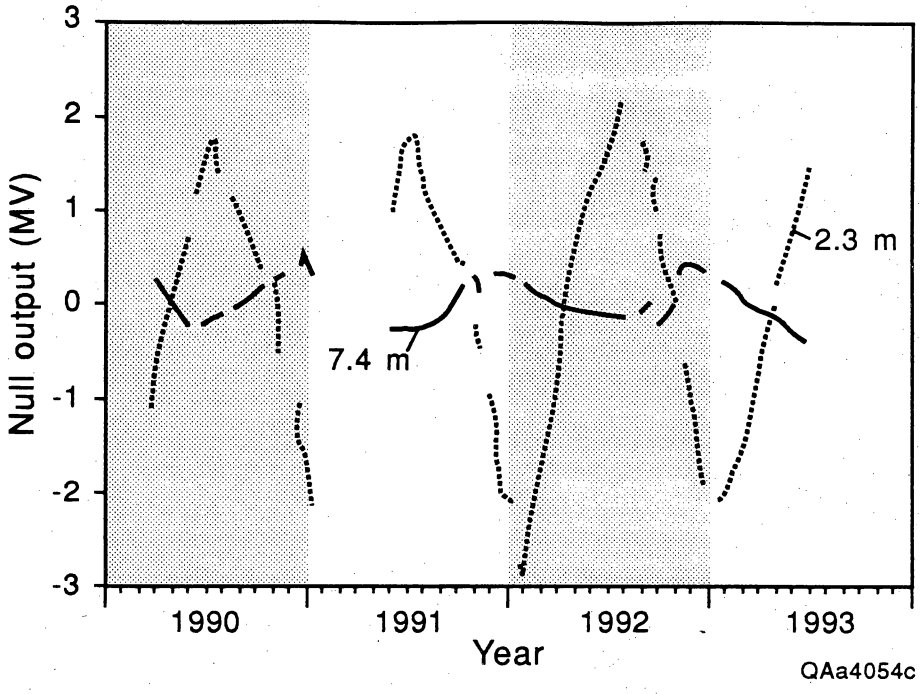

Figure 9. Seasonal variations in the null output monitored by psychrometers at 2.3 and 7.4 m depth.

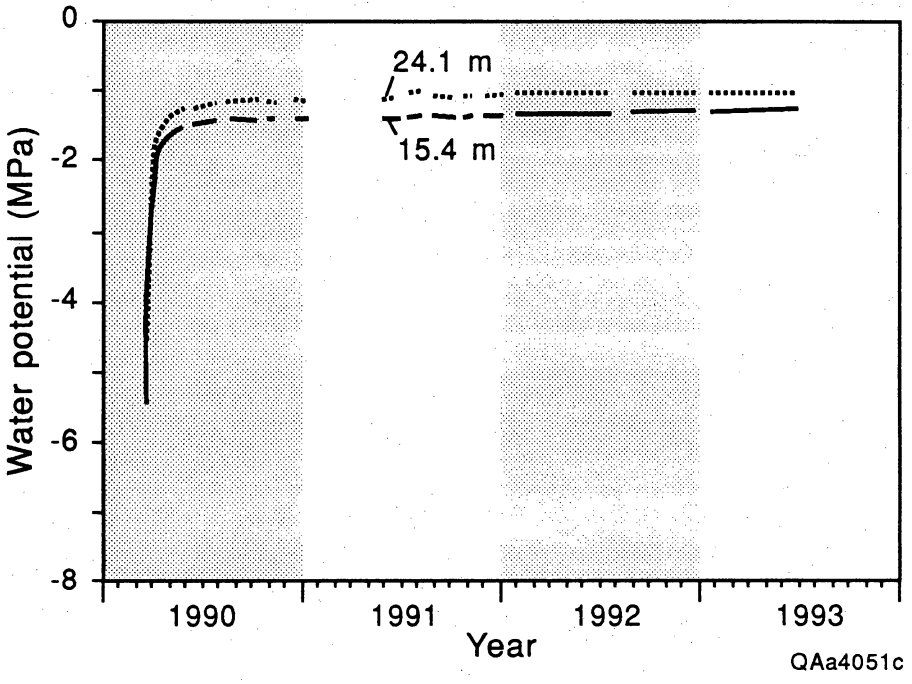

Figure 10. Water potentials monitored by psychrometers at 15.4 m and 24.1 m depth.

Comparison of Laboratory and Field Measured Water Potentials

Laboratory measured water potentials of soil samples collected from borehole 74 in September 1989 were compared with field monitored water potentials in September 1990 (Fig. 11). This comparison should be valid for depths greater than 1.4 m because temporal variations in water potential were small below this depth. The general shape of the laboratory and field water potential profiles was similar. Both profiles have predominantly upward water potential gradients except in the shallow subsurface.

Laboratory measured water potentials were much lower than field measured water potentials, particularly in the coarse grained sediments that were found in the upper 7.5 m. Water potentials measured at approximately the same depth differed by up to 6 MPa in the coarse sediments between 2 and 8.4 m depth, whereas the maximum difference in the clay section ($\geq$ 8.4 m depth) was approximately 1.4 MPa. These differences in water potential are attributed to drying of sediments during sample collection and laboratory measurement of water potential. The effect of such drying would be greatest in coarse grained sediments because of lower initial water contents and steeper water retention functions in coarse sediments (Fig. 12). The 2.1 MPa increase in the field monitored water potentials from 5.9 to 7.4 m depth is less than the 4.6 MPa increase in the laboratory measured data from 7.5 to 8.4 m depth. The 2.1 MPa increase probably marks the sand/clay contact; however, the borehole for psychrometer installation was drilled with a solid stem auger; and soil samples could not be collected, therefore, the depth of the sand/clay contact is not known.

Comparison of Field Psychrometer Data from Different Sites in the Hueco Bolson

Water potentials were recorded by field psychrometers to 14.3 m depth in another borehole and adjacent trench (20P, Fig. 1). The calibration equation for these psychrometers (20P) is similar to equation 1 for psychrometers at 77P:

$$\psi = -0.3918V + 0.0074VT - 0.0293$$

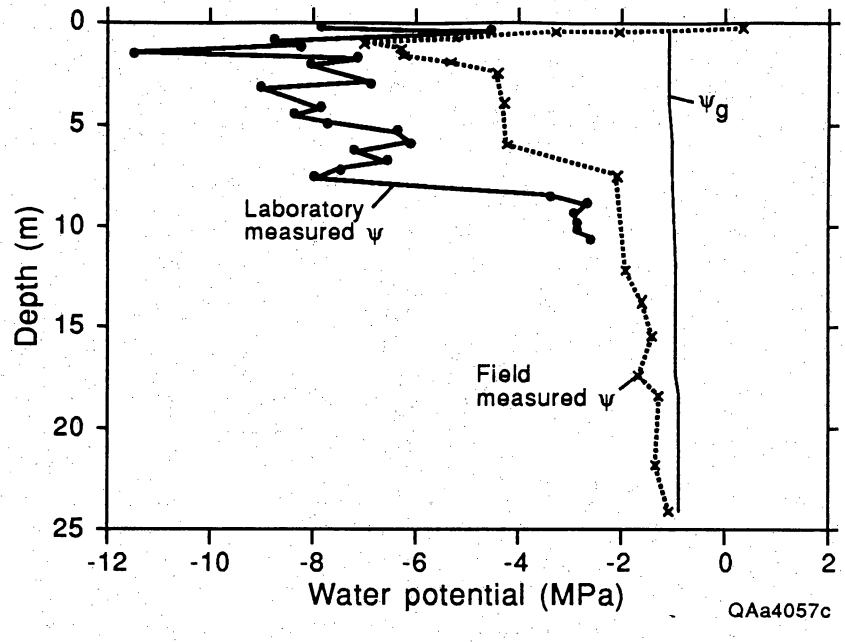

Figure 11. Comparison of laboratory-measured water potentials of soil samples collected from borehole 74 on September 25, 1989, and field-monitored water potentials in borehole 77P on September 25, 1990.

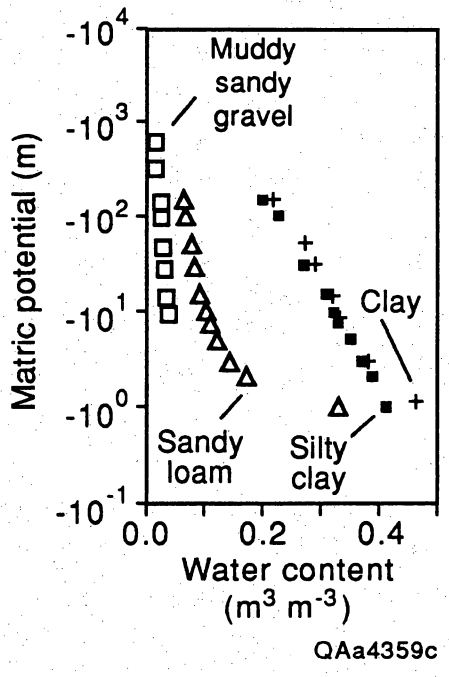

Figure 12. Laboratory-measured water retention data for different soil textures (Scanlon, 1993).

This equation has an r^2 of 0.99 and a standard error of estimate of 0.21 MPa. Monitoring data for these psychrometers from March 1989 to December 1990 were described in Scanlon (1993) and the monitoring data from March 1989 to May 1993 are described here. Psychrometers at many depths did not work because the wires in 6 of the 20 psychrometers were chewed by animals immediately after installation.

Similar trends in water potential variations found in psychrometers at 77P were also found in psychrometers at 20P. Water potentials decreased from 1989 to 1990 down to 1.4 m depth. Water potentials in the upper 0.8 m went below the calibration range in summer 1989 and stayed below this range until fall of 1990. This water potential decrease is attributed to below normal rainfall . Rainfall during 1989 (157 mm) was 53% of the long term average (296 mm) and rainfall during the first 6 months of 1990 (25 mm) was only 8% of the long term average for this period. The water potential increase during the fall of 1990 is attributed to above average rainfall from July through September (223 mm). Large increases in water potential were recorded in psychrometers down to 1.4 m depth during 1992 and 1993. Three infiltration events can be distinguished. Two of the events are similar to those recorded at 77P, and the third event was not recorded at 77P because of problems with data collection. The wetting front penetration depth was much less at 20P than at 77P. Only psychrometers at a depth of 0.3 m reached a water potential of 0 at 20P whereas psychrometers down to 0.8 m depth increased to 0 at 77P. Soil textural data from borehole 50 which is adjacent to 20P indicates that the sediments are much finer grained in the upper 1.3 m (clay loam to clay) than those near 77P (gravelly muddy sand). The finer grained sediments account for the shallower penetration of the wetting front at 20P relative to that at 77P. Attenuation and phase shift of the water potential increase with depth was recorded in both psychrometer stations. The water potential increase during the wetting phase and the decrease during the drying phase was rapid. The lag between water potential increases recorded in the upper 0.5 m was much greater during the wetting phase than

during the drying phase. Similar features of the water potential variations were recorded at 77P.

Seasonal fluctuations in water potentials were recorded by psychrometers at depths of 1.1, 1.4 and 7.6 m. Seasonal water potential fluctuations at 1.1 and 1.4 m depth were masked by water potential increases during 1992 and 1993. The water potential increase during the first ~ 2 yr at 7.6 m depth cannot readily be explained. The magnitude of seasonal fluctuations (~ 1.5 MPa at 1.1 m depth to ~ 0.1 MPa at 7.6 m depth) was similar to that recorded in 77P and the shift in seasonal maxima from summer at shallow depths to winter at greater depths was similar in 20P and 77P. There was a water potential decrease from 1989 to 1990 superimposed on the seasonal fluctuations at depths of 1.1 and 1.4 m. Maximum summer water potentials decreased by 1 and 0.4 MPa at depths of 1.1 and 1.4 m respectively. Water potential fluctuations at depths ≥ approximately 10 m were negligible. The range in water potentials from -1 to -2 MPa in this zone was similar in both 20P and 77P.

Comparison of Water Potential and Chloride Data

The chloride mass balance approach was used to evaluate subsurface water fluxes in the study area. According to this theory, chloride, originating in rainfall and dry fallout, increases in concentration through the root zone as a result of evapotranspiration and should remain constant below the root zone. If chloride input in the study area is considered constant, then, chloride concentrations in soil water are inversely proportional to water flux; low chloride concentrations indicate high water fluxes as chloride is leached out of the soil whereas high chloride concentrations indicate low water flux as chloride is concentrated by evapotranspiration. Chloride concentration data from 10 profiles in the Hueco Bolson were used to estimate subsurface water fluxes (Scanlon, 1991). The chloride profile from borehole 74 has low concentrations (≤ 300 g m-3) in the upper 1.3 m (Fig. 14) which generally corresponds to the zone of active circulation indicated by the

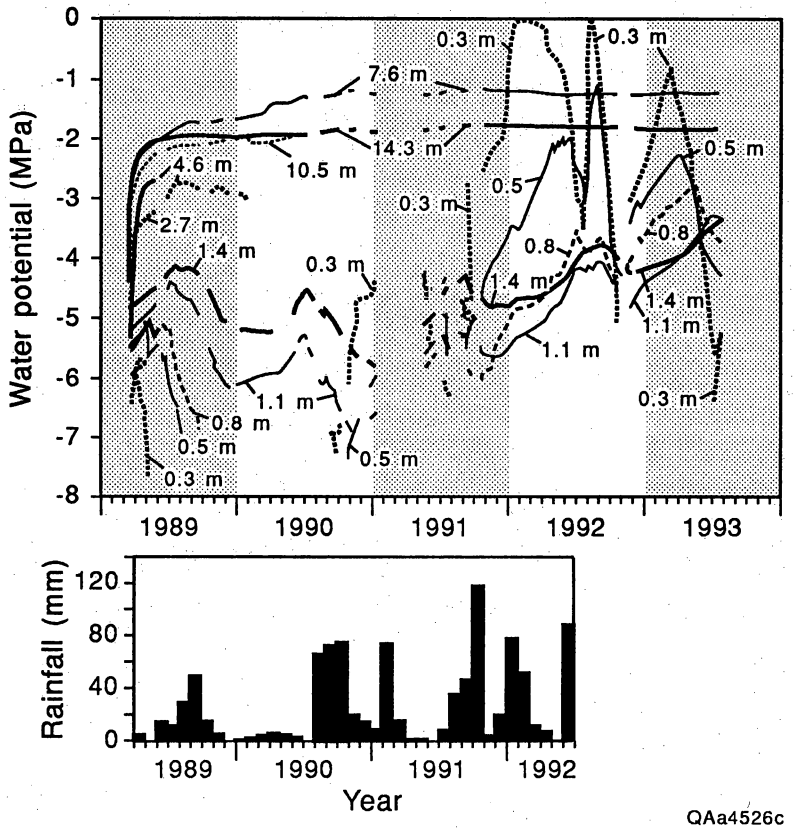

Figure 13. Temporal variations in water potential monitored by psychrometers at depths of 0.3 to 14.3 m in borehole.

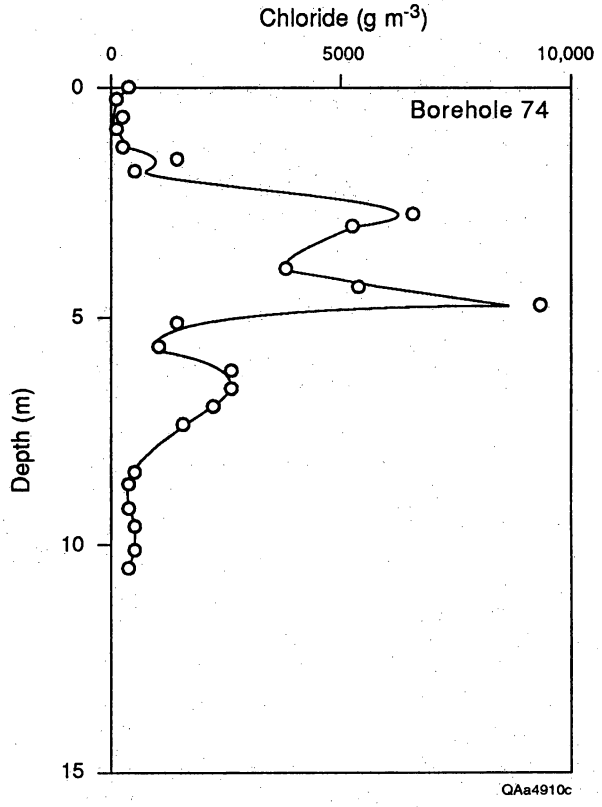

Figure 14. Chloride concentrations in soil samples from borehole 74.

water potential monitoring data (Fig. 6). A zone of high chloride was found between depths of 1.6 and 7.4 m. The reduction in chloride concentration between 7.4 and 8.4 m to concentrations ≤ 540 g m-3 occurs slightly above the sand clay contact (8.4 to 8.7 m) and corresponds to the water potential increase recorded in the laboratory and field data. The residence time of soil water chloride was calculated by dividing the total mass of chloride from the surface to 7.4 m depth by the annual chloride deposition and was approximately 13 kyr.

DISCUSSION

Comparison with Other Arid Regions

Water potential and temperature data from semiarid and arid regions are limited because of the difficulty of monitoring these parameters. Detailed monitoring of water potential and temperature was conducted near Beatty, Nevada in the Amargosa desert (Fischer, 1992). Long term average annual rainfall at this site (114 mm Beatty) is much lower than long term rainfall in the Hueco Bolson (280 mm Fort Hancock). The seasonal precipitation pattern at the two sites also differs. Most precipitation at Beatty occurs from November through March (Fischer, 1992) whereas precipitation at Fort Hancock occurs mostly from June through September. Psychrometers were installed in duplicate at the Beatty site at 1 m depth intervals from 3 to 13 m in a shaft and from 1 to 12 m in an adjacent borehole. The monitoring record reported in Fischer (1992) extends from October 1986 to February 1988. Water potentials monitored by the duplicate psychrometers at each depth were in general agreement. Water potentials monitored at 5 depths were not analyzed because the variations were considered unreasonable. Water potentials increased to > -0.5 MPa to 1.2 m depth as a result of infiltration of rainfall (total daily rainfall of 18 mm) in November 1987. Psychrometers at greater depths were not affected by this infiltration

event probably because of the capillary barrier effect of a gravel zone. Seasonal fluctuations in water potential were recorded by psychrometers at depths of 1 to 7 m. Seasonal maxima and minima also varied with depth. Seasonal water potential variations at 1.2, 1.6, 4.2 and 5 m were generally in phase with seasonal temperature fluctuations; however, water potential variations at depths of 2.8, 3, 3.4, 6.2 and 7 m were out of phase with seasonal temperature variations. It is difficult to fully evaluate the relationship between water potential and temperature with one year of data. At depths greater than 12 m water potential variations were negligible. Psychrometers installed at depths of 8 to 11.5 m showed a gradual increase in water potential throughout the monitoring period that may be natural or may be an artifact of equilibration of sediments that were dried during drilling by air injection. Many of the borehole psychrometers from depths of 8 to 12 m exhibited short term fluctuations in water potential and temperature after the November rainfall. These fluctuations were thought to be an artifact of preferential air movement in the borehole and were not observed in psychrometers installed in the shaft at similar depths. Fischer (1992) also noted that water potentials measured in the laboratory (range: -4.0 to -8.0 MPa) were equal to or lower than those measured in the field (-3.1 to -5.8 MPa) and attributed the discrepancy to drying during sample collection and analysis.

Comparison of vertical water potential profiles at Beatty and the Hueco Bolson indicate that both have upward water potential gradients and plot to the left of their equilibria lines which indicates upward driving forces for liquid and isothermal vapor movement at both sites (Fig. 15). Good agreement was found between water potentials monitored from 3 and 6 m at both sites. Below this depth water potentials at Beatty were lower than those monitored at the Hueco Bolson. Water potentials were also monitored from April 1989 to September 1990 in Ward Valley in the Sonoran Desert 35 km west of Needles California. This site is being evaluated for disposal of low-level radioactive waste. Average annual rainfall is 119 mm. The unsaturated zone is approximately 200 m thick at this site. Four psychrometers were installed at 12 different depths approximately evenly

spaced from 3 to 30 m. The data have high frequency oscillations at all depths that are up to 0.6 MPa which make it difficult to evaluate systematic variations with depth or time. Some of the short term variations are thought to be an artifact of the data collection process. A vertical profile based on data from November 7, 1990 suggests an upward water potential gradient from -3.7 MPa at 30 m depth to -5.4 MPa at 7.5 m depth (Fig. 15).

Water potentials monitored at Hanford, Washington were much higher than those recorded in the other arid sites in the southwest and ranged from 0 to -0.9 MPa at Hanford (Brownell et al., 1975). The Hanford data plot to the right of the equilibrium line, which indicates downward water flow (Fig.). This is supported by neutron probe logging and weighing lysimeter data, which recorded downward water movement (Gee and Heller, 1985). Although the mean annual precipitation at Hanford (162 mm) is much lower than that recorded in the Hueco Bolson (280 mm), much of the precipitation at Hanford occurs as snowfall when temperature and evapotranspiration are lowest and recharge potential is greatest. Also, surficial sediments are much coarser at Hanford than at the Hueco Bolson, which further contributes to drainage in this study area.

Conceptual flow model

Results from the water potential monitoring data provide detailed information on unsaturated zone processes in an arid system under natural conditions. Variations in soil texture are important in controlling the wetting front penetration depth. The wetting front penetration depth was restricted to the upper 0.3 m in the clayey soils but extended to 0.8 m in the sandy soils. Psychrometers below the wetting front down to a maximum depth of 1.4 m showed increases in water potential; however, water potentials in this zone remained less than -2 MPa and the water potential increases probably reflect negligible increases in soil water storage. Although the Hueco Bolson generally has high summer precipitation, the occurrence of water infiltration and redistribution primarily in response to above normal winter precipitation implies that winter precipitation is much more effective in percolating

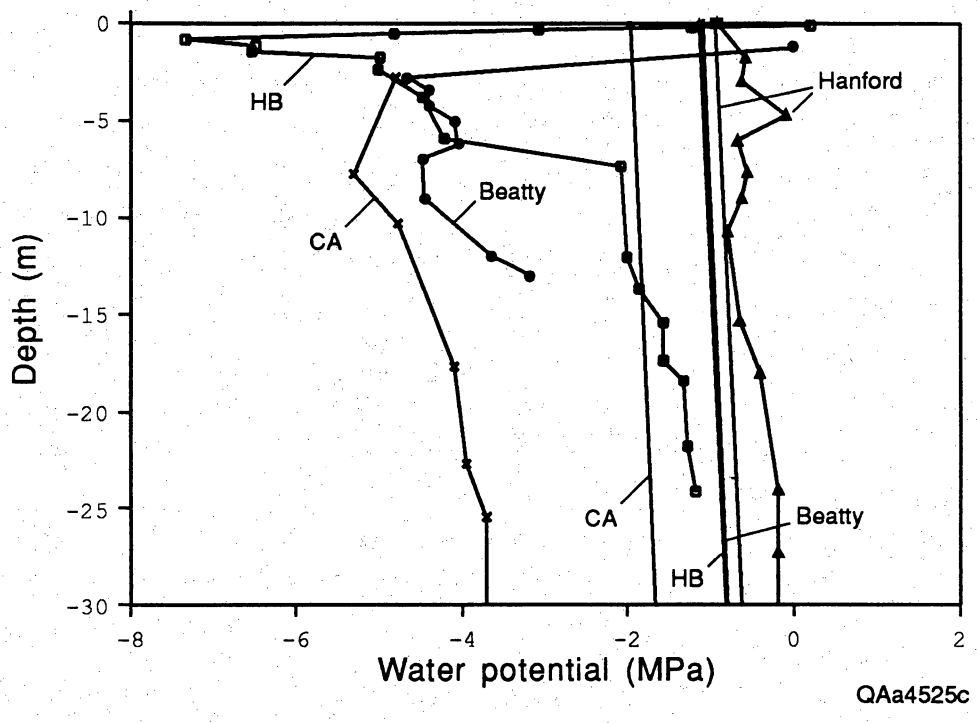

Figure 15. Comparison of water potential profiles measured in the Hueco Bolson, Texas; Hanford, Washington; Beatty, Nevada; and Needles, California.

through the soil. This is also supported by data from the Hanford site where drainage of soil water occurs in response to high winter precipitation. This also suggests that the seasonal distribution of precipitation is more important than the annual average precipitation in controlling infiltration. Large interannual variations in water infiltration and redistribution in response to interannual variations in precipitation underline the importance monitoring soil physics parameters for several years to evaluate unsaturated zone processes.

The progressive increase in water potentials with depth as water pulses move down into the unsaturated zone suggests that water at both psychrometer stations in the Hueco Bolson moves by piston flow. Evidence for piston flow was found in tracer experiments conducted in an arid site in New Mexico where the tracer front lagged the wetting front as piston displacement of initial soil water occurred (Young et al., 1992). Because piston flow is assumed in analysis of many environmental tracers such as chloride, it is important to determine the validity of this assumption.

The minimal lag between water potential decreases at each depth during the drying phase at the Hueco Bolson suggests that vegetation plays an important role in removing water from the subsurface. This is supported by data from other arid sites where comparisons of subsurface water movement between adjacent vegetated and nonvegetated sites have been made (Gee et al., 1993). At the Beatty site, evapotranspiration effectively removed subsurface water in the vegetated site, whereas water storage was much higher in the nonvegetated site. Revegetation of a previously bare lysimeter at the Hanford site removed excess water storage within a few months.

Below a depth of approximately 1.4 m in the Hueco Bolson, seasonal fluctuations in water potential are found. In the upper 1.4 m the effects of infiltration and evaporation are superimposed on seasonal fluctuations. Seasonal water potential variations from 1.4 to 7 m depth are generally in phase with seasonal temperature fluctuations. The extinction and phase shift of the water potential variations are similar to those of temperature. Numerical

simulations of subsurface water movement in the Hueco Bolson suggested that these water potential variations may be controlled by temperature fluctuations and reflect little water movement (Scanlon and Milly, 1994).

Water potential data from the Hueco Bolson and from other arid sites in the southwest all have upward gradients except in the shallow subsurface after rainfall. The water potentials at all these sites plot to the left of their respective equilibria lines. Both the upward gradients and the position of these profiles relative to equilibrium suggest an upward driving force for liquid and isothermal vapor movement. Temperature gradients in the winter are also upward and provide an upward driving force for thermal vapor movement. In contrast, temperature gradients in the summer are downward, oppose water potential gradients, and provide a downward driving force for thermal vapor movement. Numerical simulations of flow in the Hueco Bolson in response to an annual climate cycle (October 1989 through September 1990) based on water potential data monitored at 20P showed that liquid fluxes were dominant in the upper 0.3 m where downward and upward movement occurred in response to infiltration and evaporation (Scanlon and Milly, 1994). Below 0.3 m, fluxes were dominated by downward thermal vapor flux. The simulated average annual downward vapor flux below the evaporation front (0.08 m) (~ 1 mm yr-1) was within the same order of magnitude as the vapor flux estimated from the deeper penetration of bomb tritium relative to that of bomb chlorine 36 (5.6 mm yr-1).

The range in water potentials in the Hueco Bolson is similar to that found at the Beatty and California sites in the zone from 3 to 6 m. Below this depth water potentials in the Hueco Bolson increase sharply from -4.2 MPa to -2 MPa whereas water potentials at the other two sites remain low. This increase in water potentials in the Hueco Bolson probably occurs near the contact between surficial sands and underlying clays and indicates nonequilibrium conditions. The increase may reflect an increase of water potentials toward equilibrium values, or the inability of vegetation to remove water from the clays, or increased percolation in the past. The chloride data also provide evidence for increased

water flux in the past and the chloride age for this depth zone is 13 000 yr. This is consistent with Phillips (1993) analysis of environmental tracers throughout the American Southwest. Chloride data from profiles in Nevada, Arizona, New Mexico and Texas indicated an increase in water flux from 13 to 16 kyr. Water fluxes based on the chloride data agreed with water level data from closed-basin lakes in the Great Basin which also indicated a shift in the water balance about 13 kyr. The uniform regional response of subsurface flux to the Pleistocene-Holocene climate change is attributed to the replacement of mesic Pleistocene flora by a xeric Holocene flora which is much more efficient at extracting soil water.

Implications

Information on unsaturated flow processes based on soil physics monitoring has important implications for waste disposal in arid sites. Data from this study can help to design trench caps that minimize subsurface water flux. Fine textured soils in the shallow subsurface provide a large storage capacity to buffer the effect of rainfall and decrease the penetration depth of the wetting front. The psychrometer data suggest that water moves by piston flow which is more readily characterized and modeled that preferential flow. Most intense monitoring should be conducted in the shallow subsurface because water potential variations are greatest in this zone. One year of data is generally required for site characterization for a low-level radioactive waste disposal facility; however, the results from this study indicate that several years of soil physics data are required because of large interannual variations in precipitation distribution and amount. The importance of vegetation in removing water has been shown at many sites and also during the drying phase of many cycles. These data suggest that trench caps should be revegetated to minimize subsurface water movement.

CONCLUSIONS

Long term monitoring of water potentials in the Hueco Bolson provide valuable insights into unsaturated zone processes in arid systems under natural conditions. Abnormally high winter precipitation in 1992 and 1993 resulted in active water circulation to 1.4 m depth. The maximum penetration depth of the wetting front was 0.8 m in sandy soil and 0.3 m in clayey soil. Water moved down by piston flow as evidenced by the progressive increase in water potentials with depth. Water potentials remained high for long periods (120 to 70 d) at depths of 0.3 to 0.8 m. The rapid decrease in water potentials during the drying phase and the small lag between water potential decreases at different depths suggests that plants effectively remove water from the shallow subsurface. Seasonal water potential fluctuations recorded at 1.4 to 7.4 m depth were similar to seasonal temperature variations and probably do not reflect changes in water content. Below 7.4 m depth, water potentials did not vary with time. Vertical water potential profiles suggest an upward driving force for liquid and isothermal vapor movement except in the shallow subsurface after rainfall events. Temperature gradients in the winter were also upward which suggests an upward driving force for thermal vapor movement. Downward temperature gradients in the summer oppose upward water potential gradients and indicate a downward driving force for thermal vapor movement. A sharp water potential increase near the sand clay contact at 5.9 to 7.4 m depth corresponds to a chloride mass balance age of 13 kyr and suggests that the system is not at steady state and probably reflects higher recharge during the Pleistocene. Vertical profiles based on data from Beatty, Nevada; Ward Valley, California, and the Hueco Bolson showed similar water potentials in the 3 to 6 m zone; below this zone water potentials in the Hueco Bolson were up to 3 MPa higher than those recorded in the other sites. The water potential monitoring data from the Hueco Bolson suggests that fine grained sediments and vegetation are important in minimizing subsurface water movement and should be used in cap design for the facility.

REFERENCES

Brownell, L. E., Backer, J. G., Isaacson, R. E., and Brown, D. J., Soil moisture transport in arid site vadose zones, *Rep.* ARH-ST-123, 232, pp., Atlantic Richfield Hanford Company, Richland, Washington, 1975.

Enfield, C. G., Hsieh, J. J. C., and Warrick, A. W., Evaluation of water flux above a deep water table using thermocouple psychrometers, *Soil Sci. Soc. Am. Proc.*, 37, 968-970, 1973.

Gaudet, J. P., Jegat, H., Vachaud, G., and Wierenga, P. J., Solute transfer, with exchange between mobile and stagnant water, through unsaturated sand, *Soil Sci. Soc. Am. J.*, 41, 665-671, 1977.

Gee, G. W., and Heller, P. R., Unsaturated water flow at the Hanford site: a review of literature and annotated bibliography, *Rep.* PNL-5428, 42 pp., pp., Pacific Northwest Laboratory, Richland, Washington, 1985.

Gee, G. W., and Jones, T. L., Lysimeters at the Hanford site: present use and future needs, *PNL 5578 UC*, 70, 1-44, 1985.

Jones, T. L., Gee, G. W., and Heller, P. R., Psychrometric measurement of soil water potential: stability of calibration and test of pressure-plate samples, *Soil Sci.*, 150, 535-541, 1990.

Koorevaar, P., Menelik, G., and Dirksen, C., *Elements of Soil Physics*, 230 pp., Elsevier, New York, 1983.

Lang, A. R. G., Osmotic coefficients and water potentials of sodium chloride solutions from 0 to 40 C, *Aust. J. Chem.*, 20, 2017-2023, 1967.

Larkin, T. J., and Bomar, G. W., Climatic atlas of Texas, *Rep.* Publication LP-192, 151 p., pp., Department of Water Resources, Austin, Texas, 1983.

Merrill, S. D., and Rawlins, S. L., Field measurement of soil water potential with thermocouple psychrometers, *Soil Sci.*, 113, 102-109, 1972.

Meyn, R. L., and White, R. S., 1972, Calibration of thermocouple psychrometers : a suggested procedure for development of a reliable predictive model: Psychrometry in water relations research, Logan, Utah, Utah Agricultural Experiment Station, Utah State University, p. 56-63.

Montazer, P., Weeks, E. P., Thamir, F., Yard, S. N., and Hofrichter, P. B., Monitoring the vadose zone in fractured tuff, Yucca Mountain, Nevada, in *Proc. on Characterization and Monitoring of the Vadose (Unsaturated) Zone,* edited by pp. 439-469, National Water Well Association, Denver, Colorado, 1985.

Mullican, W. F., III, Kreitler, C. W., Senger, R. K., and Fisher, R. S., 1989, Truly deep saturated zone investigations at the proposed low-level radioactive waste disposal site for Texas: Proc. of the Third National Outdoor Action Conference on Aquifer Restoration, Ground Water Monitoring and Geophysical Methods, Orlando, Florida, National Water Well Association, p. 447-461.

Nichols, W. D., Geohydrology of the unsaturated zone at the burial site for low-level radioactive waste near Beatty, Nye County, Nevada, *Rep.* Water Supply Paper 2312, 57, pp., U.S. Geological Survey, 1987.

Rawlins, S. L., and Campbell, G. S., Water potential: thermocouple psychrometry, in *Methods of Soil Analysis, Part 1, Physical and Mineralogical Methods,* edited by A. Klute, pp. 597-617, Am. Soc. Agron., Madison, Wisconsin, 1986.

Savage, M. J., and Wiebe, H. H., Voltage endpoint determination for thermocouple psychrometers and the effect of cooling time, *Agric. Forest Meteor.*, 39, 309-317, 1987.

Scanlon, B. R., Evaluation of moisture flux from chloride data in desert soils, *J. Hydrol.*, 128, 137-156, 1991.

van de Pol, R. M., Wierenga, P. J., and Nielsen, D. R., Solute movement in a field soil, *Soil Sci. Soc. Am. J.*, 41, 10-13, 1977.

Winograd, I. J., Radioactive waste disposal in thick unsaturated zones, *Sci*, 212, 1457-1464, 1981.

Young, M. H., Wierenga, P. J., Hills, R. G., and Vinson, J., Evidence for piston flow in two large-scale field experiments, Las Cruces trench site, *EOS, Trans. AGU*, 73, 156, 1992.